Experimental Approaches to Acute Myocardial Infarction

André Uitterdijk

Experimental Approaches to Acute Myocardial Infarction

André Uitterdijk

Experimental Approaches to Acute Myocardial Infarction

Thesis Erasmus Medical Center, Rotterdam

ISBN: 978-94-6299-160-6
Printed by: Ridderprint BV - www.ridderprint.nl
Lay-out by: Nikki Vermeulen - Ridderprint BV - www.ridderprint.nl
Cover design: Remko Burger
Friese vertaling: Baukje Stavinga - www.letterfretter.nl

Experimental Approaches to Acute Myocardial Infarction

Experimentele benaderingen van het acute hartinfarct

Proefschrift

ter verkrijging van de graad van doctor aan de
Erasmus Universiteit Rotterdam

op gezag van de rector magnificus
Prof.dr. H.A.P. Pols
en volgens besluit van het College voor Promoties.

De openbare verdediging zal plaatsvinden op
woensdag 16 september 2015 om 11.30 uur

door

Drevis Berend Uitterdijk
geboren te Dokkum

Erasmus University Rotterdam

Promotiecommissie

Promotoren:
Prof.dr. D.J. Duncker
Prof.dr. W.J. van der Giessen († juni 2011)

Overige leden:
Prof.dr. R.J. van Geuns
Prof.dr. P. Koudstaal
Prof.dr. N. van Royen

Copromotoren:
Dr. D. Merkus
Dr. H.M.M. van Beusekom

The studies in this thesis have been performed at the Erasmus Medical Center at the department of Cardiology, Rotterdam, the Netherlands.

Financial support by the Dutch Heart Foundation for the publication of this thesis is gratefully acknowledged.

Additional financial support was generously provided by Cardialysis, OctoPlus BV and the Erasmus MC.

Foar Heit & Memke en foar mysels, wês mar grutsk

CONTENTS

Chapter 1	General introduction and outline of the thesis	11
Part I	**Experimental Approaches to Myocardial Ischemia and Myocardial Infarction**	**29**
Chapter 2	Quantification of myocardial blood flow by adenosine-stress CT perfusion imaging in pigs during various degrees of stenosis correlates well with coronary artery blood flow and fractional flow reserve	31
Chapter 3	Serial measurement of hFABP and high sensitivity Troponin I post PCI in STEMI. How fast and accurate can Myocardial Infarct Size and No-Reflow be predicted?	47
Chapter 4	No-reflow and reperfusion affect $VEGF_{165A}$ induced in-vitro network formation by human cardiac microvascular endothelium	65
Chapter 5	Time course of VCAM-1 expression in reperfused myocardial infarction in swine and its relation to retention of bone marrow-derived mononuclear cells	79
Part II	**Acute Myocardial Infarction and Reperfusion Injury**	**99**
Chapter 6	Limitation of Infarct Size and No-Reflow by Intracoronary Adenosine Depends Critically on Dose and Duration	101
Chapter 7	Vagal Nerve Stimulation during Early Reperfusion Limits Infarct-Size and No-Reflow	133
Part III	**Infarct Healing and Left Ventricular Remodeling**	**153**
Chapter 8	Evolution of reperfusion post-infarction ventricular remodeling: new MRI insights	155
Chapter 9	Intermittent pacing therapy favorably modifies infarct remodeling	169

Chapter 10	UM206, a selective frizzled antagonist, attenuates adverse remodeling after myocardial infarction in swine	199
Chapter 11	VEGF165A microsphere therapy for myocardial infarction suppresses acute cytokine release and increases microvascular density, but does not improve cardiac function	211
Chapter 12	Summary and General Discussion	241
Chapter 13	Nederlandse samenvatting	261
Chapter 14	Fryske gearfetting	271
	List of Publications	281
	PhD portfolio	287
	About the Author	291
	Dankwoord	295

CHAPTER 1

General introduction and outline of the thesis

EPIDEMIOLOGY OF CARDIOVASCULAR DISEASE

Cardiovascular disease remains an important cause of mortality and morbidity. In the Netherlands alone, 1 million patients suffer from cardiovascular disease (www.hartstichting.nl). In addition, more than 4 million Europeans die of cardiovascular disease every year with many more hospitalized for cardiovascular problems (1). Together with substantial effects on mortality and impairment in quality of life, the economic burden of cardiovascular disease is immense and is estimated to be over €200 billion in Europe (1). In the United States, cardiovascular disease claims the life of an American every 40 seconds and burdens economy with more than $300 billion annually (2). Finally, in countries in transition, including China and India, the incidence and prevalence of cardiovascular disease continues to rise, making it the predicted number one cause of death in 2020 worldwide (3). Consequently, and notwithstanding tremendous advances in cardiovascular care over the past 50 years, a large proportion of the global population will succumb to cardiovascular disease in a direct or indirect way. These epidemiological observations clearly highlight the importance of optimizing current and developing novel treatment strategies to ameliorate the burden of cardiovascular disease.

ATHEROSCLEROSIS

In industrial countries, ischemic heart disease is a dominant contributor to the cardiovascular disease burden (4). A major cause of ischemic heart disease is atherosclerosis (5,6). Atherosclerosis is a chronic inflammatory disease of artery walls and is characterized by regional accumulation of white blood cells, lipids and lipoproteins resulting in a regional inflammatory entity within the arterial wall with or without calcifications and cholesterol crystals (7,8). Such regional accumulations are termed atheromatous plaques. The disease is progressive but can remain asymptomatic for decades (9). The composition and thickness of the fibrous cap, which is the part of the atheromatous plaque in continuous contact with the blood vessel lumen and subject to blood flow, determine the stability of the plaque (10); the upstream border of the fibrous cap is most vulnerable to rupture (11).

CORONARY STENOSIS AND MYOCARDIAL ISCHEMIA

When atheromatous plaques increase in size and the vasculature can no longer compensate for the plaque's obstructive properties by virtue of outward vessel growth, the lumen of the artery-at-risk progressively narrows (6,7). Advanced narrowing with stable plaques increases resistance of the proximal coronary

blood flow. This increase in proximal resistance is initially compensated by vasodilation of the distal coronary microvasculature, a phenomenon termed autoregulation (12,13). However, when vasodilator reserve is exhausted, the stenosis becomes flow-limiting and distal myocardial perfusion is reduced (13). This impaired perfusion of myocardial tissue results in a disbalance in regional supply to, and demand of oxygen and nutrients of the myocardium, i.e. ischemia, that results in angina pectoris (14). This relative disbalance between supply and demand of oxygen and nutrients initially occurs only during heavy exercise, when oxygen demand is high, but may ultimately also occur at mild levels of exercise, and initiate repetitive episodes of ischemia, resulting in myocardial stunning progressing towards hibernation, characterized by chronic contractile dysfunction, ultrastructural myocardial abnormalities, and ultimately left-ventricular remodeling (14-17). Conversely, repetitive ischemia is a strong stimulus for the development of collateral blood vessels that form an alternative route of myocardial blood supply and thereby act to (partially) restore myocardial perfusion (18,19).

CORONARY STENOSIS, PLAQUE RUPTURE AND MYOCARDIAL INFARCTION

When an atherosclerotic plaque ruptures or erodes and the resulting intraluminal thrombotic event abruptly progresses to an acute coronary occlusion, perfusion of the distal myocardium is suddenly interrupted (6,20). Cessation of the blood supply to the myocardium will almost instantaneously lead to disturbed contraction within the hypoperfused myocardium, and result in changes in left ventricular function, i.e. abnormalities in contraction and relaxation of the ventricle (14). In addition, changes in the electrical activity occur, which, depending on the location of the hypoperfused tissue, can be discernable as elevation of the ST-segment on the electrocardiogram and are often associated with potentially life-threatening ventricular arrhythmias (21). Damage of the hypoperfused cardiac muscle distal to the culprit lesion is initially reversible (stunning), but when ischemia persists beyond 20 min, irreversible loss of cardiac tissue occurs (necrosis) (16,17). This so-called acute myocardial infarction (AMI) is accompanied by leakage of proteins such as troponins and heart specific fatty acid binding protein from the damaged cardiomyocytes, that can be used as biomarkers to determine irreversible damage and estimate infarct size (22,23).

MYOCARDIAL INFARCTION, AREA AT RISK, INFARCT SIZE, NO-REFLOW AND MYOCARDIAL SALVAGE

The myocardial territory normally perfused by the occluded coronary artery is termed the “area at risk” (Figure 1A). The part of the area at risk that eventually succumbs to necrosis is termed the infarct area (Figure 1B). Infarct size is the infarct area expressed as a percentage of the area at risk. When blood flow to the area at risk is (partially) restored, either spontaneously or purposely using a coronary intervention, blood flow to certain parts within the infarct zone often remains compromised, which is termed the no-reflow phenomenon (24) (Figure 1C), and is associated with poor prognosis (25,26). Although the pathophysiology of the no-reflow phenomenon remains incompletely understood it has been proposed to be the consequence of microvascular obstruction (27), microvascular hemorrhage (28), microvascular spasms (29), microvascular damage (30) and/or microvascular mechanical compression due to post-infarct edema (24). Theoretically, the potential infarct size approximates the full area at risk. The percentual difference between the actual infarct size and the potential infarct size is termed myocardial salvage (31) and enables to quantify efficacy of interventions. The aim of novel interventions is to increase myocardial salvage by further optimization of (mechanical) reperfusion strategies and targeting reperfusion injury including early no-reflow.

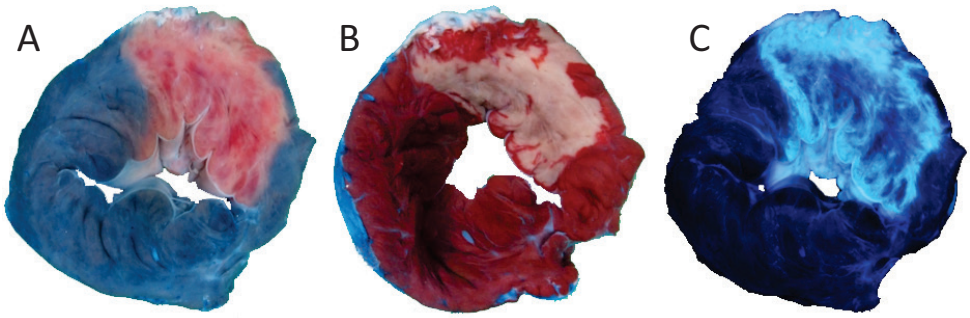

Figure 1. *Midventricular transversal slice of an infarcted porcine left ventricle stained for A: area at risk (= unstained) , B: Infarct area (white = metabolically inactive) and using UV-light for C: no-reflow (dark, non-perfused sections within bright area at risk). Please note that the staining for infarct area slightly changes geometry.*

POST-INFARCT MYOCARDIAL REMODELING, DYSFUNCTION AND WOUND HEALING

Following myocardial infarction, a plethora of immunological processes, that aim to acutely stabilize the vulnerable wound, start immediately (32). This regional wound healing process is not completely understood but a large body of evidence shows that myocardial infarction activates the innate immunity (32,33). Thus, in the acute phase, necrotic tissue is replaced by granulation tissue with negligible regenerative potential (33), which consists of cells involved in extracellular matrix turnover such as fibroblasts and myofibroblasts (34). It was recently reported that myofibroblasts in the infarct region are generally associated with improved outcome after myocardial infarction (35). Simultaneously, detrimental effects of myofibroblasts have been suggested as well (36). As a consequence, orchestrating intra-infarct myofibroblast content is emerging as a novel therapeutic target (37). Also, regional angiogenesis is activated and leucocytes such as macrophages and neutrophils are involved in phagocytizing damaged tissue (38,39). This process may be regarded as a double edged sword as this early response may initially aggravate injury (i.e. neutrophil plugging) (40,41) while being essential for wound healing and scar stabilization by phagocytosis of cell debris and forming a rigid, non-contractile substitute for cardiac muscle (42). Thus, modulation of the delicate post-infarct immune response with e.g. pharmacotherapy or neurohumoral stimulation is an important novel treatment modality for AMI.

When a substantial part of the heart and in particular the left ventricle is irreversibly damaged as a result of AMI, the heart undergoes extensive changes in geometry termed post-infarct remodeling, consisting of eccentric remodeling in particular of the surviving myocardium (Figure 2) (43,44). Although this process is intended to maintain stroke volume and hence cardiac output, it may ultimately precipitate progressive LV dilation and dysfunction and eventually lead to overt heart failure (45,46). Treatment modalities for heart failure are limited while the public health and economic burden increase (47). Especially since percutaneous coronary interventions have become the number one treatment for acute coronary syndromes, peri-AMI mortality has decreased significantly and more patients with AMI survived and will ultimately develop heart failure (48).

Traditionally, research has focused on targeting hypertrophic remodeling of the surviving myocardium to ultimately prevent heart failure, yielding inhibitors of the renin–angiotensin–aldosterone system and beta-adrenergic signaling as effective novel targets of post-AMI remodeling (49,50) However in the past 10 years

research efforts have shifted focus towards the healing processes within the infarct area as a potential therapeutic target.

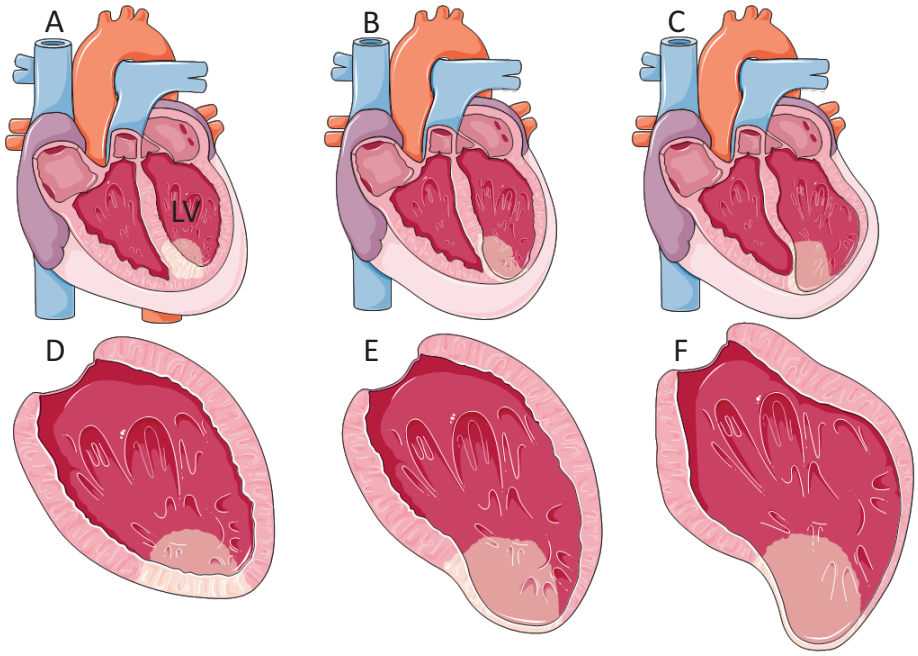

Figure 2. *Left ventricular remodeling over time showing progressive wall thinning, changes in left-ventricular geometry and infarct expansion. White area within the left ventricle (LV) is antero-septal infarct in A: the acute phase (≤hours post-infarction), B: sub-acute (several days post-infarction) and C: chronic, (weeks to months post-infarction). D, E and F are detailed left-ventricular representations of A, B and C respectively. Images provided by, and used with permission of Servier Medical Art (http://creativecommons.org/licenses/by/3.0/)*

CONVENTIONAL TREATMENT FOR ACUTE MYOCARDIAL INFARCTION AND REPERFUSION INJURY

To date, the single most effective treatment for AMI, remains early and successful restoration of myocardial blood flow of the impaired region by percutaneous coronary intervention (51). In addition, a broad spectrum of drugs and lifestyle changes are recommended in the treatment or prevention of AMI (52). However, despite its profound benefits, reperfusion therapy has been shown to produce irreversible myocardial damage, beyond that inflicted by the preceding period of ischemia, which partially offsets its benefits; this phenomenon has been termed ”lethal reperfusion-injury” (53,54). The mechanisms underlying reperfusion-

injury remain incompletely understood, but may include perturbations in calcium homeostasis (55), oxidative stress (56), acute inflammation (57), and a miscellany of microvascular impairment (58). Proof for the existence of lethal reperfusion injury stems from experimental studies showing that pharmacological (59,60) and mechanical (61,62) interventions administered during early reperfusion enhance the benefit of reperfusion and further limit infarct size. Thus, in addition to the myocardial salvage afforded by timely reperfusion, further salvage is attainable by modifying the reperfusion conditions.

RECENTLY INTRODUCED TREATMENT STRATEGIES FOR ACUTE MYOCARDIAL INFARCTION

The 21st century may be regarded as the dawn of a new era as characterized by an increasing number of novel adjunctive approaches being tested for the treatment of acute myocardial infarction, alongside reperfusion therapy (63,64). Technological developments and scientific progress are fundament of a plethora of experimental approaches that can be classified by approach or treatment target. Treatment targets include, but are not limited to, reducing infarct size and the extend of no-reflow, and stimulating regional angiogenesis or (immuno)modulating underlying principles of wound healing and scar tissue formation all in order to favorably attenuate infarct remodeling and thereby global LV remodeling (Figure 3).

Novel pharmacological therapies for myocardial infarction

The largest pool of novel adjunctive therapies for treatment and salvage following myocardial infarction aim at the pharmacological modulation of infarct development and infarct expansion and attenuating reperfusion injury including no-reflow (63). A substantial number of pharmacological conditioning studies are under investigation, both in basic research and clinical translation (65,66). Important examples aiming to attenuate acute necrosis and/or reperfusion injury include adenosine (67), exenatide (68,69) and bendavia (58,70) and results are ambiguous yet encouraging (63). Adenosine therapy i.e., resulted in controversial results (71,72) but is subject to improvement and of continued interest (73). Moreover, peptide based drugs that target Wnt/Frizzled signaling gained increased interest and aim at improving infarct healing by myofibroblast modulation with promising first results in mice (35,74,75).

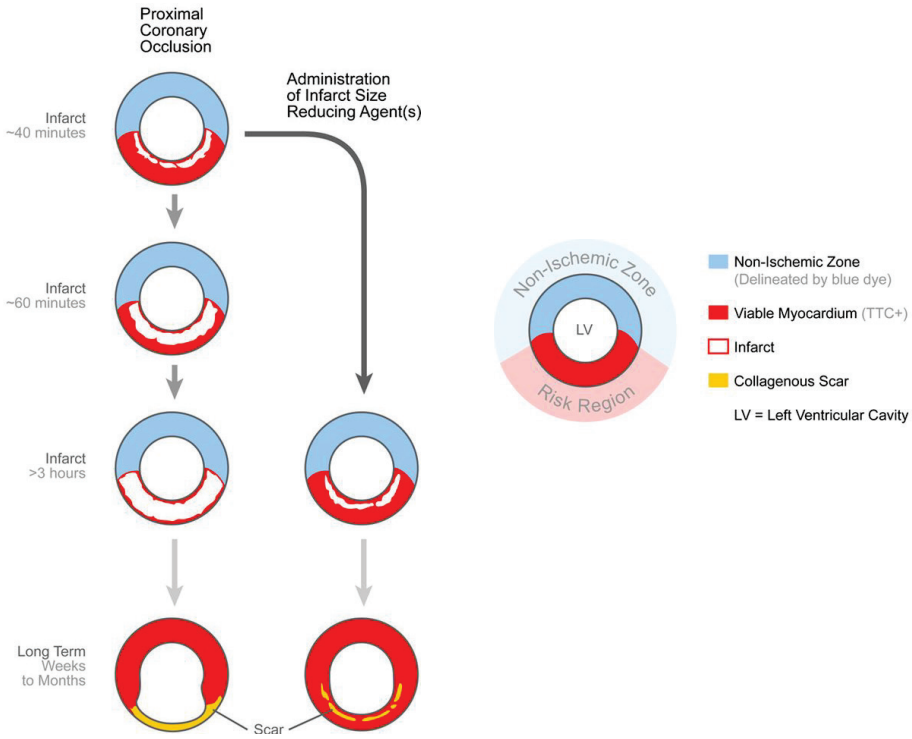

Figure 3. *Visualisation of the theoretical impact of left-ventricular and infarct expansion limiting therapies after acute myocardial infarction. LV = left ventricle, TTC+ = triphenyltetrazolium chloride which stains metabolically active myocardium. Picture taken from Kloner, 2013, Circ Res.*

Novel mechanical and device therapies for myocardial infarction

In addition to the pharmacological approach to treat myocardial infarction beyond conventional methodology, another approach exists. There are several adjunctive methods under investigation that all have a mechanical approach (76) or are device driven (77). These approaches aim at reducing infarct size or attenuate no-reflow, therefore ultimately, preventing or postponing heart failure. Currently, ischemic postconditioning, a method in which brief periods of ischemia are purposely administered immediately after reperfusion, is very promising (78), although contradictory evidence exists (79) which may be the result of differences in the number of balloon inflations (80). Also hypothermia of the infarcted heart, either induced directly or endovascularly, has shown promising results (81-83). Other (electro)mechanical or device therapies include, but are not limited to, pacing-induced dyssynchrony to attenuate infarct size (84,85). In addition, device driven neuro-humoral stimulation such as electrically triggering the efferent vagal nerve are under development to change post-infarct detrimental inflammatory cascades (86,87).

Cell Therapy for myocardial infarction

The year 2001, with the exiting publication of Orlic et al (88), was a turning point in adjunctive therapies for acute myocardial infarction that focus on the administration of either autologous, allogeneic or even xenogeneic cells. Although it has subsequently fallen subject to skepticism (89) and concern (90), that study initiated mainstream interest in the use of stem cells to treat the infarcted myocardium. Purported mechanisms of action included trans-differentiation of introduced cells into functional, electrically coupled cardiomyocytes that replace and repopulate affected areas, or paracrine actions exerting regional anti-inflammatory or anti-apoptotic effects to limit early post-infarct damage and/or facilitate local angiogenesis (91). To date, results of stem cell studies have been only modestly successful (92,93). Stem cell studies for myocardial infarction appear to be successful predominantly in the controlled setting of animal experiments where (small) animals are relatively young and have healthy cells whereas patients in clinical trials often suffer from comorbidities such as diabetes, hypertension, obesity and smoking that impair autologous cell function (94). Many parameters for stem cell treatment efficacy are still under study and remain to be optimized (95), including the optimal cell type (91) and timing (96) and route of cell administration (97). In all studies, retention of infused cells is consistently very low (98-100), which appears to be independent of the route of administration (101). Increasing regional retention by identifying and increasing its endogenous ligands may prove to be essential for increased efficacy of cell therapy.

AIMS AND OUTLINE OF THE THESIS

Despite major advances over the past 50 years, contemporary treatment and diagnosis modalities for acute myocardial infarction (AMI) and post-infarct remodeling are still limited and continue to be subject to improvement. Consequently, the aim of this thesis is to investigate recent novel diagnostic and therapeutic aspects of AMI in a preclinical large animal model, using state-of-the-art techniques and bio-assays.

Part I of this thesis covers novel experimental approaches to improve diagnosis and our understanding of myocardial ischemia and myocardial infarction. In **Chapter 2** we investigated the suitability of state-of-the-art dual energy computed tomography to quantify myocardial blood flow in the presence of flow limiting coronary stenoses of increasing severity in a porcine model of stable angina pectoris. In **Chapter 3**, we investigated the rediscovered marker, heart specific fatty acid binding

protein for acute infarct size and the extent of no-reflow, in a preclinical model of reperfused AMI. Next, in **Chapter 4,** we investigated the importance of cell type and experimental conditions in the in-vitro angiogenic evaluation of angiogenic agents and specifically the growth factor $VEGF_{165A}$ for growth factor therapy in the treatment of myocardial infarction. Finally, **Chapter 5** is dedicated to optimization of stem cell retention after myocardial infarction. This multilayered study investigated the longitudinal expression of post-infarction vascular cellular adhesion molecule 1 and its correlation with bone marrow-derived stem cell retention, again in a porcine model of reperfused AMI.

Part II of the thesis is dedicated to novel therapies for AMI, with a particular emphasis on their ability to attenuate reperfusion injury. In **Chapter 6**, acute treatment of infarct size and no-reflow with intracoronary administered adenosine pharmacotherapy in a porcine model of acute myocardial infarction was investigated using different therapeutic parameters with an emphasis on dosing and duration. Next, in **Chapter 7** a novel therapy for acute myocardial infarction and reperfusion injury is presented in which the vagal nerve of swine with acute myocardial infarction was stimulated for a very brief period of time during early reperfusion.

Finally, **Part III** of this thesis is dedicated to novel strategies to improve infarct healing and post-infarct remodeling of the left ventricle. In **Chapter 8**, a novel magnetic resonance imaging based method is presented that precisely shows the process of infarct expansion over a 5 week period after a 2 hour occlusion of the left circumflex coronary artery followed by reperfusion in swine. This state-of-the-art method that enabled us to study longitudinal changes in infarct geometry in swine with AMI was subsequently applied in **Chapter 9** to evaluate a novel, pacemaker based, therapy to attenuate post-AMI remodeling in a porcine model. In **Chapter 10**, we studied UM206, a selective Frizzled antagonist and a novel, peptide-based pharmacotherapeutic agent, to attenuate adverse remodeling in swine with AMI. Following this, **Chapter 11** describes a porcine study in which the growth factor $VEGF_{165A}$ was locally administered via controlled release microsphere therapy using percutaneous methodology in a porcine model of reperfused myocardial infarction with cardiac function and infarct characteristics measured with magnetic resonance imaging.

Finally, in **Chapter 12**, this thesis is summarized and discussed, and recommendations for future research are presented.

REFERENCES

1. Nichols M, Townsend N, Scarborough P, Rayner M. Cardiovascular disease in Europe 2014: epidemiological update. Eur Heart J 2014;35:2929-33.
2. Go AS, Mozaffarian D, Roger VL et al. Heart disease and stroke statistics--2014 update: a report from the American Heart Association. Circulation 2014;129:e28-e292.
3. Murray CJ, Lopez AD. Alternative projections of mortality and disability by cause 1990-2020: Global Burden of Disease Study. Lancet 1997;349:1498-504.
4. Yusuf S, Reddy S, Ounpuu S, Anand S. Global burden of cardiovascular diseases: part I: general considerations, the epidemiologic transition, risk factors, and impact of urbanization. Circulation 2001;104:2746-53.
5. Davies MJ. Stability and instability: two faces of coronary atherosclerosis. The Paul Dudley White Lecture 1995. Circulation 1996;94:2013-20.
6. Burke AP, Virmani R. Pathophysiology of acute myocardial infarction. Med Clin North Am 2007;91:553-72; ix.
7. Libby P, Theroux P. Pathophysiology of coronary artery disease. Circulation 2005;111:3481-8.
8. Sakakura K, Nakano M, Otsuka F, Ladich E, Kolodgie FD, Virmani R. Pathophysiology of atherosclerosis plaque progression. Heart Lung Circ 2013;22:399-411.
9. Toth PP. Subclinical atherosclerosis: what it is, what it means and what we can do about it. Int J Clin Pract 2008;62:1246-54.
10. Finn AV, Nakano M, Narula J, Kolodgie FD, Virmani R. Concept of vulnerable/unstable plaque. Arterioscler Thromb Vasc Biol 2010;30:1282-92.
11. Dirksen MT, van der Wal AC, van den Berg FM, van der Loos CM, Becker AE. Distribution of inflammatory cells in atherosclerotic plaques relates to the direction of flow. Circulation 1998;98:2000-3.
12. Zhang C RP, Merkus D, Muller-Delp JM, Tiefenbacher CP, Potter B, Knudson JD, Rocic P, Chilian WM. Regulation of Coronary Microvascular Resistance in Health and Disease. Comprehensive Physiology, 2008:521-549.
13. Duncker DJ, Koller A, Merkus D, Canty JM, Jr. Regulation of coronary blood flow in health and ischemic heart disease. Prog Cardiovasc Dis 2015;57:409-22.
14. Canty JM, Jr. , Duncker DJ. Coronary Blood Flow and Myocardial Ischemia. Braunwald's Heart Disease: A Textbook of Cardiovascular Medicine, 10th Edition, 2014:1029-1067.
15. Rahimtoola SH, Dilsizian V, Kramer CM, Marwick TH, Vanoverschelde JL. Chronic ischemic left ventricular dysfunction: from pathophysiology to imaging and its integration into clinical practice. JACC Cardiovasc Imaging 2008;1:536-55.
16. Kloner RA, Jennings RB. Consequences of brief ischemia: stunning, preconditioning, and their clinical implications: part 1. Circulation 2001;104:2981-9.
17. Kloner RA, Jennings RB. Consequences of brief ischemia: stunning, preconditioning, and their clinical implications: part 2. Circulation 2001;104:3158-67.
18. Duncker DJ, Bache RJ. Regulation of coronary blood flow during exercise. Physiol Rev 2008;88:1009-86.
19. Schaper W. Collateral circulation: past and present. Basic Res Cardiol 2009;104:5-21.
20. Fuster V, Stein B, Ambrose JA, Badimon L, Badimon JJ, Chesebro JH. Atherosclerotic plaque rupture and thrombosis. Evolving concepts. Circulation 1990;82:II47-59.
21. Durak I, Kudaiberdieva G, Gorenek B. Prognostic implications of arrhythmias during primary percutaneous coronary interventions for ST-elevation myocardial infraction. Expert Rev Cardiovasc Ther 2015;13:85-94.
22. Chan D, Ng LL. Biomarkers in acute myocardial infarction. BMC Med 2010;8:34-35.

23. Chia S, Senatore F, Raffel OC, Lee H, Wackers FJ, Jang IK. Utility of cardiac biomarkers in predicting infarct size, left ventricular function, and clinical outcome after primary percutaneous coronary intervention for ST-segment elevation myocardial infarction. JACC Cardiovasc Interv 2008;1:415-23.
24. Reffelmann T, Kloner RA. The “no-reflow” phenomenon: basic science and clinical correlates. Heart 2002;87:162-8.
25. Ndrepepa G, Tiroch K, Fusaro M et al. 5-year prognostic value of no-reflow phenomenon after percutaneous coronary intervention in patients with acute myocardial infarction. J Am Coll Cardiol 2010;55:2383-9.
26. Ndrepepa G, Tiroch K, Keta D et al. Predictive factors and impact of no reflow after primary percutaneous coronary intervention in patients with acute myocardial infarction. Circ Cardiovasc Interv 2010;3:27-33.
27. Jaffe R, Charron T, Puley G, Dick A, Strauss BH. Microvascular obstruction and the no-reflow phenomenon after percutaneous coronary intervention. Circulation 2008;117:3152-6.
28. Betgem RP, de Waard GA, Nijveldt R, Beek AM, Escaned J, van Royen N. Intramyocardial haemorrhage after acute myocardial infarction. Nat Rev Cardiol 2015;12:156-67.
29. Hellstrom HR. Coronary artery stasis after induced myocardial infarction in the dog. Cardiovasc Res 1971;5:371-5.
30. Ito H. No-reflow phenomenon and prognosis in patients with acute myocardial infarction. Nat Clin Pract Cardiovasc Med 2006;3:499-506.
31. Pennell D. Myocardial salvage: retrospection, resolution, and radio waves. Circulation 2006;113:1821-3.
32. Latet SC, Hoymans VY, Van Herck PL, Vrints CJ. The cellular immune system in the post-myocardial infarction repair process. Int J Cardiol 2015;179:240-7.
33. Hofmann U, Frantz S. Role of Lymphocytes in Myocardial Injury, Healing, and Remodeling After Myocardial Infarction. Circ Res 2015;116:354-367.
34. Daskalopoulos EP, Janssen BJ, Blankesteijn WM. Myofibroblasts in the infarct area: concepts and challenges. Microsc Microanal 2012;18:35-49.
35. Laeremans H, Hackeng TM, van Zandvoort MA et al. Blocking of frizzled signaling with a homologous peptide fragment of wnt3a/wnt5a reduces infarct expansion and prevents the development of heart failure after myocardial infarction. Circulation 2011;124:1626-35.
36. Turner NA, Porter KE. Function and fate of myofibroblasts after myocardial infarction. Fibrogenesis Tissue Repair 2013;6:5-15.
37. Daskalopoulos EP, Hermans KC, Blankesteijn WM. Cardiac (myo)fibroblast: Novel strategies for its targeting following myocardial infarction. Curr Pharm Des 2014;20:1987-2002.
38. Frangogiannis NG. The inflammatory response in myocardial injury, repair, and remodelling. Nat Rev Cardiol 2014;11:255-65.
39. Swirski FK. Inflammation and repair in the ischaemic myocardium. Hamostaseologie 2015;35:34-6.
40. Chatelain P, Latour JG, Tran D, de Lorgeril M, Dupras G, Bourassa M. Neutrophil accumulation in experimental myocardial infarcts: relation with extent of injury and effect of reperfusion. Circulation 1987;75:1083-90.
41. Lefer DJ. Do neutrophils contribute to myocardial reperfusion injury? Basic Res Cardiol 2002;97:263-7.
42. Anzai T. Post-infarction inflammation and left ventricular remodeling: a double-edged sword. Circ J 2013;77:580-7.

43. Pfeffer MA, Braunwald E. Ventricular remodeling after myocardial infarction. Experimental observations and clinical implications. Circulation 1990;81:1161-72.
44. Sutton MG, Sharpe N. Left ventricular remodeling after myocardial infarction: pathophysiology and therapy. Circulation 2000;101:2981-8.
45. Braunwald E, Pfeffer MA. Ventricular enlargement and remodeling following acute myocardial infarction: mechanisms and management. Am J Cardiol 1991;68:1D-6D.
46. Braunwald E. Heart failure. JACC Heart Fail 2013;1:1-20.
47. Stewart S, MacIntyre K, Capewell S, McMurray JJ. Heart failure and the aging population: an increasing burden in the 21st century? Heart 2003;89:49-53.
48. Bui AL, Horwich TB, Fonarow GC. Epidemiology and risk profile of heart failure. Nat Rev Cardiol 2011;8:30-41.
49. Mentz RJ, Bakris GL, Waeber B et al. The past, present and future of renin-angiotensin aldosterone system inhibition. Int J Cardiol 2013;167:1677-87.
50. White DC, Hata JA, Shah AS, Glower DD, Lefkowitz RJ, Koch WJ. Preservation of myocardial beta-adrenergic receptor signaling delays the development of heart failure after myocardial infarction. Proc Natl Acad Sci U S A 2000;97:5428-33.
51. Zijlstra F. Primary angioplasty is the most effective treatment for an acute myocardial infarction. Br Heart J 1995;73:403-4.
52. Task Force on the management of STseamiotESoC, Steg PG, James SK et al. ESC Guidelines for the management of acute myocardial infarction in patients presenting with ST-segment elevation. Eur Heart J 2012;33:2569-619.
53. Cerra FB, Lajos TZ, Montes M, Siegel JH. Hemorrhagic infarction: A reperfusion injury following prolonged myocardial ischemic anoxia. Surgery 1975;78:95-104.
54. Hausenloy DJ, Yellon DM. Myocardial ischemia-reperfusion injury: a neglected therapeutic target. J Clin Invest 2013;123:92-100.
55. Garcia-Dorado D, Ruiz-Meana M, Inserte J, Rodriguez-Sinovas A, Piper HM. Calcium-mediated cell death during myocardial reperfusion. Cardiovascular research;94:168-80.
56. Zweier JL, Talukder MA. The role of oxidants and free radicals in reperfusion injury. Cardiovascular research 2006;70:181-90.
57. Hawkins HK, Entman ML, Zhu JY et al. Acute inflammatory reaction after myocardial ischemic injury and reperfusion. Development and use of a neutrophil-specific antibody. The American journal of pathology 1996;148:1957-69.
58. Brown DA, Hale SL, Baines CP et al. Reduction of early reperfusion injury with the mitochondria-targeting peptide bendavia. J Cardiovasc Pharmacol Ther 2014;19:121-32.
59. Kloner RA, Hale SL, Dai W et al. Reduction of ischemia/reperfusion injury with bendavia, a mitochondria-targeting cytoprotective Peptide. Journal of the American Heart Association;1:e001644.
60. Hausenloy DJ, Yellon DM. The therapeutic potential of ischemic conditioning: an update. Nature reviews;8:619-29.
61. Hausenloy DJ, Yellon DM. The therapeutic potential of ischemic conditioning: an update. Nat Rev Cardiol 2011;8:619-29.
62. Vinten-Johansen J, Zhao ZQ, Zatta AJ, Kin H, Halkos ME, Kerendi F. Postconditioning--A new link in nature's armor against myocardial ischemia-reperfusion injury. Basic Res Cardiol 2005;100:295-310.
63. Kloner RA. Current state of clinical translation of cardioprotective agents for acute myocardial infarction. Circ Res 2013;113:451-63.
64. Schmidt MR, Pryds K, Botker HE. Novel adjunctive treatments of myocardial infarction. World J Cardiol 2014;6:434-43.

65. Roubille F, Lacampagne A. New drug avenues for cardioprotection in patients with acute myocardial infarction. Am J Cardiovasc Drugs 2014;14:73-7.
66. Ndrepepa G. Improving myocardial injury, infarct size, and myocardial salvage in the era of primary PCI for STEMI. Coron Artery Dis 2015;26:341-5.
67. Toombs CF, McGee S, Johnston WE, Vinten-Johansen J. Myocardial protective effects of adenosine. Infarct size reduction with pretreatment and continued receptor stimulation during ischemia. Circulation 1992;86:986-94.
68. Lonborg J, Kelbaek H, Vejlstrup N et al. Exenatide reduces final infarct size in patients with ST-segment-elevation myocardial infarction and short-duration of ischemia. Circ Cardiovasc Interv 2012;5:288-95.
69. Lonborg J, Vejlstrup N, Kelbaek H et al. Exenatide reduces reperfusion injury in patients with ST-segment elevation myocardial infarction. Eur Heart J 2012;33:1491-9.
70. Dai W, Shi J, Gupta RC, Sabbah HN, Hale SL, Kloner RA. Bendavia, a mitochondria-targeting peptide, improves post-infarction cardiac function, prevents adverse left ventricular remodeling and restores mitochondria-related gene expression in rats. J Cardiovasc Pharmacol 2014;64:543-53.
71. Niccoli G, Rigattieri S, De Vita MR et al. Open-label, randomized, placebo-controlled evaluation of intracoronary adenosine or nitroprusside after thrombus aspiration during primary percutaneous coronary intervention for the prevention of microvascular obstruction in acute myocardial infarction: the REOPEN-AMI study (Intracoronary Nitroprusside Versus Adenosine in Acute Myocardial Infarction). JACC Cardiovasc Interv 2013;6:580-9.
72. Fokkema ML, Vlaar PJ, Vogelzang M et al. Effect of high-dose intracoronary adenosine administration during primary percutaneous coronary intervention in acute myocardial infarction: a randomized controlled trial. Circ Cardiovasc Interv 2009;2:323-9.
73. Nazir SA, Khan JN, Mahmoud IZ et al. The REFLO-STEMI trial comparing intracoronary adenosine, sodium nitroprusside and standard therapy for the attenuation of infarct size and microvascular obstruction during primary percutaneous coronary intervention: study protocol for a randomised controlled trial. Trials 2014;15:371.
74. Daskalopoulos EP, Hermans KC, Janssen BJ, Matthijs Blankesteijn W. Targeting the Wnt/frizzled signaling pathway after myocardial infarction: a new tool in the therapeutic toolbox? Trends Cardiovasc Med 2013;23:121-7.
75. Daskalopoulos EP, Janssen BJ, Blankesteijn WM. Targeting Wnt signaling to improve wound healing after myocardial infarction. Methods Mol Biol 2013;1037:355-80.
76. Zhao ZQ, Corvera JS, Halkos ME et al. Inhibition of myocardial injury by ischemic postconditioning during reperfusion: comparison with ischemic preconditioning. Am J Physiol Heart Circ Physiol 2003;285:H579-88.
77. Vlaar PJ, Svilaas T, van der Horst IC et al. Cardiac death and reinfarction after 1 year in the Thrombus Aspiration during Percutaneous coronary intervention in Acute myocardial infarction Study (TAPAS): a 1-year follow-up study. Lancet 2008;371:1915-20.
78. Khan AR, Binabdulhak AA, Alastal Y et al. Cardioprotective role of ischemic postconditioning in acute myocardial infarction: A systematic review and meta-analysis. Am Heart J 2014;168:512-521 e4.
79. Kim EK, Hahn JY, Song YB et al. Effect of ischemic postconditioning on myocardial salvage in patients undergoing primary percutaneous coronary intervention for ST-segment elevation myocardial infarction: cardiac magnetic resonance substudy of the POST randomized trial. Int J Cardiovasc Imaging 2015;31:629-37.
80. Yetgin T, Magro M, Manintveld OC et al. Impact of multiple balloon inflations during primary percutaneous coronary intervention on infarct size and long-term clinical outcomes in ST-segment elevation myocardial infarction: real-world postconditioning. Basic Res Cardiol 2014;109:403.
81. Duncker DJ, Klassen CL, Ishibashi Y, Herrlinger SH, Pavek TJ, Bache RJ. Effect of temperature on myocardial infarction in swine. Am J Physiol 1996;270:H1189-99.

82. Hale SL, Herring MJ, Kloner RA. Delayed treatment with hypothermia protects against the no-reflow phenomenon despite failure to reduce infarct size. J Am Heart Assoc 2013;2:e004234.
83. Erlinge D, Gotberg M, Grines C et al. A pooled analysis of the effect of endovascular cooling on infarct size in patients with ST-elevation myocardial infarction. EuroIntervention 2013;8:1435-40.
84. Vanagt WY, Cornelussen RN, Baynham TC et al. Pacing-induced dyssynchrony during early reperfusion reduces infarct size. J Am Coll Cardiol 2007;49:1813-9.
85. Waltenberger J, Gelissen M, Bekkers SC et al. Clinical pacing post-conditioning during revascularization after AMI. JACC Cardiovasc Imaging 2014;7:620-6.
86. Shinlapawittayatorn K, Chinda K, Palee S et al. Vagus nerve stimulation initiated late during ischemia, but not reperfusion, exerts cardioprotection via amelioration of cardiac mitochondrial dysfunction. Heart Rhythm 2014;11:2278-87.
87. He X, Zhao M, Bi X et al. Novel strategies and underlying protective mechanisms of modulation of vagal activity in cardiovascular diseases. Br J Pharmacol 2014.
88. Orlic D, Kajstura J, Chimenti S et al. Bone marrow cells regenerate infarcted myocardium. Nature 2001;410:701-5.
89. Murry CE, Soonpaa MH, Reinecke H et al. Haematopoietic stem cells do not transdifferentiate into cardiac myocytes in myocardial infarcts. Nature 2004;428:664-8.
90. The Lancet E. Expression of concern: the SCIPIO trial. Lancet 2014;383:1279.
91. Boyle AJ, Schulman SP, Hare JM, Oettgen P. Is stem cell therapy ready for patients? Stem Cell Therapy for Cardiac Repair. Ready for the Next Step. Circulation 2006;114:339-52.
92. Assmus B, Leistner DM, Schachinger V et al. Long-term clinical outcome after intracoronary application of bone marrow-derived mononuclear cells for acute myocardial infarction: migratory capacity of administered cells determines event-free survival. Eur Heart J 2014;35:1275-83.
93. Delewi R, Hirsch A, Tijssen JG et al. Impact of intracoronary bone marrow cell therapy on left ventricular function in the setting of ST-segment elevation myocardial infarction: a collaborative meta-analysis. Eur Heart J 2014;35:989-98.
94. Dimmeler S, Leri A. Aging and disease as modifiers of efficacy of cell therapy. Circ Res 2008;102:1319-30.
95. Dai W, Kloner RA. Bone marrow-derived cell transplantation therapy for myocardial infarction: lessons learned and future questions. Am J Transplant 2011;11:2297-301.
96. Jiang CY, Gui C, He AN et al. Optimal time for mesenchymal stem cell transplantation in rats with myocardial infarction. J Zhejiang Univ Sci B 2008;9:630-7.
97. Sheng CC, Zhou L, Hao J. Current stem cell delivery methods for myocardial repair. Biomed Res Int 2013;2013:547902.
98. Tossios P, Krausgrill B, Schmidt M et al. Role of balloon occlusion for mononuclear bone marrow cell deposition after intracoronary injection in pigs with reperfused myocardial infarction. Eur Heart J 2008;29:1911-21.
99. Moelker AD, Baks T, van den Bos EJ et al. Reduction in infarct size, but no functional improvement after bone marrow cell administration in a porcine model of reperfused myocardial infarction. Eur Heart J 2006;27:3057-64.
100. Penicka M, Widimsky P, Kobylka P, Kozak T, Lang O. Images in cardiovascular medicine. Early tissue distribution of bone marrow mononuclear cells after transcoronary transplantation in a patient with acute myocardial infarction. Circulation 2005;112:e63-5.
101. Hou D, Youssef EA, Brinton TJ et al. Radiolabeled cell distribution after intramyocardial, intracoronary, and interstitial retrograde coronary venous delivery: implications for current clinical trials. Circulation 2005;112:I150-6.

PART

Experimental Approaches to Myocardial Ischemia and Myocardial Infarction

CHAPTER 2

Quantification of myocardial blood flow by adenosine-stress CT perfusion imaging in pigs during various degrees of stenosis correlates well with coronary artery blood flow and fractional flow reserve

*Alexia Rossi
***André Uitterdijk**
Marcel Dijkshoorn
Ernst Klotz
Anoeshka Dharampal
Marcel van Straten
Willem J van der Giessen†
Nico Mollet
Robert-Jan M van Geuns
Gabriel P Krestin
Dirk J Duncker
Pim J de Feyter
Daphne Merkus

*Both authors contributed equally

Eur Heart J Cardiovasc Imaging 2013 Apr;14(4):331-8

ABSTRACT

Aims Only few preliminary experimental studies demonstrated the feasibility of adenosine stress CT myocardial perfusion to calculate absolute myocardial blood flow (MBF), thereby providing information whether a coronary stenosis is flow-limiting. Therefore the aim of our study was to determine whether adenosine stress myocardial perfusion imaging by Dual Source CT (DSCT) enables non-invasive quantification of regional myocardial blood flow (MBF) in an animal model with various degrees of coronary flow reduction.

Methods and Results In seven pigs, a coronary flow probe and an adjustable hydraulic occluder were placed around the left anterior descending coronary artery to monitor the distal coronary artery blood flow (CBF) while several degrees of coronary flow reduction were induced. CT perfusion (CT-MBF) was acquired during adenosine stress with no CBF reduction, an intermediate (15-39%) and a severe (40-95%) CBF reduction. Standards of reference were CBF and fractional flow reserve measurements (FFR). FFR was simultaneously derived from distal coronary artery pressure and aortic pressure measurements. CT-MBF decreased progressively with increasing CBF reduction severity from 2.68 [2.31-2.81] ml/g/min (normal CBF) to 1.96 [1.83-2.33] ml/g/min (intermediate CBF-reduction) and to 1.55 [1.14-2.06] ml/g/min (severe CBF-reduction) (both $p<0.001$). We observed very good correlations between CT-MBF and CBF ($r=0.85$, $p<0.001$) and CT-MBF and FFR ($r=0.85$, $p<0.001$).

Conclusion Adenosine stress DSCT myocardial perfusion imaging allows quantification of regional MBF under various degrees of CBF reduction.

INTRODUCTION

Current guidelines indicate that in patients with stable angina pectoris both anatomy and functional severity of coronary obstructions should be assessed for guiding patient management (1). Optimal medical treatment is preferred in symptomatic patients with no or moderate ischemia, while revascularization is required in symptomatic patients with substantial myocardial ischemia, (2-4) and Percutaneous Coronary Intervention (PCI) is recommended for lesions with impaired Fractional Flow Reserve (FFR) in patients with multi-vessel disease (5-8).

Coronary CT Angiography (CTA) is a well-established, non-invasive imaging modality for detection and ruling-out coronary atherosclerosis (9-11). Coronary CTA cannot, however, accurately predict whether an intermediate lesion is flow-limiting therefore requiring the use of additional functional testing (12,13). Yet, little information is available about the ability to use CT for the quantitative assessment of myocardial blood flow (MBF) at different levels of coronary artery stenosis. Only few preliminary experimental studies demonstrated the feasibility of adenosine stress CT myocardial perfusion to determine absolute MBF, thereby providing information about the functional severity of coronary lesions (2,14,15).

The purpose of our study was two-fold: 1) to quantify regional CT-derived MBF (CT-MBF) at different degrees of coronary flow reduction in a well-established large animal model; 2) to correlate CT-MBF with coronary artery blood flow (CBF), the experimental reference standard, and with FFR, the clinical reference standard.

MATERIALS AND METHODS

Animal preparation

All procedures were conducted in compliance with the “Guide for the Care and Use of Laboratory Animals” (NIH Publication No. 85-23 revised 1996), and with prior approval of the Animal Care Committee of our institution. Nine, 5-6 months old, crossbred Yorkshire X Landrace swine (34.2±3.6kg) were sedated with an intramuscular injection of ketamine (20 mg/kg, Anisane, Raamsdonksveer, The Netherlands), midazolam (1 mg/kg, Actavis, Baarn, The Netherlands) and atropine sulphate (1mg, Pharmachemie, Haarlem, The Netherlands). Anesthesia was induced with an intravenous injection of pentobarbital sodium (15 mg/kg, Faculty of Veterinary Medicine, Utrecht, The Netherlands). Animals were intubated and mechanically ventilated with a mixture of O_2 and N_2 (1:2 v/v) (16). Anesthesia was maintained by intravenous pentobarbital sodium infusion (15mg/kg/h). A left

thoracotomy was performed in the fourth intercostal space and the pericardium was opened. Fluid-filled polyvinylchloride catheters were placed in the aortic arch, for measurement of pressure and for blood gas analysis to maintain blood gases within the physiological range. Catheters were also placed in the pulmonary artery for infusion of drugs and contrast material. Subsequently, the left anterior descending coronary artery (LAD) was dissected free for placement of a flow probe (Transonic Systems Europe B.V., Maastricht, The Netherlands) and a remote controlled silicone hydraulic vascular occluder (Fine Science Tools GmbH, Heidelberg, Germany). In addition, a fluid-filled polyvinylchloride angiocatheter for the measurement of distal coronary pressure and determination of FFR was into the LAD distal to the occluder. Flow probe, occluder and catheters were exteriorized, the chest was closed and anesthetized animals were transported to the CT suite using a mobile ventilator (Carina™, Dräger Medical, Best, The Netherlands).

Experimental and CT imaging protocols

A dual source CT (DSCT) scanner (SOMATOM Definition Flash, Siemens Healthcare, Forchheim, Germany) was used for perfusion imaging. All animals were placed in supine position. First, animals underwent DSCT myocardial perfusion imaging at rest. Subsequently, DSCT myocardial perfusion imaging was performed during maximal vasodilation. Maximal vasodilation was obtained during the infusion of 500 μg/kg/min adenosine (Adenoscan, Sanofi-Aventis Frankfurt, Germany). At this dose, adenosine resulted in marked systemic vasodilation and hypotension. In order to maintain blood pressure, the α_1-adrenoceptor agonist phenylephrine was co-infused (~5μg/kg/min iv, Pharmacy Erasmus MC, Rotterdam, The Netherlands) with adenosine. Since swine lack significant α_1-adrenergic coronary microvascular constrictor responses (17), phenylephrine can be used to oppose the systemic effects of adenosine, while leaving adenosine-induced coronary vasodilation unperturbed (16). Under maximal vasodilation the hydraulic occluder was manually inflated to sequentially obtain at least one intermediate degree of flow-limiting coronary stenosis and at least one severe degree of flow-limiting stenosis. Total occlusion was performed to delineate the LAD perfusion territory. CT perfusion imaging was repeated at each severity level of flow reduction using a novel electrocardiogram (ECG) triggered dynamic scan mode. All scans were performed in cranio-caudal direction during end-expiratory breath-hold obtained by interrupting the mechanical ventilator. The data were acquired at two alternative table positions while the table was moving back and forth (18). Image acquisition was triggered at 200ms after the R-wave. The scan coverage was 73mm resulting from a detector width of 38.4mm and 10% overlap

between both scan ranges. The minimum cycle time for the alternating scan is 950ms. For the range of heart rates in this study we acquired data every second or third heartbeat. Hence volume scan of the total heart was obtained every 2 to 3 seconds. The tube voltage was 100 kV for each X-ray tube and the total tube current-time product was 300mAs/rot. Prior to each scan 36ml of contrast material (Ultravist 370, Bayer Schering Pharma, Berlin, Germany) was injected through a pulmonary artery line at a flow rate of 6mL/s, followed by a saline chaser of 30mL at 6mL/s. Data acquisition started 2 seconds before the contrast medium injection and lasted for 30s. The delay between two consecutive scans was 20 minutes. Depending on the heart rate, the volume CT dose index (CTDIvol) ranged from 115.1 to 168.5 (mean 149.5±80.0) mGy. The corresponding dose length product (DLP) was 844.0 to 1129.0 (mean 1012.2±14.1) mGycm.

During each experiment heart rate, aortic pressure, mean coronary artery pressure and coronary blood flow (CBF) were continuously recorded (Codas, DATAQ) and stored for off-line analysis using a custom written software in MatLab (the Math Works). FFR was calculated as the ratio of distal coronary artery pressure and aortic pressure.

At the end of the experiment, animals were sacrificed with an intravenous overdose of pentobarbital sodium.

Data analysis

All CT images were evaluated by one cardiac radiologist with four years of experience in cardiac imaging (AR). To assess intra- and inter-observer agreement, MBF of the ischemic myocardial territories was measured on 10 randomly chosen CT datasets by two independent observers (AR and AD). One observer (AR), who was blinded to the previous results, measured the datasets twice, separated by at least 12 weeks. Both observers were blinded to all CBF and FFR measurements. CT images were reconstructed with a slice thickness of 3mm and an increment of 1.5mm using a medium-smooth kernel (B30f). The dynamic data were analyzed using commercial software, Volume Perfusion CT Body on a standard workstation (MMWP, Siemens Healthcare, Germany). Reconstruction and post-processing analysis of the CT perfusion images was previously described (14). Briefly, the left ventricular myocardium was segmented manually placing a volume of interest (VOI) and using a combination of a system of blood pool removal and HU thresholding (***Figure 1 - A1 and A2***). Afterwards, the arterial input function was sampled drawing a region of interest (ROI) in the descending aorta at the cranial

and the caudal ends of the two image stacks (***Figure 1B***). The data from both ROIs were then combined into one arterial input function (***Figure 1C***) and time attenuation curves (TAC) were built for each voxel within the VOI. A dedicated parametric deconvolution technique based on a two-compartment model of intra- and extravascular space was applied to fit the TACs (***Figure 2 B1 and B2***). CT-derived MBF (CT-MBF) in ml/100ml/min of each voxel was then calculated using the maximum slope of the fit curves and quantitative three-dimensional color maps representing the MBF distribution in the myocardium were generated (***Figure 2A***). CT myocardial perfusion in ml/g/min was calculated assuming a myocardium specific density of 1.05 g/ml.

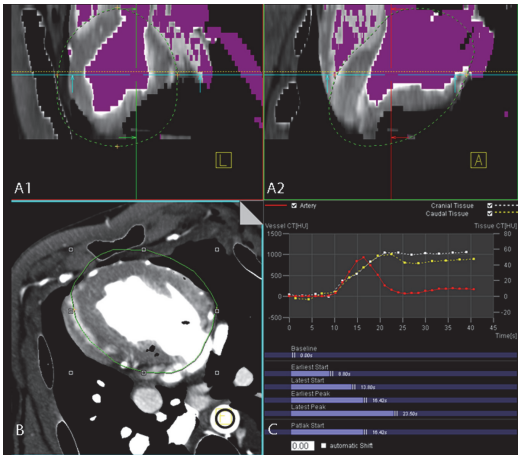

Figure 1. *CT-perfusion imaging post-processing. Screenshot of the post-processing software. Panels A1 and A2 show the segmentation of the left ventricle. The left ventricle myocardium is isolated using in combination a Hounsfield unit based thresholding and a peak enhancement analysis within a volume of interest, VOI (green line). The arterial input function is sampled from two regions of interest placed in the descending aorta of the cranial (panel B) and caudal part of the image stack. One arterial input function is then obtained (red time-attenuation curve, TAC) in panel C combining the information of both ROIs.*

The LAD perfusion territory of each animal was first defined using the color code MBF maps during total occlusion of the LAD. Afterwards a VOI was manually placed in the most representative ischemic area of the LAD territory for each degree of CBF reduction within the same animal. A VOI was manually drawn also in the remote myocardium (inferior wall). CT-MBF was then obtained for both regions.

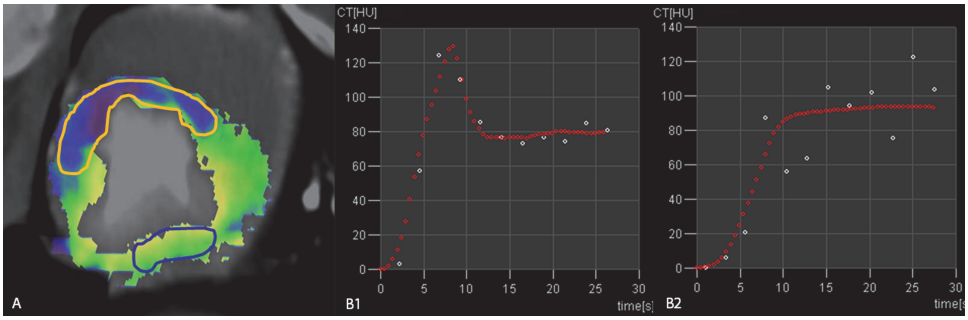

Figure 2. *Ischemic and remote myocardial territory.*
Quantitative three-dimensional color-map representing the distribution of myocardial blood flow (A). During maximal vasodilation the ischemic anterior wall shows reduced perfusion (blue area) whereas the normal myocardium appears greenish (remote myocardium). A dedicated parametric deconvolution technique based on a two compartment model of intra- and extravascular space was used to fit the TACs in a representative normal (B1) and ischemic (B2) myocardium. The white dots are the measured enhancement values. The upslope of the time attenuation curve of the ischemic myocardium is less steep compared to the remote myocardium.

Statistical analysis

Statistical analysis was performed using a dedicated statistical software program (SPSS PASW, version 17.0.2, IMB, Chicago, Illinois, USA). Measurements are presented as median [interquartile range]. All measurements were pooled and afterwards classified in three groups according to CBF: no-CBF reduction, intermediate CBF reduction (range: 15-39%), severe CBF reduction (range: 40-95%). When CBF measurements were not available the classification in different groups was based on FFR measurements. All measurements at rest and during maximal vasodilation were compared using Wilcoxon Signed Rank test. For each degree of coronary flow reduction CT-MBF were compared between the ischemic and remote myocardial territories using Wilcoxon Signed Rank test. CT-MBF, CBF and FFR were compared between different degrees of CBF reduction applying Kruskal-Wallis test for multiple independent samples. Mann-Whitney test was applied for post hoc comparison. Correlation analysis was performed to evaluate the association between CT-MBF and CBF and FFR. Linear regression models were then fitted to asses the value of CT-MBF to predict CBF and FFR. A p-value <0.05 was considered statistically significant.

RESULTS

Two pigs died before CT imaging due to ventricular fibrillation. In 7 animals instrumentation and CT myocardial perfusion imaging were successfully performed, and a total of 32 datasets were obtained. One CT dataset was excluded because of poor image quality. In one pig (4 datapoints), measurements of FFR could not be obtained due to a clot in the coronary artery catheter. Due to probe malfunction (lack of contact between probe and vessel), 11 measurements of CBF could not be obtained. Consequently, a total of 21 CBF measurements, 28 FFR measurements, and 31 CT datasets obtained in 7 swine were analyzed (***Table 1***).

At maximal vasodilation, a homogeneous increase in MBF was observed throughout the entire myocardium (***Figure 3***). At each level of CBF reduction the ischemic region in the LAD territory was clearly visible as defect in the color MBF maps in all 7 animals. Moreover, a progressive increase of the size of the ischemic territory was observed in each animal with increasing the severity of CBF reduction.

Table 1. *Number of datasets included in the analysis*

pigs\datasets	CT	FFR	CBF
CT	7p\31ds	28ds	20ds
FFR	6p	6p\28ds	17ds
CBF	5p	4p	5p\21ds

p: number of pigs, ds: number of datasets

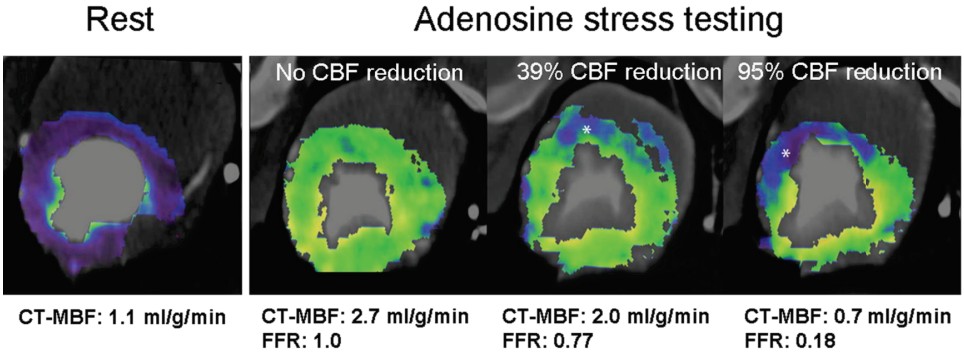

Figure 3. *Response of CT-derived myocardial blood flow (CT-MBF) to different levels of coronary blood flow (CBF) reduction. Example of CT-MBF color maps of the myocardium during maximal vasodilation, intermediate CBF reduction and severe CBF reduction. The ischemic area (*) is well visible in the color-map. A progressive decrease of CT-MBF occurs with increasing severity of CBF reduction.*

Hemodynamic parameters

Despite the infusion of phenylephrine, blood pressure decreased from 95±3 mmHg at baseline to 85±3 mmHg during infusion of adenosine, while heart rate increased from 96±15 to 136±19 beats per minute. Animals showed a slight hemodynamic deterioration with increasing severity of coronary flow reduction as shown by the progressive decrease of aortic pressure *(**Table 2**)*.

Table 2. *Hemodynamic parameters and CBF, FFR, and CT-MBF of ischemic and remote myocardium during different levels of coronary blood flow CBF at the time of CT acquisition. Data are presented as median and interquartile range*

CBF reduction [Range%]	No [0%]	Intermediate [15-39%]	Severe [40-95%]	p-value*
HR (bpm)	136 [117-154]	129 [118-147]	128 [116-143]	0.788
AoP (mmHg)	88 [78-99]	89 [86-94]	82 [74-91]	0.269
Distal CAP (mmHg)	80 [65-91]	73 [66-80]	44 [37-62] †‡	0.002
Distal CBF (ml/min)	148 [135-170]	116 [113-125] †	61 [30-83] †‡	<0.001
FFR	0.90 [0.84-1.00]	0.76 [0.65-0.91]	0.60 [0.51-0.69] †‡	<0.001
CT-MBF- ischemic (ml/g/min)	2.68 [2.31-2.81]	1.96 [1.83-2.33] †	1.55 [1.14-2.06] †ὸ	<0.001
CT-MBF-remote (ml/g/min)	2.76 [2.47-3.65]	2.51 [2.03-3.05]	3.02 [2.79-3.68]	0.162

HR: heart rate; AoP: aortic pressure; CAP: coronary artery pressure; CBF: coronary artery blood flow; FFR: fractional flow reserve; CT-MBF: CT-derived myocardial blood flow. *p-value between CBF reduction groups (Kruskal-Wallis test), †p-value<0.05 vs no CBF reduction (Mann-Whitney test), ‡p-value<0.05 severe vs intermediate CBF reduction (Mann-Whitney test), ὸp-value<0.05 between CT-MBF of the LAD ischemic territory and CT-MBF of the remote myocardium (Wilcoxon Signed-Rank test).

CT-MBF of ischemic and remote myocardium

During normal coronary arterial inflow, maximal vasodilation with adenosine resulted in a 2.8 fold increase of CT-MBF from 0.99 [0.95-1.30] ml/g/min to 2.76 [2.47-3.65] ml/g/min (p=0.001) and a 3.7 fold increase of CBF, from 40 [25-83] ml/min to 149 [135-170] ml/min (p=0.006).

In all swine, CT-MBF of the ischemic territory decreased progressively with increasing severity of stenosis (p<0.001; ***Table 2***). A typical response of CT-MBF to progressive flow reductions is presented in ***Figure 3***. CT-MBF of ischemic myocardial territories was markedly lower than CT-MBF of the remote myocardium (p<0.001) at severe CBF reduction.

CT-MBF correlated strongly with absolute flow measurement represented by CBF during no and various levels of CBF reduction (r= 0.85, p<0.001 ***Figure 4A***). CT-MBF showed a similarly strong correlation with FFR (r=0.85, p<0.001) (***Figure 4B***).

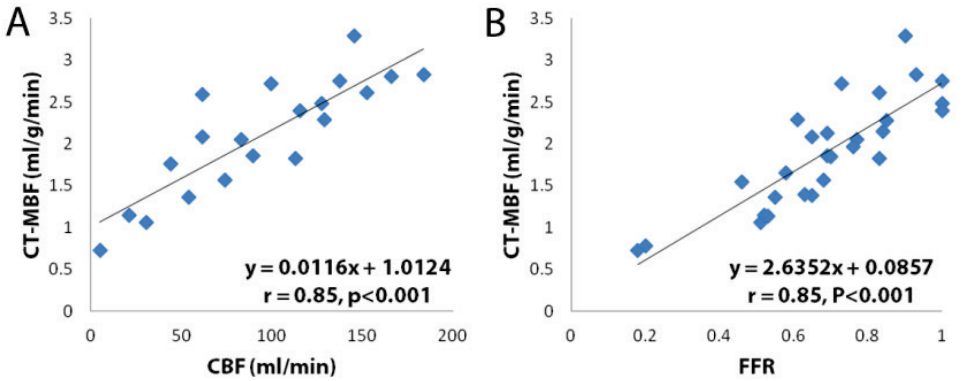

Figure 4. *CT-derived myocardial blood flow (CT-MBF) versus coronary blood flow (CBF) and fractional flow reserve (FFR). Correlation between CT-MBF and (A) CBF measured by the flow probe and (B) FFR.*

Intra- and inter-observer agreement

The mean difference (measure of precision) of CT-MBF was 0.07 ml/g/min with a standard deviation (measure of accuracy) of 0.18 ml/g/min for intra-observer measurements ($r = 0.96$; $p<0.001$). Mean difference (±standard deviation) for inter-observer measurements was 0.10 (± 0.40) ml/g/min ($r = 0.764$; $p=0.006$).

DISCUSSION

The present study assessed the diagnostic accuracy of stress dynamic DSCT quantification of MBF in ischemic and remote myocardium in a large animal model with controlled reduction in CBF under maximal vasodilation (from normal to moderate to severe CBF reduction) compared to the experimental standard of reference, CBF, and the clinical reference standard, FFR measurements. The major finding was that adenosine stress dynamic DSCT perfusion imaging provided regional quantification of MBF of ischemic and remote myocardium under experimental conditions which correlated very well with CBF and FFR .

CT quantification of MBF

Static myocardial perfusion imaging during adenosine stress has been recently investigated in humans and showed a diagnostic accuracy comparable to SPECT to detect significant coronary stenoses (19,20). However, static perfusion imaging provides only qualitative information of the myocardial perfusion by comparing the attenuation of the ischemic area to the attenuation of the remote myocardium. Quantification of myocardial perfusion is possible using dynamic CT scanning and it was already investigated by electron beam CT (EBCT) in the late 1980's. EBCT

was a remarkable technical development with an excellent temporal resolution allowing dynamic perfusion imaging but was limited by a rather small coverage and thick slices. Nevertheless, studies in animal models (21) and healthy humans (22) reported good correlations between EBCT -derived MBF versus microspheres (21) and versus indicator dilution methods (22), respectively. EBCT technology has been replaced by multidetector CT technology and, due to improved temporal resolution and coverage, the latest generation scanners now allow quantitative myocardial perfusion imaging (23).Thus, George et al proved the ability of CT to quantify MBF in an experimental model using 64-multidetector CT.(15) Mahnken et al (14) and Bamberg et al (24) showed the feasibility of a novel ECG-triggered dynamic shuttle-mode scan with data being acquired at two alternating table positions in the quantification of MBF in animal and human studies, respectively. The use of two alternating table positions increased the scan coverage and the presence of two x-ray tubes provided a better temporal resolution as compared to 64-multidetector CT. The main criticism of studies so far has been that CT-MBF underestimates MBF. We observed a higher CT-MBF in the ischemic as well as in the remote myocardium than Mahnken et al (14), and Bamberg et al (24). which can be explained by the higher dose of adenosine in our study (500 mg/kg/min) as compared to Mahnken et al (14) (240 mg/kg/min) and to Bamberg et al (24) (140 mg/kg/min). In conjunction, the use of phenylephrine resulted in a relatively well-maintained aortic blood pressure during adenosine infusion. Additionally, the 6 second contrast bolus was injected directly into the pulmonary artery in our study instead of a 10 seconds bolus into a peripheral ear vein. This yielded a much better defined arterial input function with better tissue discrimination and more accurate modeling. The values of MBF may differ in humans because a peripheral venous access is commonly used for contrast injection.

Comparison of CT-MBF with CBF and FFR

In our study we found an excellent correlation between CT-MBF and the experimental reference standard, CBF, over a wide range of blood flows. In our experimental set-up CBF provided a direct measurement of the blood flow distal to a coronary stenosis caused but direct measurements of CBF are not available in the clinical environment, although coronary blood velocity can be measured using a flow wire. Clinically, FFR was therefore introduced as indirect parameter of myocardial perfusion. FFR has been well-established as an accurate, yet invasive, parameter to assess the functionality of a coronary stenosis independent from heart rate, blood pressure and left ventricular function. In the present study we found a good correlation between CT-MBF and FFR over a wide range of coronary

flow reductions, suggesting that absolute MBF measurements with CT can provide clinically relevant information about stenosis severity. Indeed, Bamberg et al (24). recently showed the feasibility of dynamic CT perfusion imaging for the detection of hemodynamically significant coronary artery stenoses, as defined with FFR, in a human study. These authors found a cut-off point of 75 mL/100mL/min to provide the highest discriminatory power between hemodynamically significant and non-significant coronary artery lesions. This cut-off value needs further validation in different patient populations after a standardized CT protocol developed.

Limitations

Our study has some limitations that are either related to our animal model or are more general limitations of CT technology

Animal model: First, our study was designed as a feasibility study using a relatively small number of animals. Yet, the use of multiple measurements per animal and the well-defined experimental conditions make the results reliable and reproducible as further evidenced by high correlation coefficients between CT-MBF, CBF and FFR. Second, we did not use microspheres as experimental gold standard for in vivo measurement of myocardial blood flow. Bamberg et al provided good correlation between CT-MBF and microsphere-derived myocardial flow in pig model of LAD obstruction using the same CT technology (25). Third, our experimental setup was designed as a single vessel LAD obstruction, therefore our results cannot be extrapolated to multi-vessel coronary artery disease. Nevertheless, we expect that this CT technology will give good results also in the situation of three vessel disease because it provides absolute quantification of regional myocardial blood flows rather than relative flows as obtained in SPECT imaging. Fourth, the pigs (mean weight±standard deviation: 34.2±3.6kg) were relatively small compared to adult humans, which may imply the need to use higher kV and mAs settings during the CT acquisition in humans. However, in a recent study performed in patients Bamberg et al (24) used successfully 100 kV and 300 mAs as we used in pigs.

CT-technology: There are several technical aspects that need further considerations. 1) An important technical limitation is the volume coverage. 64-slice CT scanners used to be limited to a single detector up to 40 mm that was not sufficient to cover the whole heart. Nowadays two alternatives are available: first, a CT system with 320 rows that can cover the whole heart in one gantry rotation (26-28), the second alternative is the shuttle mode acquisition used in our study. Although the acquisition coverage of the shuttle mode technique of 73 mm was sufficient for encompassing the entire heart of the pigs, this coverage

may be not sufficient in humans, even when triggering in the systolic phase, due to the larger size of the human heart. Indeed Bamberg et al found that one third of the scans provided incomplete coverage of the myocardium (24). Thus, further improvements in CT technology should aim in increasing the coverage along the z-axis. 2) We used central venous access for contrast injection, which provided a tighter input function and likely resulted in higher values of myocardial blood flow. These values may not be reproducible in patients because a peripheral venous access is commonly used in the clinical routine. 3) The addition of dynamic perfusion CT imaging to the conventional clinical cardiac CTA protocol will increase the total amount of radiation dose. Optimization of radiation dose reduction protocols should be developed with preservation of image quality. 4) Finally iodinated contrast medium in the left ventricular cavity can negatively affect the assessment of myocardial perfusion. However, this may be circumvented by using beam-hardening artifact correction algorithms to increase the accuracy of CT perfusion imaging in the quantification of myocardial blood flow (29).

Clinical implications and challenges

Our study shows that CT myocardial perfusion imaging can quantitatively measure MBF in experimental animals, and thereby can be used to assess stenosis severity. This observation is supported by a few small sized studies showing that CT myocardial perfusion imaging is also feasible in patients (24,26,30-32). Thus, the addition of CT myocardial perfusion imaging to the standard coronary CTA provides complementary anatomical and functional information in a single, non-invasive examination which may improve patient management. Future improvements in CT technology, aimed at increasing the coverage and reducing the radiation exposure, would facilitate implementation of this non-invasive imaging technique in clinical practice.

CONCLUSIONS

The present study demonstrates that dynamic dual source CT can identify regional reductions of MBF, during pharmacological coronary vasodilation, over a wide range of flow-limiting coronary artery obstruction severities with a good correlation with coronary artery blood flow and fractional flow reserve.

ACKNOWLEDGEMENTS

We would like to dedicate this manuscript to Prof. Wim van der Giessen who sadly passed away in June 2011.

REFERENCES

1. Fox K, Garcia MA, Ardissino D et al. Guidelines on the management of stable angina pectoris: executive summary: The Task Force on the Management of Stable Angina Pectoris of the European Society of Cardiology. Eur Heart J 2006;27:1341-81.
2. Shaw LJ, Berman DS, Maron DJ et al. Optimal medical therapy with or without percutaneous coronary intervention to reduce ischemic burden: results from the Clinical Outcomes Utilizing Revascularization and Aggressive Drug Evaluation (COURAGE) trial nuclear substudy. Circulation 2008;117:1283-91.
3. Hachamovitch R, Hayes SW, Friedman JD, Cohen I, Berman DS. Comparison of the short-term survival benefit associated with revascularization compared with medical therapy in patients with no prior coronary artery disease undergoing stress myocardial perfusion single photon emission computed tomography. Circulation 2003;107:2900-7.
4. Boden WE, O'Rourke RA, Teo KK et al. Optimal medical therapy with or without PCI for stable coronary disease. N Engl J Med 2007;356:1503-16.
5. Legalery P, Schiele F, Seronde MF et al. One-year outcome of patients submitted to routine fractional flow reserve assessment to determine the need for angioplasty. Eur Heart J 2005;26:2623-9.
6. Pijls NH, van Schaardenburgh P, Manoharan G et al. Percutaneous coronary intervention of functionally nonsignificant stenosis: 5-year follow-up of the DEFER Study. J Am Coll Cardiol 2007;49:2105-11.
7. Tonino PA, De Bruyne B, Pijls NH et al. Fractional flow reserve versus angiography for guiding percutaneous coronary intervention. N Engl J Med 2009;360:213-24.
8. Pijls NH, Fearon WF, Tonino PA et al. Fractional flow reserve versus angiography for guiding percutaneous coronary intervention in patients with multivessel coronary artery disease: 2-year follow-up of the FAME (Fractional Flow Reserve Versus Angiography for Multivessel Evaluation) study. J Am Coll Cardiol 2010;56:177-84.
9. Budoff MJ, Dowe D, Jollis JG et al. Diagnostic performance of 64-multidetector row coronary computed tomographic angiography for evaluation of coronary artery stenosis in individuals without known coronary artery disease: results from the prospective multicenter ACCURACY (Assessment by Coronary Computed Tomographic Angiography of Individuals Undergoing Invasive Coronary Angiography) trial. J Am Coll Cardiol 2008;52:1724-32.
10. Meijboom WB, Meijs MF, Schuijf JD et al. Diagnostic accuracy of 64-slice computed tomography coronary angiography: a prospective, multicenter, multivendor study. J Am Coll Cardiol 2008;52:2135-44.
11. Miller JM, Rochitte CE, Dewey M et al. Diagnostic performance of coronary angiography by 64-row CT. N Engl J Med 2008;359:2324-36.
12. Meijboom WB, Van Mieghem CA, van Pelt N et al. Comprehensive assessment of coronary artery stenoses: computed tomography coronary angiography versus conventional coronary angiography and correlation with fractional flow reserve in patients with stable angina. J Am Coll Cardiol 2008;52:636-43.
13. Sarno G, Decraemer I, Vanhoenacker PK et al. On the inappropriateness of noninvasive multidetector computed tomography coronary angiography to trigger coronary revascularization: a comparison with invasive angiography. JACC Cardiovasc Interv 2009;2:550-7.
14. Mahnken AH, Klotz E, Pietsch H et al. Quantitative whole heart stress perfusion CT imaging as noninvasive assessment of hemodynamics in coronary artery stenosis: preliminary animal experience. Invest Radiol 2010;45:298-305.
15. George RT, Jerosch-Herold M, Silva C et al. Quantification of myocardial perfusion using dynamic 64-detector computed tomography. Invest Radiol 2007;42:815-22.

16. Sorop O, Merkus D, de Beer VJ et al. Functional and structural adaptations of coronary microvessels distal to a chronic coronary artery stenosis. Circ Res 2008;102:795-803.
17. Duncker DJ, Stubenitsky R, Verdouw PD. Autonomic control of vasomotion in the porcine coronary circulation during treadmill exercise: evidence for feed-forward beta-adrenergic control. Circ Res 1998;82:1312-22.
18. Bamberg F, Klotz E, Flohr T et al. Dynamic myocardial stress perfusion imaging using fast dual-source CT with alternating table positions: initial experience. Eur Radiol 2010;20:1168-73.
19. Blankstein R, Shturman LD, Rogers IS et al. Adenosine-induced stress myocardial perfusion imaging using dual-source cardiac computed tomography. J Am Coll Cardiol 2009;54:1072-84.
20. Cury RC, Magalhaes TA, Borges AC et al. Dipyridamole stress and rest myocardial perfusion by 64-detector row computed tomography in patients with suspected coronary artery disease. Am J Cardiol 2010;106:310-5.
21. Rumberger JA, Feiring AJ, Lipton MJ, Higgins CB, Ell SR, Marcus ML. Use of ultrafast computed tomography to quantitate regional myocardial perfusion: a preliminary report. J Am Coll Cardiol 1987;9:59-69.
22. Bell MR, Lerman LO, Rumberger JA. Validation of minimally invasive measurement of myocardial perfusion using electron beam computed tomography and application in human volunteers. Heart 1999;81:628-35.
23. Flohr TG, Klotz E, Allmendinger T, Raupach R, Bruder H, Schmidt B. Pushing the envelope: new computed tomography techniques for cardiothoracic imaging. J Thorac Imaging 2010;25:100-11.
24. Bamberg F, Becker A, Schwarz F et al. Detection of Hemodynamically Significant Coronary Artery Stenosis: Incremental Diagnostic Value of Dynamic CT-based Myocardial Perfusion Imaging. Radiology 2011;260:689-98.
25. Bamberg F, Hinkel R, Schwarz F et al. Accuracy of dynamic computed tomography adenosine stress myocardial perfusion imaging in estimating myocardial blood flow at various degrees of coronary artery stenosis using a porcine animal model. Invest Radiol 2012;47:71-7.
26. Ko BS, Cameron JD, Meredith IT et al. Computed tomography stress myocardial perfusion imaging in patients considered for revascularization: a comparison with fractional flow reserve. Eur Heart J 2012;33:67-77..
27. George RT, Arbab-Zadeh A, Cerci RJ et al. Diagnostic performance of combined noninvasive coronary angiography and myocardial perfusion imaging using 320-MDCT: the CT angiography and perfusion methods of the CORE320 multicenter multinational diagnostic study. AJR Am J Roentgenol 2011;197:829-37.
28. George RT, Arbab-Zadeh A, Miller JM et al. Computed tomography myocardial perfusion imaging with 320-row detector computed tomography accurately detects myocardial ischemia in patients with obstructive coronary artery disease. Circ Cardiovasc Imaging 2012;5:333-40.
29. Kitagawa K, George RT, Arbab-Zadeh A, Lima JA, Lardo AC. Characterization and correction of beam-hardening artifacts during dynamic volume CT assessment of myocardial perfusion. Radiology 2010;256:111-8.
30. Bastarrika G, Ramos-Duran L, Rosenblum MA, Kang DK, Rowe GW, Schoepf UJ. Adenosine-stress dynamic myocardial CT perfusion imaging: initial clinical experience. Invest Radiol 2010;45:306-13.
31. Ho KT, Chua KC, Klotz E, Panknin C. Stress and rest dynamic myocardial perfusion imaging by evaluation of complete time-attenuation curves with dual-source CT. JACC Cardiovasc Imaging 2010;3:811-20.
32. George RT, Arbab-Zadeh A, Miller JM et al. Adenosine stress 64- and 256-row detector computed tomography angiography and perfusion imaging: a pilot study evaluating the transmural extent of perfusion abnormalities to predict atherosclerosis causing myocardial ischemia. Circ Cardiovasc Imaging 2009;2:174-82.

CHAPTER 3

Serial measurement of hFABP and high sensitivity Troponin I post PCI in STEMI. How fast and accurate can Myocardial Infarct Size and No-Reflow be predicted?

André Uitterdijk
Stefan Sneep
Richard WB van Duin
Ilona Krabbendam-Peters
Charlotte Gorsse-Bakker
Dirk J Duncker
Willem J van der Giessen†
Heleen MM van Beusekom

Am J Physiol Heart Circ Physiol 2013 305:H1104-10

ABSTRACT

Objective To compare heart specific fatty acid binding protein (hFABP) and high sensitive troponin I (hsTnI) via serial measurements to identify early time points to accurately quantify infarct size and no-reflow in a preclinical swine model of ST-elevated myocardial infarction (STEMI).

Background Myocardial necrosis, usually confirmed by hsTnI or TnT, takes several hours of ischemia before plasma levels rise in absence of reperfusion. We evaluated the fast marker hFABP in comparison to hsTnI to estimate infarct size and no-reflow upon reperfused and non-reperfused STEMI in swine.

Methods In STEMI (n=4) and STEMI+reperfusion (n=8) induced in swine, serial blood samples were taken for hFABP and hsTnI and compared to triphenyl tetrazolium chloride and thioflavin-S staining for infarct size and no-reflow at sacrifice.

Results hFABP increased faster than hsTnI upon occlusion (82±29 vs. 180±73 min, $p<0.05$) and increased immediately upon reperfusion while hsTnI release was delayed 16±3 min ($p<0.05$). Peak hFABP and hsTnI reperfusion values were reached 30±5 and 139±21 min. respectively ($p<0.05$). Infarct size (containing 84±0.6% no-reflow) correlated well with area under the curve for hFABP ($r^2=0.92$) but not hsTnI ($r^2=0.53$). At 50 and 60 minutes reperfusion, hFABP correlated best with infarct size ($r^2=0.94$ and 0.93) and no-reflow ($r^2=0.96$ and 0.94) and showed high sensitivity for myocardial necrosis (2.3±0.6 and 0.4±0.6 gram)

Conclusions hFABP rises faster and correlates better with infarct size and no-reflow than hsTnI in STEMI+reperfusion when measured early after reperfusion. The highest sensitivity detecting myocardial necrosis, 0.4±0.6 gram at 60 minutes post reperfusion, provides an accurate and early measurement of infarct size and no-reflow.

INTRODUCTION

For the assessment of novel therapies to treat acute ST-elevated myocardial infarction (STEMI), it is of great importance that at baseline, infarct size and no-reflow are determined precisely to be able to validate, tailor or adjust experimental therapies. The efficacy of treatment for STEMI in (pre)clinical studies can only be accurately determined if the outcome can be compared to initial infarct size and subsequent area of no-reflow. Contemporary imaging modalities for determination of these parameters such as cardiac magnetic resonance imaging or echocardiography are often unsuitable for this purpose because of practical, temporal, resolutional or economic considerations. These imaging modalities are also inadequate to assess relatively small infarct sizes (1). Furthermore, it is unclear whether the development of acute edema, often used to determine the area at risk, interferes with acute assessment of these parameters (2).

Standard, fast detectable markers such as creatin-kinase and myoglobin may be regarded as considerably unspecific. Myoglobin for example, the faster marker, with peak values at 12 hours after onset of infarction and at 1 to 2 hours after onset of reperfusion in patients (3), is not cardiac specific and is also prevalent in skeletal muscle tissue. Baseline values are especially high in a setting of soft tissue trauma or extreme exercise (4,5). Creatin-kinase MB (CKMB), specific for heart and brain, and the cardiospecific troponins are of great predictive value for presence of myocardial necrosis but are bound to the contractile apparatus and therefore released relatively slow. As a consequence of slow troponin clearance, late (72 hr) assessment is very accurate but by its nature does not allow early detection of efficacy in acute interventions (6). Both CKMB and Troponin T show peak values following reperfusion between 7 and 8 hours (7). This disqualifies troponins and CKMB both as early and acute markers for infarct size determination. Consequently, a heart specific, early released and accurately detectable marker for an early estimation of infarct size and no-reflow is needed (8,9).

Such a candidate could be heart specific fatty acid binding protein (hFABP) which is a small (15kDa) protein and is located in the cytoplasm (10). hFABP is a heart specific isoform of a larger family of FABP members and ten times more specific for cardiac tissue than myoglobin (11). In view of its small size and cytoplasmic localization, an early, diffusion driven, and perfusion facilitated release pattern is expected. However, the performance of hFABP as a biomarker of necrosis has not been explored in a large animal model of STEMI. Consequently, to determine whether this rediscovered marker is suitable for the determination of infarct size

upon reperfusion, we compared timing and release of hFABP to the gold standard hsTnI (24kDa) following STEMI (sustained and reperfused) in swine using planimetrical infarct size determination by triphenyl tetrazolium chloride (TTC). In addition, we aimed to understand the release of these biomarkers in relation to no-reflow which was determined by thioflavin-S staining.

METHODS

Experiments were performed in 5-6 month old farmbred swine (38±1 kg, n=14) of either sex as described before (12). Experiments were conducted in compliance with the "Guide for the Care and use of Laboratory Animals" and after written approval of the Animal ethics Committee of the Erasmus MC. In short, animals were sedated with an intramuscular injection of midazolam (1 mg/kg, Actavis, Baarn, The Netherlands) and ketamine (20 mg/kg, Anisane, Raamsdonksveer, The Netherlands). Following an intravenous ear catheter placement, anaesthesia was induced with an intravenous injection of 600 mg pentobarbital. Animals were intubated and mechanically ventilated (O_2:N_2 = 1:3). Anesthesia was maintained with pentobarbital (15 mg/kg/h). Physiological temperature was continuously measured and when necessary adjusted with heating pads (12). Fluid loss was compensated for by an intravenous drip (100 ml/h saline). After the placement of an intra-arterial sheath (9F, Super Sheath®, Boston Scientific, Nieuwegein, The Netherlands) 10.000 units of heparin and 250mg acetylsalicylic acid (Aspégic®, Sanofi Aventis, Gouda, The Netherlands) were administered for anticoagulation followed by 5.000 units of heparin every additional hour.

STEMI model and blood sampling

The left circumflex coronary artery (LCx) was catheterized with a standard clinical guiding catheter (JL3.5, Boston Scientific) and quantitative coronary angiography (CAAS II, PIE Medical, Maastricht, the Netherlands) was performed following 1 mg isosorbidedinitrate (Cedocard®, Nycomed, Hoofddorp, The Netherlands) and using iodixanol as a contrast agent (Visipaque™, GE Healthcare BV, Eindhoven, The Netherlands). Then, an over the wire coronary angioplasty balloon (Apex™ PTCA Dilatation Catheter, Boston Scientific) on a standard guide wire (Luge™, 0.37 mm x 128 cm, moderate support, Boston Scientific) was carefully positioned under fluoroscopic guidance to create a broad range of infarct sizes. Following balloon inflation, occlusion of the target vessel was confirmed by angiography at baseline and every subsequent hour.In the sustained occlusion group (n=4), the occlusion was maintained for 8 hours without reperfusion. In the STEMI+reperfusion group (n=10, for a range in infarct size) the occlusion was released after 2 hours,

followed by 6 hours of reperfusion. A minimum of 2 hours of occlusion was chosen to ascertain a transmural infarction that corresponds with the plateau phase of infarct development in swine (13).

Blood samples (BD Vacutainer®, 10.8 mg K2E, Becton Dickinson, Breda, The Netherlands) were immediately put on ice prior to centrifugation and plasma was stored (-80º C) for later marker analyses. Blood samples were collected at baseline and every 30 min. during occlusion, every 10 min. upon the first hour of reperfusion followed by every 30 min. during the remaining hours.

Determination of Risk Area, Infarct Size and No-Reflow

After finalizing blood sampling, a sternotomy was performed and the balloon was reinflated to re-occlude the LCx artery. In the STEMI+reperfusion group, 10 ml 4% (w/v) thioflavin-S solution (Sigma, Zwijndrecht, The Netherlands) was slowly and manually injected intracoronary through the lumen of the balloon catheter to visualize no-reflow within the area at risk. Next, in both groups a bolus of 20 ml of a 15% (w/v) Evans Blue solution was injected into the left atrium for negative staining of the area at risk. Animals were euthanized with an overdose of pentobarbital and the heart was immediately excised. The left ventricle was isolated and sectioned into 5 transversal slices. Using UV light, regions of no-reflow were quantified in all sections as described (14). Cardiac slices were subsequently incubated in a 3% solution (w/v) of the redox indicator TTC at 37 °C for 15 min. to discriminate between metabolically active and dead myocardium to macroscopically assess infarct size as described before (12,15). Correcting for slice weight, total left ventricular infarct size and no-reflow in grams were calculated.

Biomarker analysis

All blood samples were kept on ice immediately after withdrawal and were centrifuged for 10 minutes at 1460g and 4°C within 4 hours. Plasma was aliquoted and cryopreserved at -80°C until analysis within 6 months after storage (16,17). Then, quickly thawed plasma samples were diluted (2-64x) using the standard diluent provided with the kit, and analyzed by enzyme-linked immunosorbent assays according to manufacturer's instructions for porcine hFABP and porcine hsTnI (plasma kits, Life Diagnostics, West Chester, PA, USA). Absorbance was measured at 450 nm with a microplate photometer (Multiskan EX, Thermo Scientific, Etten-Leur, The Netherlands) and converted to concentration via the standard (calibration) curve. Samples diluted such as to be in the linear range of the calibration curve, were used for further analyses.

Statistical analysis

All data are given as mean ± SEM. Data were analyzed with Sigmastat (version 2.03.0, SPSS Inc., USA). Differences in timing of release were assessed using ANOVA on ranks followed by a post-hoc Student-Newman-Keuls test when appropriate. Statistical significance was accepted when $p<0.05$ (two-tailed). AUC, regression lines and intercepts were calculated using Graphpad Prism (version 4.03, Graphpad Software Inc., USA).

RESULTS

Peri-procedural complications and hemodynamics

A total of 14 animals were included in the study, 4 in the chronic occlusion group and 10 in the reperfusion group. In the latter, one animal died due to ventricular fibrillation and one animal was excluded due to unreliable preparation (unexplained and uncontrolled ischemic injury outside the area at risk).

Peri-procedural hemodynamics (Table 1) show a moderate increase in average heart rate the first 2 hours of occlusion (67±6 to 79±3 bpm, $p<0.05$). Where in the 8 hour occlusion group the heart rate continued to rise (+24±1 bpm, $p<0.01$), the rise in heart rate was larger in reperfused animals (+63±11 bpm, $p<0.05$). These values however, remained near normal for awake swine of this size and therefore thought not to affect wash-out of the markers due to changes in coronary perfusion patterns. MAP slightly decreased during 2 hours occlusion (78±7 to 72±4 mmHg, p=N.S.) and decreased further in both groups (-15±4 vs. -11±3 ($p<0.05$) mmHg).

Table 1. *Peri-procedural hemodynamics.*

		BL	CAO		Δ from 2h CAO	
			1h	2h	4h	8h
HR (bpm)	8hr CAO	67 ± 6	68 ± 3	79 ± 3	18 ± 6	24 ± 1
	2hr CAO				38 ± 12	63 ± 11
MAP (mmHg)	8hr CAO	78 ± 7	68 ± 4	72 ± 4	-6 ± 13	-15 ± 4
	2hr CAO				-1 ± 4	-11 ± 3

Hemodynamic monitoring during sustained occlusion (8h CAO, n=4) and during 2h occlusion and 6h reperfusion (2h CAO, n=8). Data are expressed as mean ± SEM. HR = heart rate; MAP = mean arterial pressure; CAO = coronary artery occlusion; BL = baseline. *P<0.05 vs. corresponding 2h CAO time point; **P<0.10 vs. corresponding 2h CAO time point, †P<0.05 vs. change in 8h CAO group.

Risk Area, Infarct size and no-reflow by Evans-Blue, TTC and Thioflavin S

The different infarct sizes, created by inflating the balloon at different locations along the coronary tree, resulted in a risk area of 8.3±1.3 gram (7.6-15.5% of LV) and 19.4±3.4 gram (12.2-43.3% of LV) in the chronic occlusion and reperfusion group respectively. Weight of the infarcted tissue varied from 7.9±3.9 gram (7.3-15.5% of LV) and 14.9±3.6 gram (4.6-39.4% of LV) in the chronic occlusion and reperfusion group respectively. Linear regression showed that infarct size as a ratio of area at risk was similar for the two groups with a slope of 0.94±0.09 (r^2=0.98) and 1.06±0.12 (r^2=0.94) respectively.

Correlation between No-Reflow and Infarct Size

A very tight correlation was found between no-reflow and infarct size (figure 1, r^2=0.97) suggesting that no-reflow is dictated by infarct size. This duration of ischemia, chosen to reflect the maximum development of no-reflow as determined in rabbits (14), showed that approximately 84±0.06% of the infarct size contained no-reflow, regardless of infarct size when larger than approximately 1.55 gram. Only with small infarcts will no-reflow be negligible or fall below detectable levels with the demonstrated techniques.

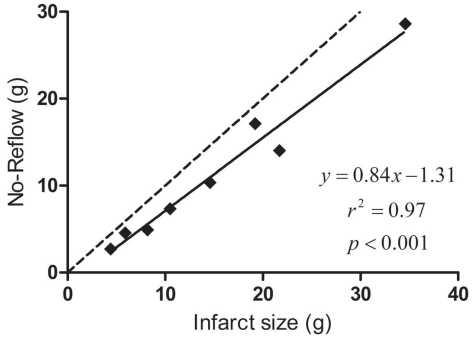

Figure 1. *Infarct size vs. no-reflow in reperfused STEMI*
Infarct size and no-reflow show a high and linear correlation with an r^2 of 97%. The x-intercept of 1.55g indicates that below this threshold no-reflow is negligible under the chosen circumstances. Dotted line is the line of identity.

Marker release during sustained occlusion

hFABP increased significantly faster than hsTnI upon occlusion in all animals with sustained 8 hour occlusions (82±29 vs. 180±73 min, p<0.05) but peak values were

not reached within the course of the experiment (Figure 2, panel A). Area under curve (AUC) for hFABP and hsTnI (76.2±14.2 and 10±3.1, p<0.004, corrected for baseline values of 6±1, 0.3±0.1 resp.) showed a moderate correlation (r^2=0.57 vs. r^2=0.34) with infarct size (11±2% of LV) produced by the 8 hour sustained occlusions.

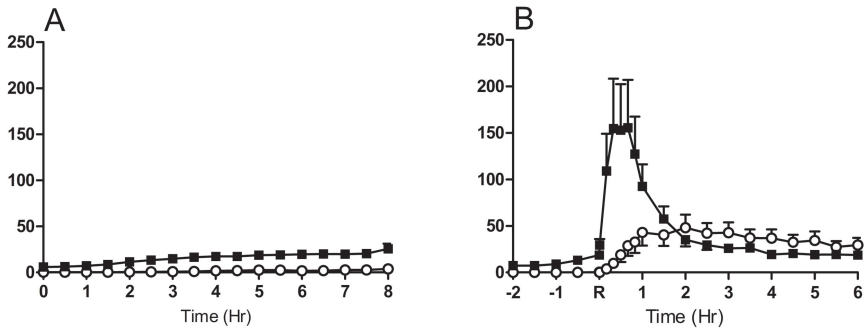

Figure 2. *Biomarker release patterns during sustained and reperfused STEMI*
Caption: Biomarker release patterns of hFABP (■) and hsTnI (○) in non-reperfused (sustained occlusion) STEMI (n=4, panel A) and reperfused STEMI (n=8, panel B, R=reperfusion), data are expressed as mean ± SEM. The graph shows how reperfusion (B) results in the acute release of biomarkers and illustrates the difference between the two markers.

Marker release upon reperfusion: Infarct Size

Reperfusion after two hours of ischemia resulted in an immediate increase in hFABP while hsTnI release was only apparent after 16±3 min (Figure 2, panel B, p<0.05). hFABP and hsTnI peak values were reached in 30±5 min. and 139±21 min (p<0.05), respectively. Infarct size by TTC correlated very well with 8 hour AUC for hFABP (Figure 3, panel A, r^2=0.91) but only moderately for hsTnI (Figure 3, r^2=0.51). Reperfusion peak values showed an equally good correlation with infarct size for hFABP (Figure 3, panel C, r^2=0.92) and a similarly moderate correlation for hsTnI (r^2=0.56). The highest correlation was found at 50 minutes post reperfusion (r^2=0.94) with hFABP.

Marker release upon reperfusion: No-Reflow

No-reflow correlated well with hFABP AUC (figure 3, panel B, r^2=0.94) but again only moderately with hsTnI (figure 3, panel B, r^2=0.48). Reperfusion peak values of hFABP also correlated well (figure 3, panel D, r^2=0.91) and again hsTnI performed poorly (r^2=0.48). The highest correlation with no-reflow was found at 50 minutes post reperfusion (r^2=0.96) with hFABP.

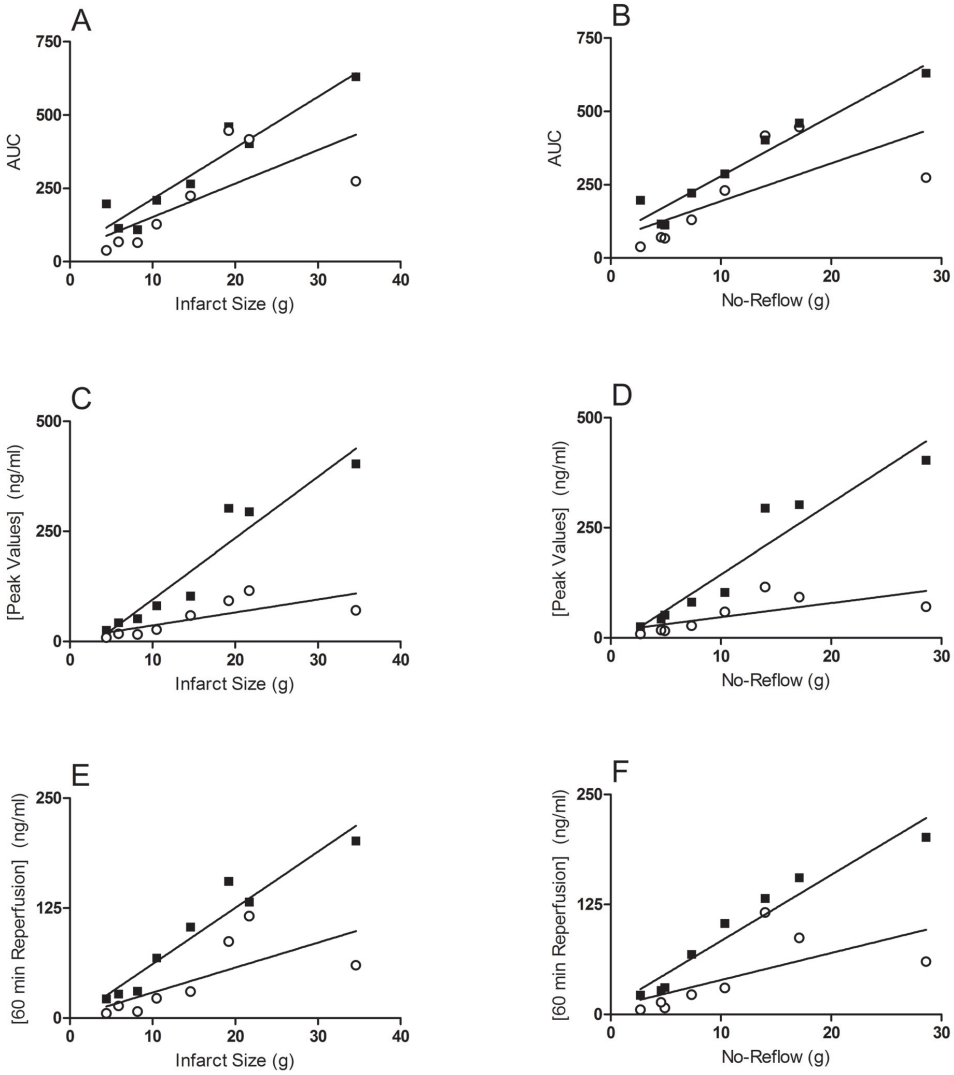

Figure 3. *Correlation of the Area Under Curve and reperfusion values to infarct size and no-reflow in reperfused STEMI*

The relation between release of hFABP (■) and hsTnI (○) with infarct size (A, C) and no-reflow (B, D) as determined by the area under curve (AUC), reperfusion peak values and values at 60 min. post reperfusion in reperfused STEMI (n=8). No-reflow correlated well with hFABP AUC (B, r^2=0.94) but only moderately with hsTnI (B, r^2 =0.48). Reperfusion peak values of hFABP again correlated well with no-reflow (D, r^2=0.91) and again hsTnI performed poorly (D, r^2=0.48). At 60 min. post reperfusion, the correlation was optimal for detecting myocardial necrosis (<0.4±0.6 gram) (E, r^2=0.93) and no-reflow (F, r^2=0.94).

Optimal timepoints and lower levels of detection for myocardial necrosis and no-reflow

We examined which time points correlated best with infarct size and no-reflow by plotting the coefficients of determination of all time points analyzed before reperfusion and of those time points in which an average discernable marker elevation was apparent (Figure 4). HsTnI did not show any strong correlations with a maximum of r^2=0.59 at 120 min. post reperfusion and continued fluctuating with a lower limit of r^2=0.40 at 210 min. within the chosen timeframe.

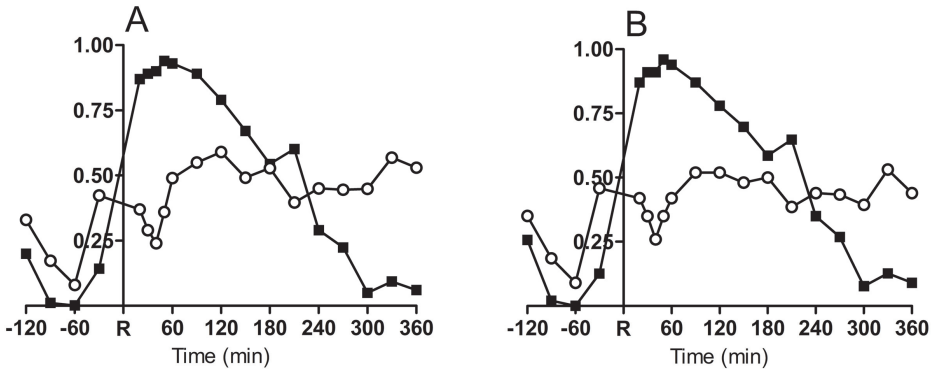

Figure 4. *Temporal changes in coefficients of determination for circulating biomarkers vs. infarct size and no-reflow*
Temporal changes in coefficients of determination (i.e. r^2) for the circulating plasma concentrations of hFABP (■) and hsTnI (○) for infarct size (A) and no-reflow (B). Data show a window of opportunity between 20 and 90 minutes of reperfusion. The major consideration for choosing an optimal timepoint is the sensitivity to detect small myocardial infarctions. R=onset of reperfusion.

Correlation for hFABP remained high and was best at 50 and 60 min. post reperfusion for both infarct size as well as no-reflow (r^2=0.94 and 0.93; r^2=0.96 and 0.94, (figure 3E, F)). In addition, the first 90 min. post reperfusion continuously produced useful correlations with regard to hFABP levels (infarct size: r^2=0.87-0.94; no-reflow: r^2=0.87-0.96). The major consideration for choosing the 50 or 60 min. timepoint is the sensitivity to detect small myocardial infarctions (2.3±0.6 and 0.4±0.6 gram (2.7 and 0.5% of LV)) and no-reflow (0.6 gram (4% of infarct size)) by determining the x-intercept at y=0.

DISCUSSION

The aim of the present study was to determine the value of hFABP for in vivo assessment of infarct size and no-reflow in a large animal model of reperfused STEMI. We found that hFABP rose within 60 minutes after onset of occlusion and, upon reperfusion, showed an immediate and steep incline. We observed a strong correlation between infarct size and hFABP reperfusion peak values (r^2=0.92) at 30±5 minutes of reperfusion. While a good correlation can be found as early as 10 minutes post reperfusion (r^2=0.88) the sensitivity to detect small amounts of myocardial necrosis is low (4.6±0.8) gram. An optimal correlation with infarct size was found at 50-60 minutes post reperfusion (r^2=0.94-0.96) allowing detection of 2.3±0.6 and 0.4±0.6 gram of necrotic myocardium.

No-reflow, as quantified by absence of thioflavin S, correlated excellently with infarct size (r^2=0.97). Consequently, the correlation of hFABP with no-reflow was equally good with AUC (r^2=0.94) and reperfusion peak values (r^2=0.91), but best at 50-60 minutes reperfusion (r^2=0.96-0.94). Lower limit detection of no-reflow was calculated to be <0.6 gram.

HsTnI performed consistently worse than hFABP and peak values were obtained significantly later ($p<0.005$).

Release patterns of cardiac markers following injury

The delayed release of biomarkers in sustained occlusion is due to the fact that release is diffusion driven and perfusion facilitated. The cytosolic localization of hFABP and subsequent fast release is reflected in the significantly faster release as compared to hsTnI ($p<0.05$).

hFABP, a small cytosolic protein, is easily released from injured and permeabilised cardiomyocytes. In contrast, cardiac troponins are bound to the contractile apparatus which significantly delays release (18). Indeed our results show significant differences in release of hFABP and hsTnI, both in terms of onset of release and time to peak.

No-reflow upon reperfusion is characterized by microvascular obstruction, microvascular damage and mechanical compression by myocyte oedema (19) and could theoretically affect the release of markers due to decreased perfusion. However, the fast release of hFABP, which takes place predominantly before the major onset of no-reflow (>30 min post reperfusion (20)), qualifies hFABP as

an appropriate marker for baseline infarct size determination, regardless of the development of no-reflow.

Our study showed a strict correlation between infarct size and the extent of no-reflow with 84% of the infarction showing no-reflow. Hence the relation between biomarker release was equally strong for infarct size and no-reflow. Interestingly, no-reflow is increasingly being appreciated as important prognosticator for long-term outcome and was recently suggested to be, at least in part, independent of myocardial necrosis thus questioning the well-established concept that no-reflow is dictated by infarct size (21,22). Future studies using interventions to affect no-reflow independently of its effects on necrosis can shed light on the influence of no-reflow on washout kinetics of hFABP.

Since hFABP is washed out fast by renal clearance, this is responsible for the differences in the plasma elimination rates as cardiac troponins are known to remain elevated for longer periods of time (6,23). It indicates the need for proper timing when sampling hFABP and indicates why hsTnI is more sensitive as a late marker for ischemia when hFABP is no longer detectable.

Sensitivity of hFABP for infarct size and no-reflow

Our data are the first to describe the precise “rise and fall” of circulating plasma levels of hFABP upon reperfusion of STEMI in a large animal model. Previously, only a single time point was measured in swine at 2 hours post reperfusion (24). We performed the same analysis and found a good correlation with infarct size (r^2=0.78) but this resulted in a lower sensitivity to detect small infarctions (lower level of detection 5.6g). In comparison, peak and 50-60 minutes post reperfusion values show a calculated lower level of detection of 3.1, 2.3 and 0.4g necrotic myocardial tissue which on average corresponds with 3.6, 2.7 and 0.5% of the LV. Therefore, these values are not only obtained faster but result in a higher sensitivity to detect necrosis and no-reflow.

Infarct size, and to an increasing extend no-reflow, are the main determinants of LV remodeling. When therapy is started within 24h a reliable assessment of infarct size and no reflow is mandatory for assessment of therapeutic efficacy, especially in small treatment groups. Both contemporary imaging modalities as well as enzyme or biomarker release studies remain inadequate, non-economic or impractical for acute assessment of these endpoints and (7) more noise reduces their sensitivity. Here, we demonstrate that hFABP AUC, hFABP peak values and

primarily 50-60 minutes post reperfusion biomarker levels correlate very well with acute infarct size and no-reflow in reperfused STEMI. Although high sensitivity troponin assays continue to improve (25), hFABP is of great value for settings where onset of reperfusion is closely controlled. Especially for longitudinal studies aiming to employ long-term follow-up, this relatively easy and fast sampling method allows both an accurate in vivo infarct size and no-reflow quantification method without the need for additional imaging modalities early after infarction.

Clinical relevance

hFABP can be of added clinical value, especially in a multimarker approach (26-30) but contradictory evidence exists (31-33). This may stem from difficulties in estimating the time from onset of ischemia to presentation, as well as variations in onset of spontaneous reperfusion and presence of retrograde flow. In combination with rapid renal clearance, hFABP in this setting, is difficult to interpret without this awareness (32). It does not disqualify hFABP as a useful marker for infarct size or no-reflow determination, especially in the setting of post-PCI reperfusion in STEMI. In absence of spontaneous reperfusion for example, hFABP will yield an accurate and early determination of infarct size. Data can be obtained in the lab prior to opportunities such as MRI for determination of these prognostic parameters, especially with the recent development of fast (15-20 min) qualitative point-of-care tests (34). Moreover, no-reflow is increasingly being appreciated for its great additional prognostic value and hFABP was shown efficacious in long-term prediction (35,36). In the clinical setting, the timing is of crucial importance and must be taken into account when studying the relevance of this marker.It must be noted that while hFABP remains of interest for clinical application, the current study principally demonstrates the suitability of serial hFABP measurement for pre-clinical purposes.

Study limitations

The range of infarct sizes tested in this study was limited to 4.6 to 39.4% of the LV. The predictive value of hFABP for infarct size or no-reflow determination in smaller or larger infarcts therefore remains to be determined, but the lower limit of detection is expected to be <1g of myocardial tissue in animals of 38±1 kg. An important limitation of the work is the limited follow-up time of 6 hours post reperfusion as it is apparent that troponins continue to rise for 72 hours (6). The data presented here, should therefore be interpreted in light of the very early phase post reperfusion, taking into account that the study was designed for hFABP validation for baseline infarct size determination in an acute, preclinical setting.

CONCLUSIONS

HFABP release shows an early and distinct release pattern, correlates strongly to infarct size and no-reflow and is detectable significantly earlier than hsTnI.
hFABP plasma levels at 50-60 minutes post reperfusion, provide an excellent, sensitive, accurate and early biomarker to assess infarct size and no-reflow for longitudinal preclinical infarct-reperfusion studies and holds promise for clinical applications such as the controlled post-PCI setting.

ACKNOWLEDGEMENTS

This study is dedicated to our beloved friend and colleague WJvdG, deceased.

REFERENCES

1. Giannitsis E, Steen H, Kurz K et al. Cardiac magnetic resonance imaging study for quantification of infarct size comparing directly serial versus single time-point measurements of cardiac troponin T. J Am Coll Cardiol 2008;51:307-14.
2. Arai AE. Magnetic resonance imaging for area at risk, myocardial infarction, and myocardial salvage. Journal of cardiovascular pharmacology and therapeutics;16:313-20.
3. Ellis AK, Little T, Zaki Masud AR, Klocke FJ. Patterns of myoglobin release after reperfusion of injured myocardium. Circulation 1985;72:639-47.
4. Kahn P, Aldor E. [Serum myoglobin and myocardial infarction (author's transl)]. Wien Klin Wochenschr 1980;92:538-40.
5. Delanghe JR, De Buyzere ML, Cluyse LP, Thierens HM, Clement DL. Acute myocardial infarction size and myoglobin release into serum. Eur J Clin Chem Clin Biochem 1992;30:823-30.
6. Chia S, Senatore F, Raffel OC, Lee H, Wackers FJ, Jang IK. Utility of cardiac biomarkers in predicting infarct size, left ventricular function, and clinical outcome after primary percutaneous coronary intervention for ST-segment elevation myocardial infarction. JACC Cardiovasc Interv 2008;1:415-23.
7. Hedstrom E, Astrom-Olsson K, Ohlin H et al. Peak CKMB and cTnT accurately estimates myocardial infarct size after reperfusion. Scand Cardiovasc J 2007;41:44-50.
8. Katus HA, Giannitsis E. Who is David and who is Goliath? There is an urgent need to improve the reference standards for estimation of myocardial infarct size. Jacc;4:534-6.
9. Dekker MS, Mosterd A, van 't Hof AW, Hoes AW. Novel biochemical markers in suspected acute coronary syndrome: systematic review and critical appraisal. Heart (British Cardiac Society);96:1001-10.
10. Glatz JF, van Bilsen M, Paulussen RJ, Veerkamp JH, van der Vusse GJ, Reneman RS. Release of fatty acid-binding protein from isolated rat heart subjected to ischemia and reperfusion or to the calcium paradox. Biochim Biophys Acta 1988;961:148-52.
11. Pelsers MM, Hermens WT, Glatz JF. Fatty acid-binding proteins as plasma markers of tissue injury. Clin Chim Acta 2005;352:15-35.
12. Duncker DJ, Klassen CL, Ishibashi Y, Herrlinger SH, Pavek TJ, Bache RJ. Effect of temperature on myocardial infarction in swine. Am J Physiol 1996;270:H1189-99.
13. Klein HH, Schubothe M, Nebendahl K, Kreuzer H. Temporal and spatial development of infarcts in porcine hearts. Basic Res Cardiol 1984;79:440-7.
14. Hale SL, Dae MW, Kloner RA. Hypothermia during reperfusion limits 'no-reflow' injury in a rabbit model of acute myocardial infarction. Cardiovasc Res 2003;59:715-22.
15. Hale SL, Kloner RA. Cardioprotection with adenosine-regulating agent, GP531: effects on no-reflow, infarct size, and blood flow following ischemia/ reperfusion in the rabbit. Journal of cardiovascular pharmacology and therapeutics;15:60-7.
16. van den Besselaar AM, Witteveen E, van der Meer FJ. Long-term stability of frozen pooled plasmas stored at -70 degrees C, -40 degrees C, and -20 degrees C for prothrombin time and International Normalized Ratio (INR) assessment. Thromb Res 2013;131:349-51.
17. Gillis JM, Dunselman P, Jarausch J, de Jong N, Cobbaert CM. Preanalytical storage does not affect 99th percentile cardiac troponin T concentrations measured with a high-sensitivity assay. Clin Chem 2013;59:442-3.
18. Takeda S, Yamashita A, Maeda K, Maeda Y. Structure of the core domain of human cardiac troponin in the Ca(2+)-saturated form. Nature 2003;424:35-41.
19. Vrints CJ. Pathophysiology of the no-reflow phenomenon. Acute Card Care 2009;11:69-76.
20. Reffelmann T, Kloner RA. Microvascular reperfusion injury: rapid expansion of anatomic no reflow during reperfusion in the rabbit. Am J Physiol Heart Circ Physiol 2002;283:H1099-107.

21. Ndrepepa G, Tiroch K, Fusaro M et al. 5-year prognostic value of no-reflow phenomenon after percutaneous coronary intervention in patients with acute myocardial infarction. J Am Coll Cardiol 2010;55:2383-9.
22. Hale SL, Herring MJ, Kloner RA. Delayed treatment with hypothermia protects against the no-reflow phenomenon despite failure to reduce infarct size. J Am Heart Assoc 2013;2:e004234.
23. Haltern G, Peiniger S, Bufe A, Reiss G, Gulker H, Scheffold T. Comparison of usefulness of heart-type fatty acid binding protein versus cardiac troponin T for diagnosis of acute myocardial infarction. Am J Cardiol 2010;105:1-9.
24. Sodha NR, Clements RT, Feng J et al. The effects of therapeutic sulfide on myocardial apoptosis in response to ischemia-reperfusion injury. Eur J Cardiothorac Surg 2008;33:906-13.
25. Collinson PO. Republished: Sensitive troponin assays. Postgrad Med J 2012;88:348-52.
26. McCann CJ, Glover BM, Menown IB et al. Investigation of a multimarker approach to the initial assessment of patients with acute chest pain. Adv Ther 2009;26:531-4.
27. Liao J, Chan CP, Cheung YC et al. Human heart-type fatty acid-binding protein for on-site diagnosis of early acute myocardial infarction. Int J Cardiol 2009;133:420-3.
28. Body R, McDowell G, Carley S, Wibberley C, Ferguson J, Mackway-Jones K. A FABP-ulous 'rule out' strategy? Heart fatty acid binding protein and troponin for rapid exclusion of acute myocardial infarction. Resuscitation 2011;82:1041-6.
29. Carroll C, Al Khalaf M, Stevens JW et al. Heart-type fatty acid binding protein as an early marker for myocardial infarction: systematic review and meta-analysis. Emerg Med J 2013;30:280-6.
30. Ruff CT, Bonaca MP, Kosowsky JM et al. Evaluation of the diagnostic performance of heart-type fatty acid binding protein in the BWH-TIMI ED chest pain study. J Thromb Thrombolysis 2013;36:361-7.
31. Kagawa Y, Toyofuku M, Masaoka Y et al. Comparison of heart-type fatty acid binding protein and sensitive troponin for the diagnosis of early acute myocardial infarction. Int J Cardiol 2013;166:347-51
32. Aldous S, Pemberton C, Troughton R, Than M, Mark Richards A. Heart fatty acid binding protein and myoglobin do not improve early rule out of acute myocardial infarction when highly sensitive troponin assays are used. Resuscitation 2012;83:e27-8.
33. Reiter M, Twerenbold R, Reichlin T et al. Heart-type fatty acid-binding protein in the early diagnosis of acute myocardial infarction. Heart 2013;99:708-14.
34. Kakoti A, Goswami P. Heart type fatty acid binding protein: structure, function and biosensing applications for early detection of myocardial infarction. Biosens Bioelectron 2013;43:400-11.
35. Schwartz BG, Kloner RA. Coronary no reflow. J Mol Cell Cardiol 2012;52:873-82.
36. Matsumoto S, Nakatani D, Sakata Y et al. Elevated serum heart-type fatty acid-binding protein in the convalescent stage predicts long-term outcome in patients surviving acute myocardial infarction. Circ J 2013;77:1026-32.

CHAPTER 4

No-reflow and reperfusion affect $VEGF_{165A}$ induced in-vitro network formation by human cardiac microvascular endothelium

André Uitterdijk
Stefan Sneep
Willem J van der Giessen†
Dirk J Duncker
Heleen MM van Beusekom

ABSTRACT

Growth factor therapy for angiogenesis in myocardial tissue is generally validated in-vitro under normoxic conditions using human umbilical vein endothelial cells (HUVEC) as opposed to the true target cell type, the human coronary microvascular endothelial cell (HCMVEC). It is unknown how HCMVEC respond to VEGF therapy in clinically relevant conditions. We therefore compared angiogenic responses to $VEGF_{165A}$ in synchronized HCMVEC and HUVECS under normoxic conditions and hypoxic conditions. Tube length and area, and the number of junctions and fields were quantified. Results showed that HCMVEC behavior not only differed significantly from HUVEC, but was also significantly affected by assay conditions. Thus, VEGF mainly affected tube formation under hypoxic conditions but less under normoxic conditions. In conclusion, VEGF primarily induces tube formation in HCMVEC under conditions mimicking no-reflow. These results indicate the necessity to validate growth factor strategies using relevant model parameters and dedicated target cells.

INTRODUCTION

Patients suffering an acute myocardial infarction are usually treated by primary percutaneous coronary interventions (pPCI) to restore blood flow in the blocked artery as soon as possible (1). Despite restoration of flow in the epicardial coronary artery, a large number of patients develop a condition called slow flow or no-reflow (2). This condition is characterized by impaired perfusion of the microvasculature in the infarct zone, often due to constriction, compression, obstruction and destruction of the myocardial microvasculature (3,4). No-reflow is associated with increased mortality and a worse lesion outcome (5) and treatment strategies for no-reflow such as angiogenesis or preservation of the existing network are needed to improve outcome for these patients.

Angiogenesis can be induced by direct vascular endothelial growth factor (VEGF) injection as well as by VEGF gene therapy and was successful in inducing collateral formation in porcine models of chronic myocardial ischemia (6) although clinical trials failed to show efficacy in chronic ischemic heart disease (7,8). Major drawbacks of VEGF therapy are its induction of systemic hypotension at relatively low doses, its short half-life, and its tumorigenic potency (6,9). Considering these drawbacks and the high cost of VEGF, optimization of delivery by determining the sensitivity of the true target cell of an organ to VEGF is essential and should preferentially be determined in a clinically relevant setting. Since pPCI is the treatment of choice for myocardial infarction, angiogenic strategies need to be studied under conditions mimicking both restored perfusion (reflow) and perturbed perfusion (no-reflow).

As swine models of myocardial infarction have shown a reduced capillary density in the heart (10), angiogenesis to improve or maintain the microvascular bed and subsequent perfusion of the infarcted myocardium, especially in the area of no-reflow, is an attractive adjunct therapy to pPCI to support cardiac wound healing and regional stability.

To reduce the number of animal experiments and the confounding factor of age and interspecies differences, this type of work is often studied in-vitro using angiogenesis assays such as tube formation assays. The gold standard is the human umbilical vein endothelial cell (HUVEC), a juvenile cell type with fast growth characteristics. While VEGF is known to amplify or increase network formation in-vitro in HUVECs, VEGF therapy has shown disappointing results in man (7,8). This could suggest that HUVEC may not sufficiently represent the patient. Indeed, the

true target cell type for cardiac therapy is the adult human cardiac microvascular endothelial cell (HCMVEC), and the response of HCMVECs to VEGF has not been reported to date.

To reflect the clinical setting of successful reperfusion as well as no-reflow, we studied the $VEGF_{165A}$ induced angiogenic response of HCMVECs in a tube formation assay that mimics network formation under conditions of no-reflow (hypoxia), and restored perfusion (normoxia). We studied the VEGF dose response at incremental cell densities by quantifying tube-area, tube-length, number of fields and number of junctions.

MATERIAL AND METHODS

Cell types

Human cardiac microvascular endothelial cells (HCMVECs) were obtained from Lonza, Breda, The Netherlands. Human Umbilical Cord Endothelial cells (HUVECs) were obtained from Cambrex, East Rutherford, USA.

No-reflow, tube formation under hypoxic conditions

HCMVECs were cultured to 70% confluence in EGM2 medium (Lonza, Breda, The Netherlands) using conventional cell culture conditions and were subsequently synchronized by nutrient depletion for 20 hours (0.5% heat inactivated fetal bovine serum (FBS) in EBmedium2, Lonza). Synchronized cells were isolated by contemporary trypsinization, centrifuged and resuspended into EBM + 0.5% heat inactivated FBS. Then, according to manufacturer's instructions, μ-slides for angiogenesis (IBIDI, Martinsried, Germany) were filled with 10μl growth factor reduced MatriGel® (MatriGel-GFR, BD Biosciences, Breda, The Netherlands) per well. Then 50μl of a range of cell suspensions ($0.65\text{-}5.2\cdot10^4$ cells/cm^2) with growth factor added (0, 30 or 100ng/ml $VEGF_{165A}$) with or without FBS (5%) was added to every well and equal distribution was ascertained (n=3 per condition). Tube formation was subsequently allowed for 18 hours at 37 °C under hypoxic (5% CO_2, 2% O_2) cell culture conditions, to mimic no-reflow. HUVECs were cultured similarly but with 0.2 and 2% FBS (synchronization and tube formation resp.).

Reperfusion, tube formation under normoxic conditions

To study the specific behavior of HCMVECs in a setting of reperfusion, i.e. angiogenesis under normoxic conditions, tube formation assays were performed (n=3 per group) as described above but under normoxic conditions (5% CO_2, 21% O_2), with and without replenishment of FBS.

Morphometry of tube formation

Following 18 hours of incubation, all wells were digitally photographed and images were subsequently processed for morphometric analyses. Total tube-length, total tube-area, number of fields and number of junctions were quantified by Clemex Vision PE (Clemex Technologies, Longueuill, Canada) and Angiosys 1.0 (TCS Cellworks, Buckingham, United Kingdom).

Statistical analysis

Data are presented as mean ± SD and were analyzed with SPSS (IBM SPSS statistics version 21.0). Statistical significance was accepted when $p<0.05$. Linear regression analysis was performed using cell type, cell density, presence of FBS and VEGF dose as independent parameters.

RESULTS

No-reflow, tube formation by HCMVEC and HUVEC under hypoxic conditions

Results are illustrated in Figure 1 and 2, and statistical analysis is summarized in Table 1. Data show that under hypoxic conditions cell type, cell density, presence of FBS and VEGF dose, all independently predict the outcome measures with an R^2 ranging from 90 to 63%. Clearly, cell type is an important predictor in these measures indicating that HUVEC and HCMVEC behave significantly different under conditions of hypoxia. Importantly, at lower cell densities HCMVECs create vascular networks more efficiently than HUVECs (Figure 2 in presence of FBS).

Since HCMVECs are specific for the intended target organ and clearly show a behavior different from HUVEC, we studied within HCMVEC the effect of hypoxia (Table 2.1) and normoxia (Table 2.2) on the VEGF response. Data for hypoxic conditions show that tube length and the number of fields and junctions were significantly enhanced by VEGF, independent of serum replenishment (FBS).

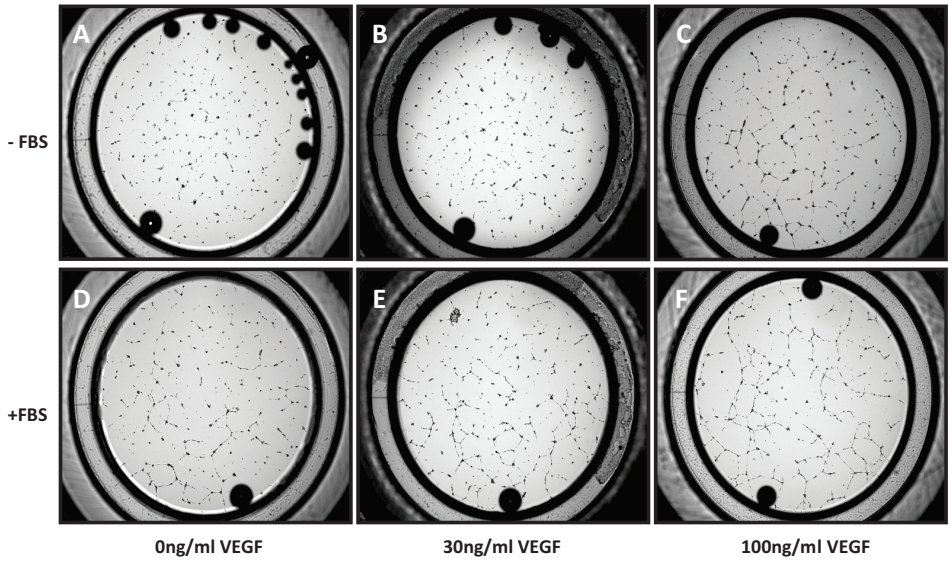

Figure 1. *Panels A-F show typical examples of endothelial network formation by HCMVEC with 3 increasing dosages of growth factor. Top row (A-C) in the absence of FBS, and bottom row (D-F) in the presence of FBS during the assay.*

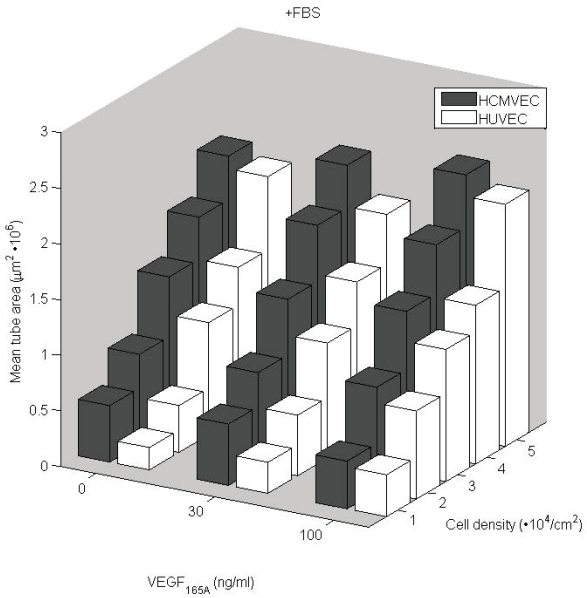

Figure 2. *Graph representing HCMVEC and HUVEC network area under hypoxic conditions in presence of FBS, showing that HCMVEC (■) create a larger network area than HUVEC (□), especially at lower densities. It shows that HCMVEC are less dependent on VEGF at lower cell densities than HUVEC.*

Table 1. *Network formation under hypoxic conditions in HUVEC and HCMVEC*

Network parameter	R^2	P-value	Model parameter:
Tube area	0.90	$1.5 \cdot 10^{-85}$	All parameters: p<0.002
Tube length	0.73	$1.2 \cdot 10^{-48}$	All parameters: p<0.003
Nr. fields	0.68	$5.8 \cdot 10^{-42}$	All parameters: p<0.002
Nr. junctions	0.63	$3.6 \cdot 10^{-37}$	All parameters: p<0.014

Summary of regression analysis to study which parameters affect network formation in HUVEC and HCMVEC under conditions of hypoxia i.e. Cell Type, Cell density, FBS presence and [VEGF]. All model parameters were independent predictors for tube formation. ±FBS = presence/absence of fetal bovine serum; [VEGF] = concentration of $VEGF_A$.

Table 2. *Regression analyses for HCMVEC tube formation behavior*

Network parameters	R^2	P-value	Model Parameters: Hypoxia, FBS, Cell density and [VEGF]	
			Significant	Trend
1. Hypoxia, conditions mimicking ischemia				
Tube area	0.90	$9.3 \cdot 10^{-42}$	FBS, Cell density	[VEGF] p=0.08
Tube length	0.71	$2.3 \cdot 10^{-15}$	FBS, Cell density, [VEGF]	
Nr. Fields	0.66	$1.7 \cdot 10^{-14}$	FBS, Cell density, [VEGF]	
Nr. Junctions	0.61	$4.0 \cdot 10^{-13}$	FBS, Cell density, [VEGF]	
2. Normoxia, conditions mimicking reperfusion				
Tube area	0.90	$7.3 \cdot 10^{-39}$	Cell density	
All other parameters	>0.75	$>5 \cdot 10^{-20}$	FBS, Cell density	[VEGF] p=0.9
3. Hypoxia vs. normoxia				
Tube area	0.90	$2.6 \cdot 10^{-85}$	FBS, Cell density	
Tube length	0.76	$2.8 \cdot 10^{-52}$	FBS, Hypoxia, Cell density	
Nr. fields	0.72	$3.2 \cdot 10^{-36}$	FBS, Hypoxia, Cell density, [VEGF]	
Nr. junctions	0.67	$1.4 \cdot 10^{-32}$	FBS, Hypoxia, Cell density	[VEGF] p=0.10

Summary of regression analysis to study which parameters affect network formation in HCMVEC under conditions mimicking chronic ischemia (hypoxia) and coditions mimicking reperfusion (normoxia). Independent model parameters to predict network formation were hypoxia, cell density, VEGF dose and FBS. Data show that VEGF only affects HCMVEC tube formation under conditions mimicking no-reflow, not under conditions mimicking reperfusion.

Reperfusion, tube formation under normoxic conditions: FBS and VEGF response

The HCMVEC response under conditions mimicking reperfusion (tube formation under normoxic conditions) is summarized in Table 2.2. Data show that cell density was the only independent predictor for tube formation. Only FBS and cell density were independent predictors for tube length and connectivity, VEGF did not affect behavior at all under conditions mimicking reperfusion.

Hypoxia versus normoxia in HCMVEC

Data comparing the effect of hypoxia, cell density, FBS and VEGF on HCMVEC network formation are summarized in Table 2.3. Analysis confirmed that hypoxia did not affect total tube area, indicating that it did not affect cell survival in this assay. It only affected tube length and connectivity (junctions, nr. of fields). VEGF was not an independent predictor with these model parameters, except for the number of fields. Under conditions mimicking successful reperfusion, i.e. tube formation under normoxic conditions, FBS and cell density are the only independent predictors, VEGF is no longer an independent predictor.

DISCUSSION

Induction of angiogenesis is a potential adjunct therapy to mechanical cardiac reperfusion therapy of ischemic myocardium by primary percutaneous coronary interventions (pPCI), to improve perfusion and hence healing of the infarct region. Results of VEGF to induce collateral formation to improve cardiac function in clinical trials have, however, been disappointing (7,8) despite in-vitro proof of concept studies (11,12). Given that the angiogenic response under experimental conditions differs between endothelial cell types (13,14), we aimed to study in vitro tube formation in human cardiac microvascular endothelial cells (HCMVEC) in comparison with conventional human umbilical vein endothelial cells (HUVEC) (15). Moreover, we studied HCMVEC behavior under conditions mimicking normal flow (successful reperfusion, normoxia) and no-reflow (hypoxia), and used $VEGF_{165A}$ as the model drug to induce angiogenesis.

The main findings of the present study are that 1) experimental parameters mimicking no-reflow (hypoxia) and successful reperfusion (normoxia), significantly affect tube formation in HMVEC and 2) VEGF affects HCMVEC tube formation only under conditions of hypoxia, not under conditions of normoxia.

Significance of cell type and model parameters for in-vitro angiogenesis

It is clearly important to be aware of the experimental conditions under which tube formation is studied and the vascular bed from which they are taken. Experimental conditions should always be aimed at mimicking relevant clinical conditions to improve external validity of these data and avoid unnecessary preclinical animal studies and negative clinical trials. The current study indicates that HCMVEC are able to form networks more easily than HUVEC under hypoxic conditions, with differences especially noted at lower cell densities. Clearly, HCMVEC are only sensitive to $VEGF_{165}$ under hypoxic conditions as tested in our experimental set-up. It is known that hypoxia affects the level of expression and the ratio between VEGF receptors 1 and 2, which affects sensitivity to $VEGF_{165A}$ and differs between cell types of different vascular beds (16-18). We suspect that the increased sensitivity of HCMVEC to VEGF under conditions of hypoxia as compared to HUVEC is the result of a change in the ratio of VEGF receptor expression (18).

The niche of VEGF in myocardial angiogenesis, treatment of no-reflow

One unsolved problem in acute cardiac revascularization, the induction of flow restoration following acute myocardial infarction, is the inability to completely restore microvascular flow despite an open coronary artery. These areas, deprived of early reperfusion with resultant prolonged ischemia, are called “No-Reflow zones” and are characterized by irreversible reperfusion injury and poor prognosis (19-21). Our data show that while VEGF was unable to induce tube formation under conditions of normoxia, it was able to improve network formation under conditions of hypoxia. It could thus be hypothesized that VEGF could exert a beneficial effect by inducing angiogenesis in these malperfused “no-reflow” areas experiencing continued hypoxia following restoration of coronary artery patency. Delivery of relevant concentrations to these specific areas of interest, in combination with prolonged delivery using novel delivery platforms such as degradable microspheres (22,23) may further improve VEGF efficacy.

CONCLUSION

In summary, we found that 1) HCMVEC behavior significantly differs from HUVEC under conditions of hypoxia 2) HCMVEC behavior is significantly affected by the conditions chosen to study tube formation such as hypoxia and normoxia. 3) VEGF primarily affects tube formation under conditions simulating hypoxia, and less during normoxia. These findings indicate that VEGF only induces tube formation in human (cardiac)microvascular endothelial cells under conditions of

hypoxia, not under conditions of normoxia. Furthermore, these findings indicate that relevant model parameters and dedicated target cells are essential when studying myocardial angiogenesis in in-vitro tube formation assays.

Acknowledgments

The authors cordially thank Dr. L. Speelman for assisting in 3D-plotting

REFERENCES

1. O'Gara PT, Kushner FG, Ascheim DD et al. 2013 ACCF/AHA Guideline for the Management of ST-Elevation Myocardial Infarction: Executive Summary A Report of the American College of Cardiology Foundation/American Heart Association Task Force on Practice Guidelines. Journal of the American College of Cardiology 2013;61:485-510.
2. Carrick D, Oldroyd KG, McEntegart M et al. A Randomized Trial of Deferred Stenting Versus Immediate Stenting to Prevent No- or Slow-Reflow in Acute ST-Segment Elevation Myocardial Infarction (DEFER-STEMI). Journal of the American College of Cardiology 2014;63:2088-2098.
3. Reffelmann T, Kloner RA. The no-reflow phenomenon: A basic mechanism of myocardial ischemia and reperfusion. Basic research in cardiology 2006;101:359-72.
4. Betgem RP, de Waard GA, Nijveldt R, Beek AM, Escaned J, van Royen N. Intramyocardial haemorrhage after acute myocardial infarction. Nature reviews Cardiology 2015;12:156-167.
5. Harrison RW, Aggarwal A, Ou FS et al. Incidence and Outcomes of No-Reflow Phenomenon During Percutaneous Coronary Intervention Among Patients With Acute Myocardial Infarction. American Journal of Cardiology 2013;111:178-184.
6. Sato K, Wu T, Laham RJ et al. Efficacy of intracoronary or intravenous VEGF165 in a pig model of chronic myocardial ischemia. J Am Coll Cardiol 2001;37:616-23.
7. Henry TD, Annex BH, McKendall GR et al. The VIVA trial: Vascular endothelial growth factor in Ischemia for Vascular Angiogenesis. Circulation 2003;107:1359-65.
8. Stewart DJ, Kutryk MJ, Fitchett D et al. VEGF gene therapy fails to improve perfusion of ischemic myocardium in patients with advanced coronary disease: results of the NORTHERN trial. Mol Ther 2009;17:1109-15.
9. Goel HL, Mercurio AM. VEGF targets the tumour cell. Nat Rev Cancer 2013;13:871-82.
10. Haitsma DB, Bac D, Raja N, Boomsma F, Verdouw PD, Duncker DJ. Minimal impairment of myocardial blood flow responses to exercise in the remodeled left ventricle early after myocardial infarction, despite significant hemodynamic and neurohumoral alterations. Cardiovasc Res 2001;52:417-28.
11. Bauters C, Asahara T, Zheng LP et al. Recovery of disturbed endothelium-dependent flow in the collateral-perfused rabbit ischemic hindlimb after administration of vascular endothelial growth factor. Circulation 1995;91:2802-9.
12. Witzenbichler B, Asahara T, Murohara T et al. Vascular endothelial growth factor-C (VEGF-C/VEGF-2) promotes angiogenesis in the setting of tissue ischemia. Am J Pathol 1998;153:381-94.
13. Baffert F, Usson Y, Tranqui L. Effects of prolonged exposure to hypoxia on morphological changes of endothelial cells plated on fibrin gel. Eur J Cell Biol 2001;80:78-86.
14. Dardik R, Livnat T, Seligsohn U. Variable effects of alpha v suppression on VEGFR-2 expression in endothelial cells of different vascular beds. Thromb Haemost 2009;102:975-82.
15. Morales DE, McGowan KA, Grant DS et al. Estrogen promotes angiogenic activity in human umbilical vein endothelial cells in vitro and in a murine model. Circulation 1995;91:755-63.
16. Gerber HP, Condorelli F, Park J, Ferrara N. Differential transcriptional regulation of the two vascular endothelial growth factor receptor genes. Flt-1, but not Flk-1/KDR, is up-regulated by hypoxia. The Journal of biological chemistry 1997;272:23659-67.
17. Olszewska-Pazdrak B, Hein TW, Olszewska P, Carney DH. Chronic hypoxia attenuates VEGF signaling and angiogenic responses by downregulation of KDR in human endothelial cells. American journal of physiology Cell physiology 2009;296:C1162-70.
18. Ulyatt C, Walker J, Ponnambalam S. Hypoxia differentially regulates VEGFR1 and VEGFR2 levels and alters intracellular signaling and cell migration in endothelial cells. Biochemical and biophysical research communications 2011;404:774-9.

19. Galasso G, Schiekofer S, D'Anna C et al. No-reflow phenomenon: pathophysiology, diagnosis, prevention, and treatment. A review of the current literature and future perspectives. Angiology 2014;65:180-9.
20. Ndrepepa G, Tiroch K, Fusaro M et al. 5-year prognostic value of no-reflow phenomenon after percutaneous coronary intervention in patients with acute myocardial infarction. J Am Coll Cardiol 2010;55:2383-9.
21. Ndrepepa G, Tiroch K, Keta D et al. Predictive factors and impact of no reflow after primary percutaneous coronary intervention in patients with acute myocardial infarction. Circ Cardiovasc Interv 2010;3:27-33.
22. Arras M, Mollnau H, Strasser R et al. The delivery of angiogenic factors to the heart by microsphere therapy. Nat Biotechnol 1998;16:159-62.
23. George EM, Liu H, Robinson GG, Mahdi F, Perkins E, Bidwell GL, 3rd. Growth factor purification and delivery systems (PADS) for therapeutic angiogenesis. Vasc Cell 2015;7:1-10.

CHAPTER 5

Time course of VCAM-1 expression in reperfused myocardial infarction in swine and its relation to retention of bone marrow-derived mononuclear cells

André Uitterdijk
Bianca CW Groenendijk
Charlotte Gorsse-Bakker
Anna Panasewicz
Stefan Sneep
Dennie Tempel
Willem J van der Giessen†
Dirk J Duncker

ABSTRACT

Intracoronary infusion of autologous bone marrow-derived mononuclear cells (BMMNC), after acute myocardial infarction (AMI), has been shown to improve myocardial function. However, therapeutic efficacy is limited, possibly because cell retention rates are very low, suggesting that optimization of cell retention might increase therapeutic efficacy. Since retention of injected BMNNC is observed only within infarcted, but not remote, myocardium, we hypothesized that adhesion molecules on activated endothelium following reperfusion was essential. Consequently, we investigated the role of adhesion molecule VCAM-1 in BMMNC retention in swine undergoing AMI produced by 120 min of LCx coronary occlusion. VCAM-1 expression in the infarct region was quantified at 1, 3, 7, 14 and 35 days post-reperfusion (n=6 per group). Since expression levels were significantly higher at 3 days (2.41±0.62%) than at 7 days (0.98±0.28%; $p<0.05$), we compared the degree of cell retention at those time points in a follow-up study, in which an average of $43 \cdot 10^6$ autologous BMMNCs were infused intracoronary at 3 or 7 days post-reperfusion (n=6 per group) and retention was quantified one hour after intracoronary infusion of autologous BMMNCs. Although VCAM-1 expression correlated with retention of BMNNC within each time point, overall BMMNC retention was similar at day 3 and day 7 (2.3±1.3% vs. 3.1±1.4%, p=0.72). This was not due to the composition of infused bone marrow cell fractions (analyzed with flow cytometry; n=5 per group), as cell composition of the infused BMNNC fractions was similar. These findings indicate that VCAM-1 expression influences, but is not the sole determinant of, BMNNC retention.

INTRODUCTION

Cell therapy with autologous bone marrow-derived cells generally produces statistically significant but only modest improvements in myocardial function after acute myocardial infarction (AMI) (1,2). With $20{\cdot}10^6$ cardiomyocytes per gram of jeopardized myocardium (3), potentially lost to infarction, it is evident that the absolute number of cells retained to regionally treat the affected area is of great importance. However, cell retention after intracoronary cell therapy is very low, varying widely between studies, possibly as a result of differences in cell type, timing of administration and initial cell dose (4-18) (see supplementary Table S1). Previous work from our laboratory showed that cell retention after intracoronary injection of BMMNCs at one week of reperfusion in a swine model of AMI, amounted 8% and 6.5%, respectively, at 1.5 hours and 4 days post-injection (13). Retention of cells was observed only within the infarcted region, whereas no cells were retained when cells were injected selectively into the non-occluded left anterior descending coronary artery (LAD). The latter findings suggest that cell adherence and retention is an active process, occurring exclusively in the reperfused infarct-zone, and not just physical entrapment of the cells due to cell size.

Following myocardial infarction, activated endothelium within the infarct region drives the expression of transmembrane adhesion molecules to orchestrate regional immune responses. These adhesion molecules serve as primary “loading-docks” for cell anchorage and their limited and transient post-AMI presence may be correlated to the limited retention of infused cells. A key player associated with endothelial adhesion of circulating immune cells includes Vascular Cell Adhesion Molecule 1 (VCAM-1). It is however, unknown to what extent VCAM-1 is present in the days following AMI and to what extent VCAM-1 presence influences BMMNC retention. Mesenchymal stem cells (MSC), a popular cell type in cell therapy, use β1-integrin (CD29) for engraftment (19) and at least 93% of MSCs express this integrin (20), which is, amongst others, part of VLA4 (α4β1-integrin), the receptor for VCAM-1. In light of these considerations, we investigated *i)* the temporal expression of VCAM-1 in infarcted and remote myocardial regions in swine with reperfused AMI; *ii),* the correlation of VCAM-1 presence to autologous bone marrow-derived cell retention and *iii)* temporal changes in AMI-induced changes in the composition of the injected BMMNCs.

MATERIAL AND METHODS

Part I: VCAM-1 expression after acute myocardial infarction

Animal experiments were performed in 48, 5-6 month old Yorkshire x Landrace swine of either sex (31.0±0.3kg). All experiments were performed in compliance with the "Guide for the Care and use of Laboratory Animals" and after written approval of the Animal Ethics Committee of the Erasmus MC.

Surgery. Myocardial infarction was produced in 33 swine (30.5±0.3kg) as previously described (21). For this purpose, swine were sedated with an intramuscular injection of midazolam (1mg/kg), ketamine (20 mg/kg) and atropine (1mg). Then, an intravenous (iv) ear catheter was placed for induction of anesthesia with thiopenthal sodium (17 mg/kg). Next, animals were intubated and mechanically ventilated (O_2:N_2 1:3 v/v), while anesthesia was maintained with fentanyl (20μg/kg/h iv). Under sterile conditions, a 9F arterial sheath was placed in a dissected carotid artery and anticoagulation was ascertained by the iv administration of 10,000 units of heparin + 5,000 units every additional hour of surgery. Physiological body core temperature was maintained with heating pads (22). Saline was infused at 100 ml/h iv to maintain fluid status of the animals, while arterial blood pressure and ECG were monitored continuously. The left circumflex coronary artery (LCx) was catheterized under fluoroscopic guidance with a 7F guiding catheter and maximal coronary artery dilation was produced with 1mg isosorbidatedinitrate for optimized balloon sizing. Next, the LCx was visualized with selective infusion of the contrast agent iodixanol and coronary diameter was measured with dedicated software (CAAS, Pie Medical, Eindhoven, The Netherlands). After the selection of the occlusion site by at least two researchers to ascertain optimal protocol adherence, the LCx was occluded for 2h distally to the first marginal branch followed by reperfusion with a standard guide wire and an appropriately sized percutaneous transluminal coronary angioplasty balloon. Following occlusion, anesthesia was switched to isoflurane inhalation anesthesia (1-3% v/v) (13,23). After 2h of occlusion the balloon was deflated and reperfusion was allowed. Anesthetized animals were monitored until hemodynamically stable. Antibiotic prophylaxis was given intramuscularly (procainebenzylpenicilline 20 mg/kg and dihydrostreptomycine sulphate 25 mg/kg). Catheters were removed, the incision site was closed and animals were allowed to recover.

Follow-Up. After 1 (n=6), 3 (n=6), 7 (n=7), 14 (n=6) or 35 (n=6) days post-AMI, animals were sedated as described above. Anesthesia was induced (15 mg iv) and maintained (15 mg/kg/h iv) with pentobarbital sodium. Following sternotomy,

the pericardium was opened and the heart was electrically induced to fibrillate. Next, the heart was excised and rinsed with ice-cold saline. The left ventricle was isolated and cut into transverse sections and both remote and infarct tissues were preserved in optimal cutting temperature compound (Tissue-Tek, Sakura Finetek, Alphen aan den Rijn, The Netherlands) using frozen CO_2 (dry ice) for future histopathological analyses.

Immunohistochemistry. Cryosections of 5*μ*m were fixed in ice-cold acetone for 10 min. Endogenous peroxidase activity was blocked with 0.3% H_2O_2 in 40% methanol for 60 min. Adjacent sections were incubated with anti-VCAM-1 (mouse-anti pig, 1:300, gift from Prof. D. Haskard, London, United Kingdom) overnight at 4 °C. Next, using the Vectastain biotinylated horse-anti mouse kit (Brunschwig Chemie, Amsterdam, The Netherlands) and diaminobenzidine (DAKO, Eindhoven, The Netherlands) expression was visualized. Stained sections were photographed with a virtual microscope (Hamamatsu NanoZoomer, 2.0-HT Slide Scanner). Whole sections, containing 5-6 high-power fields (40x) were analysed for VCAM-1 presence with dedicated software using a color threshold (BioPix iQ, 2.2.1, BioPix AB, Göteborg, Sweden). Data were expressed as a percentage of the total surface area.

Part II: Effects of VCAM-1 expression on cell retention

Based on the results obtained in the VCAM-1 expression studies described above, two time points were selected to test whether regional up-regulation of VCAM-1 leads to increased cell retention after infusion.

Surgery, Cell Isolation and -Infusion. In 15 swine (32.3±0.6kg), reperfused myocardial infarction was induced as above and serial blood for biomarker measurements was taken as described before (21). At 3 or 7 days post-AMI (n=6 surviving pigs per group), bone marrow was harvested under sterile conditions from the ileac crest and/or the proximal femur of the anesthetized pigs as described before (13). In brief, up to 160 ml bone marrow was aspirated using 5ml heparinized syringes and received in 50 ml centrifuge tubes containing 10 ml phosphate buffered saline (PBS) and 5,000 units of heparin. Bone marrow was selectively enriched for the mononuclear fraction by density centrifugation (20 min at 800g at RT), using equal amounts of Lymphoprep as a separation medium (Lucron, Milsbeek, The Netherlands). Using a sterile pipette, the mononuclear cell fraction was carefully aspirated and filtered using a 100 *μ*l cell strainer. The fraction was washed twice by centrifugation in wash buffer (PBS containing 0.1%

of autologous serum, 10 min at 600 g at RT). The obtained cells were resuspended in wash buffer and added to a red blood cell lysis solution for 10 min at RT (1:3, 8.3 g NH_4Cl + 1.0 g $KHCO_3$ + 1.8 ml 5% EDTA in 1000 ml H_2O) to remove erythrocytes. Enriched and washed cells were collected by centrifugation (2 min at 2000 g at RT). A conventional Bürker-Türk haemocytometer and trypan blue exclusion were used to count total cell number and ascertain viability. Up to $50 \cdot 10^6$ cells were labeled with the fluorescent membrane marker PKH26 (Sigma-Aldrich, Zwijndrecht, The Netherlands) and successful labeling was ascertained with fluorescence microscopy of a small aliquot. Labeled cells were then resuspended in washing buffer to obtain a density of $1.7 \cdot 10^6$ cells/ml and infused intracoronary using a multi-purpose infusion catheter into the infarcted area of the heart at a rate of $1 \cdot 10^6$ (slow, n=2 per group) or $5 \cdot 10^6$ (fast, n=4 per group) labeled cells per minute. One hour after the completion of the infusion protocol, the hearts of the animals were excised, and the complete infarct region was carefully sectioned into $1cm^2$-sized cubes and processed for histopathology as described above.

Quantification of retained cells. VCAM-1 was quantified in cell infusion treated animals as described above. Next, using a checkerboard-like approach, 5 μm cryosections from the infarcts were fixed with ice-cold acetone for 10 minutes. Sections were washed with PBS and mounted with 4',6-diamidino-2-phenylindole (Vectashield with DAPI, Brunschwig Chemie). Using a Zeiss Axiovert S100, 10x photos were taken of the stained sections and using a color threshold PKH26 positive cells were counted with ImageJ (version 1.46r, National Institutes of Health, USA). Using section thickness, average cell thickness and tissue dimensions, we calculated cell retention.

Part III: Effects of myocardial infarction on composition of the mononuclear fraction

Flow cytometry. In parallel to processing of cells for the intracoronary cell injection experiments, a representative aliquot from each bone marrow aspirate (n=5 per group) was processed for flow cytometry to assess relative contribution of the various cell types within the mononuclear fraction, in order to determine the composition of the mononuclear fraction at 3 vs 7 days post-AMI. For this purpose, we quantified the percentage of B-cells ($CD79a^+$, AbD Serotec, Puchheim, Germany), T-cells ($CD3^+$, Abcam, Cambridge, UK), α4-integrin positive cells ($CD49d^+$, AbD Serotec), β2 integrin positive cells ($CD18^+$, VMRD, Pullman, WA, USA), CD34 positive cells ($CD34^+$, R&D Systems, Abingdon, UK) and mesenchymal stem cells (as defined by $CD105^+/CD90^+/CD14^-/CD45^-$, CD105: Exbio, Prague, Czech Republic; CD90:

BD Biosciences, Breda, The Netherlands; CD14 and CD45 AbD Serotec). For the B- and T-cell staining, cells were resuspended in azide/serum/protein-free PBS at a concentration of $10 \cdot 10^6$ cells/ml. Fixable Viability Dye, for cell viability selection, was added and incubated for 30 minutes at 4 ºC. After washing with FACS Flow (BD Biosciences), CD3 antibody was incubated for 15 minutes at room temperature. Cells were washed and incubated with Leucoperm Reagent A for 15 minutes at RT followed by washing and incubation with Leucoperm Reagent B for 30 minutes at RT, final washing and resuspension in FACS Flow. For CD18, CD34, CD49d and their combinations with $CD14^-$ and $CD45^-$ staining, cells were resuspended in FACS Flow and incubated with the first primary antibodies (CD18, CD49d or CD34) for 15 minutes at room temperature. After washing, cells were incubated with secondary antibodies for 30 minutes at room temperature, followed by washing and incubation with the second set of primary antibodies (CD14 and CD45) for 15 minutes at room temperature. For cell viability selection 7-amino-actinomycin D (7-AAD, BD Biosciences) was added and cells were washed and resuspended in FACS Flow. For the MSC analysis, cells were resuspended in FACS Flow and incubated with the primary antibodies (CD105, CD90, CD14 and CD45) for 15 minutes at room temperature followed by addition of 7-AAD. After washing, cells were resuspended in FACS Flow. Flow cytometric analysis was performed on a FACSCanto (BD Biosciences) and subsequent data analysis by use of FlowJo software (Tree Star Inc, Ashland, OR, USA).

Statistics

Data are presented as mean ± SEM. Data were analyzed with Sigmaplot (Version 11.0, Drunen, The Netherlands), using two-way (time x treatment) ANOVA followed by post-hoc Bonferroni correction when appropriate. Statistical significance was accepted when $p<0.05$.

RESULTS

Part I: VCAM-1 expression after acute myocardial infarction

Mortality and Exclusion. Two swine out of 33 that encountered ventricular fibrillation during the ischemia-reperfusion protocol could not be converted to normal sinus rhythm. Of the remaining 31 animals that completed the protocol, 6 tissue-sets were ultimately not suitable for final analyses as a result of cryopreservation-induced tissue deformities leaving 25 analyzable datasets.

VCAM-1 expression after Myocardial Infarction. Figure 1 illustrates that VCAM-1 presence in remote tissue remained low at all times (0.20±0.03%). In contrast, VCAM-1 presence in the infarct region was elevated at 3 days (2.41±0.62%, n=4, p<0.001) and 7 days (0.98±0.28%, n=5, p=0.01) post-AMI. Importantly, VCAM-1 expression peaked at 3 days post-infarction and showed a transient pattern with normalization 14 days post-infarct.

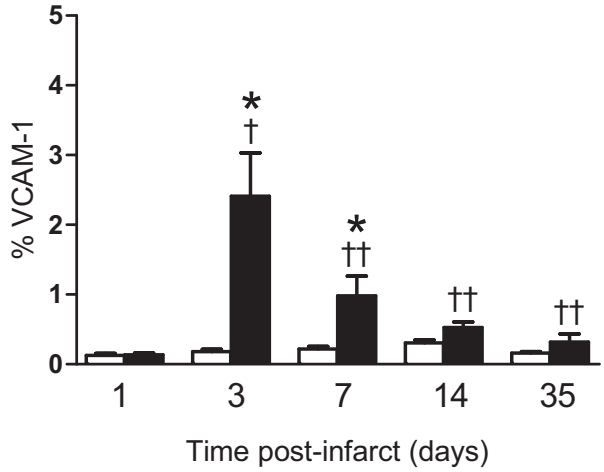

Figure 1. *Temporal VCAM-1 expression 1 (n=4), 3 (n=4), 7 (n=5), 14 (n=6) and 35 days (n=6) after myocardial infarction. Data are expressed as mean ± SEM. □ = remote tissue, ▮ = infarct tissue. *=p<0.05 vs. corresponding remote; † = p<0.05 vs. day **1;** †† = p<0.05 vs. day 3.*

Part II: Effects of VCAM-1 expression on cell retention

Mortality and Infarct Mass. Three out of 15 swine did not complete the protocol. Two swine that encountered ventricular fibrillation could not be converted to normal sinus rhythm and one swine died prematurely because of electromechanical dissociation during ischemia. Importantly, no animals died before stratification into the 3 or 7 days post-AMI group or during cell infusion. Infarct mass at baseline, estimated from the plasma concentration of heart specific fatty acid binding protein determined at 50 min of reperfusion (21), was similar between groups (11±2 g vs. 13±4 g, p=0.65).

VCAM-1 Expression. VCAM-1 showed similar levels of expression as compared to the experiments in part I (3 days post-AMI: 2.09±0.60 vs. 2.41±0.62%, p=0.73; 7 days post-AMI: 0.99±0.21 vs. 0.98±0.28%, p=0.97).

Cell Retention. Initial analyses did not show significant differences between fast (n=4 per group, 1.2±1.1% at day 3 vs. 2.8±1.7% at day 7, p=0.44) or slow (n=2 per group, 4.4±4.4% at day 3 vs. 3.5±3.3% at day 7, p=0.92) infusion rates. Consequently, fast and slow infusion results were pooled for further analyses and results are presented in Figure 2. Similar numbers of cells were infused in every group, 42±6·10^6 cells at 3 days post-AMI vs. 43±4·10^6 at 7 days post-AMI (p=0.93). An average of 8.4±0.8 individual tissue samples were selected per animal and an average of 40±6 photo's per animal were quantified for PKH26-positive cells. Results show that the absolute number of retained cells was not different at 3 or 7 days post-AMI (0.7·10^6±0.4·10^6 cells vs. 1.1·10^6±0.5·10^6, p=0.52), with similar results when data were expressed as a percentage of the initially infused number of cells (2.3±1.3% vs. 3.1±1.4%, p=0.72). Moreover, when results were corrected for infarct mass at baseline, results were again not statistically different for both absolute retention (0.05·10^6±0.03·10^6 cells/g vs. 0.08·10^6±0.04·10^6 cells/g, p=0.51) as well as relative retention (0.17±0.11%/g vs. 0.24±0.12%/g, p=0.65).

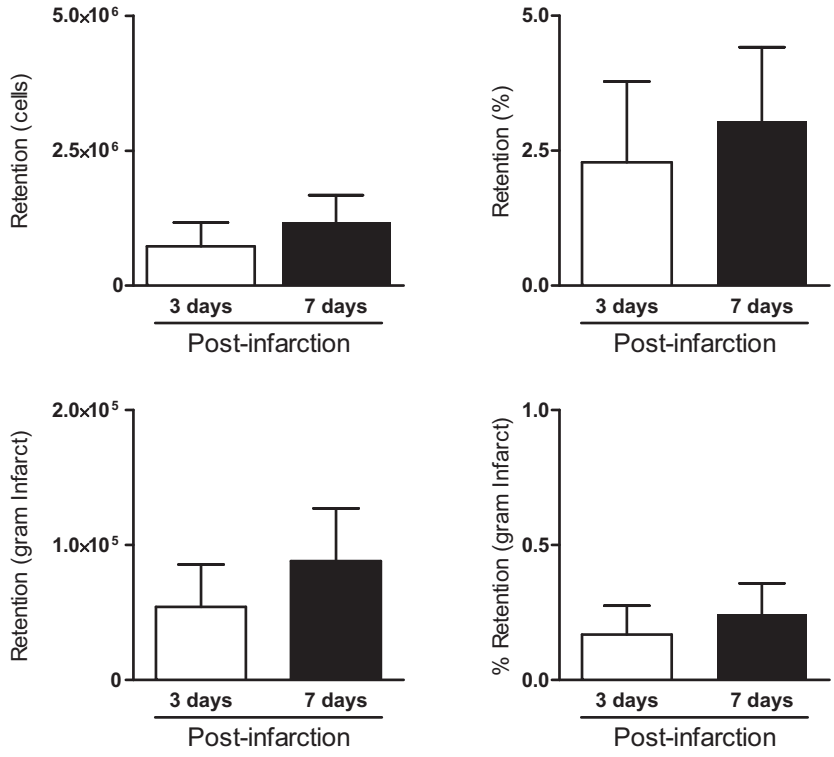

Figure 2. *Retention of cells in infarcted myocardium 3 or 7 days post infarction expressed as absolute numbers or as a percentage of the initial dose and corrected for infarct mass. Data are expressed as mean ± SEM.*

VCAM-1 expression and Cell Retention. Although cell retention levels did not differ between 3 and 7 days post-AMI, whereas VCAM-1 expression levels were significantly higher at 3 compared to 7 days post-AMI, there were significant correlations between VCAM-1 expression and cell retention at 3 days (r^2=0.69, p=0.03) and 7 days (r^2=0.74, p=0.04) post-AMI, so that higher expression of VCAM-1 was associated with a higher rate of cell retention (Figure 3). These findings suggest that while VCAM-1 is a determinant of cell retention, other factors must also play a role. One such factor could be the cell-composition of the mononuclear cell fraction that was harvested and injected at 3 days vs 7 days post-AMI.

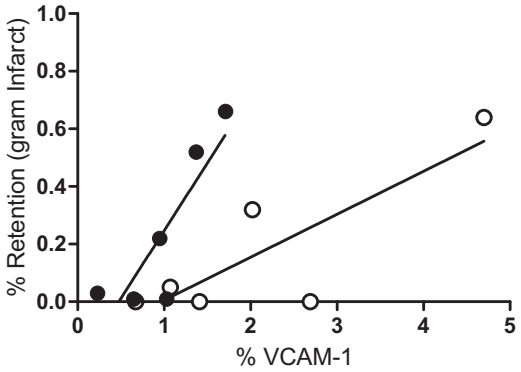

Figure 3. *Regression analysis of VCAM-1 expression at 3 (○, r^2=0.69, p=0.03) and 7 days (●, r^2=0.74, p=0.04) post-infarction vs. % of retained autologous bone marrow-derived cells per gram infarct.*

Part III: Effects of myocardial infarction on composition of the mononuclear fraction

Figure 4 shows that the contribution of B-cells, T-cells, CD34+ cells and MSCs to the mononuclear cell fraction was similar at both time points. Furthermore, cell surface adhesion molecules α4 (part of VCAM-1) integrin and β2 (part of ICAM-1) integrin showed similar expression levels in both groups. Thus, no differences in composition of the infused fraction were observed between 3 and 7 days post-AMI. Similarly, there were no significant correlations noted between composition of the injected cells and magnitude of cell retention (data not shown).

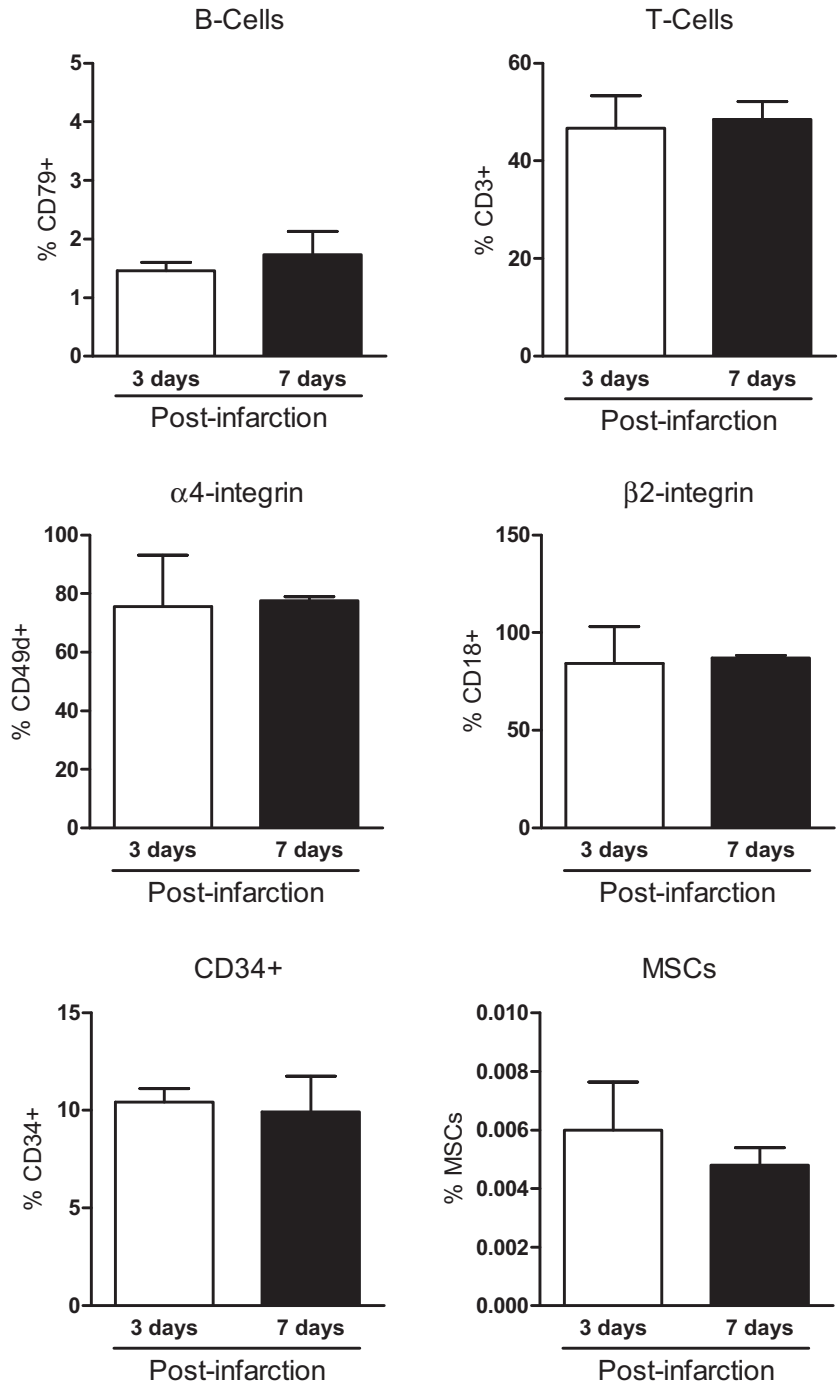

Figure 4. *Composition of autologous infused bone marrow-derived mononuclear cells at 3 and 7 days post infarction. MSC = mesenchymal stem cell. Data are expressed as mean ± SEM*

DISCUSSION

The present study investigated the temporal pattern of VCAM-1 expression in infarcted and remote myocardial regions in swine with reperfused AMI, and its correlation with retention of bone marrow mononuclear cells harvested and injected at 3 or 7 days post-AMI. The major findings were that: (*i*) vascular cell adhesion molecule 1 (VCAM-1) expression is upregulated in the microcirculation of infarct-impaired myocardial tissue in a transient manner with VCAM-1 expression peaking at 3 days (~12-fold) and 7 days (~5-fold) post-AMI, with normalization to baseline values within 14 days post-AMI; (*ii*) VCAM-1 expression correlated with the magnitude of cell retention both at 3 days and 7 days post-AMI, but average cell retention was not different at 3 days vs. 7 days, indicating that cell retention was not only dependent on VCAM-1 expression; (*iii*) composition of the mononuclear fraction was not different 3 or 7 days post-AMI and selected types individually did not correlate with retention. The implications of these findings will be discussed.

Cell retention after cell therapy

The limited therapeutic efficacy of cell therapy reported in clinical studies (1,2) could, at least in part, be due to the relatively low retention rates of administered cells. Retention rates as high as 57.7% of the infused fraction (10) or as low as 0.8% of the infused fraction (12) have been reported after intracoronary infusion (see supplementary Table S1). Also, no uniform approach in retention studies exists as many parameters that may influence retention vary. These differences include, but are not limited to, the number and types of cells infused, as well as the timing and procedure of administration. Importantly, the preferred tracking method appears to be scintigrapy. This method however, in which cells are labeled with a radioactive tracer, may be considered suboptimal as the method does not correct for the heterogeneous label efficiency that exists when a heterogeneous cell population including differences in cell type and cell size is taken into account. This will inevitably lead to skewed results when i.e. a subpopulation of large cells containing much radiolabel is retained primarily (24). Also radiolabeled cell debris may result in false-positive retention. Here we assessed BMMNC retention in great detail using a histopathological approach of the complete infarct. This detailed approach, not affected by false positive scoring or differences in label efficiency, may explain our relatively low retention compared to other studies.

Post-infarct endothelial response

Upon myocardial infarction, endothelium within the affected area is activated resulting in a proinflammatory and procoagulant environment characterized by increased interactions with leukocytes (25). Numerous adhesion factors are upregulated within the affected area including VCAM-1 (26). VCAM-1 is expressed after infarct-induced cytokine release and serves as a "docking station" for leukocytes to facilitate the regional immune response (27). Understanding the post-infarct up-regulation pattern of regional VCAM-1 may reveal the optimal timing for intracoronary infused bone marrow-derived mononuclear cell therapy. Here, we report the temporal expression pattern of VCAM-1 in the microcirculation of porcine ischemia-reperfusion impaired myocardium. VCAM-1 expression peaked at 3 days post-AMI and was normalized after 14 days, suggesting that cell retention would be optimal when applied at a time point that VCAM-1 expression is highest. Retention of autologous BMMNC, however, when administered at time points in which VCAM-1 was significantly upregulated only partly supported our hypothesis. Thus, while a correlation between increased VCAM-1 expression and cell retention was observed both at 3 days and 7 days post-AMI, average cell retention at 3 days vs 7 days was similar despite different levels of VCAM-1 expression. These results indicate that cell retention is not only determined by VCAM-1 expression, but also by other factors, one of which could the composition of the injected BMMNC at 3 vs 7 days post-AMI.

Composition of mononuclear cell fraction

Analysis of the BMMNC fraction isolated at 3 days or 7 days post-AMI did not reveal any differences in composition. In addition, the nature of the quantification study and the scarce availability of porcine antibodies restricted the phenotypical identification of retained cells within the infarct area and is considered a major limitation of this work. For future optimization studies, is remains of the greatest interest to show which cell type is dominant in retention studies. Our results however, do enable us to exclude that retained cells are MSCs only as the average absolute number of MSCs is limited to ~2000-2500 cells per infused fraction whereas absolute retained number of cells approximate at least $0.7 \cdot 10^6$ cells. Thus, cell composition of the BMMNC isolated 3 or 7 days post-AMI did not have an effect on absolute or relative cell retention suggesting that the role of composition is not decisive.

CONCLUSIONS

The present study in swine with a reperfused AMI demonstrates that VCAM-1 is significantly upregulated in the microvasculature of infarcted myocardial tissue in a transient manner peaking at 3 days post-AMI with normalization to baseline at 14 days post-AMI. Although VCAM-1 expression correlated with the magnitude of cell retention at either 3 or 7 days post-AMI, the absolute and relative average retention of BMMNCs were similar at these time points. This was not due to the composition of infused bone marrow cell fractions, as cell composition of the infused BMNNC fractions was similar at 3 and 7 days post-AMI. Taken together, these findings indicate that VCAM-1 expression is not the sole determinant of BMNNC retention in reperfused myocardium post-AMI.

ACKNOWLEDGEMENTS

Prof. Dr. Dorian Haskard, Vascular Sciences Section, National Heart and Lung Institute, Imperial College London, is cordially thanked for providing the VCAM-1 antibody.

REFERENCES

1. Delewi R, Hirsch A, Tijssen JG et al. Impact of intracoronary bone marrow cell therapy on left ventricular function in the setting of ST-segment elevation myocardial infarction: a collaborative meta-analysis. Eur Heart J 2014;35:989-98.
2. Assmus B, Leistner DM, Schachinger V et al. Long-term clinical outcome after intracoronary application of bone marrow-derived mononuclear cells for acute myocardial infarction: migratory capacity of administered cells determines event-free survival. Eur Heart J 2014;35:1275-83.
3. Olivetti G, Capasso JM, Sonnenblick EH, Anversa P. Side-to-side slippage of myocytes participates in ventricular wall remodeling acutely after myocardial infarction in rats. Circ Res 1990;67:23-34.
4. Blocklet D, Toungouz M, Berkenboom G et al. Myocardial homing of nonmobilized peripheral-blood CD34+ cells after intracoronary injection. Stem Cells 2006;24:333-6.
5. Dedobbeleer C, Blocklet D, Toungouz M et al. Myocardial homing and coronary endothelial function after autologous blood CD34+ progenitor cells intracoronary injection in the chronic phase of myocardial infarction. J Cardiovasc Pharmacol 2009;53:480-5.
6. Doyle B, Kemp BJ, Chareonthaitawee P et al. Dynamic tracking during intracoronary injection of 18F-FDG-labeled progenitor cell therapy for acute myocardial infarction. J Nucl Med 2007;48:1708-14.
7. Freyman T, Polin G, Osman H et al. A quantitative, randomized study evaluating three methods of mesenchymal stem cell delivery following myocardial infarction. Eur Heart J 2006;27:1114-22.
8. Goussetis E, Manginas A, Koutelou M et al. Intracoronary infusion of CD133+ and CD133-CD34+ selected autologous bone marrow progenitor cells in patients with chronic ischemic cardiomyopathy: cell isolation, adherence to the infarcted area, and body distribution. Stem Cells 2006;24:2279-83.
9. Hofmann M, Wollert KC, Meyer GP et al. Monitoring of bone marrow cell homing into the infarcted human myocardium. Circulation 2005;111:2198-202.
10. Hong KU, Guo Y, Li QH et al. c-kit+ Cardiac Stem Cells Alleviate Post-Myocardial Infarction Left Ventricular Dysfunction Despite Poor Engraftment and Negligible Retention in the Recipient Heart. PLoS One 2014;9:e96725.
11. Hou D, Youssef EA, Brinton TJ et al. Radiolabeled cell distribution after intramyocardial, intracoronary, and interstitial retrograde coronary venous delivery: implications for current clinical trials. Circulation 2005;112:I150-6.
12. Ly HQ, Hoshino K, Pomerantseva I et al. In vivo myocardial distribution of multipotent progenitor cells following intracoronary delivery in a swine model of myocardial infarction. Eur Heart J 2009;30:2861-8.
13. Moelker AD, Baks T, van den Bos EJ et al. Reduction in infarct size, but no functional improvement after bone marrow cell administration in a porcine model of reperfused myocardial infarction. Eur Heart J 2006;27:3057-64.
14. Moreira Rde C, Haddad AF, Silva SA et al. Intracoronary stem-cell injection after myocardial infarction: microcirculation sub-study. Arq Bras Cardiol 2011;97:420-6.
15. Musialek P, Tekieli L, Kostkiewicz M et al. Randomized transcoronary delivery of CD34(+) cells with perfusion versus stop-flow method in patients with recent myocardial infarction: Early cardiac retention of (9)(9)(m)Tc-labeled cells activity. J Nucl Cardiol 2011;18:104-16.

16. Musialek P, Tekieli L, Kostkiewicz M et al. Infarct size determines myocardial uptake of CD34+ cells in the peri-infarct zone: results from a study of (99m)Tc-extametazime-labeled cell visualization integrated with cardiac magnetic resonance infarct imaging. Circ Cardiovasc Imaging 2013;6:320-8.
17. Penicka M, Widimsky P, Kobylka P, Kozak T, Lang O. Images in cardiovascular medicine. Early tissue distribution of bone marrow mononuclear cells after transcoronary transplantation in a patient with acute myocardial infarction. Circulation 2005;112:e63-5.
18. Tossios P, Krausgrill B, Schmidt M et al. Role of balloon occlusion for mononuclear bone marrow cell deposition after intracoronary injection in pigs with reperfused myocardial infarction. Eur Heart J 2008;29:1911-21.
19. Ip JE, Wu Y, Huang J, Zhang L, Pratt RE, Dzau VJ. Mesenchymal stem cells use integrin beta1 not CXC chemokine receptor 4 for myocardial migration and engraftment. Mol Biol Cell 2007;18:2873-82.
20. Mareschi K, Ferrero I, Rustichelli D et al. Expansion of mesenchymal stem cells isolated from pediatric and adult donor bone marrow. J Cell Biochem 2006;97:744-54.
21. Uitterdijk A, Sneep S, van Duin RW et al. Serial measurement of hFABP and high-sensitivity troponin I post-PCI in STEMI: how fast and accurate can myocardial infarct size and no-reflow be predicted? Am J Physiol Heart Circ Physiol 2013;305:H1104-10.
22. Duncker DJ, Klassen CL, Ishibashi Y, Herrlinger SH, Pavek TJ, Bache RJ. Effect of temperature on myocardial infarction in swine. Am J Physiol 1996;270:H1189-99.
23. Cason BA, Gamperl AK, Slocum RE, Hickey RF. Anesthetic-induced preconditioning: previous administration of isoflurane decreases myocardial infarct size in rabbits. Anesthesiology 1997;87:1182-90.
24. McColgan P, Sharma P, Bentley P. Stem cell tracking in human trials: a meta-regression. Stem Cell Rev 2011;7:1031-40.
25. Frangogiannis NG. The inflammatory response in myocardial injury, repair, and remodelling. Nat Rev Cardiol 2014;11:255-65.
26. Ruparelia N, Digby JE, Jefferson A et al. Myocardial infarction causes inflammation and leukocyte recruitment at remote sites in the myocardium and in the renal glomerulus. Inflamm Res 2013;62:515-25.
27. Alon R, Kassner PD, Carr MW, Finger EB, Hemler ME, Springer TA. The integrin VLA-4 supports tethering and rolling in flow on VCAM-1. J Cell Biol 1995;128:1243-53.

***Table S1**. Studies on Intracoronary Cell Retention for Cardiac Cell Therapy*

Author	Species	# Cells injected ($1{\cdot}10^6$)	Cell type	Cell Size	Infusion parameters	Enrichment protocol	Tracking method	Timing of injection post MI	FU after injection	Cardiac Retention (%)	Cardiac Retention Absolute
Hofmann et al.(1) 2005)	Human	2540 24	BMC CD34+	-	4-5 injections	gelatine-polysuccinate immunomagnetically	Scintigraphy	5-10 days	50-75 min	2.1±0.4 25.7±7.3	$5.3{\cdot}10^7$ $6.2{\cdot}10^6$
Penicka et al.(2) (2005)	Human	2740	BMC	-	24ml total 4.5-5ml injections	-	Scintigraphy	9 days	2h 18h	5 1	$13.7{\cdot}10^7$ $27.4{\cdot}10^6$
Blocklet et al.(3) (2005)	Human	15	PBCD34$^+$	-	2-3x2ml	Cytapheresis + immunomagnetically	Scintigraphy	7-21 days	1 h	5.5±2.3	$0.8{\cdot}10^6$
Goussetis et al.(4) (2007)	Human	16	CD133$^+$ + CD133$^-$ CD34$^+$	-	5min/$2{\cdot}10^6$/min	Ficoll + immunomagnetically	Scintigraphy	45±36 months	1 h 24 h	9.2±3.6 6.8±2.4	$1.5{\cdot}10^6$ $1.1{\cdot}10^6$
Dedobbeleer et al.(5) (2009)	Human	18	CD34$^+$	-	3x2ml	Cytapheresis + immunomagnetically	Scintigraphy	20±2 months	1 h	3.2±0.6	$0.6{\cdot}10^6$
Silva et al. (2009)(6)	Human	100	BMMNC	-	10ml/3x2-3min ~$10{\cdot}10^6$ per min	Ficoll	Scintigraphy	5.5±1.3 days	4h 24h	16.1±7.1 10.3±6.4	$16.4{\cdot}10^6$ $10.3{\cdot}10^6$
Musialek et al.(7) (2010)	Human	4.2 4.5	CD34+	-	3x3.3ml in 3x3min 3x10ml bolus	Ficoll + immunomagnetically	Scintigraphy	6-14 days	1h	4.9±0.5 5.1±0.5	$0.21{\cdot}10^6$ $0.23{\cdot}10^6$
Moreira et al.(8) (2011)	Human	100	BMMNC	-	10ml/3x2-3min ~$10{\cdot}10^6$ per min	Ficoll	Scintigraphy	5.5±1.3 days	4h 24h	16.1 10.3	$16.4{\cdot}10^6$ $10.3{\cdot}10^6$
Musialek et al.(9) (2012)	Human	4.3	CD34+	-	30ml	Ficoll + immunomagnetically	Scintigraphy	5-10 days	1 h	5.2	$0.22{\cdot}10^6$
Hou et al.(10) (2005)	Pig	10	hPBMNC	-	30-45 sec	Ficoll	Scintigraphy	5-7 days	1h	2.6±0.3	$0.3{\cdot}10^6$
Freyman et al.(11) (2006)	Pig	50	Allogenic MSC	10-20μm	14ml/7x2 min $3.5{\cdot}10^6$ per min	Density gradient centrifugation	Scintigraphy	15 min	14±3 days	6	$2.9{\pm}1.0{\cdot}10^6$
Moelker et al.(12) (2006)	Pig	25	BMMNC	5-7μm	5ml/5min $5{\cdot}10^6$ per min	Lymphoprep	Histology	7 days	4 days	6.5	$1.6{\cdot}10^6$
Doyle et al.(13) (2007)	Pig	30	CPC	-	12ml/3x4ml/$2.5{\cdot}10^6$/ml $30{\cdot}10^6$ cells in 4ml/ 2min bolus/$15{\cdot}10^6$/min	Ficoll + Expansion	Scintigraphy	2 days	1 h	8.7±1.5 17.8±7.9	$2.6{\cdot}10^6$ $5.3{\cdot}10^6$
Tossios et al.(14) (2008)	Pig	100	BMMNC	-	20ml/4x1min $25{\cdot}10^6$ per min	Ficoll	Scintigraphy	5 days	1h 24h	4.1±1.1 3.0±0.6	$4.1{\cdot}10^6$ $3.0{\cdot}10^6$

***Table S1**. Continued*

Author	Species	# Cells injected ($1 \cdot 10^6$)	Cell type	Cell Size	Infusion parameters	Enrichment protocol	Tracking method	Timing of injection post MI	FU after injection	Cardiac Retention (%)	Cardiac Retention Absolute
Ly et al.(15) (2009)	Pig	20	MSC	-	5ml in 3min	Ex-vivo expansion	NIR	3-4 days	Immediately	1.3±0.8	$0.26 \cdot 10^6$
			BMMNC		$6.7 \cdot 10^6$ per min	Histopaque				0.8±0.1	$0.16 \cdot 10^6$
			PBMNC			Histopaque				0.8±0.1	$0.16 \cdot 10^6$
Hong et al.(16) (2014)	Pig	10	Allogenic	-	10ml/3x3min	-	Scintigraphy	6 days	1h	57.2±12.7	$5.7 \pm 1.0 \cdot 10^6$
			ASC		$1.1 \cdot 10^6$ per min				24h	22.6±5.5	$2.3 \pm 1.0 \cdot 10^6$
Uitterdijk et al. (2013)	Pig		BMMNC	6-12μm	$1 \cdot 10^6$ per min	Lymphoprep	Histology	3 days	1h	2.3±1.5	$0.7 \pm 0.4 \cdot 10^6$
		43			$5 \cdot 10^6$ per min			7 days		3.1±1.4	$1.1 \pm 0.5 \cdot 10^6$

BMC: bone marrow cells; PB: peripheral blood-derived; CD: cluster of differentiation; BMMNC: bone marrow-derived mononuclear cells; hPBMNC: human peripheral bone marrow mono nuclear cells; MSC: mesenchymal stem cells; CPC: circulating progenitor cells; ASC: adipose-derived stem cells.

SUPPLEMENTAL REFERENCES

1. Hofmann M, Wollert KC, Meyer GP et al. Monitoring of bone marrow cell homing into the infarcted human myocardium. Circulation 2005;111:2198-202.
2. Penicka M, Widimsky P, Kobylka P, Kozak T, Lang O. Images in cardiovascular medicine. Early tissue distribution of bone marrow mononuclear cells after transcoronary transplantation in a patient with acute myocardial infarction. Circulation 2005;112:e63-5.
3. Blocklet D, Toungouz M, Berkenboom G et al. Myocardial homing of nonmobilized peripheral-blood CD34+ cells after intracoronary injection. Stem Cells 2006;24:333-6.
4. Goussetis E, Manginas A, Koutelou M et al. Intracoronary infusion of CD133+ and CD133-CD34+ selected autologous bone marrow progenitor cells in patients with chronic ischemic cardiomyopathy: cell isolation, adherence to the infarcted area, and body distribution. Stem Cells 2006;24:2279-83.
5. Dedobbeleer C, Blocklet D, Toungouz M et al. Myocardial homing and coronary endothelial function after autologous blood CD34+ progenitor cells intracoronary injection in the chronic phase of myocardial infarction. J Cardiovasc Pharmacol 2009;53:480-5.
6. Silva SA, Sousa AL, Haddad AF et al. Autologous bone-marrow mononuclear cell transplantation after acute myocardial infarction: comparison of two delivery techniques. Cell Transplant 2009;18:343-52.
7. Musialek P, Tekieli L, Kostkiewicz M et al. Randomized transcoronary delivery of CD34(+) cells with perfusion versus stop-flow method in patients with recent myocardial infarction: Early cardiac retention of (9)(9)(m)Tc-labeled cells activity. J Nucl Cardiol 2011;18:104-16.
8. Moreira Rde C, Haddad AF, Silva SA et al. Intracoronary stem-cell injection after myocardial infarction: microcirculation sub-study. Arq Bras Cardiol 2011;97:420-6.
9. Musialek P, Tekieli L, Kostkiewicz M et al. Infarct size determines myocardial uptake of CD34+ cells in the peri-infarct zone: results from a study of (99m)Tc-extametazime-labeled cell visualization integrated with cardiac magnetic resonance infarct imaging. Circ Cardiovasc Imaging 2013;6:320-8.
10. Hou D, Youssef EA, Brinton TJ et al. Radiolabeled cell distribution after intramyocardial, intracoronary, and interstitial retrograde coronary venous delivery: implications for current clinical trials. Circulation 2005;112:I150-6.
11. Freyman T, Polin G, Osman H et al. A quantitative, randomized study evaluating three methods of mesenchymal stem cell delivery following myocardial infarction. Eur Heart J 2006;27:1114-22.
12. Moelker AD, Baks T, van den Bos EJ et al. Reduction in infarct size, but no functional improvement after bone marrow cell administration in a porcine model of reperfused myocardial infarction. Eur Heart J 2006;27:3057-64.
13. Doyle B, Kemp BJ, Chareonthaitawee P et al. Dynamic tracking during intracoronary injection of 18F-FDG-labeled progenitor cell therapy for acute myocardial infarction. J Nucl Med 2007;48:1708-14.
14. Tossios P, Krausgrill B, Schmidt M et al. Role of balloon occlusion for mononuclear bone marrow cell deposition after intracoronary injection in pigs with reperfused myocardial infarction. Eur Heart J 2008;29:1911-21.
15. Ly HQ, Hoshino K, Pomerantseva I et al. In vivo myocardial distribution of multipotent progenitor cells following intracoronary delivery in a swine model of myocardial infarction. Eur Heart J 2009;30:2861-8.
16. Hong KU, Guo Y, Li QH et al. c-kit+ Cardiac Stem Cells Alleviate Post-Myocardial Infarction Left Ventricular Dysfunction Despite Poor Engraftment and Negligible Retention in the Recipient Heart. PLoS One 2014;9:e96725.

PART II

Acute Myocardial Infarction and Reperfusion Injury

CHAPTER 6

Limitation of Infarct Size and No-Reflow by Intracoronary Adenosine Depends Critically on Dose and Duration

*Tuncay Yetgin
***André Uitterdijk**
Maaike te Lintel Hekkert
Daphne Merkus
Ilona Krabbendam-Peters
Heleen MM van Beusekom
Robert Falotico
Patrick W Serruys
Olivier C Manintveld
Robert-Jan M van Geuns
Felix Zijlstra
Dirk J Duncker

*Both authors contributed equally

Submitted

ABSTRACT

Objectives In the absence of effective clinical pharmacotherapy for prevention of reperfusion-mediated injury, we re-evaluated the effects of intracoronary adenosine on infarct size (IS) and no-reflow in a porcine model of acute myocardial infarction (AMI) using clinical bolus and experimental high-dose infusion regimens.

Background Despite the clear cardioprotective effects of adenosine, when administered prior to ischemia, studies on cardioprotection by adenosine when administered at reperfusion have yielded contradictory results both in the pre-clinical and clinical setting.

Methods Swine (~60 kg) were subjected to a 45-min mid-LAD occlusion followed by 2 h of reperfusion. In protocol A, an intracoronary bolus of 3 mg adenosine injected over 1 min (n=5) or saline (n=10) was administered at reperfusion. In protocol B, an intracoronary infusion of 50 μg/kg/min adenosine (n=15) or saline (n=21) was administered starting 5 min prior to reperfusion and continued throughout the 2-h reperfusion period.

Results In protocol A, area-at-risk, IS and no-reflow were similar between groups. In protocol B, risk zones were similar, but administration of adenosine resulted in significant reductions in IS from 59±3% of the area-at-risk in control swine to 46±4% (p=0.02), and no-reflow from 49±6% of the infarct-area to 26±6% (p=0.03).

Conclusion During reperfusion, intracoronary adenosine can limit IS and no-reflow in a porcine model of AMI. However protection was only observed when adenosine was administered via prolonged high-dose infusion, and not via short-acting bolus injections. These findings warrant reconsideration of adenosine as an adjuvant therapy during early reperfusion.

INTRODUCTION

Timely reperfusion remains the single most effective treatment of acute myocardial infarction (AMI) for salvaging ischemic myocardium, leading to improved residual ventricular function and clinical outcome (1). However, reperfusion itself initiates a cascade of harmful events, termed lethal reperfusion-injury, which is characterized by mitochondrial damage and cardiomyocyte death (2,3), and by ultrastructural damage to capillary endothelium, leading to microvascular obstruction, termed no-reflow (4). Since lethal reperfusion injury may account for up to 50% of the final myocardial infarct size (IS) (3), while no-reflow is associated with poor clinical prognosis (5), it is clear that reperfusion-injury constitutes a key therapeutic target.

Adenosine exerts a variety of actions that may attenuate many of the proposed mechanisms of reperfusion-mediated injury, including inhibition of neutrophil-mediated vascular damage and preservation of microvascular flow, restoration of calcium homeostasis, inhibition of oxidative stress and mediation of pre-, post- and remote conditioning (6-9). Yet, attempts to achieve cardioprotection with administration of adenosine at reperfusion have yielded mixed results in both pre-clinical and clinical studies (6-9). For example, recent clinical studies utilizing adenosine bolus injections in AMI were unable to reduce IS (10,11). Inconsistent results may be related to several factors, including the availability of adenosine at an optimal concentration at reperfusion and a brief window for therapeutic application. In addition, the optimal dosage for efficacious adenosine treatment in AMI has remained undefined in both experimental and clinical settings. Given the present clinical lack of adjuvant pharmacotherapy to prevent reperfusion-mediated injury, re-evaluation of adenosine in the setting of AMI would be of great interest, taking aforementioned considerations into account.

Accordingly, we employed an appropriate translational porcine model of ischemia-reperfusion to re-evaluate the effects of intracoronary bolus injections of adenosine at reperfusion on IS and no-reflow with doses equivalent to clinical trials. Subsequently, we investigated the cardioprotective effects of a high-dose, prolonged intracoronary infusion of adenosine.

METHODS

Experiments were performed in Yorkshire x Landrace swine of either sex weighing 55-60 kg in the ischemia-reperfusion study. All procedures were performed in compliance with the *"Guiding principles in the care and use of animals"* as approved

by the Council of the American Physiological Society and under the regulations of the Animal Care Committee of the Erasmus University Rotterdam.

Experimental protocol

All animals were subjected to regional ischemia by occluding the mid-LAD for 45 min followed by 2 h of reperfusion. In protocol A, animals received an intracoronary adenosine bolus injection at reperfusion (3 mg in 1 ml injected over 1 min) or intracoronary saline. The dose per kg bodyweight and timing of injection approximated or was similar to that employed in clinical studies (**Supplemental Table S1**). In protocol B, animals received an intracoronary adenosine infusion of 50 μg/kg/min starting at 40 min of occlusion (5 min prior to reperfusion) and continuing until the end of reperfusion (infusion rate: 0.67 ml/min) or saline. The dose of 50 μg/kg/min adenosine was determined in dose-finding studies available in the **Supplemental Study**.

Surgical preparation and procedures

Swine were sedated with ketamine (20 mg/kg, i.m.) and midazolam (1 mg/kg, i.m.), anesthetized with sodium pentobarbital (15 mg/kg, i.v.), intubated, and placed on a positive-pressure ventilator (O_2:N_2=1:3 v/v). Electrocardiographic electrodes for the limb leads were placed subcutaneously. Catheters were inserted into the right external jugular vein for infusion of saline, drugs and sodium pentobarbital (10-15 mg/kg/h) to maintain anesthesia. A micromanometer-tipped catheter (Millar Instruments, Houston, TX, USA) was advanced into the left ventricle (LV) via the right external carotid artery to measure LV pressure and its first derivative (dP/dt). A fluid-filled catheter was inserted via the left femoral artery into the aorta to measure arterial pressure and to obtain blood samples for measurement of arterial blood gases. A Swan-Ganz catheter was advanced into the pulmonary artery via the left femoral vein to measure pulmonary artery pressure and to monitor core temperature. Arterial blood gases were checked periodically and ventilation settings were adjusted as necessary to maintain blood gases within the physiological range.

A median sternotomy was performed and the pericardium was opened. An electromagnetic flow probe was placed around the ascending aorta for measurement of cardiac output. A segment (2-3 cm) of the left anterior descending coronary artery (LAD) was isolated just distal to the first diagonal branch. Following isolation, the LAD was instrumented from proximal to distal with a surgical monofilament ligature around the vessel for later occlusion; a transit-time flow probe (Transonic

Systems, Ithaca, NY, USA) for coronary blood flow (CBF) measurements; and a 22-gauge, non-obstructing, intracoronary catheter for administration of adenosine or saline. The anterior interventricular vein was cannulated with a 20-gauge catheter for coronary venous blood sampling. For measurement of atrial pressure, a catheter was inserted into the left atrial appendage. For measurement of regional contractile function, two pairs of ultrasonic crystals (Triton Technology Inc., San Diego, USA) were implanted in the mid-myocardium of area-at-risk (AR) and remote myocardium (12).

After completion of surgical instrumentation, a stabilization period of 30 min was permitted to assure hemodynamic stability before the onset of coronary occlusion. Systemic and coronary hemodynamics, regional contractile function, electrocardiographic changes and core temperature were monitored and recorded throughout the experiment. Arterial and coronary venous blood samples were obtained serially at several time points. Anticoagulation was ensured using heparin (5000 IU/h, i.v.). Animals that developed ventricular fibrillation (VF) during the protocol were defibrillated using internal paddles (30-50 J, direct current).

Myocardial oxygen balance

Measurements of Po_2 (mmHg), Pco_2 (mmHg), pH, oxygen saturation and hemoglobin concentration (grams/100 ml) were performed with a blood gas analyzer (ABL 800, Radiometer, Copenhagen, Denmark). Blood oxygen content, myocardial oxygen delivery, myocardial oxygen consumption in the LAD region and myocardial oxygen extraction were computed as previously described (13).

Area-at-risk, infarct size and no-reflow

At the end of the 2-h reperfusion period, the LAD was perfused with 5 ml of 4% thioflavin-S (Sigma, Zwijndrecht, the Netherlands) for determination of no-reflow area (NA) (14). Hereafter, the LAD was re-occluded and 40 ml of 16% Evans Blue (Sigma, Zwijndrecht, the Netherlands) was infused intra-atrial for AR determination (12). The heart was then excised and the LV was isolated and sectioned into 5 transversal segments of equal thickness parallel to the atrioventricular groove from apex to base. The AR and NA (using UV-light) of each slice were demarcated on an acetate sheet (14). The slices were incubated for 15 min in 3% buffered triphenyltetrazolium chloride (Sigma, Zwijndrecht, the Netherlands) at 37°C for determination of the infarct area (IA) (12,14). Myocardial IS was calculated as ratio (expressed as a percentage) of summed IA and summed LV (IA/LV•100%) or summed AR (IA/AR•100%). No-reflow was calculated as ratio (expressed as

a percentage) of summed NA and summed LV (NA/LV•100%), summed AR (NA/AR•100%) or summed IA (NA/IA•100%).

Neutrophils

Sections of IA, with either reflow or no-reflow, and remote non-AR (posterior wall) LV tissue were fixed in 4% buffered formaldehyde for at least 24 hours, dehydrated in graded ethanol, cleared in xylene and embedded in paraffin. 4-μm sections were stained to identify acute influx of neutrophils (Azurocidin, mouse anti human, 1:100, Abnova, Heidelberg, Germany) following antigen retrieval (10 min citrate buffer boil [pH 6]). Rabbit anti mouse secondary antibodies were used (1:100, horseradish peroxidase label, DAKO, Heverlee, Belgium) with diaminobenzidine as chromogen. Primary antibodies were omitted as a negative control. Three randomly selected high power fields (90.000 μm^2/field) per section were morphometrically quantified (Clemex Vision PE, version 6.0.010A, Clemex Technologies inc, Longueuil, Canada).

Statistical analysis

Data are presented as mean±SEM. Hemodynamic variables, myocardial metabolism, global and regional ventricular function and neutrophil infiltration were analyzed with a repeated-measures two-way analysis of variance (time x treatment) followed by the Student-Newman-Keuls post-hoc test. Infarct and no-reflow data were compared with unpaired Student's *t*-test. Computations were performed with SigmaPlot version 12.5 (Systat Software Inc., San Jose, CA, USA), with statistical significance set at $P<0.05$ (two-tailed).

RESULTS

Numbers of animals enrolled in each group and the exclusions are summarized in **Table 1**. A total number of 70 swine were enrolled, of which 51 swine were included in the final analysis. An overview of arrhythmias during the protocols is provided in **Table 2**.

Regional myocardial function and myocardial metabolism of animals are available in **Supplemental Tables S2** and **S3**, respectively.

Table 1. *Enrollment summary*

	Bolus Injection		Prolonged Infusion	
	Control	Adenosine	Control	Adenosine
Animals entered	11	11	26	22
Exclusions				
Technical failure*	0	3	1	1
Staining failure†	1	0	0	1
Death				
Non-convertible ventricular fibrillation during occlusion‡	0	3	2	4
Acute pump failure	0	0	2	1
Final number entered in analysis	**10**	**5**	**21**	**15**

Data presented as *N*. *Technical difficulties resulting in failure to complete entire protocol. †Staining difficulties compromising accurate measurement of infarct size and/or no-reflow. ‡Occurring during the first 40 min of occlusion, i.e. prior to adenosine treatment; none of the animals developed non-convertible ventricular fibrillation during reperfusion

Table 2. *Arrhythmias in surviving animals*

	Bolus Injection		Prolonged Infusion	
	Control (*N* = 10)	Adenosine (*N* = 5)	Control (*N* = 21)	Adenosine (*N* = 15)
Convertible VF, *N*	9	5	13	9
Occlusion 0-40 min, *N*	9	4	13	8
No. of episodes, mean ± SEM*	2.2 ± 0.4	4.3 ± 1.5	2.0 ± 0.3	2.0 ± 0.3
Occlusion 40-45 min, *N*	0	0	0	1
No. of episodes, mean ± SEM*	0	0	0	1.0
Reperfusion, *N*	3	1	1	1
No. of episodes, mean ± SEM*	1.0 ± 0.0	1.0	2.0	1.0

VF indicates ventricular fibrillation. *Mean number of episodes only in animals developing ventricular fibrillation.

Systemic hemodynamics

Changes in hemodynamic data for heart rate, mean aortic pressure, cardiac output, systemic vascular resistance, LV dP/dt_{P40}, and LV end-diastolic pressure in protocols A and B are summarized in **Table 3**. Coronary occlusion was associated with similar increases in heart rate and LV end-diastolic pressure, and similar decreases in mean aortic pressure, cardiac output and dP/dt_{P40} in the adenosine and control groups in both protocols. Treatment with adenosine during reperfusion did not affect any of the systemic hemodynamic variables compared to controls.

Table 3. *Systemic hemodynamics and global left ventricular function*

			Coronary Artery Occlusion			Reperfusion			
		Baseline	**5 min CAO**	**40 min CAO**	**45 min CAO**	**5 min Rep**	**15 min Rep**	**60 min rep**	**120 min Rep**
Bolus Injection									
HR (bmp)	Control	98 ± 4	99 ± 4	103 ± 3	102 ± 3	103 ± 4	99 ± 3	105 ± 5	111 ± 5
	Adenosine	120 ± 5	117 ± 1	120 ± 12	118 ± 11	119 ± 13	123 ± 10	122 ± 9	125 ± 12
MAP (mmHg)	Control	86 ± 2	73 ± 4*	67 ± 3*	66 ± 3*	66 ± 3*	65 ± 2*	62 ± 3*	61 ± 3*
	Adenosine	89 ± 5	89 ± 7	69 ± 9*	69 ± 9*	63 ± 6*	67 ± 10*	66 ± 9*	67 ± 7*
CO (L/min)	Control	3.3 ± 0.2	2.9 ± 0.2*	2.9 ± 0.2*	2.8 ± 0.2*	3.0 ± 0.2*	3.0 ± 0.2*	2.8 ± 0.2*	2.2 ± 0.3*
	Adenosine	4.1 ± 0.4†	4.3 ± 0.4	3.9 ± 0.3	3.8 ± 0.3	2.9 ± 0.6	3.3 ± 0.8	3.7 ± 0.3	2.7 ± 0.4*
SVR (L/min/mmHg)	Control	27 ± 2	27 ± 3	24 ± 2	25 ± 3	23 ± 2	23 ± 2	22 ± 2	30 ± 3
	Adenosine	23 ± 1	21 ± 3	21 ± 1	21 ± 1	20 ± 1	21 ± 2	21 ± 1	29 ± 5
$LVdPdt_{P40}$ (mmHg/s)	Control	1380 ± 100	1080 ± 90*	1030 ± 80*	990 ± 80*	1010 ± 70*	1010 ± 70*	940 ± 100*	830 ± 90*
	Adenosine	1690 ± 220	1660 ± 450	1170 ± 280*	1190 ± 280*	870 ± 210*	1180 ± 300*	1160 ± 240*	1190 ± 270*
LVEDP (mmHg)	Control	11 ± 1	13 ± 1	13 ± 1*	14 ± 1	15 ± 1*	15 ± 1*	13 ± 1	12 ± 1
	Adenosine	10 ± 1	10 ± 1	13 ± 1	13 ± 1	15 ± 2*	13 ± 1*	12 ± 1	12 ± 1

Table 3. *Continued*

			Coronary Artery Occlusion			Reperfusion			
		Baseline	**5 min CAO**	**40 min CAO**	**45 min CAO**	**5 min Rep**	**15 min Rep**	**60 min rep**	**120 min Rep**
Prolonged infusion									
HR (bmp)	Control	100 ± 4	102 ± 4	109 ± 5*	108 ± 5	11 ± 4*	107 ± 4	109 ± 4*	105 ± 3
	Adenosine	94 ± 4	98 ± 6	97 ± 5	96 ± 4	103 ± 4	100 ± 4	101 ± 4	101 ± 4
MAP (mmHg)	Control	90 ± 2	76 ± 2*	78 ± 3*	77 ± 2*	70 ± 2*	72 ± 2*	68 ± 2*	67 ± 3*
	Adenosine	88 ± 2	75 ± 3*	79 ± 3*	76 ± 3*	71 ± 4*	71 ± 3*	65 ± 3*	64 ± 3*
CO (L/min	Control	3.6 ± 0.2	3.2 ± 0.2*	3.1 ± 0.1*	3.0 ± 0.1*	3.0 ± 0.1*	2.9 ± 0.1*	2.8 ± 0.1*	2.4 ± 0.1*
	Adenosine	2.9 ± 0.2†	2.6 ± 0.2*	2.7 ± 0.2	2.6 ± 0.2	2.6 ± 0.2	2.7 ± 0.2	2.6 ± 0.2*	2.5 ± 0.1*
SVR (L/min/mmHg)	Control	26 ± 1	25 ± 1	26 ± 1	26 ± 1	24 ± 1*	25 ± 1	25 ± 1	28 ± 1*
	Adenosine	31 ± 2†	30 ± 1	31 ± 2	30 ± 2	28 ± 2*	28 ± 2*	26 ± 2*	26 ± 1*
$LVdPdt_{P40}$ (mmHg/s)	Control	1500 ± 100	1270 ± 70*	1260 ± 60*	1250 ± 50*	1140 ± 60*	1220 ± 70*	1120 ± 60*	1030 ± 50*
	Adenosine	1310 ± 120	1050 ± 80*	1170 ± 110	1160 ± 110*	1070 ± 110*	1110 ± 100*	1010 ± 100*	960 ± 90*
LVEDP (mmHg)	Control	13 ± 1	14 ± 1	15 ± 1*	14 ± 1*	16 ± 1*	16 ± 1*	15 ± 1*	14 ± 1*
	Adenosine	12 ± 1	13 ± 1	13 ± 1	13 ± 1	14 ± 1*	14 ± 1*	13 ± 1	12 ± 1

Data are presented as mean ± SEM. *P<0.05 vs. corresponding baseline. †P<0.05 vs. corresponding control. CAO indicates coronary artery occlusion; CO cardiac output; $dP/dt_{P=40}$, index of cardiac contractility during LV pressure of 40 mmHg; HR, heart rate; LV, left ventricular; LVEDP, left ventricular end-diastolic pressure; MAP, mean arterial pressure; Rep, reperfusion and SVR, systemic vascular resistance (MAP/CO).

Coronary hemodynamics

Release of the coronary ligature resulted in reactive hyperemia reflected by increases in CBF and coronary vascular conductance in both groups (**Table 4; Figure 1**). In protocol A, adenosine did not increase CBF beyond the reactive hyperemia produced by the ischemic period. In protocol B, adenosine infusion enhanced reactive hyperemia reaching significance at 5 min of reperfusion, which was maintained throughout the remainder of the 2-h reperfusion period, with a maximum fourfold increase relative to baseline at 30 min of reperfusion (**Figure 1**).

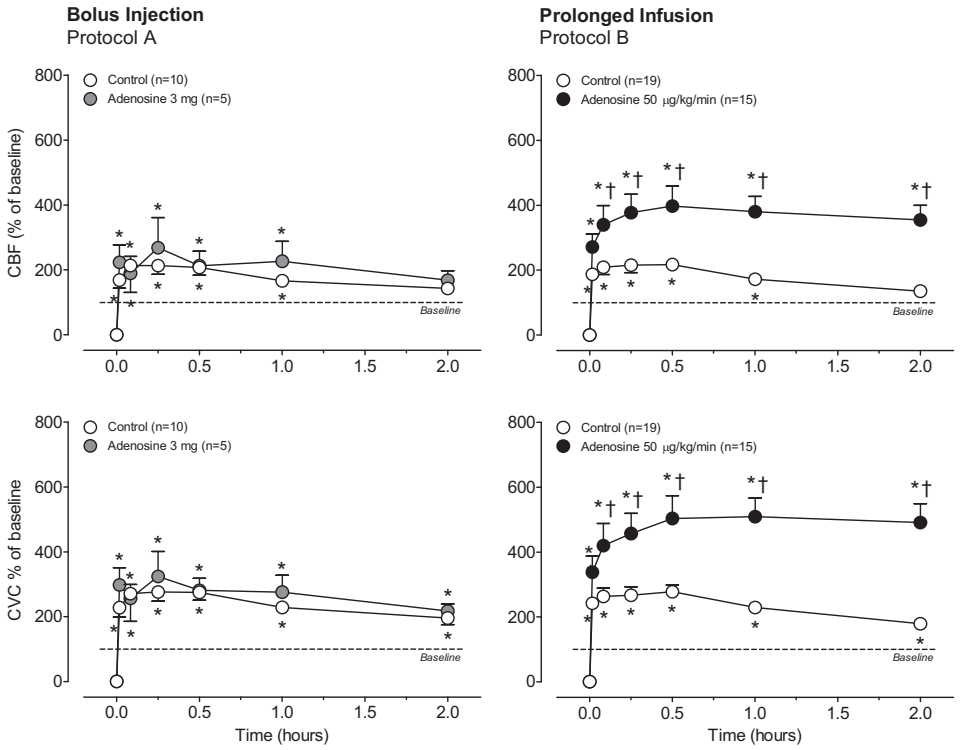

Figure 1. *Coronary Blood Flow*
**P<0.05 vs. corresponding baseline. †P<0.05 vs. corresponding control. Intracoronary adenosine infusion significantly increased coronary blood flow and coronary vascular conductance compared with controls throughout the 2-h reperfusion period, whereas bolus injections did not.*

Table 4. *Coronary hemodynamics*

			Reperfusion				
		Baseline	**1 min Rep**	**5 min Rep**	**15 min Rep**	**60 min Rep**	**120 min Rep**
Bolus Injection							
CBF (mL/min)	Control	15 ± 1	24 ± 2*	31 ± 3*	31 ± 4*	25 ± 3*	21 ± 3
	Adenosine	15 ± 5	28 ± 7*	25 ± 7	33 ± 9*	30 ± 7*	24 ± 8
CVC (mL/min/mmHg)	Control	0.18 ± 0.02	0.37 ± 0.03*	0.46 ± 0.05*	0.48 ± 0.05*	0.42 ± 0.05*	0.34 ± 0.05*
	Adenosine	0.16 ± 0.05	0.44 ± 0.09*	0.37 ± 0.10*	0.46 ± 0.10*	0.43 ± 0.12*	0.34 ± 0.10*
Prolonged Infusion							
CBF (mL/min)	Control	17 ± 2	29 ± 3*	31 ± 3*	32 ± 4	27 ± 3*	21 ± 2*
	Adenosine	11 ± 1	27 ± 4*	32 ± 3*	37 ± 3*	38 ± 4*‡	35 ± 3*‡
CVC (mL/min/mmHg)	Control	0.19 ± 0.03	0.41 ± 0.03*	0.43 ± 0.04*	0.43 ± 0.04*	0.39 ± 0.04*	0.31 ± 0.03*
	Adenosine	0.13 ± 0.01	0.38 ± 0.05*	0.45 ± 0.03*	0.51 ± 0.04*	0.58 ± 0.05*‡	0.55 ± 0.04*‡

Data are presented as mean ± SEM. *P<0.05 vs. corresponding baseline. ‡P<0.05 vs. change by control. CBF indicates coronary blood flow and CVC, coronary vascular conductance.

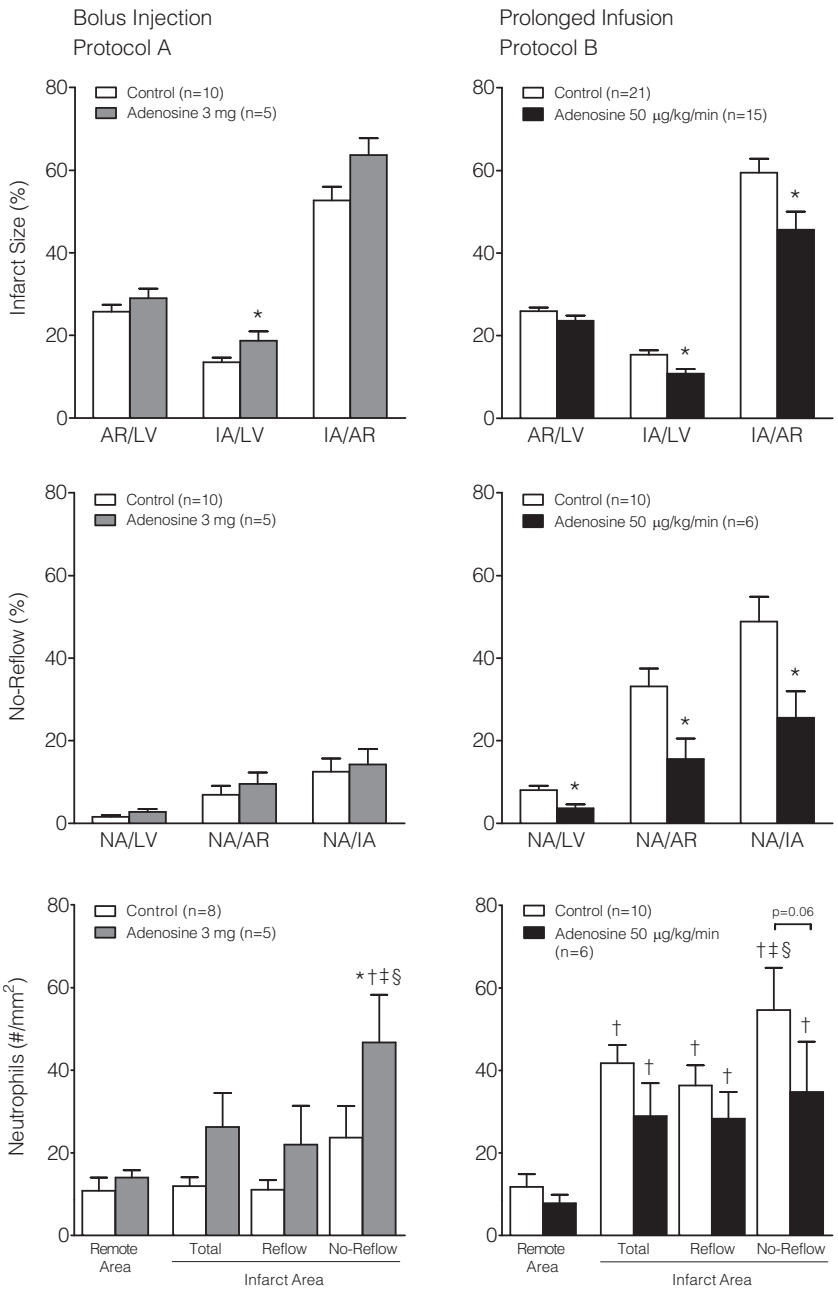

Figure 2. *Infarct size, no-reflow and neutrophil influx*
*Values are group means with SEM. *P<0.05. †P<0.05 vs. remote. ‡P<0.05 vs. reflow IA. §P<0.05 vs. total IA. Risk zone (AR/LV) was similar between groups in both protocols. Intracoronary adenosine infusion significantly reduced infarct size (IA/AR), no-reflow (NA/IA) and neutrophil influx in both infarct and no-reflow areas compared with controls, whereas bolus injections did not.*

Area-at-risk, infarct size, no-reflow

The area-at-risk, infarct size and extent of no-reflow are shown in **Figure 2**. AR was similar between adenosine and control groups in both protocols. Bolus injection of adenosine did not reduce IS (64±4% vs. 53±3% in controls; p=0.07) or no-reflow (14±4% vs. 12±3% in controls; p=0.74). Infusion of adenosine during reperfusion significantly reduced IS (46±4% vs. 59±3%; p=0.02) as well as no-reflow (26±6% vs. 49±6%; p=0.03) compared with controls.

Neutrophils

Neutrophil influx in remote and IA in both protocols are shown in **Figure 2** (bottom panels). Adenosine bolus did not attenuate neutrophil influx into the NA, whereas adenosine infusion blunted (p=0.06) neutrophil-influx in the NA.

DISCUSSION

In the present study, an intracoronary infusion of high-dose adenosine (50 μg/kg/min) initiated shortly before the onset of reperfusion and maintained throughout the 2-h reperfusion period resulted in a significant decrease in both infarct size and no-reflow in an open-chest porcine model subjected to 45 min of coronary occlusion and 2 h of reperfusion. In contrast, a single bolus of adenosine (3 mg over 1 min) during the first min of reperfusion was ineffective. This is, to our knowledge, the first study to directly compare the cardioprotection afforded by adenosine in a clinical bolus regimen versus a prolonged infusion regimen, against infarction and no-reflow in a large animal model of regional ischemia-reperfusion.

The present study confirms recent clinical studies that have failed to demonstrate any significant advantage on either IS (10,11,15) or no-reflow (10,11,16), using intracoronary adenosine bolus injections. Considering the extremely short half-life of adenosine, the bolus injections probably were inadequate to reach therapeutic concentrations, as reflected by unaltered coronary hemodynamics in protocol A. In this regard, prolonged intracoronary delivery initiated just before reperfusion may increase local drug concentration several fold and may achieve adequate concentration levels in the target microvascular bed, thereby potentially improving therapeutic efficacy. Consequently, in protocol B, intracoronary infusion of adenosine was initiated 5 min before the onset of reperfusion, enabling therapeutic drug levels at reperfusion, and thereby contributing to the attenuation of lethal reperfusion injury by inhibiting detrimental events in the early minutes of reperfusion as reflected by significant IS reduction. However, the beneficial effects

observed in the current study with prolonged infusion of adenosine also suggest that maintaining a high therapeutic drug level in the coronary microcirculation is necessary to afford protection against reperfusion-mediated injury. Indeed, intracoronary adenosine produced a 3- to 4-fold increase in CBF relative to baseline and remained stably elevated throughout the 2-h infusion period compared with control animals, affording adequate concentration levels in the target microvascular bed. In addition, administration of adenosine resulted in reduced neutrophil influx into the IA, including NA. These observations suggest that adenosine attenuated no-reflow, at least in part, through vasodilation of coronary arterioles and reduction of neutrophil activation. These aspects in turn likely contributed to decreased neutrophil adherence to endothelial cells, thereby leading to preserved capillary endothelial patency, as evidenced by thioflavin-S staining.

Although the current results in swine are in agreement with earlier studies in rabbits and dogs demonstrating IS reduction with adenosine infusions at reperfusion, not all pre-clinical studies have shown cardioprotective effects (**Supplemental Table S4**). Inspection of **Table S4** does not readily reveal a methodological explanation for these mixed results. Thus, differences in species, duration of ischemia and reperfusion, varying routes and timing and duration of administration of adenosine do not appear to separate positive from negative studies in rabbits and dogs. Interestingly, none of the aforementioned negative (and positive) studies specifically assessed the optimal dose for infusion of adenosine. Thus, it cannot be excluded that in several studies, the dose employed may have been insufficient to afford myocardial protection for a given duration of ischemia and reperfusion. This is particularly true in the case of intravenous adenosine administration, as maximal doses are difficult to achieve in view of the marked systemic hypotension that is associated with higher adenosine doses. That cardioprotection was still observed in some of the intravenous studies may have been the result of stimulation of remote pathways of cardioprotection (17,18). Whether maximal adenosine dosages were achieved in clinical studies using intravenous adenosine is also unclear. The AMISTAD-I trial tested a 3-h intravenous adenosine infusion (10-70 μg/kg/min) in patients receiving thrombolysis and demonstrated adenosine to be effective in reducing IS in the subgroup with anterior infarction only (19). In the AMISTAD-II trial, adenosine infusions (50 or 70 μg/kg/min) were utilized for anterior infarction prior to revascularization with IS reduction observed only in the high-dose group (20) and a reduction in major clinical endpoints observed only in patients receiving early reperfusion (within 3.2 h of symptom onset) (21).

In contrast, the intracoronary route allows administration of much higher adenosine doses without direct systemic adverse effects. However, in the clinical setting, the administration of adenosine via the intracoronary route has been studied mainly using bolus injections (**Supplemental Table S1**). One could assume that the very short biological half-life of adenosine (<15 s) makes a bolus injection unlikely to be effective. Indeed, in the present study, mimicking a typical clinical protocol of intracoronary adenosine bolus administration, we failed to observe any increase in CBF or coronary vascular conductance upon reperfusion. This lack of effect on the coronary microvasculature may explain that intracoronary bolus injections of adenosine failed to reduce either IS (10,11,15) or no-reflow (10,11,16). Another important issue in the clinical context is patient selection. Despite the failure to significantly impact on IS, adenosine bolus regimens have been found to improve various indices of reperfusion in patients presenting with TIMI flow ≤2 (15,22), whereas, trials also recruiting patients with presenting TIMI-3 flow (i.e. patients experiencing spontaneous reperfusion) were unable to demonstrate any advantage of intracoronary bolus injections of adenosine on IS or reperfusion markers (10,11). These data suggest that adenosine should be administered before or, at least, at the very onset of reperfusion and highlight the brief window of opportunity. The only clinical trial that did utilize a continuous intracoronary infusion regimen (albeit for only 5-10 min) showed accelerated recovery of microvascular perfusion in case of persistent ST-elevation after percutaneous coronary intervention (23). This suggests that adenosine can still be effective even after suboptimal myocardial reperfusion provided adequate dosing and duration of administration is utilized, a finding consistent with the present results. Interestingly, recent data have pointed to an increased beneficial effect of a combined adenosine bolus (120 μg) and infusion (2 mg in 2 min) regimen as evidenced by a reduced IS and an improved microvascular perfusion (24) which translated into an improvement of LV remodeling at 1-year clinical follow-up (25).

Barriers to clinical translation

The obvious differences between the experimental setting and the clinical reality constitute important barriers to efficacious clinical translation. Patient co-morbidities and concurrent use of medication with cardioprotective properties may be potential confounding factors blunting the benefits reported in the pre-clinical setting. Perhaps more importantly, therapeutic optima for adenosine treatment at reperfusion in animal models of ischemia-reperfusion have not been established. Therefore, it is not surprising that results obtained from clinical studies are inconclusive, as optimal conditions for efficacious adenosine administration remain

undefined. Notwithstanding these issues, pre-clinical and clinical data suggest that only (sustained) high doses of adenosine, reaching the coronary microcirculation immediately before or at the onset of reflow, are able to afford protection against reperfusion-mediated injury at a time when the amount of potentially salvageable myocardium is large.

Limitations

First, we employed healthy juvenile animals in our experiments without co-morbidities as encountered in patients. Second, the exact mechanisms of adenosine-mediated protection were not assessed. Nonetheless, there is abundant data regarding the mechanisms through which adenosine is effective in ameliorating reperfusion-mediated injury (6). Third, likely as a result of seasonal variation (unpublished observations), NA/AR was smaller in controls in protocol A compared with controls in protocol B. Importantly, control swine were time-matched to the adenosine swine within each protocol.

CONCLUSIONS

Prolonged high-dose intracoronary infusion of adenosine starting just prior to reperfusion, but not a single bolus of adenosine administered during early reperfusion, significantly reduced IS and no-reflow in a porcine model of AMI. Considering that there is currently no successful clinical pharmacological treatment for prevention of reperfusion-mediated injury, the findings in the present study warrant further clinical studies in patients with AMI, using prolonged high-dose intracoronary adenosine infusion.

ACKNOWLEDGEMENTS

The authors are indebted to Prof. Wim J. van der Giessen who contributed significantly to the study design, but passed away before finalizing the present work.

REFERENCES

1. Task Force on the management of STseamiotESoC, Steg PG, James SK et al. ESC Guidelines for the management of acute myocardial infarction in patients presenting with ST-segment elevation. Eur Heart J 2012;33:2569-619.
2. Braunwald E, Kloner RA. Myocardial reperfusion: a double-edged sword? J Clin Invest 1985;76:1713-9.
3. Yellon DM, Hausenloy DJ. Myocardial reperfusion injury. N Engl J Med 2007;357:1121-35.
4. Kloner RA, Ganote CE, Jennings RB. The “no-reflow” phenomenon after temporary coronary occlusion in the dog. J Clin Invest 1974;54:1496-508.
5. Ndrepepa G, Tiroch K, Fusaro M et al. 5-year prognostic value of no-reflow phenomenon after percutaneous coronary intervention in patients with acute myocardial infarction. J Am Coll Cardiol 2010;55:2383-9.
6. Forman MB, Stone GW, Jackson EK. Role of adenosine as adjunctive therapy in acute myocardial infarction. Cardiovasc Drug Rev 2006;24:116-47.
7. Hausenloy DJ, Yellon DM. Remote ischaemic preconditioning: underlying mechanisms and clinical application. Cardiovasc Res 2008;79:377-86.
8. Cohen MV, Downey JM. Adenosine: trigger and mediator of cardioprotection. Basic Res Cardiol 2008;103:203-15.
9. Dirksen MT, Laarman GJ, Simoons ML, Duncker DJ. Reperfusion injury in humans: a review of clinical trials on reperfusion injury inhibitory strategies. Cardiovasc Res 2007;74:343-55.
10. Desmet W, Bogaert J, Dubois C et al. High-dose intracoronary adenosine for myocardial salvage in patients with acute ST-segment elevation myocardial infarction. Eur Heart J 2011;32:867-77.
11. Fokkema ML, Vlaar PJ, Vogelzang M et al. Effect of high-dose intracoronary adenosine administration during primary percutaneous coronary intervention in acute myocardial infarction: a randomized controlled trial. Circ Cardiovasc Interv 2009;2:323-9.
12. Koning MM, Gho BC, van Klaarwater E, Opstal RL, Duncker DJ, Verdouw PD. Rapid ventricular pacing produces myocardial protection by nonischemic activation of KATP+ channels. Circulation 1996;93:178-86.
13. Te Lintel Hekkert M, Dube GP, Regar E et al. Preoxygenated hemoglobin-based oxygen carrier HBOC-201 annihilates myocardial ischemia during brief coronary artery occlusion in pigs. Am J Physiol Heart Circ Physiol;298:H1103-13.
14. Uitterdijk A, Sneep S, van Duin RW et al. Serial measurement of hFABP and high-sensitivity troponin I post-PCI in STEMI: how fast and accurate can myocardial infarct size and no-reflow be predicted? Am J Physiol Heart Circ Physiol 2013;305:H1104-10.
15. Grygier M, Araszkiewicz A, Lesiak M et al. New method of intracoronary adenosine injection to prevent microvascular reperfusion injury in patients with acute myocardial infarction undergoing percutaneous coronary intervention. Am J Cardiol 2011;107:1131-5.
16. Hendler A, Aronovich A, Kaluski E et al. Optimization of myocardial perfusion after primary coronary angioplasty following an acute myocardial infarction. Beyond TIMI 3 flow. J Invasive Cardiol 2006;18:32-6.
17. Liem DA, Verdouw PD, Ploeg H, Kazim S, Duncker DJ. Sites of action of adenosine in interorgan preconditioning of the heart. Am J Physiol Heart Circ Physiol 2002;283:H29-37.
18. Manintveld OC, te Lintel Hekkert M, Keijzer E, Verdouw PD, Duncker DJ. Intravenous adenosine protects the myocardium primarily by activation of a neurogenic pathway. Br J Pharmacol 2005;145:703-11.
19. Mahaffey KW, Puma JA, Barbagelata NA et al. Adenosine as an adjunct to thrombolytic therapy for acute myocardial infarction: results of a multicenter, randomized, placebo-controlled trial: the Acute Myocardial Infarction STudy of ADenosine (AMISTAD) trial. J Am Coll Cardiol 1999;34:1711-20.

20. Ross AM, Gibbons RJ, Stone GW, Kloner RA, Alexander RW. A randomized, double-blinded, placebo-controlled multicenter trial of adenosine as an adjunct to reperfusion in the treatment of acute myocardial infarction (AMISTAD-II). J Am Coll Cardiol 2005;45:1775-80.
21. Kloner RA, Forman MB, Gibbons RJ, Ross AM, Alexander RW, Stone GW. Impact of time to therapy and reperfusion modality on the efficacy of adenosine in acute myocardial infarction: the AMISTAD-2 trial. Eur Heart J 2006;27:2400-5.
22. Marzilli M, Orsini E, Marraccini P, Testa R. Beneficial effects of intracoronary adenosine as an adjunct to primary angioplasty in acute myocardial infarction. Circulation 2000;101:2154-9.
23. Stoel MG, Marques KM, de Cock CC, Bronzwaer JG, von Birgelen C, Zijlstra F. High dose adenosine for suboptimal myocardial reperfusion after primary PCI: A randomized placebo-controlled pilot study. Catheter Cardiovasc Interv 2008;71:283-9.
24. Niccoli G, Rigattieri S, De Vita MR et al. Open-Label, Randomized, Placebo-Controlled Evaluation of Intracoronary Adenosine or Nitroprusside After Thrombus Aspiration During Primary Percutaneous Coronary Intervention for the Prevention of Microvascular Obstruction in Acute Myocardial Infarction: The REOPEN-AMI Study (Intracoronary Nitroprusside Versus Adenosine in Acute Myocardial Infarction). JACC Cardiovasc Interv 2013;6:580-9.
25. Niccoli G, Spaziani C, Crea F, Investigators R-A. Left ventricular remodeling and 1-year clinical follow-up of the REOPEN-AMI trial. J Am Coll Cardiol 2014;63:1454-5.

Table S1. *Randomized clinical studies investigating the effects of intracoronary adenosine in patients with acute myocardial infarction undergoing primary percutaneous coronary intervention.*

Study	*N*	Eligibility	Ischemic Time (min)*	Type of Administration	Dose of Administration	Administration Time (min)	Start and Site of Adenosine Administration	Infarct Size	Reperfusion Markers
Marzilli et al. (2000) (1)	54	SO<3 h, pre-TIMI 0-2	106	Bolus	4 mg in 2 ml	1	After wire crossing and balloon inflation distal to PCI site	↓ peak CK/CK-MB (p=NS)	↓ No-Reflow (↓ ≥1 TIMI grades final angio rel. to post-PCI angio)
Hendler et al. (2006) (2)	20	SO<12 h, post-TIMI 3 with MBG 0/1	120	Bolus	60-120 μg	NA	Catheter site	—	↔ STR, TMPG
Stoel et al. (2008) (3)	49	STR <70% post-PCI	196	Infusion	6 mg/ml	5-10	>10 min after last balloon inflation at catheter site	Trend ↓ peak CK-MB (p=0.08)	↑ STR >70%, MBG, ↓TFC
Fokkema et al. (2009) (4)	448	SO<12 h, pre-TIMI 0-3	180	Bolus (2 x)	2 x 120 μg in 20 ml	NA	1st bolus after TA, 2nd after stenting in IRA	↔ peak CK/ CK-MB	↔ ST-deviation, STR, MBG, post-TIMI flow
Desmet et al. (2011) (5)	110	SO<12 h, pre-TIMI 0-3	215	Bolus	4 mg in 5 ml	1	After wire crossing distal to target lesion site	↔ AUC CK/CK-MB/TnI, MSI or IS MRI 4 months	↔ STR, MBG, TFC, post-TIMI flow or MVO MRI 2-3 days
Grygier et al. (2011) (6)	70	SO<6 h, pre-TIMI 0-2	273	Bolus (2 x)	2 x (1 mg for RCA and 2 mg for LCA) in 10 ml	NA	1st bolus after wire crossing, 2nd after balloon inflation at occlusion site	↔ peak CK/CK-MB/TnI	↑ STR >50%, corrected TFC, MBG 3, post-TIMI 3 flow
Niccoli et al. (2013) (7)	160	SO<12 h, pre-TIMI 0/1	277	Bolus + (Brief) Infusion	120 μg + 2 mg in 33 ml	1st bolus fast + 2	After wire crossing and TA beyond occlusion site	↓ peak CK-MB/ TnT	↑ STR >70%, ↓ MVO (TFG≤2 or MBG<2)
Garcia-Dorado et al. (2013) (8)	201	SO<6 h, persistent TIMI 0/1 after wire crossing	NA	(Brief) Infusion	4 mg	2	Immediately before reperfusion mostly with TA and direct stenting distal to culprit lesion	↔ IS MRI 2-7 days or 6 months, ↓ IS in pts with SO<200 min (n=84)	↔ MVO MRI 2-7 days or 6 months

**Ischemic time in the adenosine groups. ↓ indicates reduced; ↑, improved; ↔, unchanged; AUC, area under the curve; CK, creatine kinase; CK-MB, creatine kinase myocardial band; IRA, infarct-related artery; IS, infarct size; MBG, myocardial blush grade; MRI, magnetic resonance imaging; MSI, myocardial salvage index; MVO, microvascular obstruction; NA, not available; SO, symptom onset; STR, ST-segment resolution; TA, thrombus aspiration; TFC, TIMI frame count; TIMI, Thrombolysis In Myocardial Infarction; TMPG, TIMI myocardial perfusion grade; TnI, troponin I; and TnT, troponin T.*

Table S2. *Regional myocardial function*

			Coronary Artery Occlusion			Reperfusion			
		Baseline	**5 min CAO**	**40 min CAO**	**45 min CAO**	**5 min Rep**	**15 min Rep**	**60 min rep**	**120 min Rep**
Bolus Injection									
EDL_{LAD} (mm)	Control	10.0 ± 0.0	13.0 ± 1.4*	12.4 ± 1.2*	12.0 ± 0.8*	9.5 ± 0.3*	10.0 ± 0.3	9.9 ± 0.3	9.8 ± 0.2
	Adenosine	10.0 ± 0.0	11.0 ± 0.5	10.4 ± 0.5	10.4 ± 0.5	8.8 ± 0.7	9.2 ± 0.6	9.2 ± 0.6	9.3 ± 0.5
SS_{LAD} (%)	Control	19.5 ± 0.8	-10.0 ± 3.5*	-9.0 ± 3.5*	-6.4 ± 2.4*	0.4 ± 2.2*	3.4 ± 1.8*	2.8 ± 1.4*	1.1 ± 1.4*
	Adenosine	16.9 ± 2.2	-8.5 ± 5.9*	-7.3 ± 3.1*	-6.8 ± 2.8*	-3.4 ± 3.8*	-0.9 ± 3.1*	0.4 ± 1.9*	-0.8 ± 2.3*
EDL_{LCX} (mm)	Control	10.0 ± 0.0	10.5 ± 0.2	10.1 ± 0.3	10.0 ± 0.2	9.7 ± 0.2	9.7 ± 0.2	9.5 ± 0.2	9.3 ± 0.3*
	Adenosine	10.0 ± 0.0	10.2 ± 0.1	10.6 ± 0.5	10.8 ± 0.6	10.9 ± 0.9	10.5 ± 0.8	10.1 ± 0.3	10.0 ± 0.3
SS_{LCX} (%)	Control	20.0 ± 0.8	15.6 ± 4.4	17.5 ± 3.5	16.3 ± 2.8	17.5 ± 2.0	16.9 ± 2.6	14.8 ± 2.3	13.0 ± 2.2*
	Adenosine	14.4 ± 1.9	15.8 ± 3.3	15.4 ± 2.1	15.2 ± 2.2	17.1 ± 3.8	16.3 ± 4.2	13.3 ± 2.3	11.2 ± 2.3
Prolonged infusion									
EDL_{LAD} (mm)	Control	10.0 ± 0.0	11.3 ± 0.1*	11.5 ± 0.1*	11.5 ± 0.2*	9.3 ± 0.2*	9.7 ± 0.2	9.8 ± 0.2	9.9 ± 0.2
	Adenosine	10.0 ± 0.0	10.8 ± 0.1*	11.0 ± 0.1*	10.9 ± 0.1*	9.2 ± 0.2*	9.7 ± 0.2	9.7 ± 0.2	9.7 ± 0.2
SS_{LAD} (%)	Control	19.1 ± 0.9	-10.8 ± 1.6*	-8.2 ± 1.2*	-7.1 ± 1.2*	-1.3 ± 0.9*	0.8 ± 1.0*	1.4 ± 0.9*	0.6 ± 0.9*
	Adenosine	18.7 ± 2.0	-6.0 ± 1.7*	-4.3 ± 1.5*	-3.0 ± 1.5*	-0.4 ± 1.7*	2.3 ± 1.8*	1.5 ± 1.4*	3.0 ± 1.3*
EDL_{LCX} (mm)	Control	10.0 ± 0.0	10.2 ± 0.1	10.0 ± 0.1	9.9 ± 0.1	9.8 ± 0.1	9.8 ± 0.1*	9.6 ± 0.2*	9.5 ± 0.2*
	Adenosine	10.0 ± 0.0	10.2 ± 0.1	10.1 ± 0.1	10.0 ± 0.1	9.7 ± 0.1*	9.5 ± 0.1*	9.5 ± 0.1*	9.4 ± 0.1*
SS_{LCX} (%)	Control	16.5 ± 1.3	14.5 ± 2.2	13.1 ± 1.9*	13.2 ± 1.9*	14.7 ± 1.5	14.3 ± 1.6	12.6 ± 1.6	11.1 ± 1.5*
	Adenosine	17.8 ± 1.1	15.9 ± 1.4*	14.1 ± 1.4*	14.1 ± 1.4*	13.8 ± 1.2*	13.9 ± 1.3*	13.0 ± 1.2*	12.7 ± 1.2*

Data are presented as mean ± SEM. *P<0.05 vs. corresponding baseline. EDL indicates end-diastolic segment length; LAD, left anterior descending coronary artery perfusion territory; LCX, left circumflex coronary artery perfusion territory; and SS, % shortening of the segment length during systole.

Table S3: *Myocardial metabolism*

			Reperfusion			
		Baseline	**5 min Rep**	**15 min Rep**	**60 min Rep**	**120 min Rep**
Bolus Injection						
CV pO_2 (mmHg)	Control	25 ± 1	51 ± 2*	58 ± 2*	57 ± 2*	53 ± 2*
	Adenosine	26 ± 1	45 ± 2*	50 ± 3*	52 ± 4*	52 ± 4*
MVO_2 (μmol/min)	Control	61 ± 4	73 ± 8	38 ± 4*	38 ± 4*	35 ± 5*
	Adenosine	64 ± 19	53 ± 18	56 ± 13	44 ± 15	40 ± 11
Prolonged Infusion						
CV pO_2 (mmHg)	Control	26 ± 1	49 ± 1*	55 ± 2*	55 ± 2*	54 ± 2*
	Adenosine	26 ± 1	47 ± 1*	53 ± 2*	58 ± 3*	60 ± 3*
MVO_2 (μmol/min)	Control	82 ± 17	56 ± 6*	37 ± 5*	32 ± 5*	27 ± 4*
	Adenosine	52 ± 6†	57 ± 6	45 ± 8	35 ± 5	32 ± 4

Data are presented as mean ± SEM. *P<0.05 vs. corresponding baseline. †P<0.05 vs. corresponding control. CV pO_2 indicates coronary venous pO_2 and MVO_2, myocardial oxygen consumption.

Table S4. *Pre-clinical studies investigating the effects of adenosine on infarct size and no-reflow*

Study	Species	Ischemic Time (min)	Reperfusion period (h)	Dose of Adminis-tration	Infusion Time (min)	Start Adenosine Adminis-tration	Concomitant Lidocaine	Determination of Optimal Dose for Infusion	Infarct Size Reduction, %	No-Reflow Reduction, %
Left atrium infusion										
Zhao et al. (1999) (9)	Dog	60	6	140 μg/kg/min	125	5 min before R	No	No	Yes, 48	Yes (↓PMN), 58
Intravenous infusion										
Goto et al. (1991) (10)	Rabbit	30	3, 72	150, 370 μg/kg/min	60	5 min before R	Yes/No	No	No (with or without L)	—
Norton et al. (1991) (11)	Rabbit	30	48	0.1, 0.3, 0.55 mg/min	65	5 min before R	Yes	No	Yes (all doses), 32-40	—
Pitarys et al. (1991) (12)	Dog	90	72	150 μg/kg/min	155	5 min before R	Yes	No	Yes, 52	Yes (↓NP; p=NS)
Norton et al. (1992) (13)	Rabbit	30	48	0.001, 0.01, 0.1 mg/min	65	5 min before R	Yes	No	Yes (all 3 doses), 31-53	—
Vander Heide et al. (1996) (14)	Dog	90	3	150 μg/kg/min	155	5 min before R	Yes/No	No	No (with or without L)	—
Budde et al. (2000) (15)	Dog	60	24	140 μg/kg/min	120	5 min before R	No	No	No	No (-PMN)
Budde et al. (2004) (16)	Dog	60	6, 24, 48	140 μg/kg/min	120*	5 min before R	No	No	Yes, 50†	Yes (↓PMN)†

Table S4. *Continued*

Study	Species	Ischemic Time (min)	Reperfusion period (h)	Dose of Administration	Infusion Time (min)	Start Adenosine Administration	Concomitant Lidocaine	Determination of Optimal Dose for Infusion	Infarct Size Reduction, %	No-Reflow Reduction, %
Intracoronary infusion										
Olafsson et al. (1987) (17)	Dog	90	24	3.75 mg/min	60	At R	Yes	No	Yes, 76	Yes (↓NP; p=NS)
Babbitt et al. (1990) (18)	Dog	180	72	3.75 mg/min	60	At R	Yes	No	No	No (-NI)
Homeister et al. (1990) (19)	Dog	90	6	150 μg/kg/min	60	At R	Yes	No	Yes (only with L), 56	—
Velasco et al. (1991) (20)	Dog	40	72	3.75 mg/min	60	At R	Yes	No	Yes, 63	—
Forman et al. (1993) (21)	Dog	120	24	3.75 mg/min	60	At R	Yes	No	Yes, 75	—

*Same study dose readministered at 2, 6, 12 and 18 h of reperfusion in groups with 24-h and 48-h reperfusion periods. †Significant infarct size and polymorphonuclear neutrophil reduction with single-dose adenosine in the 6-h reperfusion group vs. controls in the 6-h reperfusion group. Significant infarct size and polymorphonuclear neutrophil reduction with multidose adenosine in the 24-h and 48-h reperfusion groups (vs. controls in the 6-h and 24-h reperfusion groups). IC indicates intracoronary; IV, intravenous; L, lidocaine; NI, neutrophil infiltration; NP, neutrophil plugging of capillaries; PMN, polymorphonuclear neutrophils; and R, reperfusion.

SUPPLEMENTAL REFERENCES

1. Marzilli M, Orsini E, Marraccini P, Testa R. Beneficial effects of intracoronary adenosine as an adjunct to primary angioplasty in acute myocardial infarction. Circulation 2000;101:2154-9.
2. Hendler A, Aronovich A, Kaluski E et al. Optimization of myocardial perfusion after primary coronary angioplasty following an acute myocardial infarction. Beyond TIMI 3 flow. J Invasive Cardiol 2006;18:32-6.
3. Stoel MG, Marques KM, de Cock CC, Bronzwaer JG, von Birgelen C, Zijlstra F. High dose adenosine for suboptimal myocardial reperfusion after primary PCI: A randomized placebo-controlled pilot study. Catheter Cardiovasc Interv 2008;71:283-9.
4. Fokkema ML, Vlaar PJ, Vogelzang M et al. Effect of high-dose intracoronary adenosine administration during primary percutaneous coronary intervention in acute myocardial infarction: a randomized controlled trial. Circ Cardiovasc Interv 2009;2:323-9.
5. Desmet W, Bogaert J, Dubois C et al. High-dose intracoronary adenosine for myocardial salvage in patients with acute ST-segment elevation myocardial infarction. Eur Heart J 2011;32:867-77.
6. Grygier M, Araszkiewicz A, Lesiak M et al. New method of intracoronary adenosine injection to prevent microvascular reperfusion injury in patients with acute myocardial infarction undergoing percutaneous coronary intervention. Am J Cardiol 2011;107:1131-5.
7. Niccoli G, Rigattieri S, De Vita MR et al. Open-Label, Randomized, Placebo-Controlled Evaluation of Intracoronary Adenosine or Nitroprusside After Thrombus Aspiration During Primary Percutaneous Coronary Intervention for the Prevention of Microvascular Obstruction in Acute Myocardial Infarction: The REOPEN-AMI Study (Intracoronary Nitroprusside Versus Adenosine in Acute Myocardial Infarction). JACC Cardiovasc Interv 2013;6:580-9.
8. Garcia-Dorado D, Otaegui I, Rodriguez Palomares JF et al. Primary results of the PROMISE trial: myocardial protection with intracoronary adenosine given before reperfusion in patients with STEMI. Annual congress of the European Society of Cardiology; September 2, 2013; Amsterdam, the Netherlands.
9. Zhao ZQ, Nakamura M, Wang NP et al. Administration of adenosine during reperfusion reduces injury of vascular endothelium and death of myocytes. Coron Artery Dis 1999;10:617-28.
10. Goto M, Miura T, Iliodoromitis EK et al. Adenosine infusion during early reperfusion failed to limit myocardial infarct size in a collateral deficient species. Cardiovasc Res 1991;25:943-9.
11. Norton ED, Jackson EK, Virmani R, Forman MB. Effect of intravenous adenosine on myocardial reperfusion injury in a model with low myocardial collateral blood flow. Am Heart J 1991;122:1283-91.
12. Pitarys CJ, 2nd, Virmani R, Vildibill HD, Jr., Jackson EK, Forman MB. Reduction of myocardial reperfusion injury by intravenous adenosine administered during the early reperfusion period. Circulation 1991;83:237-47.
13. Norton ED, Jackson EK, Turner MB, Virmani R, Forman MB. The effects of intravenous infusions of selective adenosine A1-receptor and A2-receptor agonists on myocardial reperfusion injury. Am Heart J 1992;123:332-8.
14. Vander Heide RS, Reimer KA. Effect of adenosine therapy at reperfusion on myocardial infarct size in dogs. Cardiovasc Res 1996;31:711-8.
15. Budde JM, Velez DA, Zhao Z et al. Comparative study of AMP579 and adenosine in inhibition of neutrophil-mediated vascular and myocardial injury during 24 h of reperfusion. Cardiovasc Res 2000;47:294-305.
16. Budde JM, Morris CD, Velez DA et al. Reduction of infarct size and preservation of endothelial function by multidose intravenous adenosine during extended reperfusion. J Surg Res 2004;116:104-15.

17. Olafsson B, Forman MB, Puett DW et al. Reduction of reperfusion injury in the canine preparation by intracoronary adenosine: importance of the endothelium and the no-reflow phenomenon. Circulation 1987;76:1135-45.
18. Babbitt DG, Virmani R, Vildibill HD, Jr., Norton ED, Forman MB. Intracoronary adenosine administration during reperfusion following 3 hours of ischemia: effects on infarct size, ventricular function, and regional myocardial blood flow. Am Heart J 1990;120:808-18.
19. Homeister JW, Hoff PT, Fletcher DD, Lucchesi BR. Combined adenosine and lidocaine administration limits myocardial reperfusion injury. Circulation 1990;82:595-608.
20. Velasco CE, Turner M, Cobb MA, Virmani R, Forman MB. Myocardial reperfusion injury in the canine model after 40 minutes of ischemia: effect of intracoronary adenosine. Am Heart J 1991;122:1561-70.
21. Forman MB, Velasco CE, Jackson EK. Adenosine attenuates reperfusion injury following regional myocardial ischaemia. Cardiovasc Res 1993;27:9-17.

SUPPLEMENTAL DOSE RESPONSE AND PROLONGED INFUSION STUDY

METHODS

Surgical preparation

Swine of either sex were premedicated with rompun (xylazine) 2.25 mg/kg, zoletil (tiletamine + zolazepam) 5 mg/kg i.m. and atropine 1 mg, intubated, and placed on a positive-pressure ventilator (O_2:N_2=1:3 v/v) to which 0.2-1.0% (v/v) isoflurane was added. Anesthesia was maintained with midazolam (2 mg/kg, i.v.) and fentanyl (10 μg/kg/h, i.v.). Swine were instrumented under sterile conditions as previously described (1,2). Briefly, a thoracotomy was performed by opening the fourth left intercostal space after which an 8-F fluid-filled catheter was placed in the aortic arch for the measurement of aortic blood pressure and blood sampling. For measurement of aortic blood flow, a transit-time flow probe was placed around the ascending aorta (3). After the heart was exposed via opening of the pericardium, a high fidelity Konigsberg pressure transducer and an 8-F fluid filled catheter (used for calibration of the Konigsberg transducer signal) were inserted via the left ventricle apex to measure the pressure. Subsequently, 8-F fluid-filled catheters were implanted into the left atrium for pressure measurements and into the pulmonary artery for infusion of drugs. Approximately 2 cm of the left anterior descending coronary artery was dissected free from the surrounding tissue to allow placement of a transit-time flow probe for measurement of coronary blood flow and a 22-gauge angiocatheter for intra-arterial infusion of drugs (4). The anterior interventricular vein was cannulated with a 20-gauge angiocatheter for coronary venous blood sampling and to determine myocardial O_2 consumption. Subsequently, electrical wires and catheters were tunnelled subcutaneously to the back and the chest was closed. Animals were allowed to recover from surgery and received analgesia (0.3 mg buprenorphine i.m.) for two days and antibiotic prophylaxis (25 mg/kg amoxicillin and 5 mg/kg gentamycin i.v.) for five days. The dose response and prolonged infusion protocol was performed at least one week after surgery.

Experimental protocol and procedures

The effects of increasing 10-min intracoronary infusions of adenosine (2, 5, 10, 20 and 50 μg/kg/min) were studied in chronically instrumented awake swine under resting conditions. Systemic, pulmonary and coronary hemodynamics as well as regional myocardial function was recorded throughout the experimental

protocol. Arterial and coronary venous blood samples were collected at several time points. Aortic, pulmonary and left atrial pressures were measured using Combitrans pressure transducers (Braun, Melsungen, FRG) with the reference point at mid-chest level. Hemodynamic variables were continuously recorded and blood samples were collected at each 10-min infusion rate, at a time when hemodynamics had reached a steady state.

After establishing the highest dose that was without systemic hemodynamic effects, a prolonged 24-h intracoronary infusion of this selected dose was investigated to determine whether sustained and stable increases in coronary blood flow could be achieved. Hemodynamics were measured continuously during the first 4 h after start of infusion and subsequently at 24 h.

RESULTS

A total number of 10 swine were entered into the dose response and prolonged infusion study, of which 2 died due to technical difficulties during surgical instrumentation, leaving 8 swine for the final analysis.

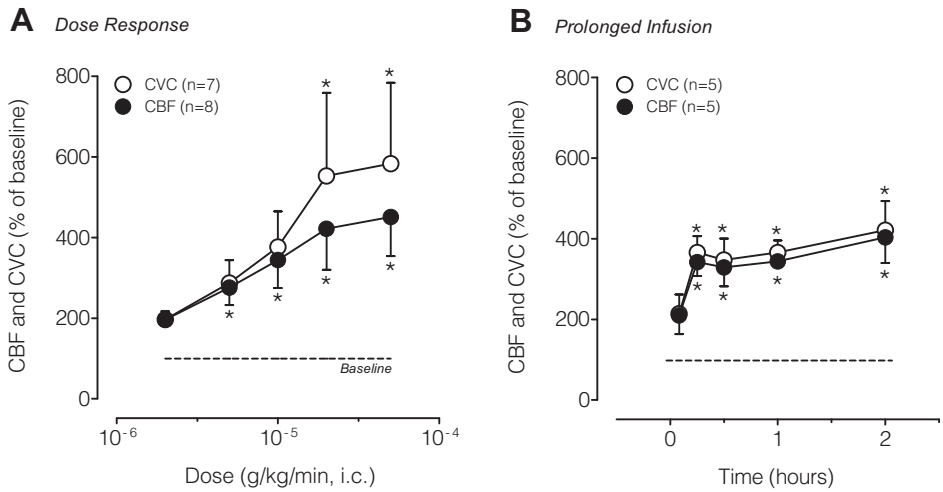

Figure 1. *Dose response and prolonged infusion*
*Data are mean ± SEM. *P<0.05 vs. corresponding baseline. Dose-dependent increases in coronary blood flow and coronary vascular conductance (% of baseline) in response to incremental 10-min intracoronary adenosine infusions (A) and to prolonged 2-h intracoronary infusions of 50 μg/kg/min (B).*

Ten-minute intracoronary infusions of adenosine, in doses up to 50 μg/kg/min, increased CBF fourfold (**Figure 1A**). Even at the highest dose adenosine resulted in negligible systemic or pulmonary hemodynamic effects (**Table 1**). Consequently, the dose of 50 μg/kg/min was selected for prolonged infusion up to 24 h.

Infusion of adenosine in a dose of 50 μg/kg/min resulted in an increase of CBF to 342 ± 35% of baseline at 15 min, which remained stable for up to 2 h (**Figure 1B**). At 24 h, coronary flow was still maintained at ~300% of baseline levels, indicating excellent and sustained coronary responsiveness, with no sign of tachyphylaxis (**Table 2**).

Table 1. *Dose responses to intracoronary infusions of adenosine*

Adenosine (n=8)		**Dose in μg/kg/min**				
	Baseline	**2**	**5**	**10**	**20**	**50**
HR (bmp)	103 ± 4	111 ± 7	106 ± 4	109 ± 4	107 ± 4	109 ± 5
MAP (mmHg)	82 ± 3	82 ± 3	80 ± 4	84 ± 5	80 ± 5	79 ± 4
PAP (mmHg)	13 ± 2	14 ± 2	13 ± 2	14 ± 2	14 ± 1	15 ± 2
LAP (mmHg)	4 ± 1	4 ± 1	4 ± 1	5 ± 1	6 ± 1	6 ± 1
CO (L/min)	3.2 ± 0.2	3.5 ± 0.3	3.3 ± 0.2	3.4 ± 0.2	3.4 ± 0.2	3.5 ± 0.3
SVC (mL/min/mmHg)	39 ± 4	43 ± 5	42 ± 5	41 ± 4	42 ± 3	44 ± 4
PVC (L/min/mmHg)	0.38 ± 0.07	0.36 ± 0.05	0.42 ± 0.08	0.53 ± 0.16	0.54 ± 0.18	0.52 ± 0.16
CBF (ml/min)	38 ± 4	72 ± 8*	97 ± 11*	116 ± 14*	140 ± 22*	151 ± 20*
CBF (% of BI)	100 ± 0	196 ± 15	276 ± 43	344 ± 69	422 ± 102*	451 ± 97*
CVC (ml/min/mmHg)	0.48 ± 0.07	0.90 ± 0.11	1.22 ± 0.14	1.55 ± 0.20	2.15 ± 0.52*	2.30 ± 0.50*
EDL LAD (mm)	10.3 ± 0.9	10.0 ± 0.8	10.0 ± 0.8	9.9 ± 0.7	10.0 ± 0.8	10.1 ± 0.8
ESL LAD (mm)	8.6 ± 0.7	8.3 ± 0.7	8.4 ± 0.8	8.2 ± 0.7	8.4 ± 0.7	8.6 ± 0.7
SS (%)	16.2 ± 1.5	17.8 ± 2.1	17.1 ± 2.6	17.6 ± 2.6	16.5 ± 2.6	14.0 ± 2.1

Data are presented as mean ± SEM. *P<0.05 vs. corresponding baseline. Analyzed with a one-way ANOVA followed by Dunnets' post-hoc test. CBF indicates coronary blood flow; CO, cardiac output; CVC, coronary vascular conductance (CBF/[MAP-LAP]); EDL LAD, end-diastolic segment length in LAD perfusion territory; ESL LAD, end-systolic segment length in LAD perfusion territory; HR, heart rate; LAP, left atrial pressure; MAP, mean arterial pressure; PAP, pulmonary artery pressure; PVC, pulmonary vascular conductance (CO/[PAP-LAP]); SS, systolic shortening (% shortening of LAD segment during systole); and SVC, systemic vascular conductance (CO/MAP).

Table 2. *Sustained effects of prolonged intracoronary infusion of adenosine*

Adenosine (n=5)		**Time after start infusion**					
	Baseline	**30 min**	**60 min**	**120 min**	**180 min**	**240 min**	**24 hours**
HR (bmp)	113 ± 8	113 ± 7	122 ± 6	120 ± 5	120 ± 5	132 ± 6	128 ± 10
MAP (mmHg)	85 ± 3	84 ± 6	83 ± 6	85 ± 4	78 ± 4	81 ± 3	77 ± 4
PAP (mmHg)	13 ± 1	15 ± 1	16 ± 1	14 ± 1	13 ± 2	15 ± 1	13 ± 2
LAP (mmHg)	2.5 ± 0.5	4.1 ± 0.8	3.8 ± 1.3	4.5 ± 1.0	2.0 ± 1.1	5.0 ± 0.5	5.6 ± 0.6*
CO (L/min)	4.2 ± 0.6	4.5 ± 0.6	4.6 ± 0.7	4.3 ± 0.5	4.4 ± 0.6	4.6 ± 0.5	4.1 ± 0.7
SVC (mL/min/mmHg)	50 ± 6	55 ± 8	57 ± 8	51 ± 6	57 ± 9	57 ± 7	53 ± 8
PVC (L/min/mmHg)	0.39 ± 0.05	0.42 ± 0.07	0.40 ± 0.07	0.44 ± 0.07	0.43 ± 0.06	0.47 ± 0.06	0.66 ± 0.13
CBF (ml/min)	46 ± 2	155 ± 28*	160 ± 15*	186 ± 29*	169 ± 20*	179 ± 18*	147 ± 24*
CBF (% of BI)	100 ± 0	329 ± 47*	344 ± 19*	404 ± 64*	364 ± 30*	386 ± 32*	313 ± 43*
CVC (ml/min/mmHg)	0.56 ± 0.03	1.99 ± 0.38*	2.07 ± 0.24*	2.36 ± 0.38*	2.25 ± 0.27*	2.36 ± 0.22*	2.05 ± 0.31*

Data are presented as mean ± SEM. *P<0.05 vs. corresponding baseline. Analyzed with a one-way ANOVA followed by Dunnets' post-hoc test. CBF indicates coronary blood flow; CO, cardiac output; CVC, coronary vascular conductance (CBF/[MAP-LAP]); HR, heart rate; LAP, left atrial pressure; MAP, mean arterial pressure; PAP, pulmonary artery pressure; PVC, pulmonary vascular conductance (CO/[PAP-LAP]); and SVC, systemic vascular conductance (CO/MAP).

REFERENCES

1. Duncker DJ, Stubenitsky R, Verdouw PD. Autonomic control of vasomotion in the porcine coronary circulation during treadmill exercise: evidence for feed-forward beta-adrenergic control. Circ Res 1998;82(12):1312-22.
2. van der Velden J, Merkus D, Klarenbeek BR, James AT, Boontje NM, Dekkers DH et al. Alterations in myofilament function contribute to left ventricular dysfunction in pigs early after myocardial infarction. Circ Res 2004;95(11):e85-95.
3. de Beer VJ, Sorop O, Pijnappels DA, Dekkers DH, Boomsma F, Lamers JM et al. Integrative control of coronary resistance vessel tone by endothelin and angiotensin II is altered in swine with a recent myocardial infarction. Am J Physiol Heart Circ Physiol 2008;294(5):H2069-77.
4. Zhou Z, Hemradj V, de Beer VJ, Gao F, Hoekstra M, Merkus D et al. Cytochrome P-450 2C9 exerts a vasoconstrictor influence on coronary resistance vessels in swine at rest and during exercise. Am J Physiol Heart Circ Physiol 2012; 302(8):H1747-55.

CHAPTER 7

Vagal Nerve Stimulation during Early Reperfusion Limits infarct size and No-Reflow

*__André Uitterdijk__
*Tuncay Yetgin
Maaike te Lintel Hekkert
Stefan Sneep
Ilona Krabbendam-Peters
Heleen MM van Beusekom
Trent M Fischer
Richard N Cornelussen
Olivier C Manintveld
Daphne Merkus
Dirk J Duncker

*Both authors contributed equally

Submitted

ABSTRACT

Vagal nerve stimulation (VNS), started prior to, or during, ischemia has been shown to reduce infarct-size. However, whether VNS affords cardioprotection when started just prior to reperfusion has not been studied to date. We therefore investigated the effect of VNS started just prior to, and continued during, early reperfusion on infarct size and no-reflow and studied the underlying mechanisms. For this purpose, swine (13 VNS, 10 Sham) underwent 45 min mid-LAD occlusion followed by 120 min of reperfusion. VNS was started 5 min prior to reperfusion and continued for a brief period of 20 min. Area-at-risk, area of no-reflow (% of infarct-area) and infarct size (% of area-at-risk), circulating cytokines, and regional myocardial leukocyte-influx were assessed. Results demonstrated that VNS significantly reduced infarct size from 67±2% in Sham to 54±5% and area of no-reflow from 54±6% in Sham to 32±6%. These effects were accompanied by reductions in neutrophil (~40%) and macrophage (~60%) infiltration in the infarct-area (all $p<0.05$), whereas systemic circulating plasma levels of TNFα and IL6 were not affected. The degree of cardioprotection did not correlate with the magnitude of VNS-induced bradycardia. In the presence of NO-synthase inhibitor LNNA (n=6), VNS (n=5) no longer attenuated infarct size and no-reflow, which was paralleled by unaltered regional leucocyte infiltration. In conclusion, VNS shows promise as a novel adjunctive therapy to limit reperfusion injury in a large animal model of acute myocardial infarction.

INTRODUCTION

The single most effective therapy to limit myocardial infarct size and improve clinical outcome after acute myocardial infarction (AMI) is early coronary reperfusion via primary percutaneous coronary intervention (1,2). However, despite its overall benefits, reperfusion-therapy has been shown to result in additional cardiomyocyte death, termed lethal reperfusion-injury (3,4), and microvascular obstruction, termed no-reflow (5). No-reflow refers to inadequate myocardial reperfusion following opening of the culprit coronary lesion, despite lack of angiographic evidence of epicardial vessel obstruction, which may be present in 30-40% of patients (6). Since both infarct size (7) and extent of no-reflow (5,8,9) are independent predictors of clinical outcome, strategies to limit these two components of reperfusion-injury have significant therapeutic potential.

A novel strategy against ischemia-reperfusion injury was recently proposed by Katare et al. (10), who demonstrated in rats that vagal nerve stimulation (VNS) limited infarct-size. This initial observation was confirmed in subsequent studies in rats (11-14), mice (15) and recently in swine (16). In these studies, the effect of VNS on no-reflow was never examined. Furthermore, VNS was started either before (10,11,14), at the very onset of (12,16), or early during (13) ischemia, which does not emulate the clinical scenario where adjuvant therapy is typically started late into ischemia or at the onset of reperfusion therapy. Consequently, the first aim of the present study was to investigate the effects of VNS, when started just prior to reperfusion, on infarct size and extent of no-reflow in a large animal model of ST-elevated myocardial infarction (STEMI).

The mechanisms behind the beneficial effect of VNS on infarct size reduction are incompletely understood, but have been proposed to include activation of muscarinic receptors (16) and blunting of the inflammatory response (13). Consequently, the second aim of the present study was to investigate potential mechanisms underlying the effects of VNS on infarct size and no-reflow, in particular anti-inflammatory actions, including circulating inflammatory cytokines and myocardial neutrophil and macrophage infiltration, and the nitric oxide synthase (NOS) signaling pathway.

MATERIALS AND METHODS

Studies were performed in 65 Yorkshire x Landrace swine (~55 kg) of either sex, in accordance with the "Guiding Principles in the Care and Use of Laboratory Animals" as approved by the Council of the American Physiological Society, and with approval of the Animal Care Committee of the Erasmus MC Rotterdam.

Animal Preparation

Swine were sedated with ketamine (20 mg/kg, i.m.) and midazolam (1 mg/kg, i.m.), anesthetized with pentobarbital (15 mg/kg i.v.), intubated and mechanically ventilated with O_2 and N_2 (1:3 v/v), and instrumented as previously described (17,18). Catheters were placed in the external jugular vein for maintenance of anesthesia (pentobarbital, 10-15 mg/kg/h) and infusion of physiological saline, and the left femoral artery for measurement of arterial blood pressure. A Swan-Ganz catheter was inserted into the left femoral vein and advanced into the pulmonary artery for body core temperature monitoring. A micro-manometer-tipped catheter (SPC-3705, Millar Instruments, Houston, USA) was inserted, via the right carotid artery, in the left ventricle (LV) for measurement of LV pressure and its first derivative (LVdP/dt). Following sternotomy, an electromagnetic flow probe (P18, Skalar Medical, Delft, The Netherlands) was placed around the ascending aorta to measure cardiac output, and a transit-time flow probe (3SB, Transonic Systems, Ithaca, USA) was placed around the left anterior descending coronary artery (LAD) for measurement of coronary blood flow. A suture was placed around the LAD, just distal to its first diagonal branch, to enable coronary artery occlusion (CAO) during the experimental protocol. Regional myocardial function was measured in the area at risk and remote myocardium using two pairs of ultrasonic crystals (P/N SL5-2, Triton Technology Inc., San Diego, USA) placed in the midmyocardium (18,19). A fluid-filled catheter was placed in the left atrium through a purse-string suture into the auricle for measurement of left atrial pressure. For coronary venous blood sampling, a custom fluid filled catheter was placed in the anterior coronary vein draining the perfusion territory of the LAD. Heparin (5000 i.u./h, i.v.) was administered throughout the experiment to prevent coagulation.

Custom-made, self-coiling cuff electrodes were placed around both the left and right vagal nerves for stimulation purposes. After completion of instrumentation, the cardiac vagal nerve reserve (maximal reduction in HR (%)) was tested in both vagal nerves (left and right) in 1 min intervals by increasing voltages (Medtronic 3625 test simulator; 2-10.5 V; 10 mA; pulse width 300 μs; 25 Hz). The maximum effect of VNS was reached during stimulation with 10.5 V. Maximum heart rate reductions during

therapy, produced by stimulation of either left (15±2%) or right vagal nerve (18±3%) were not different (p=0.41). Maximal heart rate reductions at pre-ischemia baseline were also comparable for VNS (23±2%) and Sham (21±3%) groups (p=0.69).

Experimental Protocols

Cardioprotection by VNS. After 30 min of stabilization, swine were subjected to the experimental protocol. Systemic and coronary hemodynamics and regional myocardial function were continuously recorded. Blood samples were obtained from the aorta and anterior inter-ventricular coronary vein at several time points for measurement of PO_2 (mmHg), PCO_2 (mmHg), pH, O_2 saturation, hemoglobin (Hb, in grams per 100 ml) and lactate (Acid-Base Laboratory model 800, Radiometer, Copenhagen, Denmark). Body core temperature was monitored and maintained between 37.0-38.0 ^{o}C throughout the experimental protocol (20). Swine were subjected to a 45-min CAO followed by 120 min of reperfusion. Swine encountering ventricular fibrillation (VF) were allowed to complete the protocol if conversion to sinus rhythm was successful within 2 min after onset of VF. Swine were randomly assigned to either sham-treatment (n=13) or VNS alone (n=17). VNS was started 5 min before the end of CAO and continued until 15 min into reperfusion. All VNS animals were initially subjected to stimulation of the left vagal nerve. In five animals, in which the reduction in heart rate during the first minute was less than 10%, right vagal nerve stimulation was applied during the remainder of the 20-min stimulation protocol.

Role of NO-synthase. To investigate the role of NO signaling in the protection by VNS, we performed a second series of experiments in which we studied three additional groups of swine. Animals underwent the identical 45-min CAO and 120-min reperfusion protocol, as outlined above, while receiving (*i*) sham-treatment (n=12), (*ii*) NO-synthase inhibition, using N^{ω}-Nitro-L-Arginine (LNNA, Sigma, Zwijndrecht, The Netherlands) 10 mg/kg i.v. 30 minutes before CAO (21), and sham-treatment (n=11), or (iii) LNNA and VNS (n=12).

Infarct-Size, Area of No-Reflow, Systemic and Regional Inflammation

At the end of 120 min of reperfusion, a fluid-filled catheter was inserted into the coronary artery, distal to the site of occlusion, to administer 5 ml of a 4% (w/v) thioflavin-S (Sigma) solution to determine the area of no-reflow (22,23). The coronary artery was re-occluded and the area-at-risk was delineated by intra-atrial infusion of 40 ml of 15% (w/v) Evans Blue (17,20). Then, the heart was excised, the LV was isolated and cut into 5 transverse slices of equal thickness and slices were weighed. After the area-at-risk and area of no-reflow (using UV-light) of each

slice were demarcated on an acetate sheet, slices were incubated in 3% (w/v) 2,3,5-Triphenyltetrazolium chloride at 37°C for 15 min to stain metabolically active tissue (20). The red stained non-infarcted area was also traced onto the sheet. Myocardial infarct size (IS) was defined as the ratio of the summed infarct areas (IA) and summed areas at risk (AR): IS=IA/AR*100% (17,20). Area of no-reflow (NR) was defined as the ratio of the summed no-reflow areas (NA) and summed infarct areas: NR=NA/IA*100% (22).

Systemic Inflammation

Plasma isolated from arterial blood taken at baseline, prior to CAO and the first hour of reperfusion was analyzed by ELISA according to manufacturer's instructions for porcine inflammatory markers TNFα and IL6 (R&D Systems, Abingdon, United Kingdom).

Regional Inflammation

Infarct area with either reflow or no-reflow and remote non-area-at-risk (posterior wall) LV tissue was fixed in 4% buffered formaldehyde and embedded in paraffin. To identify the acute influx of immune cells, sections of 4 μm were stained for neutrophils (Azurocidin, mouse anti human, 1:100, Abnova, Heidelberg, Germany) following antigen retrieval (10 min citrate buffer boil (pH 6)) and for macrophages (MAC387, mouse anti macrophage, 1:100, Abcam, Cambridge, United Kingdom). Staining was visualized using rabbit anti mouse secondary antibodies (1:100, horseradish peroxidase label, DAKO, Heverlee, Belgium) with 3,3'-diaminobenzidine (DAB, DAKO) and H_2O_2 as chromogen. Primary antibodies were omitted as a negative control. Three randomly selected high power fields (90,000 μm^2 per field) per section were morphometrically quantified in a blinded manner using dedicated software (Clemex Vision PE, version 6.0.010A, Clemex Technologies inc, Longueuil, Canada). Data were expressed as number of cells/mm^2.

Data and Statistical Analysis

Hemodynamic and LV global and regional function data were recorded and analysed, and myocardial oxygen and lactate consumption, and systolic and post-systolic shortening were calculated, as previously described (17,18).

Inter-group differences in AR/LV, IA/AR and NR/IA were analyzed using unpaired t-test or one-way ANOVA followed by Student-Newman-Keuls (SNK) post-hoc testing, as appropriate. Hemodynamic and LV functional data were analyzed using two-way (time x treatment) ANOVA followed by SNK test. Global and Regional

inflammation was analyzed by using two-way (treatment x location) ANOVA followed by SNK test. Values are expressed as mean ± SEM. $P<0.05$ (two-tailed) was considered statistically significant.

RESULTS

Mortality

Seven swine (3 Sham, 4 VNS) out of 30 animals that encountered VF during the 45 min CAO (prior to VNS or sham) could not successfully be converted to sinus rhythm. These 7 swine were excluded from further analysis. Percentages of animals that encountered VF, but could be converted to sinus rhythm to complete the protocol, were similar ($p=0.76$) in Sham (80%) and VNS (85%). The average number of VF episodes before start of VNS or sham treatment was similar between groups (1.8±0.4 vs. 1.4±0.4, $p=0.45$). VF did not occur during VNS or the corresponding sham period or after 15 min of reperfusion (except 1 sham animal at 11 and 15 min of reperfusion).

In the second series of experiments, 4 out of 12 Sham swine encountered irretractable VF during ischemia, while 12 out of 23 LNNA-treated swine encountered irretractable VF during ischemia (all before VNS or Sham stimulation), and hence could not complete the protocol.

Hemodynamics, Global and Regional LV function

CAO of the LAD resulted in complete loss of regional systolic segment shortening, accompanied by an increase in post-systolic shortening, in the LAD perfusion territory, which resulted in decreases in LV systolic pressure, $LVdP/dt_{P40}$, stroke volume, cardiac output, and mean aortic pressure (Table 1). Global and regional LV function only partially recovered during the 120-min reperfusion period.

The 18±4% decrease in heart rate produced by VNS was associated with a 19±2% decrease in cardiac output and a 16±4% and 13±3% decrease, respectively, in mean aortic and LV peak systolic pressure, at 45 min CAO (Table 1). VNS did not alter $LVdP/dt_{P40}$, LV end-diastolic pressure, or regional systolic and post-systolic segment shortening, indicating that VNS did not alter global or regional LV function. These effects of VNS were maintained during reperfusion, although heart rate showed partial escape from VNS during the first 5 min of reperfusion, which was likely due to the occurrence of premature ventricular contractions. Up to termination of VNS, systemic hemodynamics and global and regional LV function were no longer different between VNS and Sham swine.

Table 1. *Systemic Hemodynamics and Global and Regional Left Ventricular Function*

			Coronary Artery Occlusion		Reperfusion	
		Baseline	40 min	45 min	15 min	120 min
Systemic Hemodynamics						
HR (bpm)	Sham	111 ± 6	117 ± 8	116 ± 8	113 ± 7	109 ± 5
	VNS	103 ± 4	107 ± 4	87 ± 4*†§	89 ± 3*†§	109 ± 4
MAP (mmHg)	Sham	94 ± 3	82 ± 3*	80 ± 3*	76 ± 4*	73 ± 3*
	VNS	91 ± 3	77 ± 5*	65 ± 5*†	65 ± 4*†	71 ± 3*
CO (L/min)	Sham	4.2 ± 0.3	3.4 ± 0.1*	3.3 ± 0.1*	3.3 ± 0.2*	2.8 ± 0.1*
	VNS	3.5 ± 0.1‡	2.9 ± 0.2*	2.3 ± 0.1*†	2.4 ± 0.2*†	2.5 ± 0.1*†
SV (mL/beat)	Sham	38 ± 2	30 ± 2*	30 ± 2*	30 ± 2*	26 ± 2*
	VNS	34 ± 2	27 ± 1*	27 ± 2*	28 ± 2*	23 ± 2*
Global and Regional LV Function						
LVSP (mmHg)	Sham	109 ± 3	95 ± 3*	93 ± 3*	90 ± 3*	85 ± 4*
	VNS	106 ± 2	90 ± 5*	78 ± 5*†	79 ± 4*†	85 ± 3*
$LVdP/dt_{P40}$ (mmHg/s)	Sham	1700 ± 160	1340 ± 80*	1320 ± 60*	1330 ± 80*	1120 ± 60*
	VNS	1600 ± 70	1250 ± 80*	1060 ± 70*	1100 ± 80*	1110 ± 50*
LVEDP (mmHg)	Sham	14 ± 1	16 ± 1	15 ± 1	16 ± 1	15 ± 1
	VNS	13 ± 1	17 ± 1*	16 ± 1*	18 ± 1*	16 ± 1*
SS_{LAD} (%)	Sham	15.1 ± 1.4	-7.2 ± 1.0*	-5.9 ± 0.7*	0.7 ± 0.4*†	0.2 ± 0.6*†
	VNS	21.2 ± 1.2	-8.8 ± 1.3*	-7.0 ± 1.2*	2.0 ± 1.2*†	0.1 ± 1.3*†
SS_{LCx} (%)	Sham	13.1 ± 2.1	11.0 ± 2.6	10.8 ± 2.6	12.3 ± 1.9	9.1 ± 1.9*
	VNS	17.2 ± 1.4	17.4 ± 1.2	17.7 ± 1.3	18.1 ± 1.4	15.4 ± 1.2
PSS_{LAD}(%)	Sham	0.9 ± 0.2	10.7 ± 1.3*	9.0 ± 1.1*	2.3 ± 0.4†	2.9 ± 0.7†
	VNS	1.2 ± 0.4	15.0 ± 1.1*	12.5 ± 1.1*†	4.3 ± 1.3*†	5.0 ± 1.4*†
PSS_{LCx} (%)	Sham	0.7 ± 0.3	1.8 ± 0.7*	1.8 ± 0.8*	0.6 ± 0.3†	1.2 ± 0.6
	VNS	0.8 ± 0.2	1.1 ± 0.3	1.2 ± 0.1	1.0 ± 0.3	1.3 ± 0.6

Data are mean ± SEM; *$p<0.05$ vs. corresponding baseline; †$p<0.05$ vs. corresponding 40 min CAO; ‡$p<0.05$ vs. corresponding Sham. CO = cardiac output (L/min); $dP/dt_{P=40}$ = rate of rise in LV pressure pressure of 40 mmHg; HR = heart rate (bpm); LVEDP = left ventricular end-diastolic pressure;LVSP = left ventricular systolic pressure; MAP = mean arterial pressure (mmHg); PSS = postsystolic shortening. SS = systolic shortening; SV = stroke volume (mL/beat).

Coronary Blood Flow and Myocardial Metabolism

During reperfusion, transient increases in coronary blood flow and coronary vascular conductance were observed, together with a transient reversal from lactate consumption to production and a sustained depression of oxygen consumption (Table 2).

There were no significant differences between VNS and Sham swine in the responses of coronary blood flow, coronary vascular conductance, myocardial consumption and extraction of oxygen or lactate, during early reperfusion (Table 2).

Table 2. *Regional Coronary Blood Flow and Myocardial Metabolism*

			Reperfusion	
		Baseline	**15 min**	**120 min**
CBF (mL/min)	Sham	20 ± 4	34 ± 6*	22 ± 3
	VNS	15 ± 1	26 ± 4*	21 ± 2
CBF (mL/beat)	Sham	0.17 ± 0.03	0.30 ± 0.05*	0.21 ± 0.03
	VNS	0.14 ± 0.01	0.30 ± 0.06*	0.20 ± 0.02
MVO_2 (μmol/min)	Sham	91 ± 20	36 ± 6*	28 ± 4*
	VNS	67 ± 7	29 ± 5*	23 ± 3*
MVO_2 per beat (μmol/beat)	Sham	0.77 ± 0.13	0.32 ± 0.05*	0.26 ± 0.03*
	VNS	0.65 ± 0.07	0.33 ± 0.06*	0.21 ± 0.03*
CVC (ml/min/mmHg)	Sham	0.22 ± 0.05	0.49 ± 0.06*	0.35 ± 0.04*
	VNS	0.18 ± 0.02	0.46 ± 0.07*	0.34 ± 0.03*
Lactate Production (μmol/L/min)	Sham	-14 ± 5	10 ± 5*	-7 ± 2
	VNS	-7 ± 1	10 ± 2	-4 ± 2
O_2 Extraction (%)	Sham	73 ± 2	19 ± 2*	21 ± 3*
	VNS	71 ± 2	19 ± 2*	17 ± 2*
Lactate Extraction (%)	Sham	24 ± 4	-14 ± 7*	10 ± 2
	VNS	24 ± 5	-15 ± 3*	6 ± 3

Data are mean ± SEM; *p<0.05 vs. corresponding baseline. CBF = coronary blood flow; CVC = coronary vascular conductance (CBF/[MAP-LAP]); MVO2 = myocardial oxygen consumption; O_2 Extraction = myocardial oxygen extraction.

Infarct-Size and Area of No-Reflow

Ligation of the LAD distal to the first diagonal branch resulted in an average area-at-risk of 26±1% of the LV (Figure 1) and did not differ between Sham (26±1%) and VNS (27±1%; p=0.60). CAO of 45-min resulted in an infarct size in Sham swine of 67±2% of the area-at-risk and a no-reflow area of 54±6% of the infarct area. VNS limited infarct size to 54±5% which was accompanied by a reduction in

no-reflow area of 32±6% (both p=0.03). There were no differences between swine undergoing left or right VNS, in terms of infarct size (left 52±6% vs. right 58±7%, p=0.56) or no-reflow area (left 32±9% vs. right 32±10%, p=1.00). The degree of bradycardia produced by VNS was not predictive of either infarct size (r^2=0.21, p=0.12) or no-reflow area (r^2=0.15, p=0.19).

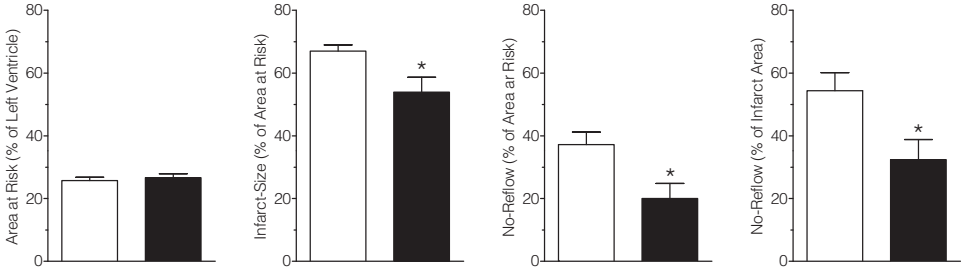

Figure 1. *Effects of VNS on infarct size and No-Reflow*
*Effects of treatment on infarct size and no-reflow of Sham (□) and VNS (■) animals. Data are mean±SEM; *p<0.05 vs. sham.*

Systemic and Regional Inflammation

Systemic TNFα levels did not rise in the early phase after reperfusion while IL6 increased significantly compared to baseline but no differences between treatment groups were found (Figure 2).

Neutrophil and macrophage numbers were increased in the infarcted areas as compared to the remote myocardium, after 120 min of reperfusion. VNS attenuated both neutrophil and macrophage influx into the infarcted area (Figure 3).

Role of NO-synthase

LNNA had no effect on infarct size, no-reflow area or leukocyte influx (Table 3). However, LNNA prevented the VNS-induced limitation of infarct size (71±6% in LNNA+VNS versus 65±5% in LNNA+sham) and no-reflow (22±5% in LNNA+VNS versus 13±4% in LNNA+sham), which was paralled by similar regional leucocyte scores (Table 3).

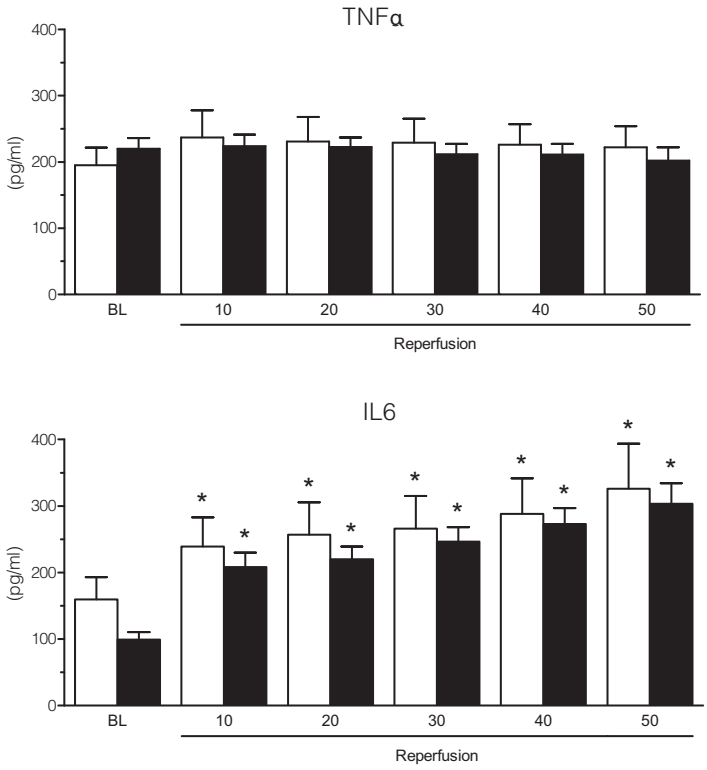

Figure 2. *Effects of VNS on Early markers for Inflammation*
*Legend: Effects of treatment on TNFα and IL6 levels in circulating plasma of sham (□) and VNS (■) animals. Data are mean ± SEM; *P<0.05 vs. corresponding baseline*

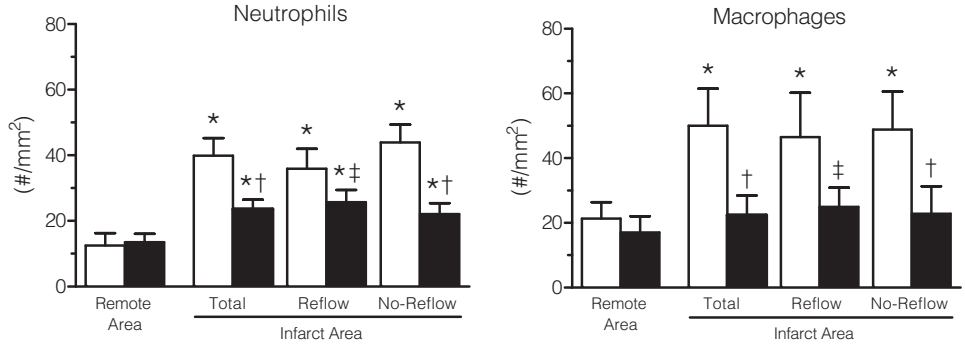

Figure 3. *Effects of VNS on Regional Inflammation*
*Legend: Effects of treatment on neutrophil and macrophage numbers in remote, total infarct, infarct reflow and infarct no-reflow tissue of sham (□) and VNS (■) animals. Data are mean±SEM; *p<0.05 vs. corresponding remote; †p<0.05 vs. sham; ‡p<0.10 vs. sham.*

Table 3. *Effects of NO-synthase inhibition*

	Sham n=8	LNNA+Sham n=5	LNNA+VNS n=6
Area at Risk (% LV)	26 ± 2	25 ± 3	27 ± 2
Infarct-Size (% AR)	50 ± 4	65 ± 5	71 ± 6
No-Reflow (% AR)	4 ± 1	8 ± 2	16 ± 4
No-Reflow (% IS)	9 ± 2	13 ± 4	22 ± 5
Cell influx in infarct area			
Neutrophils (#/mm^2)	12 ± 2	7 ± 2	25 ± 6†
Macrophages (#/mm^2)	58 ± 13	86 ± 35	62 ± 17

Data are Mean ± SEM; *p<0.05 LNNA+Sham vs. Sham; †p<0.05 LNNA+Sham vs. LNNA+VNS. AR = Area at Risk; IS = Infarct-Size; LV = Left Ventricle.

DISCUSSION

The present study is the first to investigate the effect of VNS during early reperfusion on both infarct size and extent of no-reflow in a large animal model of ST-elevation acute myocardial infarction using a clinically translational protocol. The main findings were that (*i*) VNS significantly limited infarct size and extent of no-reflow; (*ii*) these effects were accompanied by reductions in regional infiltration of neutrophils and macrophages; (*iii*) Inhibition of NO-synthase prevented the cardioprotection by VNS against necrosis and no-reflow and leukocyte-influx.

Infarct-Size

Several studies, though not all (24,25), indicate that VNS limits infarct-size, when started prior to (10,11,14), at (12,15,16) or shortly after (13,26) the onset of myocardial ischemia (Table 4). The majority of these studies have been performed in rodents or rabbits, which are sympathetically dominant, and are therefore likely to have a different sympathico-vagal balance than larger mammalian species such as pigs and humans. Although this may increase the effects of VNS in these smaller animal species with low baseline vagal activity, a recent study in swine also found that VNS started at the onset of ischemia (16) limited myocardial infarct-size. From these studies (10-16,24-26), it is difficult to determine whether the protective effect of VNS occurred during ischemia or whether a reduction in lethal reperfusion-injury contributed as well. However, two studies in which no reperfusion was allowed (12,15), suggest that at least part of the protective effect is targeted against ischemic cell death, leaving the question of whether VNS can protect against reperfusion injury unanswered. This question is important because

patients with a pending myocardial infarction typically receive adjuvant therapy only late into the ischemic episode, or just prior to reperfusion. In light of these considerations, we investigated whether VNS can afford cardioprotection when started just prior to reperfusion in a large animal model of STEMI. The results demonstrate that even when started just prior to reperfusion, VNS was still able to limit myocardial infarct-size, thus showing its protection against lethal reperfusion-injury. The observed protection may well depend on the algorithm of VNS applied. This is suggested by a very recent study showing that intermittent VNS (consisting of 21 sec VNS bouts interspersed by 30 sec of no stimulation), started at the very onset of reperfusion and sustained throughout the entire 120 min of reperfusion (Table 4), failed to attenuate infarct size (26). These discordant findings between the latter and the present study may well reflect the importance of full VNS during the golden minute(s) of reperfusion (27).

The mechanism by which VNS limits infarct size is presently incompletely understood, but appears to be independent of the reduction in heart rate produced by VNS. Thus, Calvillo et al. (11) showed that restoring heart rate to baseline levels by atrial pacing did not affect cardioprotection by VNS. Moreover, several studies, including the present one, have shown a lack of correlation between the reduction in heart rate and the reduction in infarct size by VNS (10,11,16). These findings suggest that the VNS-mediated cholinergic activation (11) and muscarinic receptor stimulation (16) protect against necrosis via a direct myocardial mechanism. We therefore studied the involvement of the reperfusion injury signaling kinase pathway, distal to the muscarinic receptor, by investigating the role of NO-synthase (28). The results show that NO-synthase activity was critical for VNS-mediated infarct size and no-reflow limitation. These observations are in line with studies from our laboratory (29,30) that have shown an important role for nitric oxide in cardioprotection against reperfusion-injury, likely by limiting opening of the mitochondrial permeability transition pore (16,22,26). Future studies are needed to further investigate the molecular underpinnings of VNS-mediated cardioprotection.

No-Reflow

Reperfusion following a prolonged period of myocardial ischemia is associated with microvascular obstruction, termed no-reflow (5). No-reflow is the result of endothelial cell damage, deterioration of the glycocalyx, increased neutrophil-plugging, micro-embolization, microvessel-rupture and edema (5,31). No-reflow has been shown to be a strong clinical prognosticator for long-term mortality (5,9), which is, at least in part, due to its close correlation with infarct size (7,23). However,

recent studies suggest that not only infarct size (32), but also the extent of no-reflow (5,8,9) is an independent predictor of clinical outcome, which is supported by experimental studies reporting reductions in no-reflow by hypothermia (8) or pharmacological intervention (21), independent of a limitation in myocardial infarct-size. These recent insights clearly suggest that novel strategies to limit no-reflow have significant therapeutic potential.

The present study is to our knowledge the first to investigate the effects of VNS on the extent of no-reflow. The results indicate that VNS markedly reduced no-reflow, which was accompanied by a reduction in recruitment of macrophages and neutrophils to the infarct area. These findings suggest that VNS modulates the regional immune response and are consistent with activation of the cholinergic anti-inflammatory pathway by VNS (11, 13, 33). VNS-induced reduction of no-reflow in the infarct area was prevented by NO-synthase inhibition in parallel with the abolition of infarct size limitation, indicating that NO-signaling is critical for the cardioprotective effects of VNS against both cardiomyocyte necrosis and microvascular obstruction.

Methodological Considerations

A potential limitation of the present study is that we studied only the very early effects of VNS on infarct size and no-reflow in swine with AMI, with a follow-up limited to 2h post reperfusion. This time-point was chosen in view of the demonstrated lack of development of infarct size and no-reflow over time between 2h and 5h of reperfusion (34), so that we do not expect that infarct size and no-reflow would have evolved much further beyond the 2h point. However, the 2h reperfusion time was clearly insufficient to allow the VNS-mediated infarct size reduction to translate into significant improvements in regional and global LV function. Future studies are required to investigate the long-term effects of infarct size and no-reflow reductions by VNS on LV remodeling and function.

Another limitation of the present study is that only a single VNS protocol was studied and hence it is likely that other VNS algorithms may afford greater cardioprotection (12). Optimization of the VNS protocol may include changes in stimulation frequency (35) and extending the duration of stimulation beyond 15 min of reperfusion.

Table 4. *Studies on the Cardioprotective effects of Vagal Nerve Stimulation*

Author	Species	I/R time	Start VNS	Duration VNS		Infarct-Size (% AR)	No-Reflow (% IA)
Pre / Onset-Ischemia							
Katare et al. (10)	Rat	30min/2h	5 min pre-ischemia	35 min	Sham	85 ± 3	-
					VNS	34 ± 2*	
Calvillo et al. (11)	Rat	30min/24h	5 min pre-ischemia	40 min	Sham	53 ± 5	-
					VNS	7 ± 1*	
Zhao et al. (14)	Rat	60min/2h	15 min pre-ischemia	75 min	Sham	47 ± 4	-
					VNS	27 ± 3*	
Kong et al. (12)	Rat	4h/0h	Onset ischemia	240 min	Sham	52 ± 2	-
					VNS	28 ± 2*	
Katare et al. (15)	Mouse	3h/0h	Onset ischemia	180 min	Sham	56 ± 1	-
					VNS	24 ± 2*	
Buchholz et al. (25)	Rabbit	45min/4h	10 min pre-ischemia	10 min	Sham	45 ± 2	-
					VNS	63 ± 3*	
Buchholz et al. (24)	Rabbit	30min/3h	10-15 min pre-ischemia	10 min	Sham	52 ± 4	-
					VNS	71 ± 4*	
					I-VNS	30 ± 3*	
Shinlapawittayatorn et al. (16)	Swine	60min/2h	Onset ischemia	180 min	Sham	46 ± 5	-
					VNS	19 ± 4*	
					I-VNS	5 ± 2*	
Early / Mid-Ischemia							
Shinlapawittayatorn et al. (26)	Swine	60min/2h	30 min into ischemia	150 min	Sham	46 ± 3	-
					I-VNS	19 ± 3*	
Wang et al. (13)	Rat	30min/2h	15 min into ischemia	30 min	Sham	72 ± 2	-
					VNS	47 ± 3*	
Pre / Onset-Reperfusion							
Shinlapawittayatorn et al. (26)	Swine	60min/2h	Onset reperfusion	120 min	Sham	46 ± 3	-
					I-VNS	44 ± 3	
Uitterdijk et al.	Swine	45min/2h	5 min pre-reperfusion	20 min	Sham	67 ± 2	54 ± 6
					VNS	54 ± 5*	32 ± 6*

Data are Mean ± SEM; *P<0.05 vs. corresponding Sham. All studies were conducted in-vivo except (13) AR = Area at Risk; IA = Infarct Area; I/R = Infarct/Reperfusion time; IS = Infarct-Size; VNS = Vagal Nerve Stimulation; I-VNS = Intermittent Vagal Nerve Stimulation (Buchholz: 10s On/50s Off; Shinlapawittayatorn: 21s On/30s Off).

Clinical Implications

The present study demonstrates that VNS starting just prior to, and lasting only 15 min into, reperfusion is effective in reducing infarct size and no-reflow in a large animal model of reperfused STEMI. VNS thus appears to be an attractive potential adjuvant therapy to limit reperfusion-injury in patients with STEMI. Current technology includes implantable stimulators (36), but with the ongoing development of transvenous and transdermal approaches, that do not require dissection of the vagal nerve, investigation of VNS in the clinical setting of AMI appears warranted.

CONCLUSIONS

The present study in a porcine model of acute myocardial infarction, demonstrated that vagal nerve stimulation (VNS) during early reperfusion limited infarct size and the extent of no-reflow. The cardioprotection appeared to occur independently of the VNS-induced decrease in heart rate and was not associated with a reduction in systemic markers of inflammation. However, VNS did result in reduced neutrophil and macrophage influx into the infarct area. Finally, NO-synthase activity was required for the VNS-induced limitation in infarct size and no-reflow. Taken together, our findings indicate that VNS is a promising novel adjunctive therapy to limit lethal reperfusion-injury.

REFERENCES

1. Silber S, Albertsson P, Aviles FF et al. Guidelines for percutaneous coronary interventions - The task force for percutaneous coronary interventions of the European Society of Cardiology. European heart journal 2005;26:804-847.
2. Task Force on the management of STseamiotESoC, Steg PG, James SK et al. ESC Guidelines for the management of acute myocardial infarction in patients presenting with ST-segment elevation. European heart journal 2012;33:2569-619.
3. Dirksen MT, Laarman GJ, Simoons ML, Duncker DJGM. Reperfusion injury in humans: A review of clinical trials on reperfusion injury inhibitory strategies. Cardiovascular research 2007;74:343-355.
4. Yellon DM, Hausenloy DJ. Myocardial reperfusion injury. N Engl J Med 2007;357:1121-35.
5. Schwartz BG, Kloner RA. Coronary no reflow. Journal of molecular and cellular cardiology 2012;52:873-882.
6. Niccoli G, Burzotta F, Galiuto L, Crea F. Myocardial no-reflow in humans. Journal of the American College of Cardiology 2009;54:281-92.
7. Masci PG, Ganame J, Francone M et al. Relationship between location and size of myocardial infarction and their reciprocal influences on post-infarction left ventricular remodelling. European heart journal 2011;32:1640-8.
8. Hale SL, Herring MJ, Kloner RA. Delayed Treatment With Hypothermia Protects Against the No-Reflow Phenomenon Despite Failure to Reduce Infarct Size. Journal of the American Heart Association 2013;2:e004234.
9. Ndrepepa G, Tiroch K, Fusaro M et al. 5-Year Prognostic Value of No-Reflow Phenomenon After Percutaneous Coronary Intervention in Patients With Acute Myocardial Infarction. Journal of the American College of Cardiology 2010;55:2383-2389.
10. Katare RG, Ando M, Kakinuma Y et al. Vagal nerve stimulation prevents reperfusion injury through inhibition of opening of mitochondrial permeability transition pore independent of the bradycardiac effect. J Thorac Cardiov Sur 2009;137:223-231.
11. Calvillo L, Vanoli E, Andreoli E et al. Vagal Stimulation, Through its Nicotinic Action, Limits Infarct Size and the Inflammatory Response to Myocardial Ischemia and Reperfusion. Journal of cardiovascular pharmacology 2011;58:500-507.
12. Kong SS, Liu JJ, Hwang TC et al. Optimizing the Parameters of Vagus Nerve Stimulation by Uniform Design in Rats with Acute Myocardial Infarction. PloS one 2012;7:e42799.
13. Wang Q, Cheng Y, Xue FS et al. Postconditioning with vagal stimulation attenuates local and systemic inflammatory responses to myocardial ischemia reperfusion injury in rats. Inflammation Research 2012;61:1273-1282.
14. Zhao M, He X, Bi XY, Yu XJ, Wier WG, Zang WJ. Vagal stimulation triggers peripheral vascular protection through the cholinergic anti-inflammatory pathway in a rat model of myocardial ischemia/reperfusion. Basic Research in Cardiology 2013;108:345.
15. Katare RG, Ando M, Kakinuma Y, Arikawa M, Yamasaki F, Sato T. Differential regulation of TNF receptors by vagal nerve stimulation protects heart against acute ischemic injury. Journal of molecular and cellular cardiology 2010;49:234-244.
16. Shinlapawittayatorn K, Chinda K, Palee S et al. Low-amplitude, left vagus nerve stimulation significantly attenuates ventricular dysfunction and infarct size through prevention of mitochondrial dysfunction during acute ischemia-reperfusion injury. Heart rhythm : the official journal of the Heart Rhythm Society 2013;10:1700-1707.
17. Koning MM, Gho BC, van Klaarwater E, Opstal RL, Duncker DJ, Verdouw PD. Rapid ventricular pacing produces myocardial protection by nonischemic activation of KATP+ channels. Circulation 1996;93:178-86.

18. Te Lintel Hekkert M, Dube GP, Regar E et al. Preoxygenated hemoglobin-based oxygen carrier HBOC-201 annihilates myocardial ischemia during brief coronary artery occlusion in pigs. American journal of physiology 2010;298:H1103-13.
19. de Zeeuw S, Trines SA, Krams R, Verdouw PD, Duncker DJ. Cardiovascular profile of the calcium sensitizer EMD 57033 in open-chest anaesthetized pigs with regionally stunned myocardium. British journal of pharmacology 2000;129:1413-22.
20. Duncker DJ, Klassen CL, Ishibashi Y, Herrlinger SH, Pavek TJ, Bache RJ. Effect of temperature on myocardial infarction in swine. The American journal of physiology 1996;270:H1189-99.
21. Li XD, Yang YJ, Geng YJ et al. Tongxinluo reduces myocardial no-reflow and ischemia-reperfusion injury by stimulating the phosphorylation of eNOS via the PKA pathway. American journal of physiology 2010;299:H1255-61.
22. Reffelmann T, Kloner RA. Microvascular reperfusion injury: rapid expansion of anatomic no reflow during reperfusion in the rabbit. Am J Physiol-Heart C 2002;283:H1099-H1107.
23. Uitterdijk A, Sneep S, van Duin R et al. Serial measurement of hFABP and high sensitivity Troponin I post PCI in STEMI. How fast and accurate can Myocardial Infarct Size and No-Reflow be predicted? American journal of physiology 2013;305:H1104-10.
24. Buchholz B, Donato M, Perez V et al. Changes in the loading conditions induced by vagal stimulation modify the myocardial infarct size through sympathetic-parasympathetic interactions. Pflugers Arch 2015;467:1509-22.
25. Buchholz B, Donato M, Perez V et al. Preischemic efferent vagal stimulation increases the size of myocardial infarction in rabbits. Role of the sympathetic nervous system. International journal of cardiology 2012;155:490-491.
26. Shinlapawittayatorn K, Chinda K, Palee S et al. Vagus Nerve Stimulation Initiated Late During Ischemia, but not Reperfusion, Exerts Cardioprotection via Amelioration of Cardiac Mitochondrial Dysfunction. Heart rhythm 2015;467:1509-22.
27. Skyschally A, van Caster P, Iliodromitis EK, Schulz R, Kremastinos DT, Heusch G. Ischemic postconditioning: experimental models and protocol algorithms. Basic Research in Cardiology 2009;104:469-483.
28. Davidson SM, Hausenloy D, Duchen MR, Yellon DM. Signalling via the reperfusion injury signalling kinase (RISK) pathway links closure of the mitochondrial permeability transition pore to cardioprotection. Int J Biochem Cell B 2006;38:414-419.
29. Manintveld OC, Hekkert MTL, van der Ploeg NT, Verdouw PD, Duncker DJ. Interaction Between Pre- and Postconditioning in the In Vivo Rat Heart. Exp Biol Med 2009;234:1345-1354.
30. Manintveld OC, Sluiter W, Dekkers DHW et al. Involvement of reperfusion injury salvage kinases in preconditioning depends critically on the preconditioning stimulus. Exp Biol Med 2011;236:874-882.
31. Galasso G, Schiekofer S, D'Anna C et al. No-Reflow Phenomenon: Pathophysiology, Diagnosis, Prevention, and Treatment. A Review of the Current Literature and Future Perspectives. Angiology 2014;65:180-189.
32. Wu E, Ortiz JT, Tejedor P et al. Infarct size by contrast enhanced cardiac magnetic resonance is a stronger predictor of outcomes than left ventricular ejection fraction or end-systolic volume index: prospective cohort study. Heart 2008;94:730-6.
33. Johnston GR, Webster NR. Cytokines and the immunomodulatory function of the vagus nerve. Brit J Anaesth 2009;102:453-462.
34. Hale SL, Dae MW, Kloner RA. Hypothermia during reperfusion limits 'no-reflow' injury in a rabbit model of acute myocardial infarction. Cardiovascular research 2003;59:715-722.
35. Bonaz B, Picq C, Sinniger V, Mayol JF, Clarencon D. Vagus nerve stimulation: from epilepsy to the cholinergic anti-inflammatory pathway. Neurogastroent Motil 2013;25:208-221.
36. Wagner D, Shelton R, Adams D et al. An interactive implantable vagal nerve stimulator for real-time modulation of cardiac autonomic control. Conf Proc IEEE Eng Med Biol Soc 2012;2012:5749-52.

PART II

Infarct Healing and Left Ventricular Remodeling

CHAPTER 8

Evolution of reperfusion post-infarction ventricular remodeling: new MRI insights

*Tirza Springeling
***André Uitterdijk**
Alexia Rossi
Charlotte Gorsse-Bakker
Piotr A Wielopolski
Willem J van der Giessen†
Gabriel P Krestin
Pim J de Feyter
Dirk J Duncker
Robert-Jan M van Geuns

*Both authors contributed equally

Int J Cardiol 2013 Nov 20:169(5);354-8

ABSTRACT

Background

Our current understanding is that left ventricular (LV) remodeling after acute myocardial infarction (AMI) is caused by expansion of the infarcted myocardium with thinning of the wall and eccentric hypertrophy of the remote myocardium. To study the geometric changes in the remodeling process after reperfused AMI we used cardiac magnetic resonance imaging (CMR).

Methods

Nine juvenile swine underwent a 120-min occlusion of the left circumflex coronary artery followed by reperfusion. CMR was performed at 3 and 36 days post-infarction. Global and regional LV remodeling was assessed including geometric changes of infarcted and remote myocardium; infarct longitudinal length (mm), mean circumferential length (mm), total infarct surface (mm^2), end-diastolic wall thickness (EDWT) (mm) and transmural extent of infarction (TEI).

Results

From 3 days to 36 days post-infarction end-diastolic volume increased by 43% ($p<0.01$). Infarct mass decreased by 36% ($p<0.01$), mainly by reduction of EDWT with 26%, while mean infarct circumferential length and longitudinal infarct length did not change. Remote myocardial mass increased by 23%, which was the result of an increase in its circumferential length from 95±10 mm to 113±11 mm ($p<0.01$), with no change in its EDWT. In contrast, EDWT in the infarct, peri-infarct and border zone decreased.

Conclusions

Contrary to the widely held view this study, using CMR measurements, shows that post-infarction remodeling was not associated with expansion of the infarcted myocardium. These findings suggest that eccentric hypertrophy of the remote myocardium, but not expansion of the infarct region, is responsible for left ventricular dilatation after AMI.

INTRODUCTION

Left ventricular (LV) remodeling after acute myocardial infarction (AMI) is a dynamic process of progressive changes in LV chamber size and shape (1), which can importantly affect the function of the ventricle and is related to prognosis and survival (2). Left ventricular remodeling starts early after AMI, the extent of which depends critically on the size of the infarct (3). It is generally accepted that chamber enlargement is mainly caused by expansion of the circumferential length and thinning of the infarcted myocardium and circumferential lengthening of the remote myocardium (4). Expansion is distortion of the ventricle topography caused by alternations of the infarcted segment and no new infarcted tissue (5). These studies are mainly based on histology, ECG or echocardiography and principally examined by ex-vivo triphenyl tetrazolium chloride (TTC) coloring (5), expansion of ST-elevation or ventricular silhouettes and dyskinesia/akinesia (6,7), but are not able to assess the actual infarct size quantitatively. SPECT and contrast enhanced CMR allows delineation of the acute necrotic infarct zone and late fibrotic infarct scar. Compared to SPECT, CMR has a higher contrast-to-noise and spatial resolution, which allows more accurate analysis of the necrotic and fibrotic infarct zone (8,9). In addition, CMR cine provides quantitative information of global and regional myocardial function. This makes CMR an excellent tool to analyze post-infarction remodeling in-vivo in both humans and animal while being able to study the differences between infarcted and remote myocardium. The present study was designed to assess time-dependent geometric changes in both infarcted and remote myocardium using a large animal model. For this purpose we studied in-vivo the geometric changes in remodeling after reperfused AMI of the infarcted and the remote myocardium in swine.

METHODS

Animal model

All animal experiments conform with the “Guide for the Care and Use of Laboratory Animals” (NIH Publication 86-23, revised 1996) and were approved by the Animal Care Committee of our institution. Nine Yorkshire x Landrace swine (5-6 months old, 4 female (30.2 ± 1.2 kg) and 5 neutered male (29.1 ± 0.8 kg)) entered the study. All animals were sedated with an intramuscular injection of midazolam (1 mg/kg), ketamine (20 mg/kg) and atropine sulphate (1mg). After placement of an intravenous catheter, animals were anesthetized with thiopental sodium (17 mg/kg), intubated and mechanically ventilated with a mixture of O_2 and N_2 (1:2). Anesthesia was maintained with intravenously administered fentanyl (20 μg/kg/hr).

Subsequently all animals received antibiotic prophylaxis comprised of a mixture of intramuscular procainebenzylpenicilline and dihydrostreptomycine sulphate (20 mg/kg and 25 mg/kg). Pancuronium bromide was administered as muscle relaxant (0.13 mg/kg). Under sterile conditions, a thoracotomy of the left intercostal space was performed (10). The pericardium was opened and the proximal part of the left circumflex coronary artery was dissected. Next, the left circumflex artery was ligated for 120 minutes to induce a transmural infarction of the lateral wall (5). Immediately after ligation fentanyl infusion was stopped and anesthesia was continued using isoflurane gas anesthesia (1-2% v/v). After 120 minutes the ligation was removed and reperfusion was allowed. The pericardium and chest wall were closed and the animals were allowed to recover. Post-surgery, all animals were given buprenorphine intramuscular (10 mg/kg).

Cardiac imaging was performed 3 days and 5 weeks post-infarction. For this purpose, animals were sedated, anesthetized and intubated as described above. Anesthesia during imaging was maintained with fentanyl and if necessary thiopental sodium (bolus 50 mg). Mechanical ventilation and peri-imaging breath-holds were performed using a mobile ventilator (Carina™, Dräger Medical, Best, The Netherlands). Muscle relaxation was achieved using pancuronium bromide.

MRI protocol

The MRI examinations were performed on a 3.0-Tesla clinical scanner (Signa HD, GE Medical systems, Milwaukee, Wisconsin) using a dedicated cardiac four-channel phased array cardiac receiver coil. Repeated breath-holds and gating to the electrocardiogram were applied to minimize the influence of cardiac and respiratory motion on data collection. Both baseline and follow-up CMR protocols consisted of cine imaging and delayed enhancement (DE).

Cine imaging was performed using a steady-state, free-precession technique (FIESTA). Imaging parameters were; 24 temporal phases per slice, field of view 28-30 x 28-30 cm, matrix size was 128 x 224, repetition time 2.5-2.8 ms, number of average minimal 1.0, time to echo 1.0 ms; flip angle 55 degrees, 12 views per segment, slice thickness was 6.0 mm, slice gap was 0 mm using a standard techniques as described previously (8).

DE was performed with a gated breath hold 2-dimensional T1-inversion recovery gradient-echo sequence minimal of 10 minutes after infusion of Gadolinium DTPA (total of 0.2 mmol/kg intravenously). Imaging parameters were; field of view 28-30

x 28-30 cm, matrix size was 192 x 160, repetition time 6.3 ms, number of average minimal 2.0, time to echo 1.6 ms, flip angle 20 degrees, slice thickness was 6.0 mm, slice gap was 0, inversion time 200-300 ms (adjusted to null the signal of the remote myocardium). The slice locations of the DE images were copied from the cine images.

CMR data analysis and definitions

All images were transferred to a Microsoft Windows™ work station based personal computer for analysis using the CAAS-MRV program (version 3.3.1; Pie Medical Imaging, Maastricht, The Netherlands). Cine imaging and DE images were acquired during the same acquisition session using matching slice positions. Registration of follow-up and baseline cine imaging and DE was achieved by consensus of 2 observers using anatomic landmarks like papillary muscle and right ventricular insertion sites.

For global function the images were analyzed using the additional information of the long axis to limit the extent of volume at the base and the apex of the heart. More details about this analysis method have been described previously (11). To determine infarct mass, infarct volume was determined on short axis DE images using a semi-quantitative analysis for the detection of the DE regions (>2SD of the mean SI of the contra-lateral myocardium). The infarct volume was multiplied by 1.05 g/ml to obtain myocardial infarct mass (8).

For the geometric changes as well as regional functional analyses, only the slices with complete circumferential myocardium were used. Each slice was divided into 36 segments (figure 1). End-diastolic wall thickness (EDWT) and end-systolic wall thickness (ESWT) were measured on cine imaging and expressed in millimetres (mm). Segmental wall thickening (SWT) was calculated by subtracting the EDWT from the ESWT divided by the EDWT and multiplied by 100%.

Longitudinal infarct length was defined as the total number of slices containing infarction multiplied by slice thickness (6 mm) expressed in mm. Total circumferential length per slice was calculated by averaging the endocardial and epicardial circumferential length, expressed in mm. To distinguish between proportional changes and absolute changes we looked at total circumferential length per slice of the infarct and remote myocardium respectively expressed in degrees and in mm. The total circumferential infarct length in degrees was calculated by dividing the number of infarcted segments by the total of 36 segments multiplied by 10

degrees (figure 1). Three basal slices were selected from the basal level of each heart for analysis of the mean circumferential length. These slices were selected because the infarct pattern in this region was typical for a lateral infarction and included infarcted and remote myocardium. Slices more apical contained little to no infarcted myocardium. Mean circumferential remote length was calculated in the same way as the infarct region using the non-infarcted segments.

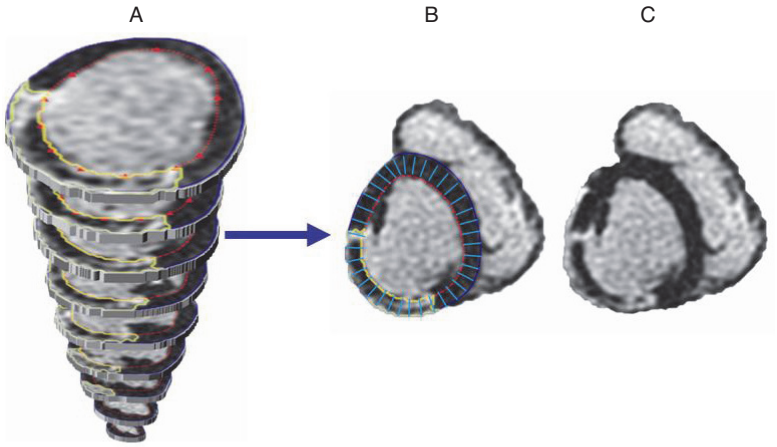

Figure 1. *Segmental analyses*
A. Complete analyzed short axis delayed enhancement from base to apex in 9 slices. B. Slice 3 short axis delayed enhancement analyzed including segmental lines. Blue: epicardial contour, Red: endocardial contour, Yellow area: infarction, Blue: segmental lines (36). C. Slice 3 short axis delayed enhancement

Total infarct surface is the sum of the total infarct area in each slice, which is calculated by multiplying circumferential length with the slice thickness of the total infarct expressed in mm^2.

Thickness to length ratio was defined as the ratio between mean EDWT and the mean circumferential length multiplied by 100%.

Transmural extent of infarction was calculated by dividing the hyperenhanced area by the total area of the pre-defined segment, expressed in %. The enhanced rim was calculated by dividing TEI by 100% multiplied by EDWT of the segment expressed in mm. The unenhanced rim was calculated by subtracting the enhanced rim from the EDWT, expressed in mm. The most lateral segment demonstrating enhancement was defined as peri-infarct. The first non-infarcted segment adjacent to the enhanced region was defined as border zone. Figure 2 depicts the various parameters of the infarcted region and remote myocardium.

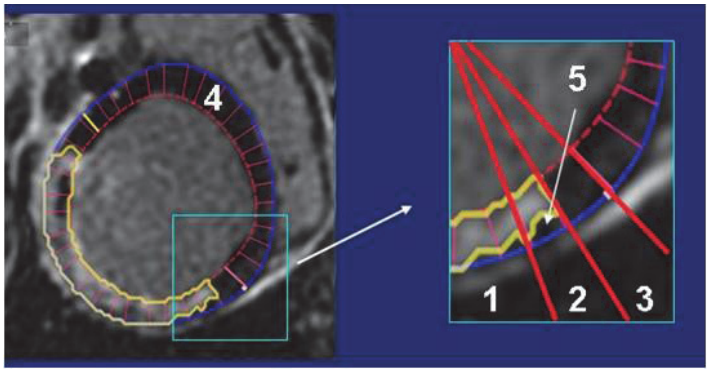

Figure 2. *Definitions of the infarcted area*
Left an analyzed short axis delayed enhancement; Blue: epicardial contour, Red: endocardial contour, Yellow area: infarction, Pink: segmental lines (36). On the right an enlargement of the borders of the infarct and definitions of the different zones 1. infarct zone, 2. peri-infarct zone, 3. border zone 4. remote myocardium. 5 unenhanced rim

Statistical analysis

Continuous data are expressed as mean values ± one standard deviation (SD), whereas dichotomous data are expressed as numbers and percentages. To test the difference in clinical characteristics and CMR findings between the infarcted and remote myocardium an unpaired t-test was used for continuous variables and Chi-squared test for categorical variables. To test the significance of changes in variables over time within each group, paired t-test was used. Statistical significance was assumed at a p-value <0.05 (two-tailed). All analyses were performed with SPSS 15.0 (SPSS Inc, Chicago, Illinois, 2006).

RESULTS

Bodyweight increased from 29±1 kg at baseline to 38±2 kg at follow-up due to normal growth. Functional imaging showed an increase in LVEF from 34±7% to 41±5% (p=0.02) between baseline and follow-up. EDV and ESV both increased between baseline and follow-up (EDV from 79±6 ml to 113±14 ml, p=0.02 and ESV from 52±6 ml to 67±9 ml, p<0.01). A small, albeit non-significant, increase in total left ventricle mass between baseline and follow-up was observed from 55±4 gram to 58±5 gram (p=0.13).

On delayed enhanced imaging all swine showed a transmural infarction of the lateral left ventricular wall which had decreased by 36% at follow-up, (from 18±4 gram to 11±3 gram, p<0.01). Conversely, remote myocardial mass increased

by 24% (38±5 to 46±3 gram, p<0.01). The largest change in dimensions in the infarct region was a 25% decrease in EDWT (table 1), while mean absolute circumferential, and longitudinal, length did not change (from 71±12 mm to 70±19 mm, p=0.79 and from 46±10 mm to 49±9 mm (p=0.18), respectively). In line with these measurements total infarct surface also did not change (from 2167±617 to 2334±822 mm^2, p=0.32). Hence the decrease in total infarct mass is principally the result of a decrease in EDWT and not due to changes in circumferential or longitudinal length. This is also reflected in the significant decrease of the thickness to length ratio (from 9±2% to 7±2%, (p=0.03)). Figure 3 shows a typical example of the difference in circumferential length at baseline and follow-up in one animal.

Table 1. *Geometric changes in the infarct region and remote myocardium.*

Geometric variable	Infarct			Remote		
	baseline	follow-up	p	baseline	follow-up	p
Myocardial mass (gram)	17 ± 4	11 ± 3	<0.01	38 ± 5	46 ± 4	<0.01
End-diastolic wall thickness (mm)	6.1 ± 0.7	4.5 ± 0.4	<0.01	5.3 ± 0.7	5.4 ± 0.4	0.70
Mean circumferential length (degrees)	134 ± 23	119 ± 30	0.01	226 ± 23	241 ± 30	0.01
Mean circumferential length (mm)	71 ± 12	70 ± 19	0.79	95 ± 10	113 ± 11	<0.01
Longitudinal length (mm)	46 ± 10	49 ± 9	0.18			
Thickness to-length ratio	8.9 ± 1.5	7.0 ± 2.5	0.03	5.9 ± 1.3	4.9 ± 1.0	<0.01

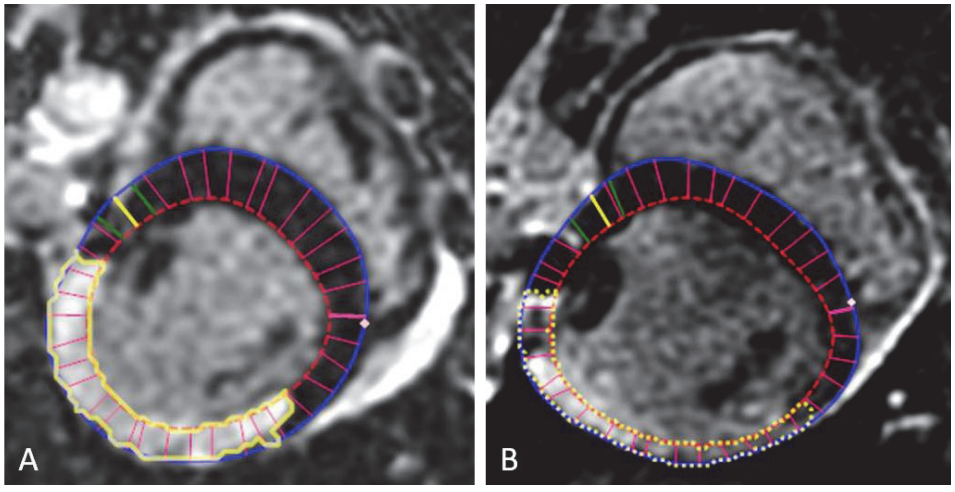

Figure 3. *Example circumferential length*
A. Analyzed short axis delayed enhancement at baseline. B. Analyzed short axis delayed enhancement at follow-up. Circumferential infarct length decreased from 134 degrees at baseline to 107 degrees at follow-up.

The remote myocardium showed almost the opposite remodeling with no change in EDWT between baseline and follow-up and a significant increase in mean circumferential length of the remote myocardium in mm between baseline and follow-up (from 95±10 mm to 113±11 mm, p<0.01).

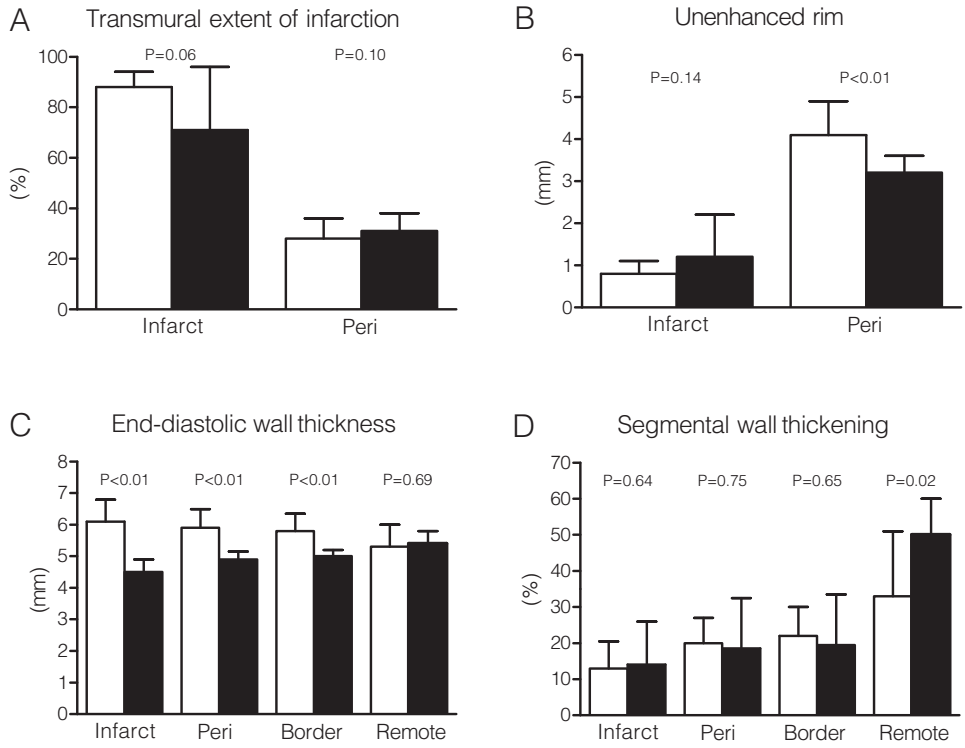

Figure 4. *Regional infarct analyses*
Regional infarct analyses in the infarct zone, peri-infarct zone, border zone and remote myocardium at baseline (□) and follow-up (■). A. Transmural extent of infarction (%) B. Unenhanced rim (mm) C. End-diastolic wall thickness (mm) D. segmental wall thickening (%).

Despite the stable circumferential length of the infarct zone in mm over time, the increase of the circumferential length of the remote region translated into a decrease in relative infarct size from 134±23 to 119±30 degrees (p=0.01).

Regional remodeling and function (TEI, unenhanced rim, EDWT and SWT) in the infarct, peri-infarct, border and remote zones are shown in figure 4. In the infarct zone TEI was reduced from 88±6% to 71±25% (p=0.06) due to a decrease in EDWT with no change in the unenhanced rim thickness. In the peri-infarct zone, TEI was less (28±8%) and stable over time (31±7%, p=0.10), as EDWT and the unenhanced

rim thickness similarly decreased. By definition the border zone showed no TEI but, interestingly, showed abnormal function (SWT 22±7%). At follow-up this area also demonstrated significant remodeling with a decrease in EDWT without a recovery of function. True remote areas showed also acute dysfunction (SWT 35±19%), but with significant improvement over time. Remodeling in these areas did not include a change of EDWT (5.3±0.7 mm to 5.4±0.4 mm, p=0.69)

DISCUSSION

Remodeling after AMI has been a process with alterations in structure and function in response to hemodynamic load and/or cardiac injury involving both infarcted and non-infarcted myocardium. Despite optimal treatment of AMI with primary percutaneous coronary intervention, remodeling still occurred in the majority of patients, which is a major determinant of heart failure (12). To understand this global LV enlargement, regional and geometric changes of the LV-wall have to be studied in order to unravel the various components that contribute to the remodeling process of reperfused AMI. CMR allows precise assessment of these changes.

The present study was designed to assess time-dependent changes in geometry of the infarcted and remote myocardium using CMR in a large animal infarct-reperfusion model. The major finding of the present study is that in reperfused post-infarct LV remodeling is not due to expansion of the infarct region (i.e. an increase in circumferential length of the infarcted myocardium), but rather is due to an increase in circumferential length of the remote myocardium. In addition, the present study confirms the decrease of infarct mass, but reveals that is principally due to thinning of the LV wall. Finally, the remote myocardial mass increases which is due to the increased remote circumferential length with no change in remote LV wall thickness.

Structural changes of infarcted and remote surviving myocardium

Necrosis after reperfusion of the occluded vessel in the myocardium at risk is an ongoing process. The current paradigm of post-infarction remodeling describes an increase of infarct size and microvascular obstruction in the first 48 hours after the acute event due to necrosis, apoptosis, and autophagy (13,14). In the following days and weeks the infarct mass decreases by approximately 30% caused by thinning of the wall, which is accompanied by expansion of the circumferential length (4,6,15). In the present study we also observed a 30% decrease in myocardial mass but contrary to current paradigm we demonstrated that between 72 hours and 5 weeks after reperfused infarction there was no appreciable expansion of the infarct zone,

reflected in an increase in circumferential length of the infarcted region. Hence, the infarct mass reduction was mainly caused by thinning of the wall, probably due to reversal of edema and removal of necrotic tissue, which was replaced by firm fibrotic scar tissue.

CMR demonstrated that remote myocardial mass increased by an increase of circumferential length between 72 hours and 5 weeks, without a significant change in wall thickness. This increase in circumferential length reflects eccentric hypertrophy characterized by lengthening of the cardiomyocytes with no or minimal cardiomyocyte thickening (16), and serves to maintain stroke volume and cardiac output short-term.

The present study demonstrates that the current paradigm may require adjustment. Thus, reperfused infarct remodeling was mainly due to increase of the circumferential length of the remote myocardium and was not associated with expansion of the infarct region.

The differences between the present study and previous reports is not readily explained, but several reasons could be forwarded. First, the initial studies were based on non-reperfused infarction models, while we used a model of reperfused infarction which incorporates the current treatment for the majority of AMI patients. Second, we used a large animal model which may not be fully comparable to the clinical studies which form the basis of the current paradigm (5-7). AMI in the clinical setting is accompanied by many confounders, including collaterals, diabetes, unknown ischemia time, etc. Studies in healthy large animal models, like swine, are not affected by those confounders that can influence the infarcted and remote myocardium (9). Thirdly, there are striking differences in the assessment of LV remodeling. For example, Hutchins and Bulkley examined histology of human hearts, but they had no serial comparison. These authors evaluated LV remodeling only at a single time-point and by studying the cardiac geometry indirectly by ventricular topography (5). Erlebach and Eaton studied distortion of geometry of the heart using echocardiography (6), which made it possible to study the remodeling process at different time points. However, echocardiography is not able to accurately identify the infarct zone and therefore this study may inadvertently have included the dysfunctional non-infarcted area which might be larger during the remodeling process resulting in conclusion that there was infarct expansion. In the present study, using state of the art CMR technology, we could clearly identify the non-infarcted remote myocardial region as the principal contributor to global LV remodeling.

Functional changes in the infarct and remote surviving myocardium

CMR has the unique capability to relate regional function to infarction. The present study demonstrated that 3 days post-AMI, infarcted as well as remote myocardial function was reduced, where only remote myocardial function recovered at 5 weeks. An explanation for the reduced function of the remote myocardium at 3 days post-AMI is not readily found, but could be due to the increase in LV radius and consequently an increase in systolic wall stress. In addition there is evidence that fibroblast infiltration and increased edema also occur in the remote myocardium and not just in the infarct region (17,18). The combination of these factors can lead to decreased cell interaction and resulting in diminished wall contraction. In the following days/weeks, edema will resolve and fibroblasts will be removed and the remote myocardial cells will adjust to the increased wall stress by compensatory increase of the cells and especially of contractile intracellular structures causing increased remote circumferential length which will improve remote function.

The border zone showed wall motion abnormalities, which did not improve in 5 weeks even though infarcted tissue was not present in this zone. Presumably the lack of improvement of the border zone was due to continued high wall stress, which is maximal in this area, and to disrupted mechanical interaction between the fibrotic tissue and border zone myocardium (19).

Methodological considerations

All our animals were 4-5 months old and were still growing during the study period, which may have influenced LV growth making it difficult to distinguish between maladaptive remodeling and physiological growth. All animals had a transmural infarction and findings may be different in smaller non-transmural infarcts; therefore our conclusion cannot be extrapolated to non-transmural infarction.

CONCLUSION

Using a combination of regional geometric imaging of infarct and remote myocardial regions, we demonstrated that the current paradigm of reperfused post-infarct remodeling requires adjustments and is not associated with expansion of the infarct region, but confirms the association with wall thinning of the infarcted myocardium and circumferential lengthening of the remote myocardium without thickening of the wall. Therefore remodeling of the remote myocardium, and not of the infarct region, is principally responsible for LV dilatation after AMI.

REFERENCES

1. Gaudron P, Eilles C, Ertl G, Kochsiek K. Compensatory and noncompensatory left ventricular dilatation after myocardial infarction: time course and hemodynamic consequences at rest and during exercise. Am Heart J 1992;123:377-85.
2. Gaudron P, Eilles C, Kugler I, Ertl G. Progressive left ventricular dysfunction and remodeling after myocardial infarction. Potential mechanisms and early predictors. Circulation 1993;87:755-63.
3. Masci PG, Ganame J, Francone M et al. Relationship between location and size of myocardial infarction and their reciprocal influences on post-infarction left ventricular remodelling. European heart journal 2011;32:1640-8.
4. Pfeffer MA, Braunwald E. Ventricular remodeling after myocardial infarction. Experimental observations and clinical implications. Circulation 1990;81:1161-72.
5. Hutchins GM, Bulkley BH. Infarct expansion versus extension: two different complications of acute myocardial infarction. Am J Cardiol 1978;41:1127-32.
6. Erlebacher JA, Weiss JL, Eaton LW, Kallman C, Weisfeldt ML, Bulkley BH. Late effects of acute infarct dilation on heart size: a two dimensional echocardiographic study. Am J Cardiol 1982;49:1120-6.
7. Eaton LW, Weiss JL, Bulkley BH, Garrison JB, Weisfeldt ML. Regional cardiac dilatation after acute myocardial infarction: recognition by two-dimensional echocardiography. N Engl J Med 1979;300:57-62.
8. Baks T, van Geuns RJ, Biagini E et al. Recovery of left ventricular function after primary angioplasty for acute myocardial infarction. European heart journal 2005;26:1070-1077.
9. Moelker AD, Baks T, van den Bos EJ et al. Reduction in infarct size, but no functional improvement after bone marrow cell administration in a porcine model of reperfused myocardial infarction. European heart journal 2006;27:3057-64.
10. van der Velden J, Merkus D, Klarenbeek BR et al. Alterations in myofilament function contribute to left ventricular dysfunction in pigs early after myocardial infarction. Circ Res 2004;95:e85-95.
11. Kirschbaum SW, Baks T, Gronenschild EH et al. Addition of the long-axis information to short-axis contours reduces interstudy variability of left-ventricular analysis in cardiac magnetic resonance studies. Invest Radiol 2008;43:1-6.
12. Dixon JA, Spinale FG. Myocardial remodeling: cellular and extracellular events and targets. Annual review of physiology;73:47-68.
13. Dixon JA, Spinale FG. Myocardial remodeling: cellular and extracellular events and targets. Annu Rev Physiol 2011;73:47-68.
14. Rochitte CE, Lima JA, Bluemke DA et al. Magnitude and time course of microvascular obstruction and tissue injury after acute myocardial infarction. Circulation 1998;98:1006-14.
15. Weisman HF, Healy B. Myocardial infarct expansion, infarct extension, and reinfarction: pathophysiologic concepts. Prog Cardiovasc Dis 1987;30:73-110.
16. Anversa P, Olivetti G, Capasso JM. Cellular basis of ventricular remodeling after myocardial infarction. Am J Cardiol 1991;68:7D-16D.
17. Rolf A, Assmus B, Schachinger V et al. Maladaptive hypertrophy after acute myocardial infarction positive effect of bone marrow-derived stem cell therapy on regional remodeling measured by cardiac MRI. Clin Res Cardiol 2011;100:983-92.
18. Yang Z, Berr SS, Gilson WD, Toufektsian MC, French BA. Simultaneous evaluation of infarct size and cardiac function in intact mice by contrast-enhanced cardiac magnetic resonance imaging reveals contractile dysfunction in noninfarcted regions early after myocardial infarction. Circulation 2004;109:1161-7.
19. Rumberger JA, Behrenbeck T, Breen JR, Reed JE, Gersh BJ. Nonparallel changes in global left ventricular chamber volume and muscle mass during the first year after transmural myocardial infarction in humans. J Am Coll Cardiol 1993;21:673-82.

CHAPTER 9

Intermittent pacing therapy favorably modifies infarct remodeling

*__André Uitterdijk__
*Tirza Springeling
Kevin CM Hermans
Daphne Merkus
Vincent J de Beer
Charlotte Gorsse-Bakker
Eric Mokelke
Evangelos P Daskalopoulos
Piotr A Wielopolski
W Matthijs Blankesteijn
Frits W Prinzen
Willem J van der Giessen†
Robert-Jan M van Geuns
Dirk J Duncker

*Both authors contributed equally

Submitted

ABSTRACT

Despite early revascularization, remodeling and dysfunction of the left ventricle (LV) after acute myocardial infarction (AMI) remain important therapeutic targets. Intermittent pacing therapy (IPT) of the LV can limit infarct-size, when applied during early reperfusion. However, the effects of IPT on post-AMI LV-remodeling and infarct-healing are unknown. We therefore investigated the effects of IPT on global LV-remodeling and infarct-geometry in swine with a 3-day old AMI. For this purpose, fifteen pigs underwent 2h ligation of the left circumflex coronary artery followed by reperfusion. A pacing lead was implanted in the peri-infarct zone. After three days, global LV-remodeling and infarct-geometry were assessed using magnetic resonance imaging (MRI). Animals were stratified into Control and IPT groups. Thirty-five days post-AMI, follow-up MRI was obtained and myofibroblast content, markers of extracellular matrix (ECM) turnover and Wnt/Frizzled signaling in infarct tissue were studied. Results show that IPT had no significant effect on global LV-remodeling, function or infarct-mass, but attenuated infarct-healing. In control pigs, infarct-mass reduction was principally due to a 26.2±4.4% reduction in infarct-thickness, in IPT pigs it was mainly due to a 35.7±4.5% decrease in the number of infarct-segments with no significant change in infarct-thickness. Myofibroblast content was higher in IPT (10.9±2.1%) compared to Control (5.4±1.6%; $P \leq 0.05$). Higher myofibroblast presence did not coincide with alterations in expression of genes involved in ECM-turnover or Wnt/Frizzled signaling at 5 weeks follow-up. Taken together, IPT limited infarct-expansion and altered infarct-composition, showing that IPT influences remodeling of the infarct zone, likely by increasing regional myofibroblast content.

INTRODUCTION

The prevalence of heart failure continues to rise worldwide (1,2). An important risk factor for heart failure is left-ventricular (LV) cardiac remodeling following acute myocardial infarction (AMI), with infarct size as its principal determinant (1,3). Despite advances in the treatment of AMI and subsequent cardiac remodeling, a need exists for novel adjunctive therapies. Current strategies under investigation for cardioprotection include pharmacological agents or application of brief mechanical interruptions of coronary blood flow either before ischemia or during early reperfusion to protect the myocardium by reducing infarct size (4,5). In addition, there is evidence that intermittent pacing therapy (IPT) is capable of limiting infarct size not only when applied prior to ischemia (6,7), but also when applied during early reperfusion (8,9), resulting in blunting of subsequent LV remodeling (10).

Presently, it is unclear whether IPT is capable of limiting LV remodeling independent of its protection against acute myocardial necrosis, i.e. when started a few days after reperfusion. Consequently, the aim of the present study was to investigate the effects of dyssynchronous IPT of the left ventricle (IPTVVI), when started in the sub-acute phase after reperfusion, in a large animal model of transmural reperfused AMI produced by a transient coronary artery occlusion (CAO). For this purpose, swine were subjected to a 120-min CAO followed by reperfusion, three days after which they underwent cine-MRI and delayed enhancement MRI (DE-MRI) to assess global LV remodeling and function as well as infarct-geometry. Subsequently animals received IPTVVI (3x5 min b.i.d.) throughout the five weeks post-AMI.

MATERIALS AND METHODS

Experiments were performed in thirty-one 5-6 month old Yorkshire x Landrace pigs of either sex and were conducted in compliance with the “Guide for the Care and use of Laboratory Animals” and after written approval of the Animal Care Committee of the Erasmus MC.

Acute effects of IPTAAI and IPTVVI on LV function

In four chronically instrumented swine we investigated the acute hemodynamic responses to intermittent dyssynchronous pacing of the left ventricle (IPTVVI) in comparison with intermittent synchronous atrial pacing (IPTAAI).

Surgery. Swine were sedated (ketamine 20 mg/kg IM; midazolam, 1 mg/kg, IM; atropine 1 mg, IM), anesthetized (thiopenthal sodium, 15 mg/kg, IV), intubated and

ventilated with O2/N2 (1/3 v/v), to which isoflurane was added (1-2% v/v). Under sterile conditions, the chest was opened and pressure catheters and flow probes were implanted to monitor hemodynamics and LV function (11,12). The proximal left circumflex coronary artery (LCx) was ligated to produce AMI (12). A bipolar atrial lead was sutured onto the right atrium and connected to the subcutaneously implanted pacing device (Insignia Entra 1296, Guidant, St Paul, MN). A unipolar epicardial pacemaker lead was positioned in the mid-anterior wall position near the LAD coronary artery. After proper functioning of the pacing setup was ascertained (Zoom 2920, Guidant, St Paul, MN, United States), the chest was closed and animals were allowed to recover. Swine received analgesia (buprenorphine, 0.01 mg/kg/day, IM) during the first 48h post-surgery.

*Experimental Protocol***.** Five days after surgery, with swine resting quietly, hemodynamic measurements were recorded. Subsequently, swine underwent three consecutive 5-min episodes of AAI or VVI pacing with heart rates at 30 beats/min above resting levels, separated by 5-min intervals of normal sinus rhythm. AAI and VVI pacing protocols were randomly performed on separate days.

Effects of chronic IPTVVI on global LV and regional infarct remodeling

*Surgery***.** Swine (n=27) were sedated, anesthetized, intubated and ventilated as described above. Anesthesia was maintained with fentanyl (20 μg/kg/hr, IV) until LCx occlusion, followed by isoflurane (1-2% v/v). Antibiotic prophylaxis consisted of procainebenzylpenicilline (20 mg/kg, IM) and dihydrostreptomycine (25 mg/kg, IM). Following thoracotomy via the third left intercostal space a polyvinylchloride catheter was placed in the aortic arch, the pericardium was opened and the proximal LCx was dissected. A unipolar epicardial lead was screwed into the anticipated infarct border zone, followed by 2h of LCx occlusion. The pericardium and chest were closed and the animals were allowed to recover, receiving analgesia (buprenorphine, 0.01 mg/kg/day, IM) for 48h. Pacemakers were interrogated weekly. Six swine died during the AMI procedure; two swine died during the first 24 hours post-AMI; one swine died during transportation to the MRI at 3 days.

Experimental Protocol. Three days after AMI, cardiac MRI was performed. Swine were sedated and intubated as described above. Mechanical ventilation and peri-imaging breatholds were performed using a mobile ventilator. During MRI, anesthesia was maintained with fentanyl (20μg/kg/h, IV) and thiopental sodium (100 mg bolus). Muscle relaxation was achieved using pancuronium bromide (2-4

mg, IV). Post-imaging, animals received antibiotic prophylactics as above and were allowed to recover. Then, animals were randomized to either Control or IPTVVI and pacemakers remained switched off (Control) or were started (IPTVVI). Importantly, none of the remaining 18 swine died prematurely after stratification into Control (n=11) or IPTVVI (n=7) groups. The IPTVVI pacing protocol was applied every 12h (6 AM and 6 PM), consisting of three times 5-min of pacing at 30 beats/min above sinus rhythm (AV-delay 10 ms) separated by 5-min of normal sinus rhythm. Post-hoc analysis of pacemaker readouts could not confirm proper pacing in one IPTVVI animal whereas in the Control group two animals received unplanned indiscriminate pacing. Consequently, for final analysis 6 swine were included in the IPTVVI group and 9 swine were included in the Control group. At one and five weeks post-AMI arterial blood samples were collected in subsets of animals (n=5 per group). Five weeks after onset of treatment, cardiac MRI measurements were repeated and animals were sacrificed for histological and molecular analysis of the infarct-zone.

Cardiac Magnetic Resonance Imaging Cardiac MRI was performed and analyzed on a 3T scanner as described before (13,14). Global and regional cardiac function and infarct geometry were assessed at baseline (3 days post-AMI), i.e. before treatment and at 5 weeks follow-up (see Supplemental Methods).

*Biomarkers***.** Arterial blood samples were collected 1 and 5 weeks post-AMI in EDTA tubes (n=5) and plasma was stored at -80 °C. Markers of inflammation (TNFα) and extracellular matrix turnover (MMP-9, TIMP-1) were quantified using enzyme-linked immunosorbent assays (ELISA) according to manufacturer's instructions (see Supplemental Methods).
Histology. At 5 weeks follow-up, transverse sections of infarct-tissue were fixed in 4% formaldehyde and embedded in paraffin. To quantify myofibroblasts in the infarct area, sections were stained for alpha smooth muscle actin (αSMA; (15); see Supplemental Methods). Data were expressed as myofibroblast area / total tissue area (%).

*RT-PCR***.** Porcine infarct tissue was homogenized and RNA was isolated. The isolated RNA was assessed for concentration and purity (A260/A280 ratio), and reverse-transcribed into cDNA (see Supplemental Methods). The expression of 17 genes related to either myofibroblast presence, regulation or differentiation were quantified as well as 6 genes involved in extracellular matrix turnover (see Table 2. and Supplemental Methods). Quantification of gene expression was performed using the comparative Ct (ΔCt) method and results are expressed as ratios to the housekeeping gene cyclophilin.

Statistical Analysis

All data are expressed as mean±SEM. Data were analyzed using two-way (time x treatment) ANOVA followed by post-hoc testing, when appropriate, of within treatment group differences with paired *t* testing, and of between treatment group differences with unpaired *t* testing (SPSS 15.0, IBM, Armonk, NY, United States). $p \leq 0.05$ (two-tailed) was considered statistically significant.

RESULTS

Acute effects of IPTAAI and IPTVVI on LV function

None of the 4 pigs experienced ventricular arrhythmias during AAI or VVI pacing. AAI to 30 beats/min (~25%) above baseline heart rates produced 10-15% increases in global LV contractility (LVdP/dtP40) and cardiac output, while stroke volume decreased by 10% likely due to the reduction in LV filling pressure. In contrast, VVI to 30 beats/min above baseline heart rates had no significant effect on LVdP/dtP40, and failed to increase cardiac output, as stroke volume decreased by ~25% (Figure 1). Importantly, these findings indicated that ventricular pacing was not associated with arrhythmias or hemodynamic instability in swine with a recent AMI.

Effects of chronic IPTVVI on global LV and regional infarct remodeling

Table 1 summarizes global LV anatomy, function and infarct-geometry data at baseline and at follow-up. Importantly, global LV and infarct-geometry parameters showed no significant differences at the 3-day post-AMI baseline.

In control animals, 2h occlusion of the LCx resulted in AMI that comprised 31±2% of the LV, resulting in a depressed ejection fraction of 33±2% (compared to 55±3% in normal healthy swine (16)). During the five weeks follow-up, ejection fraction increased to 40±2% although this increase failed to reach statistical significance ($p=0.06$). Total LV mass did not change during the subsequent 5 weeks follow-up, as the increase in mass of the remote myocardium was balanced by an equivalent decrease in infarct-mass (Table 1).

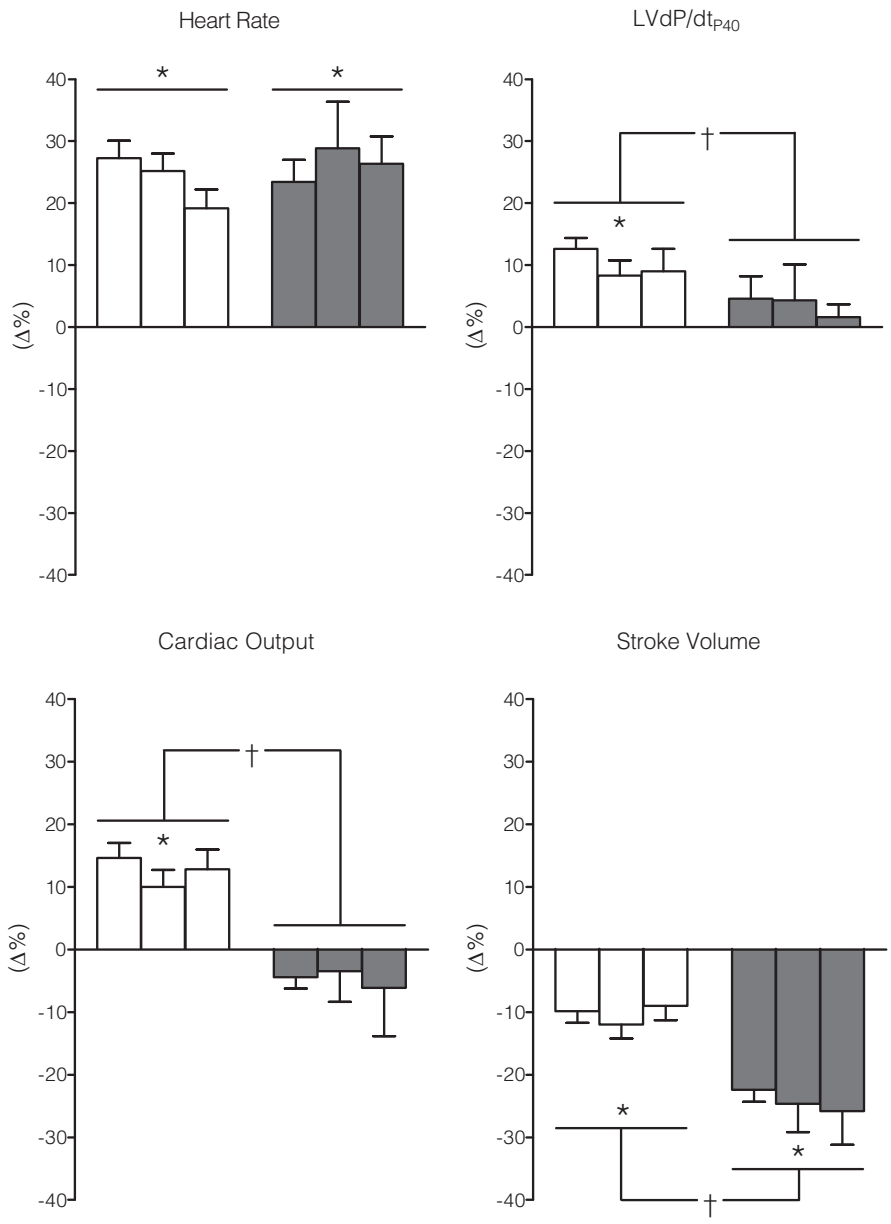

Figure 1. *Hemodynamic Effects of Atrial (AAI) versus Ventricular (VVI) Intermittent Pacing*
*Percent changes from pre-pacing baseline values produced by three consecutive 5-min pacing periods of AAI (white bars) and VVI (grey bars), interspersed by 5-min of normal sinus rhythm. Shown are heart rate, left-ventricular positive dP/dt at a left-ventricular pressure of 40 mm Hg (LVdP/dtP40), cardiac output and stroke volume. Data are Mean±SEM; n=4; *p≤0.05 from corresponding BL; †p≤0.05 AAI vs. VVI.*

Table 1. *Global LV function and infarct geometry*

		Post-MI	
		3 days BL	**37 days FU**
Global LV Anatomy and Function			
Body weight (kg)	Control	29 ± 0	38 ± 1*
	IPT	28 ± 1	37 ± 1*
LV-mass (g)	Control	56 ± 1	58 ± 1
	IPT	55 ± 2	55 ± 1
Heart Rate (bpm)	Control	93 ± 3	80 ± 6
	IPT	100 ± 6	78 ± 11
End-Diastolic Volume (ml)	Control	80 ± 3	113 ± 5*
	IPT	81 ± 2	110 ± 8*
End-Systolic Volume (ml)	Control	54 ± 3	68 ± 3*
	IPT	53 ± 2	67 ± 8
Stroke Volume (ml)	Control	27 ± 2	45 ± 4*
	IPT	28 ± 2	43 ± 3*
Ejection Fraction (%)	Control	33 ± 2	40 ± 2**
	IPT	35 ± 3	40 ± 3*
Infarct Geometry			
Remote LV mass (g)	Control	39 ± 1	47 ± 0*
	IPT	38 ± 1	46 ± 0*
Infarct-mass (g)	Control	17.6 ± 1.4	11.7 ± 0.8*
	IPT	17.1 ± 1.2	9.3 ± 0.9*††
Infarct-size (% LV)	Control	31 ± 2	20 ± 1*
	IPT	31 ± 2	17 ± 2*
Infarct-thickness (mm)	Control	6.2 ± 0.2	4.5 ± 0.2*
	IPT	5.9 ± 0.2	4.9 ± 0.3
Infarct-length (#slices)	Control	7.8 ± 0.6	8.3 ± 0.6
	IPT	8.8 ± 0.3	8.0 ± 0.5*
Infarct-length (mm)	Control	47 ± 4	50 ± 4
	IPT	53 ± 2	48 ± 3*†
Infarct-circumference (#segments)	Control	13.5 ± 0.8	12.0 ± 1.1
	IPT	13.6 ± 1.6	9.4 ± 1.3*†
Infarct-circumference (mm)	Control	62 ± 3	65 ± 6
	IPT	61 ± 5	52 ± 5
Total # infarcted segments	Control	73 ± 8	71 ± 9
	IPT	90 ± 9	58 ± 8*†

Data are Mean ± SEM; Control, n=9; IPT, n=6; *P<0.05, vs. corresponding BL; **P<0.10, vs. corresponding BL; †P<0.05, ††P<0.10, change by IPT vs. change in control. BL = baseline; FU = follow-up. LV=Left Ventricle

The changes in global LV anatomy and function were not different between IPTVVI and Control (Table 1). However, infarct-geometry responded markedly to IPTVVI (Table 1, Figure 2 and Figure 3). In control animals, infarct-mass decreased over time as a result of a significant decrease in infarct-thickness with no significant changes in infarct-length or circumference, and no changes in the total number of infarcted segments. In contrast, in IPT animals, the reduction in infarct-mass was primarily due to a decrease in total number of infarcted segments (comprised of reductions in both infarct-length and circumference), with no significant decrease in infarct-thickness. The latter could have played a role in preventing the reduction in infarct-mass from reaching statistical significance compared to Control group (P=0.07; Figure 3).

Myofibroblasts. Histological quantification of αSMA positive cells in the infarct region showed a significant higher presence of myofibroblasts, 5.4±1.6% of the infarct area in Control vs. 10.9±2.1% in IPTVVI swine (Figure 4 and 5, p=0.05).

Biomarkers of inflammation and extracellular matrix turnover. Circulating plasma levels of inflammation (TNFα) and extracellular matrix turnover (MMP-9 and TIMP-1), measured at 1 and 5 weeks post-AMI, did not differ significantly between treatment groups (Figure 6).

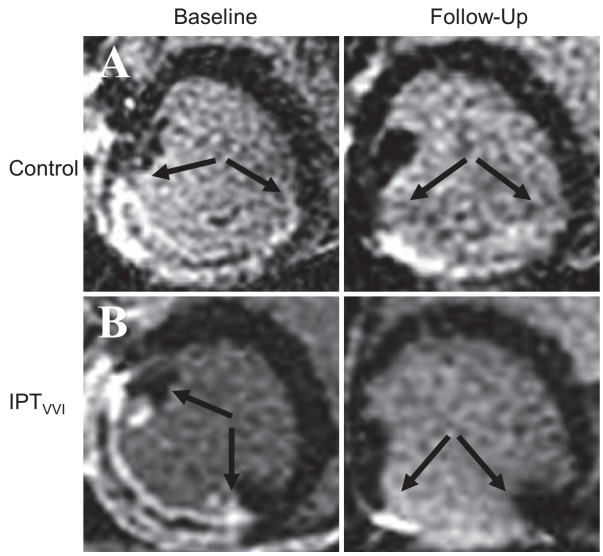

Figure 2. *Effect of IPTVVI on Infarct Circumference*
Short-axis delayed-enhancement images showing infarct characteristics at baseline (left) and follow up (right) in Control (A) and IPTVVI (B) swine. The enhanced (white) area demarcated by the arrows is the infarct-region.

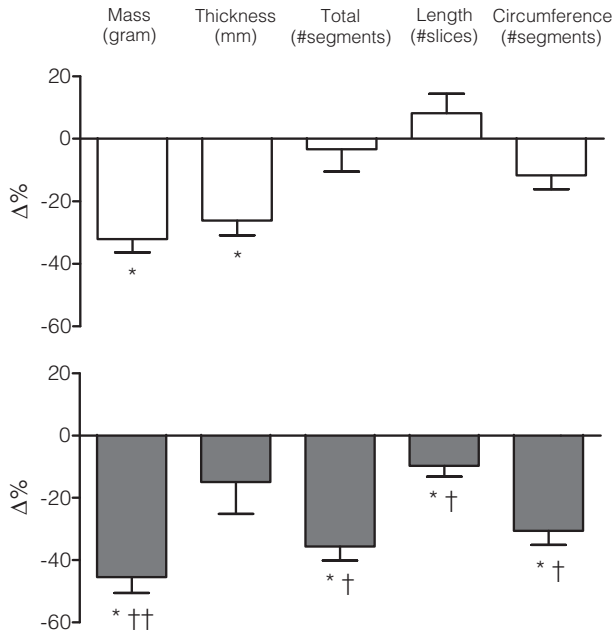

Figure 3. *Effect of IPTVVI on Infarct Geometry*
*Percent changes in infarct geometry from baseline values at 5wk follow-up in 8 Control (white bars) and 6 IPTVVI (grey bars) swine. Shown are changes in infarct-mass, infarct-thickness, total number of infarcted segments, number of infarcted slices, and average circumferential infarct-length. Data are Mean±SEM; *p≤0.05 vs. corresponding BL; †p≤0.05, ††p≤0.10, vs. change in Control.*

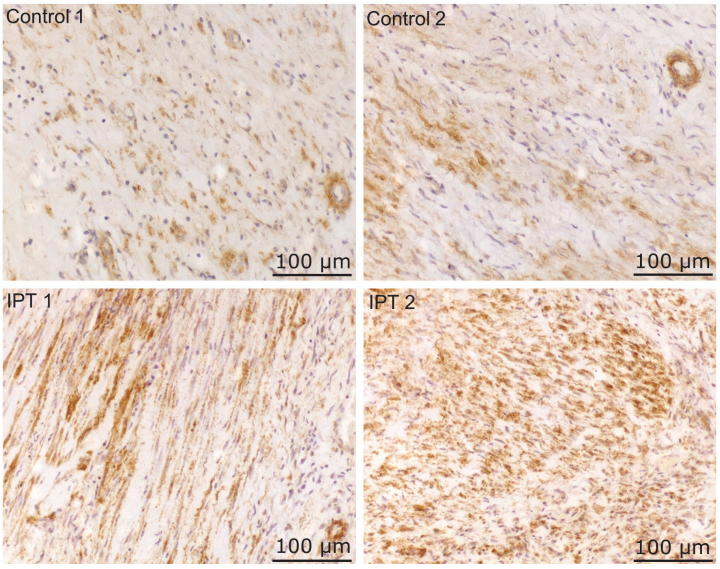

Figure 4. *IPTVVI Increases Myofibroblast Presence in the Infarct Region αSMA stained infarct-tissue of two Control and two IPTVVI swine (magnification 20x). Brown staining indicates myofibroblasts.*

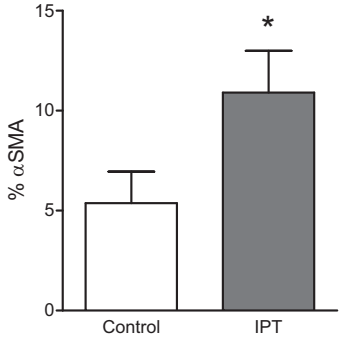

Figure 5. *IPTVVI Increases the Number of Myofibroblast in the Infarct Region Percent αSMA-positive cells in infarct tissue from 8 Control (white bar) and 6 IPTVVI (grey bar) swine. Data are Mean±SEM; *p≤0.05 vs. Control.*

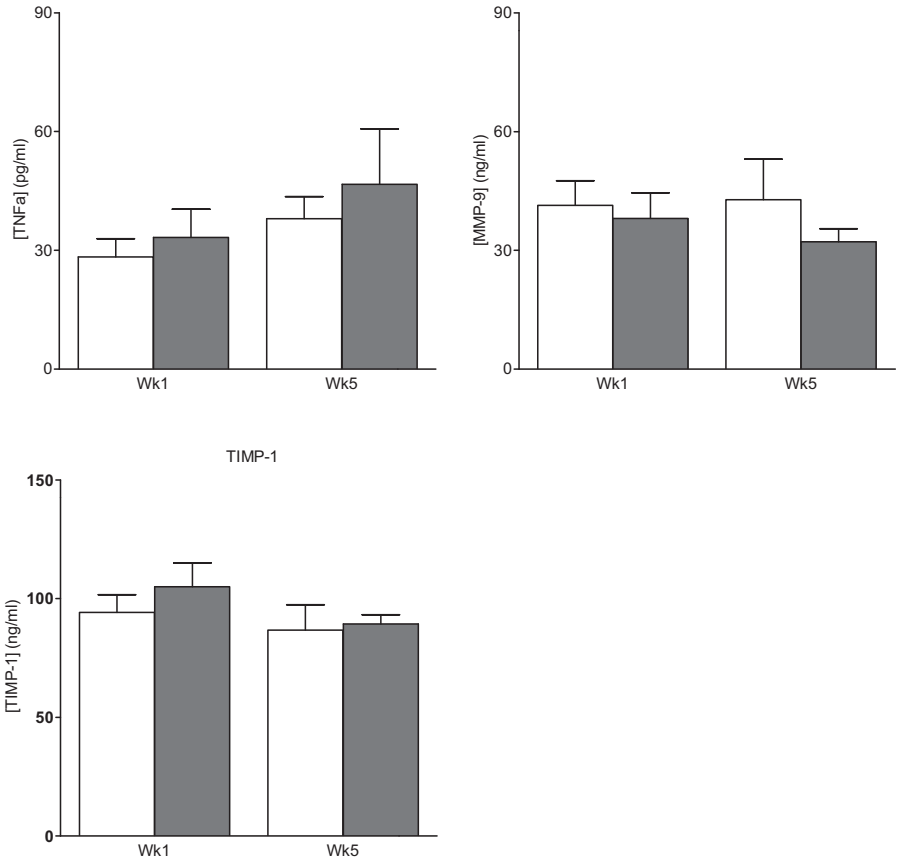

Figure 6. *Circulating Levels of Markers of Extracellular Matrix and Inflammation*
*Markers for extracellular matrix and inflammation in arterial plasma of 5 Control (white bar) and 5 IPT (grey bar) swine. Data are Mean±SEM; *p≤0.05 vs. Control.*

Quantitative expression data. At follow-up, expression data for myofibroblast presence (αSMA) supported histological findings although it remained borderline significant (p=0.06, two-tailed). Similarly a trend (p=0.08, two-tailed) towards increased α-1-type-1 collagen (Col1a1) expression at follow-up, suggesting that increased myofibroblast numbers translated into increased matrix turnover. In contrast, markers for myofibroblast differentiation and Wnt/Frizzled signaling were not different at follow-up (Table 2.).

Table 2. *RT-PCR for myofibroblasts and extracellular matrix*

	Control	**IPT**
Myofibroblast presence, regulation and differentiation		
αSMA	0.7 ± 0.1	1.2 ± 0.3**
Vimentin	1.7 ± 0.5	1.6 ± 0.4
Desmin	0.4 ± 0.1	0.3 ± 0.1
SPARC	1.6 ± 0.5	1.9 ± 0.7
Tenascin-C	1.5 ± 0.9	0.6 ± 0.2
VEGF-A	0.6 ± 0.1	0.6 ± 0.3
β-Catenin	0.6 ± 0.1	0.4 ± 0.1
TGFβ1	0.8 ± 0.1	0.6 ± 0.1
TGFβ2	1.8 ± 0.6	1.4 ± 0.1
TGFβ3	6.1 ± 2.2	5.2 ± 1.8
Fzd2	1.5 ± 0.4	1.7 ± 0.3
Fzd4	1.3 ± 0.3	0.9 ± 0.2
LRP5	0.8 ± 0.2	0.5 ± 0.2
LRP6	0.7 ± 0.1	0.7 ± 0.1
LOX	2.0 ± 0.7	3.6 ± 0.7
APC	0.8 ± 0.2	0.8 ± 0.1
Axin2	3.6 ± 1.2	3.5 ± 1.0
Extracellular matrix composition and turnover		
Col1a1	2.1 ± 0.7	4.7 ± 1.3**
Col1a2	1.9 ± 0.6	3.5 ± 1.3
Col3a1	1.7 ± 0.5	2.0 ± 0.6
MMP-2	1.7 ± 0.5	2.5 ± 0.7
MMP-9	4.5 ± 1.6	4.5 ± 1.5
TIMP-1	1.5 ± 0.4	3.4 ± 1.5

Data are ratios to housekeeping gene cyclophilin ± SEM; Control: n=9; IPT: n=6. *P≤0.05 vs. corresponding control; **P≤0.10 vs. corresponding control. APC = adenomatous polypolis coli; Axin = axis inhibition protein; αSMA = alpha smooth muscle actin; Col = collagen; Fzd = frizzled; LOX = lysil oxidase; LRP = low-density lipoprotein receptor-related protein; MMP = matrix metalloproteinase; RT-qPCR = reverse transcriptase quantitative polymerase chain reaction; SPARC = secreted protein acidic and rich in cysteine; TGF = transforming growth factor; TIMP = tissue inhibitor of metalloproteinases. VEGF-A = vascular endothelial growth factor A.

DISCUSSION

The present study is the first to investigate the effects of dyssynchronous intermittent ventricular pacing (IPTVVI), initiated three days after acute myocardial infarction (AMI) and continued for 5 weeks, on global and regional LV remodeling and infarct-geometry in a clinically relevant animal model. The major findings were that (*i*) IPTVVI had no effect on global LV remodeling or function, but (*ii*) had a marked effect on infarct-remodeling by decreasing the number of infarcted segments without changing infarct-thickness. (*iii*) Additionally, IPTVVI increased myofibroblast content in the infarcted area, (*iv*) without changing circulating markers of inflammation and extracellular matrix turnover. These findings provide evidence that intermittent electrical stimulation of the left ventricle may represent a novel means to modulate scar remodeling after MI.

IPT in AMI and post-AMI remodeling

Several studies in swine (6) and rabbits (7,9) have shown that pretreatment with ventricular, but not atrial (17), pacing is capable of limiting myocardial infarct-size. Subsequent studies have demonstrated that not only preconditioning (6,7,9), but also postconditioning with brief periods of ventricular pacing in the early reperfusion phase (8-10), can also limit myocardial infarct-size. Moreover, the effects of this early protection against myocardial necrosis was sustained over a six week period, resulting in a trend towards blunted LV remodeling and improved LV function (10). The present study is the first to investigate the effects of prolonged IPT on infarct-remodeling, independent of its protection against acute myocardial necrosis. The results of this study clearly demonstrate that IPTVVI started 3 days after reperfusion, at a time when necrosis can no longer be affected, significantly influenced remodeling of the infarct-region.

Early studies in humans in the pre-thrombolysis era, reported disproportionate thinning and stretching of the infarcted segment (18-20). Recent post-thrombolysis studies in humans with reperfused AMI confirm that regional myocardial wall thinning represents (transmural) myocardial infarction (21). Furthermore, limited scar burden is associated with improved contractility (21) and blunted remodeling (3) whereas rupture prone cardiac aneurysms are the consequence of continued ventricular wall thinning (22). Also, late dilatation of the LV after primary percutaneous intervention remains of clinical significance (23) and may represent a potential target of IPTVVI. Thus the IPTVVI-induced alteration of infarct-geometry may mitigate the sequence of events leading to ventricular wall thinning and limit LV remodeling at long-term. Although significant changes in infarct-geometry and

composition were observed in the present study, these alterations did not yet translate into favorable global LV remodeling at 5 weeks follow-up. This finding that is similar to previous observations with cell-therapy studies in swine (24), as well as humans (25), with AMI suggests that longer follow-up may be required for detecting benefits at the global LV level. In addition, it should be noted that we studied only a single algorithm of pacing therapy. Hence, it cannot be excluded that other algorithms or pacing protocols may produce larger regional effects that do translate into global LV improvements (8). Clearly, future studies, using longer follow-up, are necessary to optimize the onset, timing, duration and mode of pacing therapy.

IPT and infarct-geometry: Role of myofibroblasts

The infarct zone is increasingly being appreciated as an area with relevant biological activity and therapeutic potential (26,27). Cardiac fibroblasts, including the active collagen secreting myofibroblasts, are the dominant cell type in the infarct region and are recognized as essential in infarct remodeling (15,28,29). Myofibroblasts typically appear in the infarct-area at 4-5 days after AMI, reach a peak at 1-2 weeks and continue to reside up to at least 4 weeks (30) and possibly months to years (15). In the present study, IPTVVI, started at three days post-AMI, increased myofibroblast numbers in the infarct zone. Myofibroblasts could have contributed to the geometric changes in the infarct region produced by IPTVVI in several ways. First, in the infarcted myocardium, myofibroblasts are responsible for collagen turnover thus contributing to the delicate balance between ECM synthesis and degradation (15). Second, myofibroblasts are capable of tonical contraction and could therefore improve structural integrity of the scar and increase mechanical strength in the (sub)acute phase (15). Particularly, the latter is in concordance with the geometrical changes observed in the present study.

The exact mechanism by which IPTVVI influenced myofibroblast content was not determined in the present study. However, it is well known that LV pacing results in considerable changes in LV contraction patterns, even in the peri-infarct zone (9,31), resulting in alterations in regional stretch and loading conditions (7,32-34). Since mechanical tension is an important stimulus for cardiac fibroblast to myofibroblast differentiation (35,36), it is likely that regional alternations in myocardial stretch produced by IPTVVI stimulated resident fibroblasts to differentiate into myofibroblasts. Although expression studies at 5-week follow-up could not identify which molecular mechanisms underlie the higher myofibroblast presence, including TGFβ and the Wnt/Frizzled signaling pathway (37), it is

possible that these pathways were involved in the early phase of IPTVVI. This is also suggested by a study in swine (38), in which continuous low dose electrical stimulation within the infarct-region, not only resulted in higher numbers of myofibroblasts, but also in elevated TGFβ-R1 activity, when measured as early as one week after onset of stimulation. These observations underline the transient nature of the local molecular responses to regional electrical stimulation. However, we did not observe changes in circulating arterial plasma levels of inflammation or extracellular matrix proteins in IPTVVI versus Control swine, at either 1 or 5 weeks after AMI, indicating that the effect of pacing on release of these proteins in pigs with infarcts was not discernible in the systemic circulation even at 1 week after AMI. It is therefore likely that myofibroblasts, which are a rich source of bioactive molecules (39), modulated infarct-geometry in a paracrine manner, which is supported by the observations of Mukherjee et al (38) that TIMP-1 co-localizes with myofibroblasts within the infarct-zone.

In conclusion, the present study shows that 5 weeks of IPTVVI, a regionally targeted non-pharmaceutical approach that was safe (no arrhythmias and maintained cardiac output), favorably influenced the infarct-remodeling process, likely by increasing myofibroblast content in the infarct-region. Thus, whereas Control swine showed a reduction in infarct-mass over the 5-week follow-up period, which was principally due to infarct-thinning, IPTVVI resulted in a reduction in infarct-mass that was principally due to a decrease in the number of infarcted LV segments while infarct-thinning was prevented. Histological assessment revealed increased numbers of myofibroblasts in the infarct-zone. Taken together, these findings suggest that IPT in the peri-infarct zone represents a novel adjunctive therapy to favorably modulate infarct-healing in patients with acute myocardial infarction.

REFERENCES

1. Braunwald E. Heart failure. JACC Heart Fail 2013;1:1-20.
2. Mosterd A, Hoes AW. Clinical epidemiology of heart failure. Heart (British Cardiac Society) 2007;93:1137-1146.
3. Masci PG, Ganame J, Francone M et al. Relationship between location and size of myocardial infarction and their reciprocal influences on post-infarction left ventricular remodelling. European Heart Journal 2011;32:1640-1648.
4. Dirksen MT, Laarman GJ, Simoons ML, Duncker DJGM. Reperfusion injury in humans: A review of clinical trials on reperfusion injury inhibitory strategies. Cardiovascular Research 2007;74:343-355.
5. Hausenloy DJ, Yellon DM. Myocardial ischemia-reperfusion injury: a neglected therapeutic target. Journal of Clinical Investigation 2013;123:92-100.
6. Koning MM, Gho BC, van Klaarwater E, Opstal RL, Duncker DJ, Verdouw PD. Rapid ventricular pacing produces myocardial protection by nonischemic activation of KATP+ channels. Circulation 1996;93:178-86.
7. Vanagt WY, Cornelussen RN, Poulina QP et al. Pacing-induced dys-synchrony preconditions rabbit myocardium against ischemia/reperfusion injury. Circulation 2006;114:I264-I269.
8. Babiker FA, van Golde J, Vanagt WY, Prinzen FW. Pacing Postconditioning: Impact of Pacing Algorithm, Gender, and Diabetes on Its Myocardial Protective Effects. J Cardiovasc Transl 2012;5:727-734.
9. Vanagt WY, Cornelussen RN, Baynham TC et al. Pacing-induced dyssynchrony during early reperfusion reduces infarct size. Journal of the American College of Cardiology 2007;49:1813-1819.
10. Babiker FA, Lorenzen-Schmidt I, Mokelke E et al. Long-term protection and mechanism of pacing-induced postconditioning in the heart. Basic research in cardiology 2010;105:523-533.
11. Kappers MHW, de Beer VJ, Zhou ZC et al. Sunitinib-Induced Systemic Vasoconstriction in Swine Is Endothelin Mediated and Does Not Involve Nitric Oxide or Oxidative Stress. Hypertension 2012;59:151-157.
12. van der Velden J, Merkus D, Klarenbeek BR et al. Alterations in myofilament function contribute to left ventricular dysfunction in pigs early after myocardial infarction. Circ Res 2004;95:e85-95.
13. Baks T, van Geuns RJ, Biagini E et al. Recovery of left ventricular function after primary angioplasty for acute myocardial infarction. European Heart Journal 2005;26:1070-1077.
14. Springeling T, Uitterdijk A, Rossi A et al. Evolution of reperfusion post-infarction ventricular remodeling: New MRI insights. International Journal of Cardiology 2013;169:354-358.
15. van den Borne SW, Diez J, Blankesteijn WM, Verjans J, Hofstra L, Narula J. Myocardial remodeling after infarction: the role of myofibroblasts. Nature reviews;7:30-7.
16. Moelker AD, Baks T, Wever KM et al. Intracoronary delivery of umbilical cord blood derived unrestricted somatic stem cells is not suitable to improve LV function after myocardial infarction in swine. Journal of molecular and cellular cardiology 2007;42:735-45.
17. Marber MS, Walker DM, Eveson DJ, Walker JM, Yellon DM. A single five minute period of rapid atrial pacing fails to limit infarct size in the in situ rabbit heart. Cardiovasc Res 1993;27:597-601.
18. Hutchins GM, Bulkley BH. Infarct expansion versus extension: two different complications of acute myocardial infarction. The American journal of cardiology 1978;41:1127-32.
19. Weisman HF, Healy B. Myocardial Infarct Expansion, Infarct Extension, and Reinfarction - Pathophysiologic Concepts. Progress in cardiovascular diseases 1987;30:73-110.
20. Weiss JL, Marino PN, Shapiro EP. Myocardial Infarct Expansion - Recognition, Significance and Pathology. American Journal of Cardiology 1991;68:D35-D40.
21. Shah DJ, Kim HW, James O et al. Prevalence of Regional Myocardial Thinning and Relationship With Myocardial Scarring in Patients With Coronary Artery Disease. Jama-J Am Med Assoc 2013;309:909-918.

22. Kumar Goud P, Bakkannavar SM, Chinmayee P. Cardiac aneurysm: a nature's way of correction. Am J Forensic Med Pathol 2013;34:228-30.
23. Springeling T, Kirschbaum SW, Rossi A et al. Late Cardiac Remodeling After Primary Percutaneous Coronary Intervention - Five-Year Cardiac Magnetic Resonance Imaging Follow-up. Circulation Journal 2013;77:81-88.
24. Moelker AD, Baks T, Van den Bos EJ et al. Reduction in infarct size, but no functional improvement after bone marrow cell administration in a porcine model of reperfused myocardial infarction. European Heart Journal 2006;27:3057-3064.
25. Janssens S, Dubois C, Bogaert J et al. Autologous bone marrow-derived stem-cell transfer in patients with ST-segment elevation myocardial infarction: double-blind, randomised controlled trial. Lancet 2006;367:113-121.
26. Cleutjens JPM, Blankesteijn WM, Daemen MJAP, Smits JFM. The infarcted myocardium: Simply dead tissue, or a lively target for therapeutic interventions. Cardiovascular Research 1999;44:232-241.
27. Sun Y, Kiani MF, Postlethwaite AE, Weber KT. Infarct scar as living tissue. Basic research in cardiology 2002;97:343-347.
28. Brown RD, Ambler SK, Mitchell MD, Long CS. The cardiac fibroblast: Therapeutic target in myocardial remodeling and failure. Annual review of pharmacology and toxicology 2005;45:657-687.
29. Turner NA. Therapeutic regulation of cardiac fibroblast function: targeting stress-activated protein kinase pathways. Future cardiology;7:673-91.
30. Frangogiannis NG, Michael LH, Entman ML. Myofibroblasts in reperfused myocardial infarcts express the embryonic form of smooth muscle myosin heavy chain (SMemb). Cardiovascular Research 2000;48:89-100.
31. Lewis CW, Owen CH, Zipprich DA, Sabiston DC, Smith PK, Glower DD. The Effects of Local Ventricular Pacing on Recovery from Regional Myocardial-Ischemia. Journal of Surgical Research 1993;54:360-367.
32. Huang CH, Wang JS, Chiang SC, Wang YY, Lai ST, Weng ZC. Brief pressure overload of the left ventricle preconditions rabbit myocardium against infarction. Annals of Thoracic Surgery 2004;78:628-633.
33. Ovize M, Kloner RA, Przyklenk K. Stretch Preconditions Canine Myocardium. American journal of physiology 1994;266:H137-H146.
34. Shuros AC, Salo RW, Florea VG et al. Ventricular preexcitation modulates strain and attenuates cardiac remodeling in a swine model of myocardial infarction. Circulation 2007;116:1162-1169.
35. Hinz B, Gabbiani G. Mechanisms of force generation and transmission by myofibroblasts. Current opinion in biotechnology 2003;14:538-546.
36. Hinz B, Mastrangelo D, Iselin CE, Chaponnier C, Gabbiani G. Mechanical tension controls granulation tissue contractile activity and myofibroblast differentiation. American Journal of Pathology 2001;159:1009-1020.
37. Laeremans H, Hackeng TM, van Zandvoort MAMJ et al. Blocking of Frizzled Signaling With a Homologous Peptide Fragment of Wnt3a/Wnt5a Reduces Infarct Expansion and Prevents the Development of Heart Failure After Myocardial Infarction. Circulation 2011;124:1626-U107.
38. Mukherjee R, Rivers WT, Ruddy JM et al. Long-Term Localized High-Frequency Electric Stimulation Within the Myocardial Infarct Effects on Matrix Metalloproteinases and Regional Remodeling. Circulation 2010;122:20-U64.
39. Porter KE, Turner NA. Cardiac fibroblasts: At the heart of myocardial remodeling. Pharmacology & therapeutics 2009;123:255-278.

SUPPLEMENTAL MATERIALS AND METHODS

Cardiac MRI and Imagage analysis

MRI was performed on a 3.0-Tesla clinical scanner (Signa HD, GE Medical systems, Milwaukee, WI, United States) using a dedicated cardiac four-channel phased array cardiac receiver coil. Repeated breath holds and gating to the electrocardiogram were applied to minimize the influence of cardiac and respiratory motion on data collection. Both baseline and follow-up delayed enhanced MRI (DE-MRI) protocols consisted of cine–MRI and DE-MRI.

Cine-MRI was performed using a steady-state, free-precession technique (FIESTA, GE Medical System). Imaging parameters were: 24 temporal phases per slice, field of view 28-30 x 28-30 cm, matrix size was 128 x 224, repetition time 2.5-2.8 ms, number of average minimal 1.0, time to echo 1.0 ms; flip angle 55 degrees, 12 views per segment, slice thickness was 6.0 mm, slice gap was 0 mm. Using standard techniques to identify the major cardiac axes, two-chamber and four chamber cine-CMR images were obtained. The two- and four chamber end-diastolic images at end expiration provided the reference images to obtain a series of short axis views. This resulted in 8-12 cine breath-hold short-axis images to cover the entire left ventricle. Delayed enhancement imaging was performed with a gated breath hold 2-dimensional T1-inversion recovery gradient-echo sequence minimal of 10 minutes after infusion of Gadoliniumdiethyltriaminepentaacetic acid (0.2 mmol/kg intravenously, Gadovist, Bayern-Schering, Germany). Imaging parameters were; field of view 28-30 x 28-30 cm, matrix size was 192 x 160, repetition time 6.3 ms, number of average minimal 2.0, time to echo 1.6 ms, flip angle 20 degrees, slice thickness was 6.0 mm, slice gap was 0, inversion time 200-300 ms (adjusted to null the signal of the remote myocardium). The slice locations of the delayed enhanced images were copied from the cine-images.

Image Analysis. All images were analysed in a blinded matter using the CAAS-MRV program (version 3.3.1; Pie Medical Imaging, Maastricht, The Netherlands). Cine and delayed enhancement images were acquired during the same imaging session and were matched using identical slice positions (1,2).

Analysis of all images was achieved by consensus of 2 observers using anatomic landmarks such as papillary muscles and right ventricular insertion sites. The images were analysed using the additional information of the long axis to limit the extent of volume at the base and the apex of the heart (3). End-diastolic volume (EDV), end-systolic volume (ESV), ejection fraction (EF) and left ventricular mass

were measured by manually drawing the endocardial and epicardial contour in end-systolic and end-diastolic phase of the 2- and 4-chamber images with automatic segmentation to the short axis and if necessary corrected manually. Papillary muscles and trabeculations were considered as being part of the blood pool volume. Infarct volume was determined on short axis delayed enhancement images using semi-quantitative analyses for the detection of the delayed enhancement regions (>2SD of the mean SI of the contra-lateral myocardium). The delayed enhancement volume was multiplied by 1.05 g/ml to obtain myocardial infarct mass. For the segmental analyses, only slices with complete circumferential myocardium were used and each slice was divided into 36 segments (2). Longitudinal infarct length was defined as the total number of slices containing infarction multiplied by slice thickness (6 mm). Mean circumferential infarct length is defined as the average infarct circumferential length of 3 basal slices (2).

Biomarkers. Arterial blood samples were collected at 1 and 5 weeks post-infarct in EDTA tubes, centrifuged (10 min at 1460g and 4°C) and plasma was stored within 4h at -80 °C for later analysis of circulating biomarkers. Markers of inflammation (TNFα) and extracellular matrix turnover (MMP-9, TIMP-1) were quantified using enzyme-linked immunosorbent assays (ELISA) according to manufacturer's instructions (USCN Life Sciences, Wuhan, China; R&D systems, Minneapolis, MN, USA). Absorbance (450nm) was measured with a SpectraMax M5 plate reader (Molecular Devices Corporation, Menlo Park, CA, USA) and concentrations calculated using a standard curve.

Histology. At 5 weeks follow-up, transversal sections of infarct-tissue were fixed in 4% buffered formaldehyde for at least 24 hours and subsequently embedded in paraffin. To distinguish myofibroblasts from fibroblasts in the infarct area, sections of 4 μm were stained for alpha smooth muscle actin (4) (αSMA monoclonal antibody, 1:2000, Sigma, Zwijndrecht, The Netherlands). A minimum of five randomly selected high power fields (90.000 μm^2 per field) per section were planimetrically quantified in a blinded matter for myofibroblast numbers with vessels excluded (Qwin, Leica, Rijswijk, The Netherlands). Data were expressed as myofibroblast area / total tissue area (%).

RT-PCR. Porcine infarct tissue was homogenized and RNA was isolated using the RNeasy Fibrous Tissue Mini Kit (Qiagen, Hilden, Germany) according to manufacturer's instructions. The isolated RNA was assessed for concentration and purity (A260/A280 ratio) with a NanoDrop spectrophotometer (Thermo Fischer Scientific, USA). Next, RNA was reverse-transcribed into cDNA, using the iScript

cDNA synthesis kit (Bio-Rad, USA). Temperature gradient optimization studies were performed with pooled samples from non-infarct tissue cDNA, and the optimal annealing temperatures for each primer, along with the sequences, are shown in Table S1 of the supplemental data. IQ SYBR Green Supermix (Bio-Rad) was used for the detection of cDNA levels. Quantification of gene expression was performed using the comparative Ct (ΔCt) method and results are expressed as ratios to the housekeeping gene cyclophilin.

Table S1. *Primer sequences and annealing temperatures used in the RT-qPCR studies*

Sus Scrofa gene	Forward primer	Reverse primer	Annealing Temperature used (°C)
Fzd2	ATAGGCACGTCCTTCCTCCT	GACGGGTGTAGAACTTCCTCC	62
Fzd4	ACATGGGGCATTTCCAGGAG	TACAAGTCGCCTGGGTGAAC	65
LRP5	ACGTGATCGAGTTTGGCCTT	TGTTGTGCATGCAGTCGTTG	65
LRP6	CGTGCCAGTTGGAGGTTTTG	TCCGAAGGCTGTGGATAGGA	62
β-Catenin	ATTGAAGCTGAGGGAGCCAC	ACTCCTAAAGGATGATTTACAGGTC	62
TGFβ1	GTGGAAAGCGGCAACCAAAT	CACTGAGGCGAAAACCCTCT	65
TGFβ2	TGCCTGCGTCCACTTTACAT	AGCTGAGAACCCTGCTATGC	62
TGFβ3	ATGGAGAAGAAACCCAGAGCTT	TCCGACTCGGTGTTTTCCTG	63.5
VEGF-A	GACCAGAAACCCCACGAAGT	AAATGCTTTCTCCGCTCCGA	58
aSMA	GGACCCTGTGAAGCACCAG	GGGCAACACGAAGCTCATTG	66.4
Col1a1	AGACATCCCACCAGTCACCT	TCACGTCATCGCACAACACA	62
Col1a2	CTTGAGACTCAGCCACCCAG	CCGAATGCAGGTTTCACCAG	65
Col3a1	GCTCCCATCTTGGTCAGTCC	CCATCATTACCTCGAGCCCC	63.5
Vimentin	TCTGGAATCCCTCCCTCTGG	TTGCGCTCCTGAAAAACTGC	66.4
Desmin	GGCTCAGTACGAGACCATCG	GCATCGATCTCGCAGGTGTA	63
Tenascin-C	CACCCCGGTACTTGTTCCAT	CCTCGAAGGTGACAGTTGCT	57
SPARC	ACCCTGTCCAGGTGGAAGTAG	GGCAGAACGACAAACCATCC	57
APC	ACAAAACTGGAAACTGAGGCAT	CGGAGGGACATTTTTGACCG	63
LOX	TCCAAGCTGGCTATTCGACG	AGGATTGTACGGGTCATCGC	65
AXIN2	CAAACCCATGCCTGTCTCCT	CGGAAGAGATAAGCCCCGTC	65.5
TIMP-1	CTGGTCATCAGGGCCAAGTT	GGTCTGTCCACAAGCAGTGA	63.5
MMP-2	GCAGTGATGGCAAGTTGTGG	TTGACATCGTCGTGGGACAG	65
MMP-9	ACTTCGGAAACGCAAAAGGC	AAGAGTCTCTCGCTAGGGCA	62
Cyclophilin	AGACAGCAGAAAACTTCCGTG	AAGATGCCAGGACCCGTATG	63.5

APC = adenomatous polypolis coli; Axin = axis inhibition protein; aSMA = alpha smooth muscle actin; Col = collagen; Fzd = frizzled; LOX = lysil oxidase; LRP = low-density lipoprotein receptor-related protein; MMP = matrix metalloproteinase; RT-qPCR = reverse transcriptase quantitative polymerase chain reaction; TGF = transforming growth factor; TIMP = tissue inhibitor of metalloproteinases. VEGF-A = vascular endothelial growth factor A.

SUPPLEMENTAL REFERENCES

1. Baks T, Cademartiri F, Moelker AD et al. Multislice computed tomography and magnetic resonance imaging for the assessment of reperfused acute myocardial infarction. Journal of the American College of Cardiology 2006;48:144-152.
2. Springeling T, Uitterdijk A, Rossi A et al. Evolution of reperfusion post-infarction ventricular remodeling: New MRI insights. International Journal of Cardiology 2013;169:354-358.
3. Kirschbaum SW, Baks T, Gronenschild EH et al. Addition of the long-axis information to short-axis contours reduces interstudy variability of left-ventricular analysis in cardiac magnetic resonance studies. Investigative radiology 2008;43:1-6.
4. van den Borne SW, Diez J, Blankesteijn WM, Verjans J, Hofstra L, Narula J. Myocardial remodeling after infarction: the role of myofibroblasts. Nature reviews;7:30-7.

CHAPTER 10

UM206, a selective frizzled antagonist, attenuates adverse remodeling after myocardial infarction in swine

***André Uitterdijk**
*Kevin CM Hermans
Daphne PM de Wijs-Meijler
Evangelos P Daskalopoulos
Irwin K Reiss
Dirk J Duncker
W Matthijs Blankesteijn
Daphne Merkus

*Both authors contributed equally

Invited revision Lab Invest

ABSTRACT

Modulation of Wnt/Fzd signaling with UM206 reduced infarct expansion and prevented heart failure development in mice, an effect that was accompanied by increased myofibroblast presence in the infarct, suggesting that Wnt/Fzd signaling plays a key role in cardiac remodeling following myocardial infarction (MI). This study aims to investigate the effects of modulation of Wnt/Fzd signaling with UM206 in a swine model of reperfused myocardial infarction (MI).

For this purpose, seven swine with MI were treated with continuous infusion of UM206 for 5 weeks. Six control swine were treated with vehicle. Another 8 swine were sham-operated. Cardiac function was determined by echo in awake swine. Infarct-mass was estimated at baseline by heart specific fatty acid binding protein ELISA and at follow-up using planimetry. Components of Wnt/Frzd signaling, myofibroblast presence and extracellular matrix were measured at follow-up with qPCR and/or histology.

Results show that UM206-treatment resulted in a significant decrease in infarct-mass compared to baseline (-41±10%), whereas infarct-mass remained stable in the Control-MI group (3±17%). Progressive dilation of the LV occurred in the Control-MI group between 3 and 5 weeks after MI while adverse remodeling was halted in the UM206-treated group. mRNA expression for Fzd4 and the Frizzled co-receptor LRP5 was increased in UM206-treated as compared to Control-MI swine. Myofibroblast presence was significantly lower in infarcted tissue of the UM206-treated animals (1.53±0.43% vs 3.38±0.61%) at 5 weeks follow-up.

This study shows that UM206-treatment attenuates adverse remodeling in a swine model of reperfused MI, indicating that Wnt/Fzd signaling is a promising target to improve infarct-healing and limit post-MI remodeling.

INTRODUCTION

Although left ventricular (LV) remodeling after myocardial infarction (MI) is aimed at maintaining cardiac pump function, initial infarct size, and the subsequent progressive expansion and thinning of the infarcted area constitute the main risk factors for the development of post-MI heart failure (1). Several strategies that influence either the infarct size and/or the ensuing process of LV remodeling have been proposed as potential therapies to halt the development and progression of LV dysfunction (2,3).

Cardiac fibroblasts, that account for up to 70% of the cells present in the myocardium, regulate extracellular matrix turnover, and play an essential role in cardiac homeostasis. Fibroblasts are more resistant to ischemia than cardiomyocytes (4-6), and prolonged myocardial ischemia results in death of particularly the cardiomyocytes, while the fibroblasts survive. Fibroblasts have therefore been proposed to be a therapeutic target to influence the healing process of the myocardium (1,5,7,8). In addition to these resident fibroblasts, fibroblasts enter the infarcted tissue by migration. When present in the infarcted area, the fibroblasts gradually differentiate into their more contractile and synthetic myofibroblast phenotype. These (myo)fibroblasts play key roles both in the initial inflammatory phase as well as in the subsequent proliferative phase of the post-infarction proliferative response, that together lead to the formation of a stable, collagen-rich scar (4). Thus, increasing myofibroblast presence shortly after MI has been proposed to promote scar contraction and limit LV dilation (1,4,9). Fibroblast migration is inhibited by Wnt/Fzd signaling, and targeting the Wnt signaling pathway by modulating its ligand, the frizzled receptors, through UM206, an antagonist of Fzd1 and Fzd2, has been shown to promote fibroblast migration, limit infarct size and attenuate adverse remodeling after infarction induced by permanent ligation of the coronary artery in mice (10,11). A potential pitfall of altering fibroblast presence is that in the remote non-infarcted myocardium, local fibroblasts may remain activated in response to volume and pressure overload and may promote interstitial fibrosis (1,12).

In light of these considerations, the present study aimed to investigate whether UM206 is capable of limiting adverse LV-remodeling after MI in a preclinical setting, i.e. when tested in a large translational swine model of reperfused MI. Moreover, we aimed to elucidate if a potential beneficial effect of UM206 on remodeling of the infarct area was accompanied by changes in the remote myocardium. For this purpose, swine were subjected to 2 hours of coronary artery occlusion followed by

reperfusion. After one day, cardiac function was assessed with echocardiography and UM206 or Saline was continuously infused intra-arterially throughout the five week follow-up period. At follow-up, cardiac function was reassessed and myocardial tissue was analyzed to elucidate underlying mechanisms and signaling pathways.

MATERIALS AND METHODS

Animal experiments were performed in accordance with the *Guide for the Care and Use of Laboratory Animals* (NIH Publication No. 85-23, revised 1996) and with approval of the Erasmus Medical Center Animal Care Committee. Twenty-two pre-adolescent (2-3 months old) Yorkshire x Landrace swine (21±1 kg) of either sex were used.

Surgery

Swine were sedated with ketamine (20 mg/kg, Intramuscularly [IM]) and midazolam (0.5 mg/kg, IM), anesthetized with thiopental (10 mg/kg, intravenously [IV]), intubated and ventilated with O_2/N_2 (1/3 v/v) and anesthetized with fentanyl (20μg/kg/h) (13,14). Following a thoracotomy through the fourth left intercostal space, a polyvinyl catheter was inserted into the aorta. The heart was exposed via a small pericardial incision, the proximal left circumflex artery (LCx) was dissected and a suture was placed around it. Subsequently, a polyvinyl catheter was inserted into the left atrium. Baseline blood samples were taken. Following administration of heparin (5000 IU IV), the LCx was occluded for two hours by ligation of the suture followed by reperfusion. Administration of heparin was repeated after 1 hour of occlusion. Then catheters were tunneled to the back, filled with heparin solution to prevent clotting, and the pericardium and the chest were closed. Blood samples were taken after 50 minutes of reperfusion. One animal died during reperfusion due to recurrent fibrillation. Eight weight-matched swine that underwent a thoracotomy with placement of a catheter in the aorta, but without ischemia-reperfusion, served as sham-operated animals. All animals were allowed to recover, receiving analgesia (0.3 mg buprenorphine IM) for 2 days and antibiotic prophylaxis (25 mg/kg amoxicillin and 5 mg/kg gentamycin IV) for 5 days.

Echocardiography, Hemodynamic Measurements and Follow-up

One day after surgery, (awake) animals underwent echocardiography for the determination of LV end-diastolic cross-sectional area (EDA) and end-systolic cross-sectional area (ESA) (15,16). 2D ejection fraction (EF) was calculated

as (EDA-ESA)/EDA·100%. Also, blood samples were taken from the aorta and collected in EDTA anticoagulation tubes, centrifuged and plasma was stored at -80 °C until further analysis. Blood pressure was recorded immediately following echographic measurements using CODAS-software and analyzed using a custom written program in Matlab.

Subsequently, animals were randomly assigned to the UM206 group (7 swine) or the Control-MI group (6 swine). UM206 (target dose 0.6 µg/kg/day via the left atrium) was continuously infused at a rate of 1 ml/h, using a balloon pump (Easypump, BBraun, filled with 240 ml saline, heparin (100 IU/ml), 0.001 g EDTA and 240 µg UM206). In the Control-MI group, swine received an identical balloon-pump but without UM206. Echographic and hemodynamic measurements as well as blood sampling were repeated after 3 and 5 weeks, and the balloon pump was refilled when necessary over the course of 5 weeks.

Sacrifice. Five weeks after initial surgery, swine were re-anesthetized with pentobarbital (10-15 mg/kg per hour, IV) intubated and ventilated with a mixture of oxygen and nitrogen. A Swan-Ganz catheter was inserted via the femoral vein and advanced under fluoroscopic guidance into the pulmonary artery for measurement of pulmonary artery pressure and cardiac output (thermodilution). A Millar catheter was inserted into the left carotid artery and advanced into the left ventricle for measurement of LV pressure and its first derivative (dP/dt). After completion of all measurements, animals underwent a sternotomy, the heart was arrested by electrical fibrillation and immediately excised. The left ventricle was sectioned into transversal slices of approximately 1-2 cm, which were first weighed and photographed. Subsequently tissue from the anterior wall and infarct tissue were taken and further sub-divided for storage in liquid nitrogen, isopentane and buffered formaldehyde (3.5-4%) for further histological and molecular assessment.

Infarct mass measurements

Infarct mass at baseline. To assess infarct mass at baseline, heart specific fatty acid binding protein (hFABP) was determined with ELISA from the plasma samples obtained at 50 minutes of reperfusion according to the manufacturers description (Life Diagnostics, West Chester, PA, United States). Baseline infarct mass ($IM_{baseline}$) was estimated using the relationship between hFABP and infarct size obtained in a previous study from our laboratory (17).

Infarct mass at follow-up. Infarct mass at sacrifice was determined using the pictures of the individual rings of the heart by an experienced technician (MtLH, blinded to treatment of the animals) using planimetry. Infarct area on basal and apical side of each ring, expressed as percentage of total area of the ring was averaged and multiplied by weight of the ring. Total infarct mass at follow-up (IM_{FU}) was calculated as the sum of the weights of the infarcts in the individual rings.

ELISA, histology and molecular studies

Longitudinal circulating markers for collagen turnover. Blood samples taken at pre-infarction baseline, 24 h post-infarction and every week until 5wk follow-up were quantified for swine MMP-9 and TIMP-1 using ELISA according to manufacturer's instructions (Cusabio, Huissen, The Netherlands).

Histology. To quantify myofibroblast numbers in the infarct area, paraffin embedded sections of 4 μm were stained for alpha smooth muscle actin as described before (18) (αSMA monoclonal antibody, Sigma, Zwijndrecht, The Netherlands). Next, the infarcted area was planimetrically quantified for myofibroblast numbers in a blinded matter with vessels excluded (Qwin, Leica, Rijswijk, The Netherlands). Data were expressed as myofibroblast area / total infarct area (%).

RT-PCR. Cryopreserved infarct tissue was homogenized and RNA was isolated using the RNeasy Fibrous Tissue Mini Kit (Qiagen, Hilden, Germany) according to manufacturer's instructions. Isolated RNA was assessed for concentration and purity (A260/A280 ratio) with a NanoDrop spectrophotometer (Thermo Fischer Scientific, USA). Next, RNA was reverse-transcribed into cDNA, using the iScript cDNA synthesis kit (Bio-Rad, USA). Temperature gradient optimization studies were performed with pooled samples from non-infarct tissue cDNA (n=12). IQ SYBR Green Supermix (Bio-Rad) was used for the detection of cDNA levels. Quantification of gene expression of genes related to either myofibroblast presence, regulation or differentiation were quantified as well as genes involved in extracellular matrix turnover and Wnt/Frizzled signaling was performed using the comparative Ct (ΔCt) method and results are expressed as ratios to the housekeeping gene cyclophilin and normalized to the average of sham-operated animals. See supplemental table S1 for primer details.

Statistical analysis

Statistical analysis for the effect of UM206 on hemodynamic, echographic and expression data was performed in SPSS. Expression data were first compared between sham, Control-MI remote, and UM206-treated remote myocardium using ANOVA. Subsequently, since infarct mass variation at baseline was considerable, ranging from 9.6 to 23.5 gram, ANCOVA with UM206 as a factor and infarct size determined by plasma hFABP as a covariate was used. When hFABP was not related to expresssion, an ANOVA for repeated measures was used with area (infarct vs remote) as within-subject factor and UM206-treatment as between-subject factor. Data are given as mean±SEM. $P<0.05$ was considered statistically significant.

RESULTS

Occlusion of the LCx coronary artery resulted in infarction of the lateral wall of the left ventricle as evidenced by marked changes in the ECG (not shown) and hFABP release. Although plasma hFABP concentrations at 50 minutes of reperfusion varied considerably between the individual animals, overall plasma hFABP concentrations were similar in the Control-MI group and the UM206 group (Table 1). Estimated $IM_{baseline}$ was therefore also similar between groups.

Treatment with UM206 for 5 weeks resulted in a significant decrease in IM whereas IM remained unchanged in the Control-MI group (Figure 1A, Table 1). The alterations in infarct remodeling were accompanied by changes in LV geometry as measured with echo in awake swine. After 3 weeks follow up, LV dilation occurred as evidenced by the larger increase in LV-EDA in both Control-MI and UM206-treated swine as compared to sham-operated animals (Figure 1B, Table 2). This increase in LV-EDA was progressive between 3 and 5 weeks after MI in the Control-MI group, whereas LV-EDA remained constant in the UM206 group (Table 2), resulting in a significant reduction in dilation of the LV by UM206-treatment 5 weeks after MI (Table 2, Figure 1B). MI resulted in a significant decrease in ejection fraction at 3 and 5 weeks follow-up, but there was no overall difference in ejection fraction between UM206-treated and Control-MI swine (Table 2), due to the large variation in IM. However, IM at follow up was linearly related to LV ejection fraction (not shown), suggesting that the IM reduction by UM206 did result in improved LV function. Hemodynamics, as measured under anesthesia, were not different between groups (Table 3) although heart rate was slightly lower in vehicle-treated swine. This was most likely the result of anesthesia, as awake heart rates were not different between groups (not shown).

Table 1. *Infarct mass at baseline and Follow-up*

	Sham	Control-MI	UM206
hFABP (ng/ml)	-	141 ± 34	155 ± 20
$IM_{baseline}$ (g)	-	14.5 ± 1.5	17.7 ± 1.9
IM_{FU} (g)	-	14.2 ± 2.3	11.2 ± 2.2†
Infarct $Size_{FU}$ (%LV)	-	10.6 ± 1.7	8.7 ± 1.6
LVM/BM (g/kg)	2.31 ± 0.10	3.35 ± 0.21*	3.14 ± 0.39*
RVM/BM (g/kg)	0.75 ± 0.04	1.11 ± 0.06*	1.13 ± 0.09*

Data are expressed as mean ± SEM. *p<0.05 vs sham; †p<0.05 vs corresponding baseline. BM = body mass; hFABP = heart specific fatty acid binding protein; IM = infarct mass; LVM = left ventricular mass; RVM = right ventricular mass.

Table 2. *Echocardiographic parameters*

Days post-MI		Sham	Control-MI	UM206
	EDA (mm^2)	778 ± 49	851 ± 75	902 ± 84
Day 1	ESA (mm^2)	359 ± 22	448 ± 86	456 ± 60
	EF (%)	53.3 ± 2.3	48.8 ± 5.5	50.1 ± 3.4
	EDA (mm^2)	860 ± 50	1389 ± 76*	1266 ± 81*
Day 21	ESA (mm^2)	360 ± 41	843 ± 67*	693 ± 61*
	EF (%)	57.7 ± 4.3	39.2 ± 3.8*	45.3 ± 3.5*
	EDA (mm^2)	1052 ± 33	1781 ± 110*	1428 ± 103*†
Day 35	ESA (mm^2)	471 ± 53	1010 ± 95*	789 ± 113*
	EF (%)	55.8 ± 4.4	43.6 ± 2.5*	44.8 ± 5.2

Data are expressed as mean ± SEM. *P<0.05 vs sham; † P<0.05 vs Control-MI. EDA = end diastolic area; EF = ejection fraction; ESA = end systolic area.

Table 3. *Hemodynamic parameters at sacrifice*

	Sham	Control-MI	UM206
Heart rate (bpm)	99 ± 3	83 ± 7*	103 ± 7
Aorta pressure (mmHg)	92 ± 5	103 ± 7	103 ± 2
LVSP (mmHg)	103 ± 4	118 ± 8	115 ± 2
LVEDP (mmHg)	13 ± 2	15 ± 3	13 ± 2
dP/dtmax (mmHg/s)	1620 ± 140	1690 ± 180	1590 ± 160
dP/dtmin (mmHg/s)	-1600 ± 140	-2100 ± 140	-2100 ± 170
CO (L/min)	3.9 ± 0.3	3.4 ± 0.5	4.2 ± 0.3

LVSP: left ventricular systolic pressure; LVEDP: left ventricular end diastolic pressure; dP/dtmax: maximal rate of rise of left ventricular pressure; dP/dtmin: maximal rate of decrease in left ventricular pressure; CO: cardiac output. Data are expressed as mean ± SEM. *P<0.05 vs sham; †P<0.05 vs Control-MI.

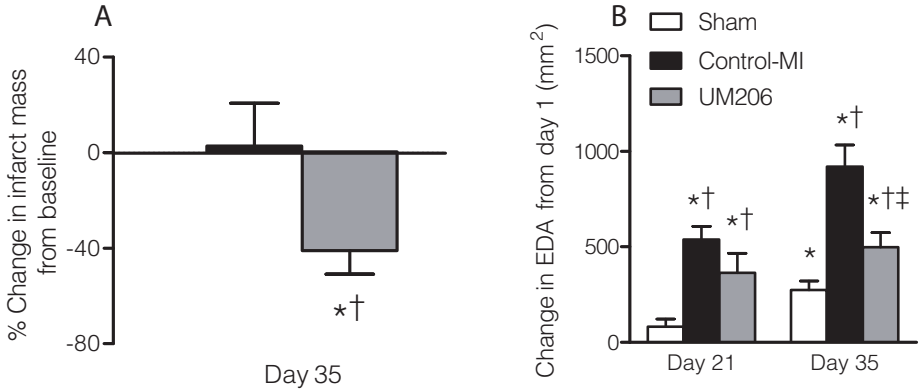

Figure 1. *Effect of UM206-treatment on infarct size and left ventricular dilatation*
*UM206-treatment decreased infarct mass (Panel A). The reduction in infarct mass was accompanied by a reduced dilation of the left ventricular end-diastolic area as measured with echocardiography (panel B). * P<0.05, vs baseline (Panel A) or day 1 post-MI (Panel B), † P<0.05 vs Sham, ‡P<0.05 UM206-treatment vs Control-MI.*

In agreement with previous observations in mice, MI resulted in the occurrence of myofibroblasts in the infarct area, activation of the Wnt/Fzd pathway, inflammation and increased expression of ECM proteins in the infarct area. Interestingly, this occurred not only in the infarcted myocardium, but also in the remote myocardium. mRNA for both Fzd2 and Fzd4 was increased in remote non-infarcted myocardium as compared to sham, and while expression of Fzd2 tended to be more increased (P=0.06) in the infarcted area, Fzd4 mRNA expression was less in infarcted as compared to the remote area (Table 4). mRNA expression of the Fzd co-receptor LRP5 was increased, while mRNA expression of the co-receptor LRP6 was decreased in remote as well as infarcted myocardium as compared to sham-operated animals. TGF-β1 and Collagen-3 were increased in remote and infarcted myocardium of swine with MI, while collagen-1 was slightly lower in remote myocardium of swine with MI as compared to sham-operated animals, but was increased in the infarcted myocardium in comparison to remote myocardium (Table 4). Moreover, LOX, one of the enzymes responsible for collagen-crosslinking, as well as tenascin-C, a glycoprotein that is expressed in the extracellular matrix following injury, were increased in the infarcted myocardium as compared to remote tissue. In the downstream part of the Wnt/Fzd signaling pathway, axin and APC were unaltered in either remote or infarcted myocardium, while β-catenin was increased in remote and infarcted myocardium of both Control-MI swine and swine treated with UM206 as compared to sham-operated swine.

Table 4. *RT-PCR for Wnt signaling, structural extracellular matrix components and growth factors*

	Remote area			Infarct Area		P-values		
	Sham	**Control-MI**	**UM206**	**Control-MI**	**UM206**	**UM206**	**Area**	**Area* UM206**
Wnt Signaling								
β-Catenin	1.0 ± 0.3	2.3 ± 0.4*	2.7 ± 0.4*	1.8 ± 0.5	3.0 ± 0.6	0.17	0.84	0.43
Fzd2	1.0 ± 0.1	3.1 ± 0.3*	2.7 ± 0.2*	4.8 ± 0.9	4.2 ± 1.0	0.45	0.06	0.89
Fzd4	1.0 ± 0.2	1.7 ± 0.2*	2.1 ± 0.2*	0.8 ± 0.1	1.4 ± 0.2	0.01	0.01	0.68
LRP5	1.0 ± 0.7	12.9 ± 1.6*	18.4 ± 2.0*†	4.1 ± 1.4	8.0 ± 2.5	0.04	0.01	0.71
LRP6	1.00 ± 0.23	0.39 ± 0.03	0.52 ± 0.04*	0.36 ± 0.06	0.52 ± 0.11	0.08	0.79	0.81
APC	1.00 ± 0.23	0.83 ± 0.12	0.97 ± 0.13	0.69 ± 0.09	0.95 ± 0.16	0.23	0.41	0.58
Axin2	1.00 ± 0.35	0.31 ± 0.14	0.41 ± 0.07	0.30 ± 0.02	0.35 ± 0.09	0.26	0.58	0.71
Structural Components and growth factors								
αSMA	1.0 ± 0.3	2.2 ± 0.4	2.0 ± 0.6	7.9 ± 3.5	2.5 ± 0.6	0.14	0.13	0.19
VEGF-A	1.0 ± 0.4	1.1 ± 0.1	1.9 ± 0.7	0.6 ± 0.2	1.1 ± 0.2	0.08	0.13	0.75
LOX	1.00 ± 0.20	0.67 ± 0.14	0.51 ± 0.04	1.38 ± 0.20	1.15 ± 0.41	0.43	0.02	0.90
Tenascin-C	1.0 ± 0.5	8.5 ± 4.3	3.6 ± 1.2	33.9 ± 6.0	21.8 ± 5.6	0.15	0.00	0.35
TGFβ1	1.0 ± 0.3	3.0 ± 0.3*	3.2 ± 0.3*	2.1 ± 0.4	2.5 ± 0.4	0.46	0.01	0.66
TGFβ2	1.00 ± 0.25	0.21 ± 0.06*	0.17 ± 0.02*	0.28 ± 0.09	0.21 ± 0.06	0.39	0.38	0.76
TGFβ3	1.0 ± 0.3	9.3 ± 3.4	5.0 ± 0.6*	17.0 ± 1.6	18.0 ± 3.8	0.54	0.04	0.36
Col1a1	1.00 ± 0.21	0.62 ± 0.06	0.48 ± 0.08*	2.37 ± 0.44	1.97 ± 0.79	0.56	0.01	0.78
Col3a1	1.0 ± 0.3	2.4 ± 0.3*	2.3 ± 0.5*	2.2 ± 0.4	3.1 ± 1.0	0.49	0.65	0.52
MMP-2	1.00 ± 0.26	0.73 ± 0.07	0.61 ± 0.09	0.83 ± 0.18	0.88 ± 0.24	0.84	0.30	0.63
MMP-9	1.00 ± 0.23	0.31 ± 0.12*	0.26 ± 0.07*	75 ± 46	1.2 ± 0.6	0.14	0.13	0.14
TIMP-1	1.0 ± 0.7	6,9 ± 0.7*	5.1 ± 0.6*	10.5 ± 2.7	7.1 ± 1.1	0.078	0.14	0.66

APC = adenomatous polypolis coli; Axin = axis inhibition protein; αSMA = alpha smooth muscle actin; Col = collagen; Fzd = frizzled; LOX = lysil oxidase; LRP = low-density lipoprotein receptor-related protein; MMP = matrix metalloproteinase; RT-qPCR = reverse transcriptase quantitative polymerase chain reaction; TGF = transforming growth factor; TIMP = tissue inhibitor of metalloproteinases. VEGF-A = vascular endothelial growth factor A. Data are ratios to housekeeping gene cyclophilin and are displayed relative to sham values ± SEM; Control-MI: n=6; UM206: n=6. *P≤0.05 vs. sham: n=8.

The infarct reduction by UM206 was accompanied by changes in infarct composition and expression of genes involved in ECM remodeling and Wnt/Fzd signaling. Histological assessment of αSMA-positive cells in the infarcted myocardium revealed a significantly lower presence of myofibroblasts in the UM206 group (Figure 2B), which when also corrected for infarct mass at baseline was corroborated by a trend towards a reduction in αSMA mRNA expression (P=0.076, Table 4). In accordance with their role in extracellular matrix turnover, the reduced presence of myofibroblasts resulted in a decrease in TIMP-1 (Figure 2C) and a trend towards a decrease in MMP-9 mRNA (P=0.085, Figure 2D) in the UM206-treated group as compared to the Control-MI group at sacrifice 5 weeks after induction of MI. The effects of UM206-treatment on local TIMP-1 and MMP-9 expression were not reflected in significant changes in MMP-9 and TIMP-1 in circulating plasma.

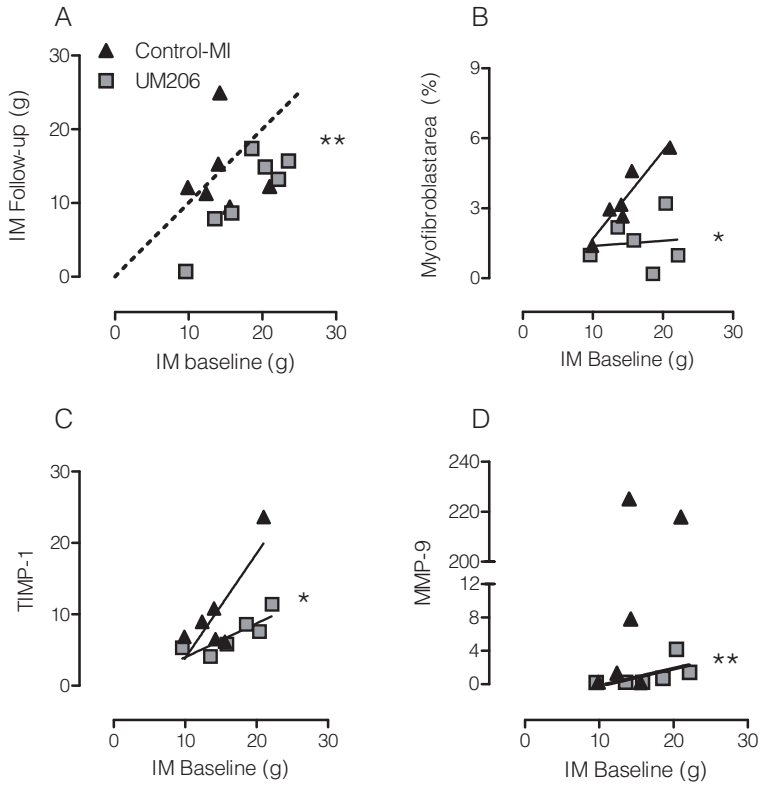

Figure 2. *Effect of UM206-treatment on infarct remodeling and expression of markers for myofibroblast presence and extracellular matrix remodeling*
*UM206-treatment for 5 weeks increased infarct reduction (Panel A). This beneficial effect of UM206 was accompanied by a reduction in myofibroblast presence (panel B), which was associated with a decrease in TIMP-1 (Panel C) and a trend towards a reduction in MMP-9 (panel D). * P<0.05, **P<0.10 UM206-treatment vs Control-MI.*

TIMP-1 levels were below the detection limit of the assay in most plasma samples and were not different between Control-MI and UM206-treated swine. MI resulted in a significant increase in plasma MMP-9 one day post-MI prior to the start of UM206-treatment (15±5 ng/ml at day 1 vs 8±4 ng/ml just prior to initiation of MI) but was not different between groups. This increase in plasma MMP-9 tended to wane over time, being 6±1 ng/ml at 5 weeks follow-up (P=0.10 vs day 1), but serial assessment of plasma MMP-9 did not show any differences between Control-MI and UM206-treated swine.

Interestingly, mRNA expression of Fzd4 was significantly higher in the infarcted myocardium of the UM206-treated animals (Table 4). This higher expression of Fzd4, a receptor thought to be involved in angiogenesis, was accompanied by a tendency towards a higher expression of VEGF in the infarcted myocardium of UM206-treated animals as compared to Control-MI.

mRNA for the Fzd co-receptors LRP5 (P=0.06) and LRP6 (P<0.05) was higher in the remote myocardium of UM206-treated animals as compared to Control-MI (Table 4), which was accompanied by a trend towards a lower TIMP-1 expression (P=0.07), suggesting that UM206-treatment may directly affect remodeling of the remote myocardium as well.

DISCUSSION

In the present study the effect of UM206, a modulator of Wnt/Fzd signaling, was investigated on infarct remodeling and LV function in a clinically relevant large animal model. The most important findings in the present study are that treatment with UM206 for 5 weeks after acute MI, resulted in *i)* IM reductions and *ii)* reduced dilation of the LV which was accompanied by *iii)* changes in expression of genes involved in ECM remodeling and Wnt/Fzd signaling. The implications of these findings will be discussed below.

Myofibroblasts and LV remodeling after MI

MI results in dilation and remodeling of the left ventricle. Although this process is aimed at maintaining pump function, dilation of the left ventricle has been shown to be an initiating factor in the process leading to heart failure. Infarct size and composition of the scar tissue, replacing the infarcted myocardium, are important determinants of the outcome of the LV remodeling process. Infarct healing occurs

in three partly overlapping phases: an initial inflammatory phase, followed by a proliferative phase and maturation of the scar. (Myo)fibroblasts play different roles in the different phases (4,9). In the initial phase, the fibroblasts act as local immune modulators and are the main effectors of fibrogenesis (1,4-6,19). In the subsequent proliferative phase of healing, fibroblasts further differentiate into myofibroblasts that not only have an augmented matrix-synthetic phenotype, but also express the contractile protein αSMA. Both the increased ECM production and the contractile properties of the myofibroblasts have been proposed to be key factors in strengthening the infarct and limiting infarct expansion, thereby reducing LV dilation (1,4,20), and therefore constitute a target to modulate infarct remodeling. Administration of UM206 promotes migration of fibroblasts to the infarcted area by inhibition of Wnt/Fzd signaling, and thereby modulates the scar formation in the infarcted area (10). In accordance with our recent study in mice (10), we found in the present study that treatment with UM206 for 5 weeks reduced infarct size and that this reduction in infarct size was accompanied by a decreased LV dilation, as measured in awake animals with echocardiography, between 3 and 5 weeks after MI in swine treated with UM206. Interestingly, infarct mass at sacrifice correlated very well with ejection fraction measured at 5 weeks follow-up, suggesting that, by promoting infarct reduction, UM206-treatment may improve cardiac function.

In both the canine (21) and the porcine (9) heart, myofibroblast presence peaks between 5 and 21 days after MI, after which myofibroblast numbers gradually decline. This has led to the concept that during the phase of infarct maturation, when the infarct is filled with matrix, myofibroblast proliferation is suppressed, and myofibroblasts become quiescent and undergo apoptosis (4). In the present study, we found that the presence of myofibroblasts, as indicated by immunohistochemistry as well as mRNA-expression for αSMA, was higher in the infarcted tissue as compared to remote tissue and correlated with infarct size at follow up. In contrast to our previous study in mice, in which UM206-treatment increased myofibroblast presence in the infarcted area (10), myofibroblast presence was lower in the infarcted myocardium of UM206-treated swine as compared to Control-MI, particularly in swine with a large MI. It should be noted however, that infarct size as a percentage of the left ventricle in mice is much larger than the infarct size in swine in the present study, and therefore mechanical stress within the murine infarcts is expected to be larger. As myofibroblast differentiation is promoted by mechanical stress (22), it is likely that the UM206-induced infarct remodeling earlier after MI attenuated mechanical stress 5 weeks after MI, and thereby reduced myofibroblast presence. This is in accordance with a recent study in swine showing that, while in control infarcts myofibroblasts presence increased

between 7 and 21 days of infarct, treatment with a biocomposite material resulted in an increased myofibroblast presence 7 days after MI, while myofibroblasts were lower at 21 days, at a time when LV dilation was reduced compared to control infarcts (9). Importantly, it has been suggested that persistent myofibroblast presence in the injured heart particularly in the remote non-infarcted myocardium, may be detrimental as it may lead to excessive fibrosis and contribute to heart failure (1,23). It is therefore important to also evaluate changes in the remote myocardium. MMP-9 was decreased while TIMP-1 and collagen-3 were increased in the remote myocardium after MI, which is suggestive of increased interstitial fibrosis (1,12), but UM206- treatment did not modulate this expression.

In humans, LV dilation was shown to correlate with circulating MMP-9 levels (24,25). In our study however, biological activity of early myofibroblast presence was not reflected in circulating levels of MMP-9 and TIMP-1, typical markers for collagen turnover. It is possible that the surgical trauma in combination with the chronic instrumentation of our animals evoked inflammatory and reparative processes that influenced the plasma levels of MMP-9, which may have masked the effect of the MI. Moreover, plasma levels of MMP-9 do not only reflect the increased expression of MMP-9 in the infarcted area but are also influenced by the decreased expression of MMP-9 in the remote-non-infarcted myocardium. In contrast to the unaltered circulating plasma levels of MMP-9, MMP-9 mRNA tended to be higher in the infarcted myocardium of Control-MI as compared to UM206-treated swine 5 weeks after MI and correlated with infarct size, which is in accordance with the increased presence of myofibroblasts, and their role in modulation of the ECM. In combination with our observation that expression of collagen 1 and 3 was unaltered by UM206, the increased levels of MMP-9 in the Control-MI swine may have resulted in enhanced degradation of the ECM, which could have contributed to the LV dilation that occurred between 3 and 5 weeks after MI.

Almost all frizzled members have been identified in the healthy heart tissue but the signaling in the adults is silent (19,23). The Wnt/Fzd signaling pathway is activated in wound healing after MI (20,26). In the present study, Fzd-receptor expression patterns were indeed different in remote vs infarcted myocardium. In accordance with a recent study in swine (27), Fzd2 was increased, while Fzd4 was decreased in infarcted myocardium as compared to remote myocardium. Although, in the present study, we focused on the effect of altering Wnt/Fzd signaling in myofibroblasts, it is possible that altering signaling in other cell-types within the myocardium may have contributed to the beneficial effects of UM206. Thus, Wnt signaling has also

been related to inflammation and angiogenesis (7) and expression of Fzd4, a receptor that has been shown to be involved in stabilization of micro vessels, was higher in animals treated with UM206 as compared to Control-MI. As micro vessel stabilization is protective against microvascular regression in the maturation phase of MI, the increased expression of Fzd4 together with the tendency towards an increase in VEGF-mRNA, is consistent with and increased angiogenic potential in UM206-treated swine, which may have contributed to the improved infarct healing.

CONCLUSION

Administration of the peptide fragment UM206 attenuates the dilation of the left ventricle after MI in a translationally relevant swine model of ischemia/reperfusion. From this observation, we conclude that inhibition of Wnt/Fzd signaling has a beneficial effect on the wound healing after MI, resulting in a reduced adverse remodeling of the heart. Although the effects on cardiac function were limited at the 5-week time point, it is attractive to speculate that prolonged administration of UM206 will prevent the deterioration of the cardiac performance that is frequently observed after infarction.

ACKNOWLEDGMENTS

The authors gratefully acknowledge technical assistance of A. Verzijl, S. Sneep, M. te Lintel Hekkert and L.A. Blonden.

REFERENCES

1. Daskalopoulos EP, Hermans KC, Blankesteijn WM. Cardiac (myo)fibroblast: Novel strategies for its targeting following myocardial infarction. Curr Pharm Des 2014;20:1987-2002.
2. Kloner RA, Jennings RB. Consequences of brief ischemia: stunning, preconditioning, and their clinical implications: part 1. Circulation 2001;104:2981-9.
3. Kloner RA, Jennings RB. Consequences of brief ischemia: stunning, preconditioning, and their clinical implications: part 2. Circulation 2001;104:3158-67.
4. Chen W, Frangogiannis NG. Fibroblasts in post-infarction inflammation and cardiac repair. Biochim Biophys Acta 2013;1833:945-53.
5. Ma Y, de Castro Bras LE, Toba H et al. Myofibroblasts and the extracellular matrix network in post-myocardial infarction cardiac remodeling. Pflugers Arch 2014;466:1113-27.
6. Turner NA, Porter KE. Function and fate of myofibroblasts after myocardial infarction. Fibrogenesis Tissue Repair 2013;6:5-15.
7. Hermans KC, Daskalopoulos EP, Blankesteijn WM. Interventions in Wnt signaling as a novel therapeutic approach to improve myocardial infarct healing. Fibrogenesis Tissue Repair 2012;5:16.
8. Porter KE, Turner NA. Cardiac fibroblasts: at the heart of myocardial remodeling. Pharmacol Ther 2009;123:255-78.
9. McGarvey JR, Pettaway S, Shuman JA et al. Targeted injection of a biocomposite material alters macrophage and fibroblast phenotype and function following myocardial infarction: relation to left ventricular remodeling. J Pharmacol Exp Ther 2014;350:701-9.
10. Laeremans H, Hackeng TM, van Zandvoort MA et al. Blocking of frizzled signaling with a homologous peptide fragment of wnt3a/wnt5a reduces infarct expansion and prevents the development of heart failure after myocardial infarction. Circulation 2011;124:1626-35.
11. Hermans KC DE, Janssen BJ and Blankesteijn W. Matthijs. UM206, a frizzled-receptor antagonist attenuates adverse remodeling and cardiac function deterioration following myocardial infarction. The FASEB Journal 2014;28:652.10.
12. Shinde AV, Frangogiannis NG. Fibroblasts in myocardial infarction: a role in inflammation and repair. J Mol Cell Cardiol 2014;70:74-82.
13. Boontje NM, Merkus D, Zaremba R et al. Enhanced myofilament responsiveness upon beta-adrenergic stimulation in post-infarct remodeled myocardium. Journal of Molecular and Cellular Cardiology 2011;50:487-499.
14. Zhou ZC, de Wijs-Meijler D, Lankhuizen I et al. Blunted coronary vasodilator response to uridine adenosine tetraphosphate in post-infarct remodeled myocardium is due to reduced P1 receptor activation. Pharmacological Research 2013;77:22-29.
15. Kuster DWD, Merkus D, Kremer A et al. Left ventricular remodeling in swine after myocardial infarction: a transcriptional genomics approach. Basic Research in Cardiology 2011;106:1269-1281.
16. van der Velden J, Merkus D, Klarenbeek BR et al. Alterations in myofilament function contribute to left ventricular dysfunction in pigs early after myocardial infarction. Circ Res 2004;95:e85-95.
17. Uitterdijk A, Sneep S, van Duin RW et al. Serial measurement of hFABP and high-sensitivity troponin I post-PCI in STEMI: how fast and accurate can myocardial infarct size and no-reflow be predicted? Am J Physiol Heart Circ Physiol 2013;305:H1104-10.
18. van den Borne SW, van de Schans VA, Strzelecka AE et al. Mouse strain determines the outcome of wound healing after myocardial infarction. Cardiovasc Res 2009;84:273-82.
19. Daskalopoulos EP, Janssen BJ, Blankesteijn WM. Myofibroblasts in the infarct area: concepts and challenges. Microsc Microanal 2012;18:35-49.

20. Daskalopoulos EP, Janssen BJ, Blankesteijn WM. Targeting Wnt signaling to improve wound healing after myocardial infarction. Methods Mol Biol 2013;1037:355-80.
21. Frangogiannis NG, Michael LH, Entman ML. Myofibroblasts in reperfused myocardial infarcts express the embryonic form of smooth muscle myosin heavy chain (SMemb). Cardiovasc Res 2000;48:89-100.
22. Hinz B, Gabbiani G. Mechanisms of force generation and transmission by myofibroblasts. Current opinion in biotechnology 2003;14:538-546.
23. Lajiness JD, Conway SJ. Origin, development, and differentiation of cardiac fibroblasts. J Mol Cell Cardiol 2014;70:2-8.
24. Kelly D, Cockerill G, Ng LL et al. Plasma matrix metalloproteinase-9 and left ventricular remodelling after acute myocardial infarction in man: a prospective cohort study. Eur Heart J 2007;28:711-8.
25. Squire IB, Evans J, Ng LL, Loftus IM, Thompson MM. Plasma MMP-9 and MMP-2 following acute myocardial infarction in man: correlation with echocardiographic and neurohumoral parameters of left ventricular dysfunction. J Card Fail 2004;10:328-33.
26. Daskalopoulos EP, Hermans KC, Janssen BJ, Matthijs Blankesteijn W. Targeting the Wnt/frizzled signaling pathway after myocardial infarction: a new tool in the therapeutic toolbox? Trends Cardiovasc Med 2013;23:121-7.
27. Prat-Vidal C, Galvez-Monton C, Nonell L et al. Identification of temporal and region-specific myocardial gene expression patterns in response to infarction in swine. PloS one 2013;8:e54785.

SUPPLEMENTAL MATERIAL

Table S1. *Primer sequences and annealing temperatures used in the RT-qPCR studies*

Sus Scrofa gene	Forward primer	Reverse primer	Annealing Temperature used (°C)
β-Catenin	ATTGAAGCTGAGGGAGCCAC	ACTCCTAAAGGATGATTTACAGGTC	62
Fzd2	ATAGGCACGTCCTTCCTCCT	GACGGGTGTAGAACTTCCTCC	62
Fzd4	ACATGGGGCATTTCCAGGAG	TACAAGTCGCCTGGGTGAAC	65
LRP5	ACGTGATCGAGTTTGGCCTT	TGTTGTGCATGCAGTCGTTG	65
LRP6	CGTGCCAGTTGGAGGTTTTG	TCCGAAGGCTGTGGATAGGA	62
APC	ACAAAACTGGAAACTGAGGCAT	CGGAGGGACATTTTTGACCG	63
AXIN2	CAAACCCATGCCTGTCTCCT	CGGAAGAGATAAGCCCCGTC	65.5
aSMA	GGACCCTGTGAAGCACCAG	GGGCAACACGAAGCTCATTG	66.4
VEGF-A	GACCAGAAACCCCACGAAGT	AAATGCTTTCTCCGCTCCGA	58
LOX	TCCAAGCTGGCTATTCGACG	AGGATTGTACGGGTCATCGC	65
Tenascin-C	CACCCCGGTACTTGTTCCAT	CCTCGAAGGTGACAGTTGCT	57
TGFβ1	GTGGAAAGCGGCAACCAAAT	CACTGAGGCGAAAACCCTCT	65
TGFβ2	TGCCTGCGTCCACTTTACAT	AGCTGAGAACCCTGCTATGC	62
TGFβ3	ATGGAGAAGAAACCCAGAGCTT	TCCGACTCGGTGTTTTCCTG	63.5
Col1a1	AGACATCCCACCAGTCACCT	TCACGTCATCGCACAACACA	62
Col3a1	GCTCCCATCTTGGTCAGTCC	CCATCATTACCTCGAGCCCC	63.5
MMP-2	GCAGTGATGGCAAGTTGTGG	TTGACATCGTCGTGGGACAG	65
MMP-9	ACTTCGGAAACGCAAAAGGC	AAGAGTCTCTCGCTAGGGCA	62
TIMP-1	CTGGTCATCAGGGCCAAGTT	GGTCTGTCCACAAGCAGTGA	63.5
Cyclophilin	AGACAGCAGAAAACTTCCGTG	AAGATGCCAGGACCCGTATG	63.5

APC = adenomatous polypolis coli; Axin = axis inhibition protein; αSMA = alpha smooth muscle actin; Col = collagen; Fzd = frizzled; LOX = lysil oxidase; LRP = low-density lipoprotein receptor-related protein; MMP = matrix metalloproteinase; RT-qPCR = reverse transcriptase quantitative polymerase chain reaction; TGF = transforming growth factor; TIMP = tissue inhibitor of metalloproteinases. VEGF-A = vascular endothelial growth factor A.

CHAPTER 11

VEGF165A microsphere therapy for myocardial infarction suppresses acute cytokine release and increases microvascular density, but does not improve cardiac function

***André Uitterdijk**
*Tirza Springeling
Matthijs van Kranenburg
Richard WB van Duin
Ilona Krabbendam-Peters
Charlotte Gorsse-Bakker
Stefan Sneep
Rorry van Haeren
Ruud Verrijk
Robert-Jan M van Geuns
Willem J van der Giessen†
Tommi Markkula
Dirk J Duncker
Heleen MM van Beusekom

*Both authors contributed equally

Am J Physiol Heart Circ Physiol 2015 309:H396-H406

ABSTRACT

Angiogenesis induced by growth-factor releasing microspheres can be an off-the-shelf and immediate alternative to stem cell therapy for acute myocardial infarction (AMI), independent of stem cell yield and co-morbidity induced dysfunction. Reliable and prolonged local delivery of intact proteins such as VEGF is however notoriously difficult. Our objective was to create a platform for local angiogenesis in human-sized hearts, using polyethylene-glycol/polybutylene-terephthalate (PEG-PBT) microsphere-based $VEGF_{165A}$ delivery. PEG-PBT microspheres were biocompatible, distribution was size dependent and a regimen of $10{\cdot}10^6$ 15μm microspheres at $0.5{\cdot}10^6$ per minute did not induce cardiac necrosis. Efficacy, studied in a porcine model of AMI with reperfusion rather than chronic ischemia used for most reported VEGF studies, shows that microspheres were retained for at least 35 days. Acute $VEGF_{165A}$ release attenuated early cytokine release upon reperfusion and produced a dose dependent increase in microvascular density at 5 weeks following AMI. However, it did not improve major variables for global cardiac function, left ventricular dimensions, infarct size or scar composition (collagen and myocyte content). Taken together, controlled $VEGF_{165A}$ delivery is safe, attenuates early cytokine release and leads to a dose dependent increase in microvascular density in the infarct zone, but does not translate into changes in global or regional cardiac function and scar composition.

INTRODUCTION

Stem cell therapy for acute myocardial infarction (AMI), sought after to facilitate cardiac repair, has shown promise to improve cardiac function and patient outcome (1). However, outcome parameters vary widely (2) and are not always reported well (3). Rather than trans-differentiation of stem cells into cardiomyocytes, the postulated mechanism of stem cell action is through paracrine factors, inducing anti-apoptotic effects, immunomodulation and regional angiogenesis (4). Improved angiogenesis or maintenance of the pre-existing microvascular bed is not only a prerequisite for cardiac regeneration, but also for cardiac healing through improved or maintained perfusion. It allows for access of leukocytes and facilitates scar stabilizing processes such as fibrosis and debridement.

Autologous stem cell therapy however, is delayed hours to days due to cell harvesting and cell culture steps, and quality and viability may vary with co-morbidities (5,6). In addition, it has been suggested that early post-AMI regional inflammation may impair stem cell function. This implies that stem cell therapy depends heavily on quality of the cells and, importantly, cannot be used immediately following a primary percutaneous coronary intervention (pPCI) which is the preferred AMI treatment. This leaves acute and reperfusion induced injury such as no-reflow untreated.

Microsphere (MSP) therapy, releasing angiogenic or other therapeutic factors, could be an off-the-shelf alternative to stem cells. It would make it independent from co-morbidity induced stem cell dysfunction and would be available for immediate delivery following pPCI. It would also allow delivery of regional angiogenic agents or other pharmacotherapeutics before onset of irreversible reperfusion injury and before development of impaired (microvascular) perfusion i.e. no-reflow.

This timing is of particular importance as delivery of therapeutic agents before the occurrence of no-reflow induced perfusion deficits, should allow optimal distribution of MSP and widens its therapeutic potential beyond angiogenesis to prolonged local delivery of other pharmaca.

We used an amphiphilic biomaterial composed of polyethylene glycol and polybutylene terephthalate (PEG-PBT) with adjustable release kinetics (PolyActive™). It is designed especially for stable protein delivery (7-11) and can theoretically harbor more than one growth factor per MSP for simultaneous release. Adjustable release kinetics of MSPs allows control of diffusion and, subsequently, sequential release of multiple growth factors is possible when a mixture of growth

factor specific MSPs with dedicated release characteristics are given. Polyactive™ MSP delivery keeps proteins intact, protects them against proteolytic degradation and has shown excellent biocompatibility in implants (12). PolyActive™ can be stored as an off-the-shelf therapy without loss of activity.

Many studies of growth factor induced angiogenesis have been performed in the past but these models invariably used chronic ischemia through permanent occlusion of a coronary artery. However, the clinical reality in Western Europe is that patients suffering an acute myocardial infarction are referred for pPCI where possible, to relieve ischemia by immediate reperfusion. We therefore studied the efficacy of MSP induced angiogenesis using $VEGF_{165A}$ as a model drug in a setting similar to that used for pPCI by using a translational animal model of ischemia-reperfusion.

MATERIALS AND METHODS

Source of $VEGF_{165A}$

Growth factor $VEGF_{165A,}$ used for both cell culture studies and preparation of loaded MSPs, was sourced from one supplier (Peprotech, New Jersey, United States). Growth factor for cell culture studies was diluted from fresh stock.

Preparation of $VEGF_{165A}$ loaded Polyactive™ microspheres

Monodisperse formulations of placebo, high dose (~0.3 pg) and low dose (~0.1 pg) $VEGF_{165A}$-loaded PolyActive™ MSPs (Octoplus, Leiden, The Netherlands) were prepared by a double emulsion (water-in-oil-in-water) method. $VEGF_{165A}$ aqueous solution (0.5 % w/v) was emulsified by high shear mixing (Ultra-Turrax) into a solution of PolyActive™, a copolymer of polyethylene glycol (PEG) and polybutylene terephthalate (PBT) with compositions, 1000PEGT80PBT20 or 1500PEGT77PBT23 (Polyvation, Groningen, The Netherlands) in dichloromethane (10 % w/w). This emulsion was pushed through a membrane (Nanomi, Oldenzaal, The Netherlands) with a uniform pore size specific for each desired MSP size, using nitrogen into a 0.5 % solution of polyvinyl alcohol (PVA, 13-23 kDa, Sigma, Zwijndrecht, The Netherlands), resulting in a suspension of uniformly sized micro droplets. Extraction and evaporation of the organic solvent resulted in formation of hardened MSP. After washing and final sieving through an absolute 20 μm sieve to remove aggregated samples, suspended MSPs were frozen in water for injection and stored at -80 °C until use.

Microsphere size distribution and surface characteristics

Size distribution and the number of MSP per ml was determined by Coulter counter analysis (Coulter Counter Multisizer 3, Beckman Coulter, Mijdrecht, The Netherlands).

MSP shape and surface characteristics were studied by scanning electron microscopy (Jeol JSM6610LV at 5KV). Hydrated MSP were dried through graded ethanol series followed by a chemical drying step using hexamethyldisilazane (Sigma). Fully dried MSP were mounted using double sided conductive carbon tape and sputter coated (gold) before examination.

In-vitro release kinetics of $VEGF_{165A}$ microspheres

Since small increments in systemic VEGF levels are difficult to determine (13), release kinetics of drug-laden MSP were only determined in vitro. Release kinetics were assessed by placing $10{\cdot}10^6$ MSP in a gently and continuously swirled extraction medium at 37 °C (PBS + 0.05% Tween20) that precludes aggregation of proteins and stabilizes them for later analysis (14). Total $VEGF_{165A}$ release was measured at <1min (mimicking acute release), 2.5h (mimicking early reperfusion), then every day for 14 days followed by 21, 28 and 35 days post incubation. These time points were selected to mimic timing of the efficacy study described below. Eluted $VEGF_{165A}$ was measured by enzyme-linked immunosorbent assays (ELISA) according to manufacturer's instructions for human $VEGF_{165A}$ (R&D Systems, Abingdon, United Kingdom). Absorbance was measured at 450 nm with a microplate photometer and converted to concentration using a standard calibration curve. MSP size was measured before and after the release kinetics studies by Coulter counter analysis.

In-Vitro angiogenic $VEGF_{165A}$ efficacy

To study the lower threshold of *$VEGF_{165A}$* efficacy in cardiac network formation, cultured human cardiac microvascular endothelial cells (HCMVECs, Lonza, Breda, The Netherlands) were starved for 20 hours (0.5% heat inactivated fetal bovine serum (FBS) in basal endothelial cell growth medium (EBM2), Lonza, Breda, The Netherlands) for synchronization. Starved cells were isolated by contemporary trypsinization and centrifugation and $2.6{\cdot}10^4$ cells/cm^2 were resuspended into EBM2 + 0.5% heat inactivated FBS. According to manufacturer's instructions, μ-slides for angiogenesis (IBIDI, Martinsried, Germany) were filled with 10μl growth factor reduced MatriGel® (MatriGel-GFR, BD Biosciences, Breda, The Netherlands) per well. Then 50μl of cell suspension with incremental $VEGF_{165A}$ (Peprotech, 0,

30 ng/g or 100 ng/g) was added to every well (n=5) and equal distribution was ascertained. Angiogenesis was subsequently allowed for 18 hours at 37 °C under hypoxic (pO_2: 2%) cell culture conditions and photographically documented. Total tube length and number of junctions were quantified (Angiosys 1.0, TCS Cellworks, Buckingham, United Kingdom) for statistical analysis.

In vivo Size finding for MSP retention, Safety and Biocompatibility

The MSP size generally used for determination of myocardial blood flow is 15 μm as it is retained by the organ without inducing arteriolar obstruction (15). However, since biomaterials can show specific behavior, we decided to test both smaller (12 μm) and larger (17 μm) MSP to confirm retention and determine potential arteriolar obstruction with PolyActive™ MSP. These experiments were performed in 5-6 month old Yorkshire-Landrace swine of either sex (34.2±0.9kg). All animal experiments were conducted in compliance with the "Guide for the Care and use of Laboratory Animals" and after written approval of the Animal Ethics Committee of the Erasmus MC. In short, swine were sedated with an intramuscular injection of midazolam (1 mg/kg) and ketamine (20 mg/kg). Following an intravenous ear catheter placement, anesthesia was induced with an intravenous injection of 600 mg pentobarbital. Animals were intubated and mechanically ventilated (O_2:N_2 = 1:3, v.v.). Anesthesia was maintained with pentobarbital (15 mg/kg/h) and animals were instrumented as described before (16).

For size finding (myocardial MSP retention), 1-5·10^6 placebo MSP ranging from 12-17μm were injected intracoronary in 11 animals for dispersion into the healthy myocardium with an infusion rate up to 1.5·10^6/min. After 2 hours, animals were euthanized and excised hearts were conventionally processed for infarct size determination by TTC (16) and histological MSP quantification by Resorcin-Fuchsin staining, which stains MSP black.

To determine whether myocardial micro-infarctions were produced by MSP infusion, we investigated the acute effects of placebo MSP infusion in 4 healthy swine. Under fluoroscopic guidance, distally to the first marginal branch of the left circumflex coronary artery (LCx, to mimic the delivery as planned for the efficacy study), 15 μm placebo MSP were infused in anesthetized swine through a microcatheter. Numbers of infused MSP varied from 5·10^6 to 20·10^6 and were infused with a rate of 0.5 or 1·10^6 MSP per minute (Table 1). Serial blood sampling and quantification of markers for necrosis and follow-up infarct size measurements were executed as described before (16).

For biocompatibility studies, the sub-acute and chronic inflammatory response to placebo MSP were assessed in 6 swine infused with $5 \cdot 10^6$ 15 μm MSP ($0.5 \cdot 10^6$/min). After 5 days (n=3) or 28 days (n=3) animals were sacrificed as described above, tissues were retrieved and prepared for routine HE histology.

Efficacy of VEGF eluting microsphere therapy for acute myocardial infarction

Thirty-two swine (31.4±0.4kg) were sedated as above and anesthesia was maintained with fentanyl (i.v. 20 μg/kg/hr). Maximal transient coronary vasodilatation was induced for quantitative angiography (selective infusion of 1 mg isosorbidedinitrate) to determine optimal balloon sizing. Coronary diameters were measured using a non-ionic contrast agent (Iodixanol) and dedicated software (CAAS, Pie medical, Eindhoven, The Netherlands). The occlusion and infusion site was carefully selected by at least two investigators and was always selected distal to the first marginal branch. An appropriately sized, coronary angioplasty balloon with a standard guide wire was carefully positioned under fluoroscopic guidance at the selected site of infusion. The LCx was occluded for 2 hours followed by reperfusion. Upon occlusion, anesthesia was switched from fentanyl to isoflurane inhalation anesthesia (17,18). Immediately upon reperfusion by deflation of the angioplasty balloon, $10 \cdot 10^6$ 15μm MSP containing placebo, low or high dose $VEGF_{165A}$ were infused (in 40ml saline, 2ml per minute, $0.5 \cdot 10^6$ particles per minute). The route of administration and the area of distribution of the MSP are illustrated in Figure 1 and shows that MSP are given through the lumen of the angioplasty balloon upon deflation while remaining at the original location, leading to MSP treatment of the area at risk only (i.e. subjected to ischemia), and not outside the area at risk. Anesthetized animals were monitored for 2.5 hours following reperfusion to serially assess biomarker release. Next, catheters were removed, the wound was closed, animals received antibiotic prophylaxis (a mixture of procainebenzylpenicillin and dihydrostreptomycine sulfate, 20mg/kg and 25mg/kg IM) and were allowed to recover.

Global and regional cardiac function by MRI

Global and regional cardiac function including microvascular obstruction was assessed, processed and analyzed in a blinded matter at one and five weeks after myocardial infarction and therapy using magnetic resonance imaging (MRI) as described before (19,20). In short, animals were sedated and intubated as described above. Anesthesia was maintained with fentanyl (20 μg/kg/h) and, when necessary, supported with thiopental sodium (100 mg bolus). Mechanical ventilation and peri-imaging breath-holds were performed using a mobile ventilator

(Carina, Draeger, Zoetermeer, The Netherlands). When necessary, and always in absence of pain reflexes, muscle relaxation was achieved using pancuronium bromide (2-4 mg bolus). Cardiac MRI examinations were performed on a 1.5-Tesla clinical scanner (Signa HD, GE Medical systems, Milwaukee, WI, United States) using a dedicated cardiac four-channel phased array cardiac receiver coil. Repeated breath-holds and gating to the electrocardiogram were applied to minimize the influence of cardiac and respiratory motion on data collection. All cardiac MRI (CMR) protocols consisted of cine–MRI (myocardial function) and delayed enhancement MRI (DE-MRI, infarct size and no-reflow). Cine-MRI was performed using a steady-state, free-precession technique (FIESTA, GE Medical System). Using standard techniques to identify the major cardiac axes, two-chamber and four chamber cine-CMR images were obtained. The two- and four chamber end-diastolic images provided the reference images to obtain a series of short axis views. This resulted in 8-12 cine breath-hold short-axis images to cover the entire left ventricle.

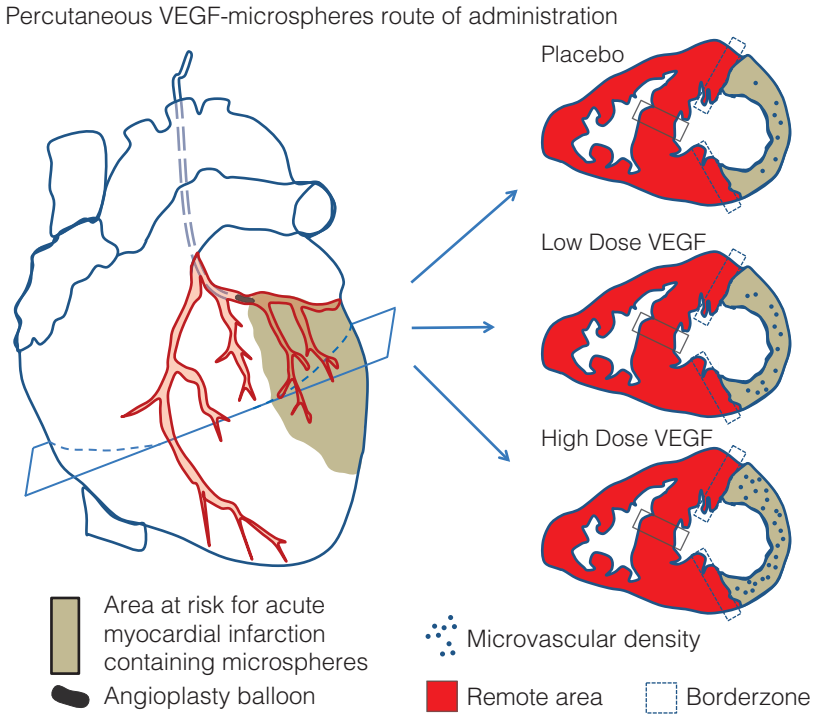

Figure 1 *Graphic representation of the AMI model showing the route of MSP administration. MSP were administered via the guidewire lumen following deflation of the "over-the-wire" angioplasty balloon used to induce ischemia. Hence, MSP were only delivered to the area at risk. The cross-sections at the right indicate the areas of interest used for histological analysis.*

Delayed enhancement imaging was performed with a gated breath-hold 2-dimensional T1-inversion recovery gradient-echo sequence minimally 10 minutes after infusion of Gadolinium-diethyl-triamine-penta-acetic-acid (0.2 mmol/kg i.v., Gadobutrol®, 1.0 mmol/ml, Bayer, Mijdrecht, the Netherlands) (20).

After MRI-imaging, animals were allowed to recover as described above (1 week post-AMI) or transported back to the operating theatre for follow-up sacrifice.

MRI image processing and analysis

All images were transferred to a Microsoft Windows™ based personal computer for blind analysis using the CAAS-MRV program (version 3.3.1; Pie Medical Imaging, Maastricht, The Netherlands). Cine and delayed enhancement images were acquired during the same imaging session and were matched using identical slice positions. Registration of follow-up and baseline cine and delayed enhancement images was achieved by consensus of 2 observers using anatomic landmarks such as papillary muscles and right ventricular insertion sites. The images were analyzed in a blind matter using the additional information of the long axis to limit the extent of volume at the base and the apex of the heart. Left ventricular end-diastolic volume (EDV), left ventricular end-systolic volume (ESV), left ventricular ejection fraction (EF), left ventricular mass and left ventricular end-diastolic wall thickness of the infarct (EDWT) were measured by semi-automatically drawing the endocardial and epicardial contour in end-systolic and end-diastolic phase of the 2- and 4-chamber images with automatic segmentation to the short axis and if necessary corrected manually. Papillary muscles and trabeculations were considered as being part of the blood pool volume and excluded from myocardial mass. Left ventricular ejection fraction (LVEF) was calculated as (LVEDV – LVESV) / LVEDV. Infarct size (IS m/m) was determined on short axis delayed enhancement images using semi-quantitative analyses for the detection of the delayed enhancement regions (2).

Histology

At sacrifice of the anesthetized animal, a sternotomy was performed, the pericardium was carefully opened and after an overdose of pentobarbital, the aorta was cross-clamped and the vena cava opened. Immediately upon euthanasia, proximally to the aorta clamp, an infusion setup was placed to flush the arrested heart with approximately one liter of ice-cold saline to remove blood and plasma from the heart. The flushed heart was excised and cut into 5 transversal slices on a cooled cutting board. Slices were sectioned into remote, border zone and infarct

tissue and subsequently fixed in 3.5-4% buffered formaldehyde, in preparation for paraffin embedding. Area at risk (see Figure 1) is defined as the area subjected to ischemia and is the only area containing MSP. Infarct area is defined as the area showing extensive fibrosis and lack of cardiomyocytes. Border zone is defined as the area bordering the infarct, and does not contain microspheres. For microvascular density of the remote area, tissue was taken from the LV wall opposite of the infarcted area (i.e. septum).

Microvascular density measurement

As arteriolar density does not change as a result of myocardial infarction (21), we measured total microvascular density in the microsphere treated infarct area reflecting changes in capillary density. To quantify microvascular density in myocardial tissue, 4μm sections of paraffin embedded infarct, border zone and remote tissue were stained with the biotin labeled lectin Dolichos Biflorus (DBA, L6533, 1:100, Sigma) followed by Streptavidin-HRP (1:4000, Sigma) and diaminobenzidine-H_2O_2 as a chromogen. Using a 40x magnification, 4 MSP containing, non-overlapping, images were taken of every section (Clemex Vision 4.0, Clemex technologies inc. Quebec, Canada). Microvascular density was quantified using an adapted Chalkley grid to rapidly and reliably quantify angiogenesis despite tortuosity (22) with a custom built ImageJ macro (version 1.46r, National Institutes of Health, USA). The adapted Chalkley grid was manually placed over every image, with a MSP in the center of the image in case of infarcted tissue. Then, with increments of 4 degrees, the automated Chalkley grid rotated 90 times for each image to determine its maximum Chalkley score. Chalkley scores were converted to absolute microvascular densities with a calibration curve.

Extracellular Matrix and regional cardiomyocyte presence

Collagen area and cardiomyocyte presence within the infarct region were quantified using a Resorcin-Fuchsin staining. MSP containing areas (designated as having been subjected to ischemia) were divided into 6 non-overlapping sections. Every section was analyzed to determine the percentage collagen (red stained areas) and cardiomyocytes (yellow stained cardiomyocytes).

Biomarkers for necrosis and inflammation

Serial blood samples were analyzed for markers of necrosis as described before (16). Also, to assess the acute anti-inflammatory response of $VEGF_{165A}$-drug-laden-MSP-therapy, tumor necrosis factor α (TNFα) and interleukin 6 (IL6) levels

were quantified in blood samples obtained at baseline, at 2.5h of reperfusion and at 5 weeks follow-up using similar procedures and performed according to manufacturer's instructions (R&D Systems).

Cumulative regional VEGF concentration per gram infarct tissue

The cumulative VEGF concentration eluted by $10{\cdot}10^6$ low and high dose MSP was calculated by dividing the mean in-vitro VEGF release in 35 days (i.e. 0.9 μg and 2.8 μg), by the weight of each infarction as determined by hFABP release at 50 min reperfusion.

Statistical analysis

Data are presented as mean ± SEM. Data were analyzed with Sigmaplot (Version 11.0, Drunen, The Netherlands) and SPSS (IBM SPSS statistics 21). Two-way (time x treatment) repeated measures ANOVA or paired samples T-Test was used followed by post-hoc Bonferroni correction when appropriate. Statistical significance was accepted when $p<0.05$.

RESULTS

In vitro studies of size distribution, surface characteristics and release kinetics of $VEGF_{165A}$ microspheres

Determination of MSP size showed a similar diameter in all formulations in the therapy study (placebo: 15.2±0.01 μm; low dose: 15.3±0.01 μm; high dose: 15.3±0.00 μm). Scanning EM was used to visually ascertain MSP integrity for the three formulations, and showed an intact and smooth surface. The release patterns of the 15 μm VEGF containing formulations is illustrated in Figure 2. Cumulative dose for low and high dose MSP was 0.92±0.05 and 2.80±0.17 μg $VEGF_{165A}$ per $10{\cdot}10^6$ MSP. Importantly, the release pattern was not statistically different between the two active formulations. All MSP showed a decrease in diameter at the end of a period of 35 days, but this was similar in all formulations (placebo: -9.8±0.1%; low dose: -10.3±0.7%; high dose: -10.5±0.1%).

In-Vitro angiogenic effects of $VEGF_{165A}$

The HCMVEC tube-formation assay under hypoxic conditions (Figure 3), as a marker for angiogenesis, showed a clear dose response to $VEGF_{165A}$ in terms of significantly increased tube length ($p=0.007$) and number of junctions ($p=0.021$). Post–hoc analysis showed that this was dictated by the difference between 100

and 0 ng/g with a trend for 30 ng/g towards improved network formation. The low dose $VEGF_{165A}$ group reflects this value and therapy was steered towards a cumulative VEGF dose approximating 100 ng/g.

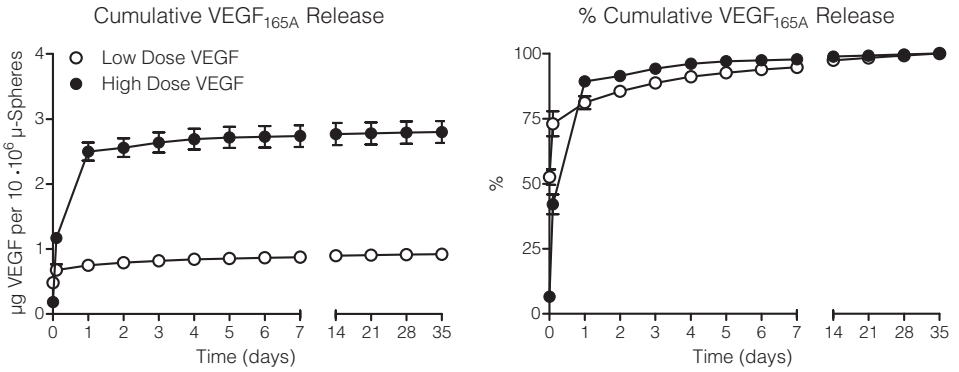

Figure 2 *Cumulative in-vitro release curves (n=3) of $10 \cdot 10^6$ MSP in low and high dose drug laden formulations, showing an early release burst of VEGF, followed by a steady increase in the cumulative release. Absolute values are given in the left panel, while release expressed as a percentage of the total cumulative dose is shown in the right panel. Data are shown as average ± SEM. White spheres represent low dose VEGF microspheres and black spheres high dose VEGF microspheres.*

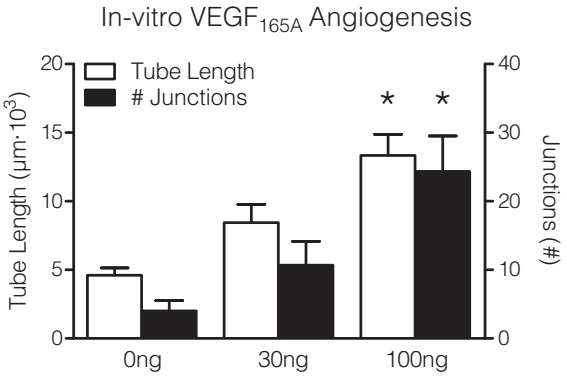

Figure 3 *In-vitro angiogenic response of human cardiac microvascular endothelial cells in a tube formation assay (n=5) under ischemic conditions to indicate the lower threshold of $VEGF_{165A}$ efficacy in the no-reflow zones. Data show a dose response with statistically significant effects at 100ng and this value was subsequently used to steer the low dose $VEGF_{165A}$ group. Data are shown as average ± SEM. White bars represent tube length and black bars number of junctions.* * = $p<0.05$ vs. corresponding 0ng measurement.*

Size finding, safety and biocompatibility

The size finding study data obtained by intracoronary infusion of MSP of different size in swine myocardium, confirmed that smaller MSP of 12 μm were not well retained (6±1% as compared to 17 μm spheres). The latter showed impaired distribution with congestion of the microvasculature although TTC staining was negative. Therefore, 15 μm diameter MSP were selected for subsequent studies of safety and biocompatibility. In the safety or dose tolerance study with 15 μm spheres, the average MSP treated area (MTA) was 21.4±3.3% of the left ventricle (17.5±3.2g cardiac tissue) in all groups. Data show that infusion of 10 and $20{\cdot}10^6$ MSP at $1{\cdot}10^6$ MSP/min, resulted in a macroscopically detectable TTC stained infarct area of resp. 2.5 and 9.7% MTA. However, MSP infusion of $5{\cdot}10^6$ ($1{\cdot}10^6$ / min) and $10{\cdot}10^6$ ($0.5{\cdot}10^6$ /min) showed no macroscopic myocardial necrosis, which was confirmed by absence of hFABP and hsTnI release (Table 1).

Table 1. *Dose Tolerance*

Nr. of Microspheres	**$5{\cdot}10^6$**	**$10{\cdot}10^6$**	**$10{\cdot}10^6$**	**$20{\cdot}10^6$**
Infusion Parameters				
Infusion Volume	10ml	20ml	40ml	40ml
Infusion Density	$5{\cdot}10^5$/ml	$5{\cdot}10^5$/ml	$2.5{\cdot}10^5$/ml	$5{\cdot}10^5$/ml
Infusion Speed	2ml/min	2ml/min	2ml/min	2ml/min
Infusion Rate	$1{\cdot}10^6$/min	$1{\cdot}10^6$/min	$0.5{\cdot}10^6$/min	$1{\cdot}10^6$/min
Myocardial Damage				
Infarct Size (% MTA)	0.00	2.54	0.00	9.67
[hsTnI] (ng/ml)	0.42	2.03	0.30	8.68
[hFABP] (ng/ml)	6.44	12.10	0.48	28.99

MTA = microsphere treated area; hsTnI = high sensitive troponin I (baseline: below detectable levels); hFABP = heart specific fatty acid binding protein (baseline: 6.1±1.1 ng/ml).

Histology confirmed adverse effects produced by the two high dose, and faster MSP infusion rates as hemorrhagic events. In contrast, the $5{\cdot}10^6$ ($1{\cdot}10^6$/min) and the $10{\cdot}10^6$ ($0.5{\cdot}10^6$/min) group did not show micro bleedings. Analysis of the biocompatibility following intracoronary infusion of MSP revealed no inflammation, neither at 5 nor at 28 days following infusion of the MSP (Figure 4) without signs of microvascular damage. These safety and biocompatibility results formed the basis for the longitudinal functional assessment of MSP therapy for myocardial infarction using $10{\cdot}10^6$ MSP at a rate of $0.5{\cdot}10^5$ MSP per minute.

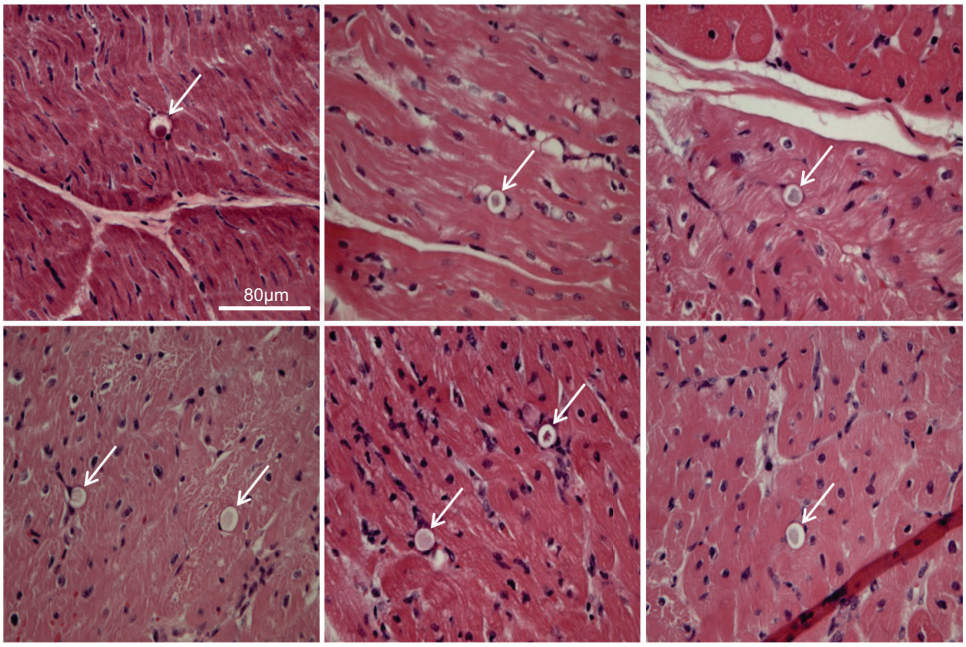

Figure 4 *Histological analysis of in vivo biocompatibility to assess safety of MSP therapy, illustrated for six different hearts, shows absence of MSP induced inflammation at 5 days (top row) and 28 days (bottom row) following infusion in healthy, non-ischemic myocardium. MSP are light pink (arrow). HE stain, bar = 80µm.*

Efficacy of VEGF eluting microsphere therapy for acute myocardial infarction

Mortality following myocardial infarction was observed in 8 swine (25%) who died prematurely. Mortality was not different between groups: Non-convertible ventricular fibrillation during the infarct-reperfusion protocol occurred in 4 swine: 2 during coronary artery occlusion and 2 during reperfusion. No animals died during infusion of MSP. Two animals died within 48h post infarction of sub-acute cardiac complications. One animal died at one week due to severe heart failure and one animal died because of technical failure. All remaining 24 swine (n=8 per group) completed the protocol and were included for final blinded analyses.

Baseline characteristics and cumulative VEGF exposure

Infarct mass at baseline by markers of necrosis. To ascertain that infarct mass at baseline was similar in all groups, circulating hFABP levels were taken at 50 min of reperfusion to calculate infarct mass (16). Infarct masses did not differ between groups (Placebo: 13±2g; Low dose: 14±2g and High dose: 16±1g; p=0.40).

Cumulative VEGF exposure. Cumulative local VEGF concentration per infarct mass (infarct mass at baseline by hFABP divided by VEGF dose) showed that per gram infarcted myocardium, the low dose group received 0.07±0.01μg $VEGF_{165A}$, the high dose group received 0.35±0.06μg $VEGF_{165A}$. Placebo MSP treated animals received no $VEGF_{165A.}$

Global and Regional cardiac function at 1 and 5 weeks post-AMI

To understand the early effects of VEGF therapy on cardiac function, one week post-AMI, global and regional myocardial function were assessed with cardiac MRI. Results (Table 2) clearly show that global and regional myocardial function are similar compared to placebo therapy.

Global and regional myocardial function were assessed again at 5wk post-AMI. Importantly, no significant differences were found between VEGF groups and placebo suggesting that VEGF did not have an effect on global and regional myocardial function either early (1wk) or late (5wk) post-AMI.

Inflammatory biomarker release

To understand the effect of VEGF therapy on inflammation, TNFα and IL6 were quantified at baseline, 2.5h of reperfusion and 5wk follow-up. Data are illustrated in Figure 5 and show that while placebo spheres showed a significant increase in TNFα release during reperfusion ($p<0.01$), levels decreased significantly to normal at 5wk follow-up ($p<0.01$). TNFα levels in both VEGF containing MSP formulations remained at baseline levels. A similar pattern for placebo was observed for IL6 and while the high dose group showed an increase at early reperfusion, this did not reach levels of statistical significance ($p=0.15$).

Table 2. *Global and Regional myocardial characteristics by MRI*

		Post-AMI	
	Treatment	**wk1**	**wk5**
LV Function and Remodeling			
Heart Rate (bpm)	Placebo	77 ± 8	80 ± 4
	Low dose	71 ± 4	71 ± 4
	High dose	64 ± 5	75 ± 7
End-Diastolic Volume (ml)	Placebo	104 ± 7	120 ± 7*
	Low dose	106 ± 3	126 ± 6*
	High dose	107 ± 8	125 ± 9*
Stroke Volume (ml)	Placebo	46 ± 2	54 ± 2*
	Low dose	42 ± 3	58 ± 3*
	High dose	48 ± 2	49 ± 3††
Ejection Fraction (%)	Placebo	46 ± 3	46 ± 2
	Low dose	40 ± 2	46 ± 2*
	High dose	46 ± 2	40 ± 4*
LV-mass (g)	Placebo	49 ± 2	54 ± 2*
	Low dose	49 ± 2	54 ± 2*
	High dose	48 ± 3	52 ± 3*
Infarct Characteristics			
Infarct Mass (g)	Placebo	8.0 ± 2.0	6.4 ± 1.6*
	Low dose	9.3 ± 0.9	6.9 ± 0.6*
	High dose	9.6 ± 1.6	7.6 ± 1.2*
Infarct Size (% LV)	Placebo	15.5 ± 3.3	11.2 ± 2.3*
	Low dose	19.4 ± 2.2	13.3 ± 1.6*
	High dose	19.4 ± 2.4	14.4 ± 1.8*
End-Diastolic Wall Thickness (mm)	Placebo	4.2 ± 0.2	4.1 ± 0.2
	Low dose	3.9 ± 0.1	3.6 ± 0.3
	High dose	4.2 ± 0.1	3.6 ± 0.3*
No-Reflow (% IM)	Placebo	9.5 ± 4.9	-
	Low dose	10.1 ± 4.6	-
	High dose	7.7 ± 2.7	-

Data are Mean ± SEM; n=8 per group; AMI = Acute Myocardial Infarction; LV = Left Ventricular; IM = Infarct Mass; - = not detectable; *P<0.05 vs. corresponding wk1; †P<0.05 vs. corresponding low dose; ††P<0.10 vs. corresponding low dose. At 5 wk post AMI, no-reflow can no longer be detected.

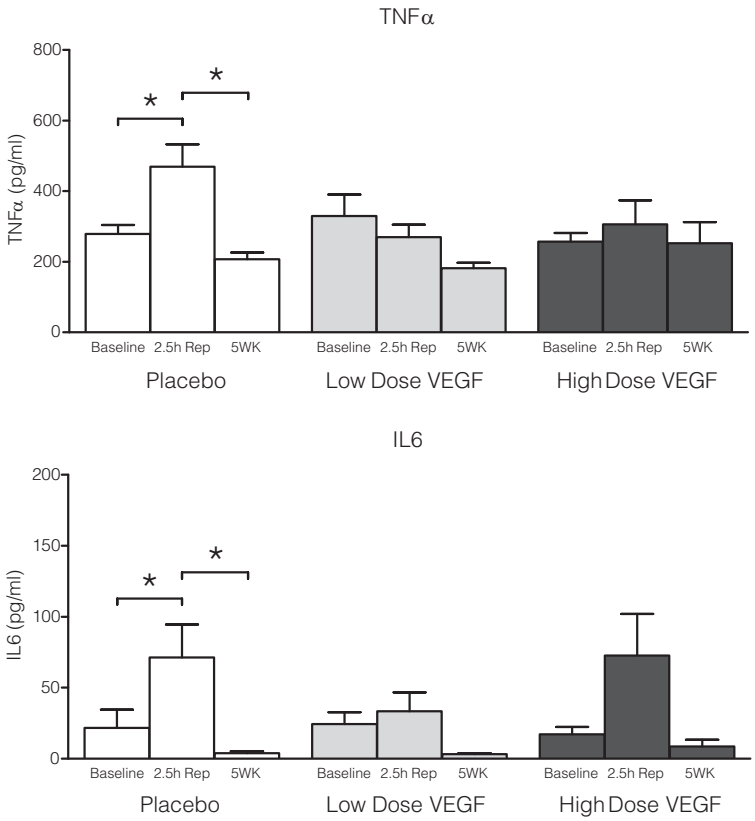

Figure 5 *Longitudinal assessment for release of inflammatory markers TNFα and IL6 in plasma as measured by ELISA shows that the VEGF release by the microspheres attenuates cytokine release at 2.5 hours reperfusion, having returned to baseline at 5 weeks follow-up. Data are presented as average ± SEM, n=8 per group. *p<0.01. BL=Baseline; Rep=Reperfusion; 5wk=5 weeks follow-up. IL6 levels at 2.5h reperfusion were not statistically different from baseline and 5 weeks follow-up (p=0.15).*

Histological analysis

Microvascular density measurements. To study the effect of VEGF on microvascular density in the infarct zone, Chalkley counts of the infarct area were normalized to the non-infarcted remote areas. In contrast to placebo treatment (13±7% decrease in Chalkley score vs. remote, Figure 6), high dose treatment resulted in a significantly higher Chalkley score (10±6%, $p<0.04$ vs. placebo). This corresponds to a difference of approximately 739±278 vessels per mm^2 ($p<0.05$). The low dose group remained similar to the remote area, indicating a dose response effect. In figure 6 typical examples of microvascular density in the infarcted area are shown. Capillary density in the border zones in the placebo, low dose VEGF and high dose VEGF group (2045±125, 2168±115, 2223±134 vessels per mm resp.) were similar

to the remote area and showed no signs of VEGF effects. Chalkley scores in MSP-containing viable rim of the infarcted tissue, reliably measureable in a few animals (n=4 to 5/group), similarly did not show differences with remote in paired analyses.

Collagen and regional cardiomyocyte presence. To study whether differences in microvascular density affected infarct healing, we quantified the presence of collagen and cardiomyocytes in the area at risk, defined as the area containing MSP (Figure 7). $VEGF_{165A}$ therapy at 5wk post-AMI did not result in differences in total collagen content (placebo: 24 ±5%; low dose: 25±3%; high dose: 33±3% surface area, p=0.25) or changes in cardiomyocyte presence compared to placebo (placebo: 41±7%; low dose 37±5; high dose 27±5, p=0.21).

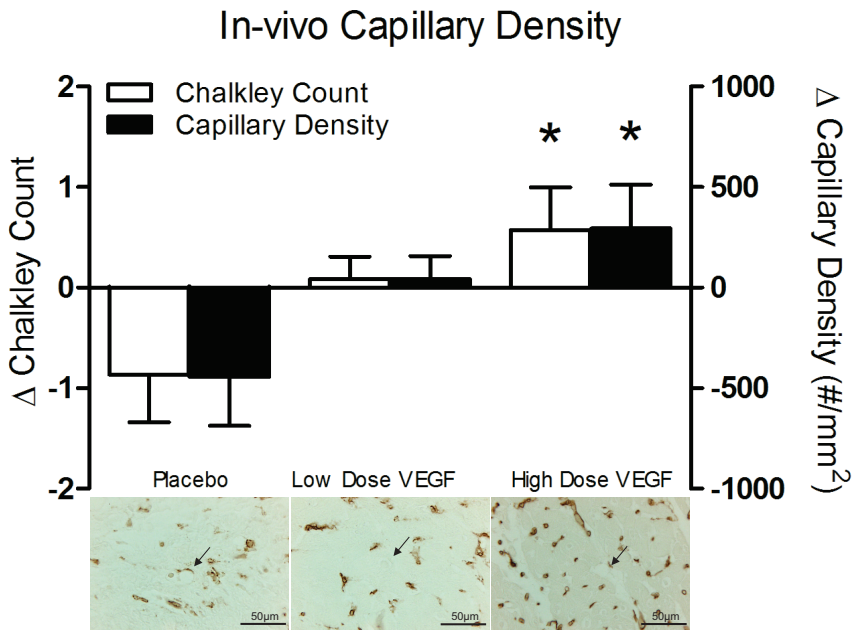

Figure 6 *Top panel showing the in-vivo relative microvascular density measurements in the area at risk as a result of $VEGF_{165A}$ therapy at 5 weeks follow-up. Data, given as the difference between infarct and remote area, are shown as average ± SEM. White bars represent differences in the Chalkley counts and black bars differences in the absolute number of capillaries * = p<0.05 vs. Placebo.*
The bottom panel illustrates the microvascular staining of the area at risk in Placebo (left), low dose VEGF (mid) and high dose VEGF (right) MSP by HRP labeled lectin Dolichos Biflorus. MSP were used to center the Chalkley grid prior to automated measurements of the microvasculature. HRP was visualized with DAB- H_2O_2. Bar = 50µm.

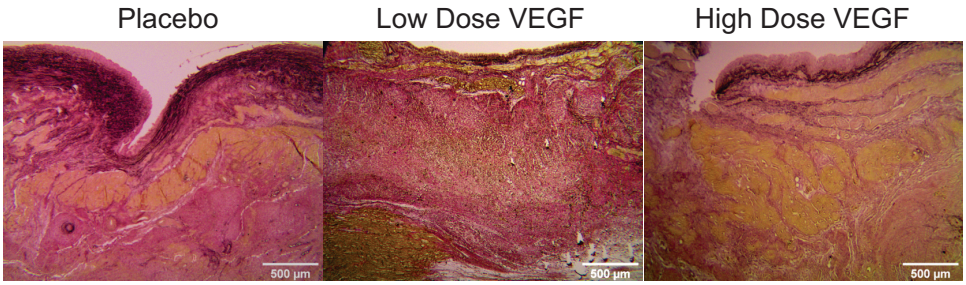

Figure 7 *Endocardial border of the infarct area in the three groups showing extensive fibrosis with endocardial survival of cardiomyocytes, with collagen stained red, and cellular elements such as muscle stained yellow. Resorcin Fuchsin stain. Bar = 500µm.*

DISCUSSION

The current study was performed to test the safety, biocompatibility and efficacy of controlled $VEGF_{165A}$ release from degradable MSP as an off-the-shelf therapy for regional angiogenic therapy following acute myocardial infarction (AMI) in a setting of percutaneous coronary interventions (PCI). Intracoronary delivery was initiated directly upon reperfusion of the infarct tissue to allow delivery of drug-loaded MSP before onset of reperfusion injury and no-reflow. This approach allows optimal MSP distribution within the area at risk before development of perfusion defects as a result of no-reflow.

Major findings

We observed that 15 μm MSP were effectively retained and distributed within the myocardium without inducing an acute or chronic local inflammatory response or (micro) infarction. MSP presence did not negatively affect cardiac function as compared to historic data with similar infarct size (heart rate 84±19 vs 80±4, stroke volume 60±11 vs 54±2) (18). VEGF-loaded MSP delivery in infarcted myocardium significantly reduced the acute release of the pro-inflammatory cytokines TNFα and IL6 during reperfusion. At follow-up, histology revealed dose dependent changes in microvascular density within the MSP treated infarct area as compared to the intrinsic non-ischemic control area. Per gram infarcted myocardium, a dose of 0.07±0.01μg $VEGF_{165A}$ maintained- while 0.35±0.06μg $VEGF_{165A}$ increased-microvascular density. However, these changes did not translate to changes in scar composition (collagen and cardiomyocyte presence), or global and regional myocardial function by cardiac MRI at 1 or 5 weeks after AMI.

Microsphere Composition and Size

We found that 15 μm diameter MSP were effectively retained by the porcine myocardium, while 12μm MSP were not, and 17μm MSP impaired optimal distribution. MSP retention may not only be dictated by size but also by material properties since Poly(lactide-co-glycolide) MSP of 7 μm diameter were described to be retained well (23). Thus, every (bio)material for local drug delivery needs to be tailored individually to the intended microvascular bed for optimal MSP sizing. Especially in case of angiogenic MSP it is prudent to regulate MSP retention to prevent angiogenesis in unwanted areas.

Timing of MSP Delivery

The timing of infusion, immediately upon reperfusion of the ischemic myocardium, allows distribution before the major onset of reperfusion injury and no-reflow (24). This opens up new therapeutic options for treatment of no-reflow as systemic drug delivery will be limited by the development of microvascular perfusion defects within half an hour after onset of reperfusion. The timing of MSP therapy upon reperfusion is of great clinical potential as MSPs can be infused directly following PCI, thus limiting additional procedural risks to the patient.

Inhibition of Acute Inflammation

Reperfusion following myocardial infarction is typically associated with the release of pro-inflammatory cytokines such as TNFα and IL6 (25). The main source of TNFα is suggested to be the monocyte/macrophage while others indicate that mast cells are the initial source of TNFα that subsequently gives rise to influx of monocyte/macrophages with the latter as the main source for IL6 (23,25). However, cardiomyocytes and endothelium can also release TNFα when stimulated (26).
Given the chronic nature of our study, we were unable to assess the acute effect of VEGF MSP infusion on cardiac macrophage accumulation and mast cell degranulation in tissue. Consequently, we were unable to identify the source of these cytokines. Whether reduction of TNFα and IL6 is detrimental or protective for the reperfused myocardium is difficult to say. TNFα reduction can attenuate infarct size but TNFα can also increase the expression of cytoprotective proteins (26). In our study it did not translate to differences in myocardial function.

VEGF therapy and global function

$VEGF_{165A}$ therapy in our study resulted in a dose-dependent increase in microvascular density but this did not translate into global or regional improvements of cardiac function as measured by cardiac MRI. However, we induced relatively small infarcts, and 5 weeks follow-up may be considered short. Previous results from our laboratory indicate that indeed, these conditions may not result in measurable global functional improvements at short term, despite regional improvements (18). Our study is the first to report MSP based VEGF release for AMI in a setting of reperfused MI in a large animal model. Interestingly, approximately 57% of small animal VEGF studies that include functional measurements report improvements in global cardiac function and 50% of large animal studies show global functional improvements (Table 3), but these are mostly studied in a setting of chronic ischemia. No clear therapeutic optima, including timing of administration and total cumulative dosage, can be distilled from this previous work. Thus, differences in experimental conditions, including animal model, infarct size and therapeutic protocol, may underlie differences in therapeutic outcome.

VEGF elicits a dose-dependent increase in cardiac microvascular density

It is remarkable that so few studies report the total cumulative dose of administered VEGF or the dose normalized to bodyweight or infarct mass. Consequently an effective VEGF dosage remains to be established and may be species dependent. For example, two rat studies that applied a bolus-like administration of VEGF both report positive effects on global function while administering a striking 458-fold difference in cumulative growth factor dosage (11μg vs. 24ng) (27,28). These results suggest that at least a broad range of therapeutic efficacy of VEGF for chronic MI exists. Our study, using a model of reperfused MI, shows that while placebo treatment resulted in loss of microvascular density in the infarct zone, a cumulative dose of 0.9μg VEGF (0.07±0.01μg per gram myocardium) preserved microvascular density whereas 2.8μg (0.35±0.06 μg per gram myocardium) resulted in an increased microvascular density as compared to remote tissue. This demonstrates that VEGF indeed elicits dose-dependent angiogenesis in the infarcted tissue.

Table 3. *Animal studies on the cardiotherapeutic effects of regional VEGF Therapy for myocardial infarction*

Author	Species	I/R time	Route of Administration	Start Therapy	Duration Therapy	Cumulative VEGF dose		Effect on Vascular Density	Effect on Global Function
Dicks et al.[33]	Dog	Permanent occlusion	IM	3 days post MI	47 days	0	Control	-	-
Saeed et al.[34]	Dog	Permanent occlusion	IM	3 days post MI	50 days	0	Control	-	↔
Ferrarini et al.[35]	Dog	Permanent occlusion	IM	240 min after onset ischemia	28 days	0	Control	-	-
Vera Janavel et al.[36]	Sheep	Permanent occlusion	IM	60 min after onset ischemia	15 days	0	Control	-	-
Bougioukas et al.[37]	Rabbit	Permanent occlusion	IM	5 min after onset ischemia	Bolus	0	Control	-	-
Wu et al.[38]	Rat	Permanent occlusion	IM	7 days post MI	35 days	0	Control	-	-
Rufaihah et al.[39]	Rat	Permanent occlusion	IM	Early after onset ischemia	30 days	-	Control	-	↓*
Hao et al.[40]	Rat	Permanent occlusion	IM	7 days post MI	28 days	0	Control	-	↓†
Gao et al.[41]	Rat	Permanent occlusion	IM	Immediately after onset ischemia	28 days	0	Control	-	-
Zhang et al.[27]	Rat	Permanent occlusion	IM	Immediately after onset ischemia	Several hours	0	Control	-	-
Oh et al.[42]	Rat	Permanent occlusion	IM	14 days post MI	28 days	0	Control	-	-
Su et al.[43]	Mouse	Permanent occlusion	IM	Immediately after onset ischemia	56 days	0	Control	-	-
Formiga et al.[44]	Rat	60 min/32 days	IM	4 days post MI	28 days	0	Control	-	-
Simón-Yarza et al.[45]	Rat	Permanent Occlusion	IM	1 week post MI	90 days	0.51μg	VEGF	↑*	↑*

Table 3. *Continued*

Author	Species	I/R time	Route of Administration	Start Therapy	Duration Therapy	Cumulative VEGF dose		Effect on Vascular Density	Effect on Global Function
Scott et al.[28]	Rat	Permanent occlusion	IV	Immediately after onset ischemia	Bolus	-	Control	-	-
Zhigang et al.[46]	Rat	Permanent occlusion	IV	3 days post MI	14 days	-	Control	-	-
Sato et al.[29]	Pig	Ameroid constrictor	IV	3 weeks after onset constriction	40-200 min.	10μg/kg	VEGF	↔	↔
			IC		40 min.	2μg/kg	VEGF	↔	↔
			IC		40 min.	10μg/kg	VEGF	↑**	↔
			IC/IV		40 min.	0	Control		↔
Uitterdijk et al.	Swine	120 min/5 weeks	IC	Onset reperfusion	35 days	0 μg	Control	↓	↔
					"	0.9 μg	VEGF	↔	↔
					"	2.8 μg	VEGF	↑*	↔

I/R = Infarct/Reperfusion time; IM =Intramyocardial (endo or epicardially); IV = Intravenous; IC = Intracoronary; - = not reported; *P<0.05 vs. Control; †P<0.05 vs. baseline functional measurements. ** effects assessed as increased regional coronary flow, not as vascular density

When we place this outcome in perspective, it is striking that the effect of VEGF therapy in all previous studies consistently resulted in a significantly higher microvascular density of the infarct zone as compared to the microvascular density of control infarcts. This effect appears independent of dosage, therapeutic protocol or timing of administration. It must be noted however, that we were the only group to compare microvascular density within the infarct region to the intrinsic control (remote area). It may well be that while VEGF increased microvascular density in infarcted tissue as compared to control infarctions, it could still be lower than in the remote zone, which could affect long term outcome.

Route of administration and AMI-model

From a translational point of view, it is evident that an intravenous or intracoronary route of administration is less invasive as opposed to injecting growth factors directly into the myocardium. Considering the potential tumorigenic potency and blood pressure lowering effects of VEGF (29), any bolus, either intravenous, intracoronary or intramyocardially, is less appropriate as it inevitably recirculates. VEGF, distributed via the microcirculation, binds avidly to endothelium and fibrin, where bound to the latter it still supports endothelial proliferation (30,31). Slow and sustained VEGF delivery via degradable biomaterials following intracoronary delivery therefore seems a viable therapy as the growth factor can be more easily bound to the tissue, and subsequent circulating levels should remain low. So far, none of the studies in Table 3 used the clinically relevant intracoronary route of biomaterial mediated VEGF administration and no conclusions can be drawn whether the outcome would have differed. We speculate however, that optimal growth factor delivery and retention will be carrier dependent and needs to be tailored as is true for cell therapy (32). Clearly a permanent occlusion, as used in the vast majority of the studies summarized in Table 3, is not representative for the clinical situation where interventions to restore perfusion of the ischemic territory is the golden standard in many countries. As a consequence, results obtained from these non-reperfused infarct studies will less likely predict the true effects of VEGF therapy following PCI for AMI.

Clinical relevance

In our model of reperfused MI, intracoronary delivery of VEGF by degradable MSP clearly resulted in an increased microvascular density, but not in improved cardiac function. Whether the changes in microvascular density would translate to a better long-term outcome beyond our 5 week period, is unknown. Thus, the long term benefit of increased microvascular density remains to be determined. The current

study does serve as a proof of principle that chronic delivery of active protein using biocompatible polymers in the broader context is feasible. It is a versatile methodology which is not limited to regional and global cardiac scar remodeling therapy or to one specific protein, but rather might serve as a general platform for local drug delivery via the microvascular bed.

Limitations

The current formulation of microspheres showed an early (burst) release of VEGF in the in vitro study, which may have protected or stabilized the vascular bed from the acute ischemic insult resulting in attenuated release of inflammatory cytokines, but also results in lower sustained VEGF levels. We cannot exclude that this may have affected efficacy of angiogenesis. In addition, multiple growth factors might also have improved efficacy of angiogenic therapy. It is also generally accepted that co-morbidities such as hypertension, diabetes and atherosclerosis, often present in patients suffering acute myocardial infarction, can affect angiogenesis. Therefore, studies in large animal models in which these risk factors are present would be useful, prior to testing angiogenic strategies in clinical trials.

CONCLUSIONS

Regional, controlled VEGF delivery leads to a dose dependent increase in microvascular density in infarcted tissue. This increase did not translate to changes in global or regional cardiac function or scar composition. Controlled regional VEGF delivery however is safe and feasible and supports the development of novel adjunctive off-the-shelf therapeutic applications.

ACKNOWLEDGEMENTS

The authors cordially acknowledge the indispensable contributions of Ayla Hoogendoorn, Frank-Jan Drost, Felix Kienjet and Bas Wijenberg. Klazina Kooiman and Tom van Rooij are thanked for their contributions in particle sizing.

REFERENCES

1. Delewi R, Hirsch A, Tijssen JG et al. Impact of intracoronary bone marrow cell therapy on left ventricular function in the setting of ST-segment elevation myocardial infarction: a collaborative meta-analysis. Eur Heart J 2014;35:989-98.
2. de Jong R, Houtgraaf JH, Samiei S, Boersma E, Duckers HJ. Intracoronary stem cell infusion after acute myocardial infarction: a meta-analysis and update on clinical trials. Circ Cardiovasc Interv 2014;7:156-67.
3. Szady AD, Pepine CJ, Sharma SV et al. A Critical Analysis of Clinical Outcomes Reported in Stem Cell Trials for Acute Myocardial Infarction: Some Thoughts for Design of Future Trials. Curr Atheroscler Rep 2013;15:341-55.
4. Pavo N, Charwat S, Nyolczas N et al. Cell therapy for human ischemic heart diseases: Critical review and summary of the clinical experiences. J Mol Cell Cardiol 2014;75C:12-24.
5. Fadini GP, Albiero M, Vigili de Kreutzenberg S et al. Diabetes impairs stem cell and proangiogenic cell mobilization in humans. Diabetes Care 2013;36:943-9.
6. Dimmeler S, Leri A. Aging and disease as modifiers of efficacy of cell therapy. Circ Res 2008;102:1319-30.
7. Bezemer JM, Grijpma DW, Dijkstra PJ, van Blitterswijk CA, Feijen J. A controlled release system for proteins based on poly(ether ester) block-copolymers: polymer network characterization. J Control Release 1999;62:393-405.
8. Bezemer JM, Grijpma DW, Dijkstra PJ, van Blitterswijk CA, Feijen J. Control of protein delivery from amphiphilic poly(ether ester) multiblock copolymers by varying their water content using emulsification techniques. J Control Release 2000;66:307-20.
9. Bezemer JM, Radersma R, Grijpma DW, Dijkstra PJ, Feijen J, van Blitterswijk CA. Zero-order release of lysozyme from poly(ethylene glycol)/poly(butylene terephthalate) matrices. J Control Release 2000;64:179-92.
10. Bezemer JM, Radersma R, Grijpma DW, Dijkstra PJ, van Blitterswijk CA, Feijen J. Microspheres for protein delivery prepared from amphiphilic multiblock copolymers. 2. Modulation of release rate. J Control Release 2000;67:249-60.
11. Bezemer JM, Radersma R, Grijpma DW, Dijkstra PJ, van Blitterswijk CA, Feijen J. Microspheres for protein delivery prepared from amphiphilic multiblock copolymers. 1. Influence of preparation techniques on particle characteristics and protein delivery. J Control Release 2000;67:233-48.
12. van Dijkhuizen-Radersma R, Hesseling SC, Kaim PE, de Groot K, Bezemer JM. Biocompatibility and degradation of poly(ether-ester) microspheres: in vitro and in vivo evaluation. Biomaterials 2002;23:4719-29.
13. Henry TD, Rocha-Singh K, Isner JM et al. Intracoronary administration of recombinant human vascular endothelial growth factor to patients with coronary artery disease. Am Heart J 2001;142:872-80.
14. Bondos SE, Bicknell A. Detection and prevention of protein aggregation before, during, and after purification. Anal Biochem 2003;316:223-31.
15. Krueger MA, Huke SS, Glenny RW. Visualizing regional myocardial blood flow in the mouse. Circ Res 2013;112:e88-97.
16. Uitterdijk A, Sneep S, van Duin RW et al. Serial measurement of hFABP and high-sensitivity troponin I post-PCI in STEMI: how fast and accurate can myocardial infarct size and no-reflow be predicted? Am J Physiol Heart Circ Physiol 2013;305:H1104-10.
17. Cason BA, Gamperl AK, Slocum RE, Hickey RF. Anesthetic-induced preconditioning: previous administration of isoflurane decreases myocardial infarct size in rabbits. Anesthesiology 1997;87:1182-90.

18. Moelker AD, Baks T, van den Bos EJ et al. Reduction in infarct size, but no functional improvement after bone marrow cell administration in a porcine model of reperfused myocardial infarction. Eur Heart J 2006;27:3057-64.
19. Kirschbaum SW, Baks T, Gronenschild EH et al. Addition of the long-axis information to short-axis contours reduces interstudy variability of left-ventricular analysis in cardiac magnetic resonance studies. Invest Radiol 2008;43:1-6.
20. Springeling T, Kirschbaum SW, Rossi A et al. Late cardiac remodeling after primary percutaneous coronary intervention-five-year cardiac magnetic resonance imaging follow-up. Circ J 2013;77:81-8.
21. Haitsma DB, Bac D, Raja N, Boomsma F, Verdouw PD, Duncker DJ. Minimal impairment of myocardial blood flow responses to exercise in the remodeled left ventricle early after myocardial infarction, despite significant hemodynamic and neurohumoral alterations. Cardiovasc Res 2001;52:417-28.
22. Fox SB, Leek RD, Weekes MP, Whitehouse RM, Gatter KC, Harris AL. Quantitation and prognostic value of breast cancer angiogenesis: comparison of microvessel density, Chalkley count, and computer image analysis. J Pathol 1995;177:275-83.
23. Arras M, Mollnau H, Strasser R et al. The delivery of angiogenic factors to the heart by microsphere therapy. Nat Biotechnol 1998;16:159-62.
24. Reffelmann T, Kloner RA. Microvascular reperfusion injury: rapid expansion of anatomic no reflow during reperfusion in the rabbit. Am J Physiol Heart Circ Physiol 2002;283:H1099-107.
25. Frangogiannis NG, Smith CW, Entman ML. The inflammatory response in myocardial infarction. Cardiovasc Res 2002;53:31-47.
26. Kleinbongard P, Schulz R, Heusch G. TNFalpha in myocardial ischemia/reperfusion, remodeling and heart failure. Heart Fail Rev 2011;16:49-69.
27. Zhang J, Ding L, Zhao Y et al. Collagen-targeting vascular endothelial growth factor improves cardiac performance after myocardial infarction. Circulation 2009;119:1776-84.
28. Scott RC, Rosano JM, Ivanov Z et al. Targeting VEGF-encapsulated immunoliposomes to MI heart improves vascularity and cardiac function. FASEB J 2009;23:3361-7.
29. Sato K, Wu T, Laham RJ et al. Efficacy of intracoronary or intravenous VEGF165 in a pig model of chronic myocardial ischemia. J Am Coll Cardiol 2001;37:616-23.
30. Jakeman LB, Winer J, Bennett GL, Altar CA, Ferrara N. Binding sites for vascular endothelial growth factor are localized on endothelial cells in adult rat tissues. J Clin Invest 1992;89:244-53.
31. Sahni A, Francis CW. Vascular endothelial growth factor binds to fibrinogen and fibrin and stimulates endothelial cell proliferation. Blood 2000;96:3772-8.
32. Campbell NG, Suzuki K. Cell delivery routes for stem cell therapy to the heart: current and future approaches. J Cardiovasc Transl Res 2012;5:713-26.
33. Dicks D, Saloner D, Martin A, Carlsson M, Saeed M. Percutaneous transendocardial VEGF gene therapy: MRI guided delivery and characterization of 3D myocardial strain. Int J Cardiol 2010;143:255-63.
34. Saeed M, Martin A, Jacquier A et al. Permanent coronary artery occlusion: cardiovascular MR imaging is platform for percutaneous transendocardial delivery and assessment of gene therapy in canine model. Radiology 2008;249:560-71.
35. Ferrarini M, Arsic N, Recchia FA et al. Adeno-associated virus-mediated transduction of VEGF165 improves cardiac tissue viability and functional recovery after permanent coronary occlusion in conscious dogs. Circ Res 2006;98:954-61.
36. Vera Janavel G, Crottogini A, Cabeza Meckert P et al. Plasmid-mediated VEGF gene transfer induces cardiomyogenesis and reduces myocardial infarct size in sheep. Gene Ther 2006;13:1133-42.

37. Bougioukas I, Didilis V, Ypsilantis P et al. Intramyocardial injection of low-dose basic fibroblast growth factor or vascular endothelial growth factor induces angiogenesis in the infarcted rabbit myocardium. Cardiovasc Pathol 2007;16:63-8.

38. Wu J, Zeng F, Huang XP et al. Infarct stabilization and cardiac repair with a VEGF-conjugated, injectable hydrogel. Biomaterials 2011;32:579-86.

39. Rufaihah AJ, Vaibavi SR, Plotkin M et al. Enhanced infarct stabilization and neovascularization mediated by VEGF-loaded PEGylated fibrinogen hydrogel in a rodent myocardial infarction model. Biomaterials 2013;34:8195-202.

40. Hao X, Mansson-Broberg A, Grinnemo KH et al. Myocardial angiogenesis after plasmid or adenoviral VEGF-A(165) gene transfer in rat myocardial infarction model. Cardiovasc Res 2007;73:481-7.

41. Gao F, He T, Wang H et al. A promising strategy for the treatment of ischemic heart disease: Mesenchymal stem cell-mediated vascular endothelial growth factor gene transfer in rats. Can J Cardiol 2007;23:891-8.

42. Oh KS, Song JY, Yoon SJ, Park Y, Kim D, Yuk SH. Temperature-induced gel formation of core/shell nanoparticles for the regeneration of ischemic heart. J Control Release 2010;146:207-11.

43. Su H, Lu R, Kan YW. Adeno-associated viral vector-mediated vascular endothelial growth factor gene transfer induces neovascular formation in ischemic heart. Proc Natl Acad Sci U S A 2000;97:13801-6.

44. Formiga FR, Pelacho B, Garbayo E et al. Sustained release of VEGF through PLGA microparticles improves vasculogenesis and tissue remodeling in an acute myocardial ischemia-reperfusion model. J Control Release 2010;147:30-7.

45. Simon-Yarza T, Tamayo E, Benavides C et al. Functional benefits of PLGA particulates carrying VEGF and CoQ10 in an animal of myocardial ischemia. Int J Pharm 2013;454:784-90.

46. Zhigang W, Zhiyu L, Haitao R et al. Ultrasound-mediated microbubble destruction enhances VEGF gene delivery to the infarcted myocardium in rats. Clin Imaging 2004;28:395-8.

CHAPTER 12

Summary and General Discussion

In the year 1997, it was estimated that cardiovascular disease would become the main cause of death in Europe in 2020 (1). Reality however, appears to swiftly overhaul this prediction as cardiovascular disease is currently the worldwide leading cause of death (WHO, Jan 2015). This increase is accompanied by high mortality rates (2) and increased incidence of heart failure with poor prognosis and substantial economic burden (3). Acute myocardial infarction (AMI) is accountable for a substantial part of these developments despite important advances in the field with percutaneous coronary intervention (PCI) were made (4). Contemporary PCI however, is intertwined with additional reperfusion injury, a state in which additional myocardial damage is inflicted beyond that of the preceding ischemic period (5-7). Despite revascularization, reperfusion injury is often accompanied by regional perfusion deficits of the affected area which is titled no-reflow (8,9) and is associated with poor prognosis (10,11). Therefore, a growing number of efforts have been made to limit additional reperfusion injury and no-reflow (12-15). These first efforts may be considered immature and preliminary in nature and altogether necessitate improvement of techniques and treatment modalities for the diagnosis and adjunctive treatment of AMI. Targets for diagnosis include adequate determination of both infarct size and no-reflow, while therapy should be aimed at limiting these processes to ultimately attenuate post-AMI LV remodeling. The aim of the current work therefore was to contribute to novel diagnostic and therapeutic approaches to AMI at the level of preclinical research. In this chapter the major results of the individual studies are summarized and their implications are discussed.

PART I: EXPERIMENTAL APPROACHES TO MYOCARDIAL ISCHEMIA AND MYOCARDIAL INFARCTION

Following a general introduction (**Chapter 1**) into the field of myocardial ischemia, AMI and secondary epiphenomena, **Chapter 2** presented a large animal model for myocardial ischemia and stable angina pectoris for the validation of dual source computed tomography (DSCT) as a novel tool to precisely assess and quantify myocardial hypoperfusion distally to various levels of flow limiting coronary stenoses. Adenosine stress dynamic DSCT perfusion imaging allowed non-invasive quantification of regional myocardial blood flow for a broad range of coronary artery stenoses. Thus, flow obtained with DSCT under controlled experimental conditions, correlated well with coronary blood flow and fractional flow reserve, suggesting that a single adenosine stress DSCT may not only provide clinically relevant information with regard to location and composition of a coronary artery stenosis, but can also quantify the severity of a stenosis in terms of distal hypoperfusion.

DSCT therefore allows diagnosis of suspected coronary artery disease such as myocardial ischemia and stable angina pectoris. In clinical practice, fractional flow reserve measurements during invasive coronary artery angiography are the golden standard for the assessment of the functional flow limitations of coronary stenoses (16,17). While they guide subsequent peri-procedural decision-making, this approach is increasingly being demonstrated to have limitations (18-20). Also, it has recently become apparent that scenarios exist in which a patient presents with stable chest pain but where invasive coronary angiography with fractional flow reserve measurements does not show obstructive coronary stenosis (21). Such cases may be the result of a dysfunctional microvasculature and not coronary artery narrowing and may result in false negative diagnoses with postponed decision-making and treatment as a consequence. Especially in such cases, non-invasive CT coronary angiography combined with the presented adenosine stress perfusion protocol may prevent or reduce false negative diagnoses in a single non-invasive measurement as it can precisely verify myocardial perfusion deficits. This approach will ultimately result in future improvements in patients. First in-patient results confirm the additional clinical value of DSCT stress myocardial perfusion imaging (22). Future research should focus on further improving sensitivity and accuracy of the method, together with a further reduction in radiation burden (23).

In **Chapter 3** the rediscovered biomarker, heart specific fatty acid binding protein (hFABP) was validated to quantify infarct size as well as the degree of no-reflow in a preclinical porcine model of reperfused AMI. hFABP results were compared to the clinical standard of high-sensitive troponin I (hsTnI). The most important result is that post-reperfusion hFABP in circulating plasma showed a very strong correlation with both infarct size as well as the area of no-reflow. The best correlation was found in plasmas taken 50-60 min post-reperfusion although analyses in plasmas taken as soon as 10 min post-reperfusion already yield excellent results. Importantly, hFABP outperformed hsTnI consistently or produced at least results with comparable precision. In addition, hFABP results were obtained significantly earlier, yielding an early baseline measure of a broad range of infarct sizes. Indeed, hFABP was capable of precisely quantifying infarct masses of only a few grams. This marker will be especially useful in a controlled laboratory setting where onset of reperfusion and subsequent timing are closely directed, and may provide an early, non-invasive and cheap alternative to conventional imaging modalities such as cardiac magnetic resonance imaging. For this reason, we applied this approach in chapters 5, 10 and 11. hFABP may also be of use as a risk stratification tool to rule-in (24,25) or rule-out (26,27) patients with suspected AMI.

There is a need for novel experimental approaches to augment or maintain regional vascular integrity in order to support the infarct-impaired heart through attenuating regional wound healing. However, angiogenic agents identified and validated under optimal experimental conditions have so far yielded disappointing results in the clinical setting (28,29). This could be the result of the confounding effects of comorbidities that are known to severely affect cell function and its subsequent response to an angiogenic stimulus (30) or dosing of the drug (29,31). Also, cell types used in the in-vitro evaluation of growth factors for angiogenic purposes are often not the true target cell type which is really subject to the growth factor in in-vivo evaluation. The majority of angiogenic agents are validated in-vitro in so-called tube formation assays. These cell-based, in-vitro assays reflect the angiogenic potency of a certain substance and can be tailored to the different required experimental needs. A possible improvement in the in-vitro studying of growth factors for angiogenic purposes in ischemic heart disease with emphasis on conditions of hypoxia and hypoperfusion (in-vitro no-reflow) is presented in **Chapter 4**, a study that assessed the angiogenic effects of the well-studied growth factor $VEGF_{165A}$ subjected to conventional in-vitro tube formation conditions as well as experimental circumstances that mimic the hostile reperfusion scenario of hypoperfusion and hypoxia. The experiments were conducted using the gold–standard, human umbilical vein endothelial cells (HUVEC), as well as the true target cell type for regional, post-infarct cardiac angiogenesis, the human cardiac microvascular endothelial cell (HCMVEC). Both cell types were assessed for their angiogenic potential under normoxic and hypoxic conditions, with and without fetal bovine serum added to mimic the hostile and diverse nutrient and oxygen depleted environment of post-infarct conditions of hypoperfusion. The major findings indicate that experimental conditions of tube formation assays, including cell type and culture conditions such as hypoxia, significantly influenced outcome. These results highlight the need for extensive in-vitro validation of therapeutic agents (growth factors) in relevant conditions and may in part explain why clinical studies that used growth factor therapy for myocardial infarction failed to attenuate infarct and left ventricular (LV) remodeling (28,29).

Part I of this thesis is concluded with a study in pigs dedicated to optimization of stem cell therapy for myocardial infarction, a field in regenerative cardiology with varying, yet encouraging results (32,33). An important bottleneck in the efficacy of stem cell therapy for myocardial infarction may be the very limited retention of administered cells within the affected area (34,35). Because cell retention after therapy appears to be an active process and not a mere process of physical entrapment (36) it is hypothesized that when the endogenous endothelial ligand is overexpressed or when cells are delivered at this time point of higher presence that retention

will be enhanced with ultimately beneficial results on post-infarct LV function. For this purpose the study described in **Chapter 5** was designed and performed.

This study investigated the temporal expression of the post-infarction vascular cellular adhesion molecule 1 (VCAM-1) within the infarct zone and its correlation with bone marrow-derived stem cell retention, again in a porcine model of reperfused AMI. In the first phase of this study, VCAM-1 presence was quantified at 1, 3, 7, 14 and 35 days post-AMI. Interesting results of phase 1 of this study showed that VCAM-1 was transiently expressed and significantly higher at 3 and 7 days post-AMI with a peak at 3 days post infarction and normalization after 14 days. Consequently, in phase 2 of this study we administered autologous bone marrow-derived stem cells intracoronary at 3 or 7 days post-AMI and histologically quantified retention of cells within the complete infarct. The results however, showed retention rates to be low and similar at 3 or 7 days post-AMI, likewise when results were corrected for infarct mass using the approach developed in chapter 3. Although VCAM-1 expression again was confirmed to be increased, comparably to phase 1, it did not increase cell retention. When results are compared to work of others (34,37), our retention rates are relatively low and suggest that increased presence of VCAM-1 does not significantly increase cell retention. In addition, flowcytometric analyses of the infused fractions showed no difference in composition between the fractions. These results do not specifically guide future efforts for the improvement of post-infarct regional autologous bone marrow-derived cell retention but may suggest that VCAM-1 should not be a primary target in increasing regional retention. Future preclinical efforts should focus on other adhesion molecules involved, in combination with elucidating which cells are primarily retained.

PART II: ACUTE MYOCARDIAL INFARCTION AND REPERFUSION INJURY

This part of the general summary and discussion is dedicated to novel therapies that are aimed at reducing acute post-infarct lethal-reperfusion injury as measured by infarct size and area of no-reflow early after AMI. The expected early results of limitation of lethal reperfusion injury are reductions in infarct size as well as no-reflow and are elementary to post-infarct myocardial salvage. Thus, arresting or limiting acute infarct and no-reflow development may result in attenuated LV-dysfunction and remodeling.

Pharmacotherapy of reperfusion injury after revascularization is promising and fundamental to the definite proof of the existence of reperfusion injury (14,15).

A well-studied drug in this field is adenosine for which results are encouraging (38,39) yet controversial (40-42). This may be the result of inconsistencies in peri-procedural parameters such as drug timing and dosing. In **Chapter 6**, we treated pigs with AMI with intracoronary administered adenosine with an emphasis on investigating duration of infusion as prime determinant in the reduction of reperfusion injury. The results showed that intracoronary administered high-dose adenosine was capable of reducing infarct size and no-reflow. Improvements were, however, only apparent when adenosine was given over a prolonged period and were absent when adenosine was administered as a high-dose bolus only. Results were reflected in attenuated regional influx of inflammatory cells augmenting the effect of adenosine on regional immune response (43,44). These results warrant reconsideration of adenosine as a post-infarct adjuvant therapy for reperfusion injury. Indeed, a recent study suggests that high-dose, prolonged intracoronary adenosine therapy may offer protection against reperfusion injury (45).

It has been hypothesized that reducing the workload of the heart during early reperfusion will result in reduced metabolic demand of the area-at-risk and improved prognosis (46).
Several studies in small animals have shown that stimulating the vagal nerve system in a supra-physiological manner results in a bradycardic response concomittant with a significant reduction in infarct size (47). These studies however, started vagal nerve therapy either before (48), at the onset of (47), or early during (49) ischemia, time points that do not reflect the clinical reality. In **Chapter 7** a clinically more relevant protocol of vagal nerve stimulation was applied by initiating vagal nerve stimulation during early reperfusion in a translational, large animal model of reperfused AMI with infarct size and area of no-reflow as primary endpoints. The results showed that vagal nerve stimulation was capable of significantly limiting both infarct size and no-reflow and that these effects were independent of the degree of bradycardia. Additional signal transduction experiments showed that nitric oxide was essential for the vagal nerve stimulation induced cardioprotection. Also, regional histological analyses of both the infarct zone as well as the area of no-reflow showed that this novel adjunctive therapy reduced regional immune cell influx with reductions in regional macrophage influx reflecting the decrease in infarct size whereas neutrophil influx within the no-reflow zone paralleled the reduction in no-reflow. Recent work in dogs confirm the anti-inflammatory effect of vagal nerve stimulation (50), thus suggesting that vagal nerve stimulating indeed is immunosuppressive and a promising novel adjunctive method for cardioprotection. Future research efforts should focus on optimization of the stimulation protocol (51) and less invasive vagal nerve stimulating methods such as transdermal stimulation (52,53).

PART III: INFARCT HEALING AND LEFT VENTRICULAR REMODELING

Following myocardial infarction, the heart undergoes extensive geometrical changes to maintain stroke volume and cardiac output (54,55). Notwithstanding the apparent appropriateness of this remodeling process, ultimately progress to overt heart failure may occur (56,57). While research has traditionally focused on the LV-remodeling process by targeting the surviving myocardium, current research, including the work in this thesis is focussing on modulating the healing process of the infarcted myocardium itself. These efforts include, but are not limited to, attenuating infarct expansion (58), which is a critical determinant of remodeling (59), attenuating regional wound healing by changing regional myofibroblast content, a cell type associated with improved prognosis (60), and increasing or maintaining regional angiogenesis with growth factors (61,62).

To precisely distinguish between the global and regional LV post-infarct expansion, we developed a magnetic resonance imaging-based method in swine with a transmural reperfused AMI measured at three and thirty-five days post-AMI. This method which was described in **Chapter 8,** allowed us to digitally divide the left ventricle into 6 mm slices and those slices were subsequently divided into 36 identical segments. The use of these slices and segments allowed us to precisely monitor the post-infarct global and regional expansion using infarct length, infarct thickness and infarct circumference.

Using this method in **Chapter 9** we studied the effects of dyssynchronous pacing of the left ventricle after AMI and its effects on attenuating global and regional LV-remodeling when applied in the sub-acute phase after AMI, at a time when protection against early necrosis is no longer possible. For this purpose, we instrumented swine with pacemakers, placed epicardial pacemaker leads in the expected border zone and produced reperfused AMI. Three and thirty-five days later, baseline global and regional cardiac function, using the method described in chapter 8, was assessed. Interestingly, dyssynchronous pacing of the left ventricle did modify infarct-geometry, which was paralleled by a significantly higher number of myofibroblasts within the scar. This differentiated subtype of resident fibroblasts is involved in extracellular matrix turnover, capable of tonic contraction and associated with improved prognosis (63). Although pacing of the left ventricle did not result in global improvements in LV-function after AMI it was capable of significantly attenuating infarct thinning and infarct composition. These promising results warrant further research, including optimization of the current and other

pacing protocols (64) as well as temporal signal transduction analyses to elucidate the mechanism underlying the increased myofibroblast content produced by dyssynchronous pacing.

There is evidence that pharmacologically increasing regional myofibroblast content after AMI yield beneficial results as evidenced in mice that were treated with a selective peptide that antagonizes the Frizzled receptor of the Wnt complex (60). This UM206 peptide was capable of significantly reducing infarct size and preventing the onset of heart failure. In **Chapter 10** we investigated the effects of UM206 on global LV-function and infarct size in swine with reperfused AMI when started 24h post-AMI and continued for 5 weeks. Cardiac function was measured weekly with echocardiography and infarct size was determined at baseline and 5 week follow-up using techniques described in chapter 3. The results showed that infarct mass decreased significantly in UM206 treated animals whereas this did not change in sham treated animals, confirming previous findings in mice (60). This reduction in infarct mass was accompanied by reduced LV-dilatation in the therapy group starting week 3 post-AMI whereas left ventricular function in sham treated animals continued to deteriorate. Surprisingly, results could not be explained by increased myofibroblast numbers in the infarct. Also, molecular expression studies at follow-up did not reveal which molecular mechanisms were responsible for the beneficial effects. We speculate that UM206 exerted a beneficial effect on the myofibroblasts that are involved in tissue repair (65), the first weeks after AMI. This however, did not translate into significant changes in the longitudinal presence of circulating markers for extracellular matrix turnover. Although UM206 yielded promising results in terms of infarct mass reduction and attenuation of LV-remodeling, it is interesting to compare results in myofibroblast presence in the infarct region to results obtained in chapter 9. Results between control experiments (infarct + sham-IPT vs infarct + sham-UM206) were statistically similar ($p=0.4$). Myofibroblast numbers within the infarcts of treated (infarct + IPT vs infarct + UM206) animals however, were statistically different ($p<0.001$). We speculate that these differences are the consequence of the moment at which the different approaches effectively exert their effect on myofibroblast numbers. In the UM206 treated animals, promoting early presence of myofibroblasts resulted in attenuation of LV dilatation, thereby likely reducing the stress on the infarcted tissue and negating the stimulus for additional myofibroblast differentiation. In contrast, in the IPT treated group, the IPT procedure resulted in a sustained stretch of the infarcted tissue and thereby enhanced the stimulus for myofibroblast differentiation. Infarct geometry changed by IPT treatment, suggesting that prolonged myofibroblast presence is still capable of beneficial modulation of LV geometry. It is however unknown whether

the effect of IPT would have been different when studied at an earlier timepoint. Future studies are therefore warranted that elucidate the optimal duration and "intensity" of myofibroblast presence and to investigate whether dyssynchronous pacing therapy and UM206 therapy exert an additive or synergistic effect on infarct healing to benefically modulate infarct geometry and LV remodeling.

Stem cell therapy for the treatment of myocardial infarction has many drawbacks. As described in chapter 5, retention rates are low (36) and beneficial results are modest at best (32,66), contradictory (67), potentially transient in nature (33) and subject to attenuation by co-morbidities affecting stem cell function (30). Together with increased evidence that cell therapy acts through paracrine mechanisms, these considerations prompted us to investigate a novel delivery system capable of selective administration of a drug of choice, with customizable release kinetics. In **Chapter 11** we investigated a polymer-based microsphere delivery system which was loaded with $VEGF_{165A}$ (chapter 4). This study showed that indeed microspheres loaded with $VEGF_{165A}$ could be successfully produced with differential release characteristics of intact drug. Next, using techniques described in chapter 3 we ascertained in-vivo retention and safety in swine without myocardial infarction. Having assessed safety and retention of the particles, we continued to test the in-vivo efficacy of drug-laden microspheres in a porcine model of reperfused AMI. Global myocardial function was tested one and five weeks post-AMI with cardiac magnetic resonance imaging and follow-up tissue was regionally analyzed for capillary density using a custom-made and automated, stereologic approach. In parallel, inflammatory markers were longitudinally assessed. The findings showed that indeed we were successful in developing a functional alternative for stem cell therapy. Regional capillary density was significantly increased or maintained in a dose-dependent manner in swine that received the active microspheres, whereas capillary density decreased in the infarcts of sham-treated animals. In addition, drug-laden microspheres attenuated early systemic markers for inflammation. Despite both this regional and systemic effect, global LV-function did not improve. Thus, we provide a very promising delivery system for regional drug delivery, which is not limited to a certain drug or target organ but is widely applicable and allows for tailored multi-drug, multi-stage release for regional pharmacotherapy (68). However, we also provide evidence that for the levels reached in this study, increased capillary density of the myocardium is not associated with improvements in cardiac function at these early time points.

CONCLUSIONS AND DIRECTIONS FOR FUTURE RESEARCH

It is evident that many successful efforts, including in the studies described in this thesis, have recently been made to improve diagnosis and treatment of AMI. These novel methods and therapies provide a solid basis for future research to translate these findings to clinic application.

First of all, improved, faster and better methods for early diagnosis of ischemic heart disease (chapter 2 and 3) will reduce the number of false negative or false positive diagnoses and will contribute to accelerated revascularization with improved outcome. Importantly, different approaches depending on sex of the patient may be inevitable and are of increased interest (69,70). Contemporary scientific knowledge including the current work provided us with several (putative) mechanisms that underlie cardioprotection. Also, post-infarct regional remodeling is an active and dynamic process where different mechanisms are dominant at different time points. These findings suggest that adjunctive efforts for cardioprotection may be more beneficial when a synergistic, complementary multi-step approach with an acute, sub-acute and a chronic component is developed. These future approaches should focus on acute infarct size limitation and the treatment of no-reflow (chapter 6 and 7) in parallel to early modulation of detrimental inflammatory events (chapter 7 and 11). In the sub-acute phase, treatment modalities may have to focus on modulating regional wound healing and infarct stabilization (chapter 9 and 10) to further limit infarct expansion and left ventricular dysfunction to ultimately delay or prevent the onset of progressive heart failure which has a poor prognosis (71) with overall annual mortality rates of 10% (72). In the long-term, which was beyond the scope of the current work, additional treatment with stem cells (73) or other delivery systems of regional drug-delivery (chapter 11) may provide additional beneficial effects. Although current work primarily focused on the infarct-impaired area, sub analyses of data from chapter 9 & 10 confirms that myocardial infarction has an effect on structural and molecular integrity of the remote, surviving myocardium areas as well. This confirms that future efforts, in continuation of earlier studies, should not neglect these remote-based therapeutical leads.

The no-reflow area is increasingly recognized as important in cardiac care (10,11) and has evolved into an independent area of interest with targeted approaches (14). Some studies suggest that no-reflow may be at least partially independent of infarct size and more than a simple epiphenomenon (74,75). These recent insights suggest that novel strategies to limit no-reflow have significant therapeutic potential

in addition to infarct size reducing efforts. Interestingly, even sex differences may have to be included in future work (76). The current work (chapter 6 and 7) may also indicate that a seasonal effect on the amount of no-reflow, independent of infarct size, may exist. Indeed, previous work already showed that a seasonal variation in myocardial infarct size exists (77). This augments the need for further research into this matter and emphasizes the need for time-matched controls.

Translation of preclinical studies into clinical practice may be hampered as relatively young and healthy animals are still used whereas cardiovascular disease most prominently occurs in the elderly, a group that is often accompanied by many comorbidities that affect many biological processes including cell function (30). Presently, efforts are made to improve animal models for cardiovascular disease including comorbidities such as diabetes mellitus (78), obesity and metabolic syndrome (79), hypertension (80) and accelerated atherosclerosis (81). In addition, there appears to be a minimal extent of myocardial damage inflicted to the left ventricle (i.e. >20%) that is required for heart failure to occur (82). This information is important for design of future experimental studies when left ventricular dysfunction or even heart failure is required. In addition, a longer post infarct follow-up period may be required in swine with AMI of the lateral wall of the left ventricle to detect beneficial effects of novel therapies although sensitive and improved techniques (chapter 2 and 8) may prove useful. Thus, a longer follow-up period using adult animals with comorbidities may increase clinical translatability of novel approaches for AMI.

The infarct-area has long been considered to be inert but is increasingly recognized as dynamic (83,84). Indeed, the current work shows that post-AMI wound healing, as evidenced in altered geometry (chapter 9), composition (chapter 9 and 10) or vascularization (chapter 11) of the scar, can successfully be modulated. These results support future work with a focus on scar modulation, including efforts to influence myofibroblast content. It is presently unknown which approach is most beneficial including optimal timing of therapy post-AMI and warrants further investigation. The future treatment of MI could be envisioned to encompass a synergistic, stepwise approach. First, upon reperfusion, myocardial necrosis and no-reflow are treated in the acute phase with approaches such as adenosine therapy (chapter 6) and vagal nerve stimulation (chapter 7). Subsequently, microspheres that contain a cocktail of growth factors (chapter 11), are infused into the affected infarct area to augment regional angiogenesis (chapter 4), to ultimately build a vascular scaffold that allows improved wound healing and enhanced sub-acute treatment with myofibroblast modulating drugs such as UM206 (chapter

10) and treatment with stem cell therapy (73), or a second wave of drug-laden microspheres tailored to release several waves of drugs at prespecified times. Cardiac perfusion imaging (chapter 2) and infarct geometry by MRI (chapter 8) allow precise monitoring of progress whereas the absence of additional hFABP release (chapter 3) ascertains safety.

REFERENCES

1. Murray CJ, Lopez AD. Alternative projections of mortality and disability by cause 1990-2020: Global Burden of Disease Study. Lancet 1997;349:1498-504.
2. Pagidipati NJ, Gaziano TA. Estimating deaths from cardiovascular disease: a review of global methodologies of mortality measurement. Circulation 2013;127:749-56.
3. Heidenreich PA, Trogdon JG, Khavjou OA et al. Forecasting the future of cardiovascular disease in the United States: a policy statement from the American Heart Association. Circulation 2011;123:933-44.
4. Bui AL, Horwich TB, Fonarow GC. Epidemiology and risk profile of heart failure. Nat Rev Cardiol 2011;8:30-41.
5. Frohlich GM, Meier P, White SK, Yellon DM, Hausenloy DJ. Myocardial reperfusion injury: looking beyond primary PCI. Eur Heart J 2013;34:1714-22.
6. Hausenloy DJ, Yellon DM. Myocardial ischemia-reperfusion injury: a neglected therapeutic target. J Clin Invest 2013;123:92-100.
7. Cerra FB, Lajos TZ, Montes M, Siegel JH. Hemorrhagic infarction: A reperfusion injury following prolonged myocardial ischemic anoxia. Surgery 1975;78:95-104.
8. Reffelmann T, Kloner RA. The “no-reflow” phenomenon: basic science and clinical correlates. Heart 2002;87:162-8.
9. Rezkalla SH, Kloner RA. No-reflow phenomenon. Circulation 2002;105:656-62.
10. Ndrepepa G, Tiroch K, Fusaro M et al. 5-year prognostic value of no-reflow phenomenon after percutaneous coronary intervention in patients with acute myocardial infarction. J Am Coll Cardiol 2010;55:2383-9.
11. Ndrepepa G, Tiroch K, Keta D et al. Predictive factors and impact of no reflow after primary percutaneous coronary intervention in patients with acute myocardial infarction. Circ Cardiovasc Interv 2010;3:27-33.
12. Ndrepepa G. Improving myocardial injury, infarct size, and myocardial salvage in the era of primary PCI for STEMI. Coron Artery Dis 2015;26:341-55.
13. Sharma V, Bell RM, Yellon DM. Targeting reperfusion injury in acute myocardial infarction: a review of reperfusion injury pharmacotherapy. Expert Opin Pharmacother 2012;13:1153-75.
14. Brown DA, Hale SL, Baines CP et al. Reduction of early reperfusion injury with the mitochondria-targeting peptide bendavia. J Cardiovasc Pharmacol Ther 2014;19:121-32.
15. Kloner RA, Hale SL, Dai W et al. Reduction of ischemia/reperfusion injury with bendavia, a mitochondria-targeting cytoprotective Peptide. J Am Heart Assoc 2012;1:e001644.
16. Pijls NH, van Schaardenburgh P, Manoharan G et al. Percutaneous coronary intervention of functionally nonsignificant stenosis: 5-year follow-up of the DEFER Study. J Am Coll Cardiol 2007;49:2105-11.
17. Pijls NH, Sels JW. Functional measurement of coronary stenosis. J Am Coll Cardiol 2012;59:1045-57.
18. Plein S, Motwani M. Fractional flow reserve as the reference standard for myocardial perfusion studies: fool’s gold? Eur Heart J Cardiovasc Imaging 2013;14:1211-3.
19. Norgaard BL, Jensen JM, Leipsic J. Fractional flow reserve derived from coronary CT angiography in stable coronary disease: a new standard in non-invasive testing? Eur Radiol 2015;25:2282-90.
20. Meijboom WB, Van Mieghem CA, van Pelt N et al. Comprehensive assessment of coronary artery stenoses: computed tomography coronary angiography versus conventional coronary angiography and correlation with fractional flow reserve in patients with stable angina. J Am Coll Cardiol 2008;52:636-43.
21. Crea F, Camici PG, Bairey Merz CN. Coronary microvascular dysfunction: an update. Eur Heart J 2014;35:1101-11.

22. Ko SM, Song MG, Chee HK, Hwang HK, Feuchtner GM, Min JK. Diagnostic Performance of Dual-Energy CT Stress Myocardial Perfusion Imaging: Direct Comparison With Cardiovascular MRI. AJR Am J Roentgenol 2014;203:W605-13.
23. Mazrani W, McHugh K, Marsden PJ. The radiation burden of radiological investigations. Arch Dis Child 2007;92:1127-31.
24. Liebetrau C, Nef HM, Dorr O et al. Release kinetics of early ischaemic biomarkers in a clinical model of acute myocardial infarction. Heart 2014;100:652-7.
25. Gami BN, Patel DS, Haridas N, Chauhan KP, Shah H, Trivedi A. Utility of Heart-type Fatty Acid Binding Protein as a New Biochemical Marker for the Early Diagnosis of Acute Coronary Syndrome. J Clin Diagn Res 2015;9:BC22-4.
26. Cappellini F, Da Molin S, Signorini S et al. Heart-type fatty acid-binding protein may exclude acute myocardial infarction on admission to emergency department for chest pain. Acute Card Care 2013;15:83-7.
27. Jacobs L, van Borren M, Gemen E et al. ANNALS EXPRESS: Rapidly rule out acute myocardial infarction by combining copeptin and H-FABP with cardiac troponin. Ann Clin Biochem 2015.
28. Stewart DJ, Kutryk MJ, Fitchett D et al. VEGF gene therapy fails to improve perfusion of ischemic myocardium in patients with advanced coronary disease: results of the NORTHERN trial. Mol Ther 2009;17:1109-15.
29. Henry TD, Annex BH, McKendall GR et al. The VIVA trial: Vascular endothelial growth factor in Ischemia for Vascular Angiogenesis. Circulation 2003;107:1359-65.
30. Dimmeler S, Leri A. Aging and disease as modifiers of efficacy of cell therapy. Circ Res 2008;102:1319-30.
31. Wang B, Cheheltani R, Rosano J, Crabbe DL, Kiani MF. Targeted delivery of VEGF to treat myocardial infarction. Adv Exp Med Biol 2013;765:307-14.
32. Delewi R, Hirsch A, Tijssen JG et al. Impact of intracoronary bone marrow cell therapy on left ventricular function in the setting of ST-segment elevation myocardial infarction: a collaborative meta-analysis. Eur Heart J 2014;35:989-98.
33. Meyer GP, Wollert KC, Lotz J et al. Intracoronary bone marrow cell transfer after myocardial infarction: 5-year follow-up from the randomized-controlled BOOST trial. Eur Heart J 2009;30:2978-84.
34. Penicka M, Widimsky P, Kobylka P, Kozak T, Lang O. Images in cardiovascular medicine. Early tissue distribution of bone marrow mononuclear cells after transcoronary transplantation in a patient with acute myocardial infarction. Circulation 2005;112:e63-5.
35. Tossios P, Krausgrill B, Schmidt M et al. Role of balloon occlusion for mononuclear bone marrow cell deposition after intracoronary injection in pigs with reperfused myocardial infarction. Eur Heart J 2008;29:1911-21.
36. Moelker AD, Baks T, van den Bos EJ et al. Reduction in infarct size, but no functional improvement after bone marrow cell administration in a porcine model of reperfused myocardial infarction. Eur Heart J 2006;27:3057-64.
37. Silva SA, Sousa AL, Haddad AF et al. Autologous bone-marrow mononuclear cell transplantation after acute myocardial infarction: comparison of two delivery techniques. Cell Transplant 2009;18:343-52.
38. Forman MB, Stone GW, Jackson EK. Role of adenosine as adjunctive therapy in acute myocardial infarction. Cardiovasc Drug Rev 2006;24:116-47.
39. Mahaffey KW, Puma JA, Barbagelata NA et al. Adenosine as an adjunct to thrombolytic therapy for acute myocardial infarction: results of a multicenter, randomized, placebo-controlled trial: the Acute Myocardial Infarction STudy of ADenosine (AMISTAD) trial. J Am Coll Cardiol 1999;34:1711-20.

40. Desmet W, Bogaert J, Dubois C et al. High-dose intracoronary adenosine for myocardial salvage in patients with acute ST-segment elevation myocardial infarction. Eur Heart J 2011;32:867-77.
41. Garcia-Dorado D, Garcia-del-Blanco B, Otaegui I et al. Intracoronary injection of adenosine before reperfusion in patients with ST-segment elevation myocardial infarction: a randomized controlled clinical trial. Int J Cardiol 2014;177:935-41.
42. Ross AM, Gibbons RJ, Stone GW, Kloner RA, Alexander RW, Investigators A-I. A randomized, double-blinded, placebo-controlled multicenter trial of adenosine as an adjunct to reperfusion in the treatment of acute myocardial infarction (AMISTAD-II). J Am Coll Cardiol 2005;45:1775-80.
43. Todd J, Zhao ZQ, Williams MW, Sato H, Van Wylen DG, Vinten-Johansen J. Intravascular adenosine at reperfusion reduces infarct size and neutrophil adherence. Ann Thorac Surg 1996;62:1364-72.
44. Zhao ZQ, Todd JC, Sato H, Ma XL, Vinten-Johansen J. Adenosine inhibition of neutrophil damage during reperfusion does not involve K(ATP)-channel activation. Am J Physiol 1997;273:H1677-87.
45. Zhang H, Tian NL, Hu ZY et al. Three hours continuous injection of adenosine improved left ventricular function and infarct size in patients with ST-segment elevation myocardial infarction. Chin Med J (Engl) 2012;125:1713-9.
46. Hjalmarson A. Significance of reduction in heart rate in cardiovascular disease. Clin Cardiol 1998;21:II3-7.
47. Katare RG, Ando M, Kakinuma Y et al. Vagal nerve stimulation prevents reperfusion injury through inhibition of opening of mitochondrial permeability transition pore independent of the bradycardiac effect. J Thorac Cardiovasc Surg 2009;137:223-31.
48. Calvillo L, Vanoli E, Andreoli E et al. Vagal stimulation, through its nicotinic action, limits infarct size and the inflammatory response to myocardial ischemia and reperfusion. J Cardiovasc Pharmacol 2011;58:500-7.
49. Wang Q, Cheng Y, Xue FS et al. Postconditioning with vagal stimulation attenuates local and systemic inflammatory responses to myocardial ischemia reperfusion injury in rats. Inflamm Res 2012;61:1273-82.
50. Zhang R, Wugeti N, Sun J et al. Effects of vagus nerve stimulation via cholinergic anti-inflammatory pathway activation on myocardial ischemia/reperfusion injury in canine. Int J Clin Exp Med 2014;7:2615-23.
51. Kong SS, Liu JJ, Hwang TC et al. Optimizing the parameters of vagus nerve stimulation by uniform design in rats with acute myocardial infarction. PLoS One 2012;7:e42799.
52. Wang Z, Yu L, Huang B et al. Low-level Transcutaneous Electrical Stimulation of the Auricular Branch of Vagus Nerve Ameliorates Left Ventricular Remodeling and Dysfunction By Down-regulation of Matrix Metalloproteinase 9 and Transforming Growth Factor beta1. J Cardiovasc Pharmacol 2015;65:342-8..
53. Van Leusden JW, Sellaro R, Colzato LS. Transcutaneous Vagal Nerve Stimulation (tVNS): a new neuromodulation tool in healthy humans? Front Psychol 2015;6:102.
54. Pfeffer MA, Braunwald E. Ventricular remodeling after myocardial infarction. Experimental observations and clinical implications. Circulation 1990;81:1161-72.
55. Sutton MG, Sharpe N. Left ventricular remodeling after myocardial infarction: pathophysiology and therapy. Circulation 2000;101:2981-8.
56. Braunwald E. Heart failure. JACC Heart Fail 2013;1:1-20.
57. Braunwald E, Pfeffer MA. Ventricular enlargement and remodeling following acute myocardial infarction: mechanisms and management. Am J Cardiol 1991;68:1D-6D.
58. Hochman JS, Choo H. Limitation of myocardial infarct expansion by reperfusion independent of myocardial salvage. Circulation 1987;75:299-306.

59. McKay RG, Pfeffer MA, Pasternak RC et al. Left ventricular remodeling after myocardial infarction: a corollary to infarct expansion. Circulation 1986;74:693-702.

60. Laeremans H, Hackeng TM, van Zandvoort MA et al. Blocking of frizzled signaling with a homologous peptide fragment of wnt3a/wnt5a reduces infarct expansion and prevents the development of heart failure after myocardial infarction. Circulation 2011;124:1626-35.

61. Chu H, Wang Y. Therapeutic angiogenesis: controlled delivery of angiogenic factors. Ther Deliv 2012;3:693-714.

62. Deveza L, Choi J, Yang F. Therapeutic angiogenesis for treating cardiovascular diseases. Theranostics 2012;2:801-14.

63. van den Borne SW, Diez J, Blankesteijn WM, Verjans J, Hofstra L, Narula J. Myocardial remodeling after infarction: the role of myofibroblasts. Nat Rev Cardiol 2010;7:30-7.

64. Babiker FA, van Golde J, Vanagt WY, Prinzen FW. Pacing postconditioning: impact of pacing algorithm, gender, and diabetes on its myocardial protective effects. J Cardiovasc Transl Res 2012;5:727-34.

65. Klingberg F, Hinz B, White ES. The myofibroblast matrix: implications for tissue repair and fibrosis. J Pathol 2013;229:298-309.

66. Assmus B, Leistner DM, Schachinger V et al. Long-term clinical outcome after intracoronary application of bone marrow-derived mononuclear cells for acute myocardial infarction: migratory capacity of administered cells determines event-free survival. Eur Heart J 2014;35:1275-83.

67. Nowbar AN, Mielewczik M, Karavassilis M et al. Discrepancies in autologous bone marrow stem cell trials and enhancement of ejection fraction (DAMASCENE): weighted regression and meta-analysis. BMJ 2014;348:g2688.

68. George EM, Liu H, Robinson GG, Mahdi F, Perkins E, Bidwell GL, 3rd. Growth factor purification and delivery systems (PADS) for therapeutic angiogenesis. Vasc Cell 2015;7:1-11.

69. Shah AS, Griffiths M, Lee KK et al. High sensitivity cardiac troponin and the under-diagnosis of myocardial infarction in women: prospective cohort study. BMJ 2015;350:g7873.

70. Yahagi K, Davis HR, Arbustini E, Virmani R. Sex differences in coronary artery disease: Pathological observations. Atherosclerosis 2015;239:260-267.

71. Hobbs FD, Kenkre JE, Roalfe AK, Davis RC, Hare R, Davies MK. Impact of heart failure and left ventricular systolic dysfunction on quality of life: a cross-sectional study comparing common chronic cardiac and medical disorders and a representative adult population. Eur Heart J 2002;23:1867-76.

72. Neubauer S. The failing heart--an engine out of fuel. N Engl J Med 2007;356:1140-51.

73. Uitterdijk A, Groenendijk BC, van Der Giessen WJ. Stem cell therapy for chronic heart failure. Hellenic J Cardiol 2009;50:127-32.

74. Hale SL, Herring MJ, Kloner RA. Delayed treatment with hypothermia protects against the no-reflow phenomenon despite failure to reduce infarct size. J Am Heart Assoc 2013;2:e004234.

75. Li XD, Yang YJ, Geng YJ et al. Tongxinluo reduces myocardial no-reflow and ischemia-reperfusion injury by stimulating the phosphorylation of eNOS via the PKA pathway. Am J Physiol Heart Circ Physiol 2010;299:H1255-61.

76. Langhans B, Ibrahim T, Hausleiter J et al. Gender differences in contrast-enhanced magnetic resonance imaging after acute myocardial infarction. Int J Cardiovasc Imaging 2013;29:643-50.

77. Kloner RA, Das S, Poole WK et al. Seasonal variation of myocardial infarct size. Am J Cardiol 2001;88:1021-4.

78. Larsen MO, Rolin B. Use of the Gottingen minipig as a model of diabetes, with special focus on type 1 diabetes research. ILAR J 2004;45:303-13.

79. Spurlock ME, Gabler NK. The development of porcine models of obesity and the metabolic syndrome. J Nutr 2008;138:397-402.

80. Fossum TW, Baltzer WI, Miller MW et al. A novel aortic coarctation model for studying hypertension in the pig. J Invest Surg 2003;16:35-44.

81. Sabe AA, Elmadhun NY, Sadek AA, Chu LM, Bianchi C, Sellke FW. Differential effects of atorvastatin on autophagy in ischemic and nonischemic myocardium in Ossabaw swine with metabolic syndrome. J Thorac Cardiovasc Surg 2014;148:3172-8.

82. Murry CE, Reinecke H, Pabon LM. Regeneration gaps: observations on stem cells and cardiac repair. J Am Coll Cardiol 2006;47:1777-85.

83. Sun Y, Weber KT. Infarct scar: a dynamic tissue. Cardiovasc Res 2000;46:250-6.

84. Pokorney SD, Rodriguez JF, Ortiz JT, Lee DC, Bonow RO, Wu E. Infarct healing is a dynamic process following acute myocardial infarction. J Cardiovasc Magn Reson 2012;14:62.

CHAPTER 13

Nederlandse samenvatting

Een goed functionerend hart en bloedvatenstelsel is essentieel voor zowel de aanvoer van zuurstof en voedingsstoffen, als de afvoer van afvalstoffen van en naar alle organen. Ziekten aan hart en vaten zijn wereldwijd dan ook verantwoordelijk voor een zeer groot aantal patiënten. Dit gaat vaak gepaard met een verminderde kwaliteit van leven en een verminderde levensverwachting. Deze hart- en vaatziekten brengen daarnaast zeer hoge kosten in de gezondheidszorg met zich mee.

Het acute hartinfarct is verantwoordelijk voor een groot gedeelte van deze problemen en wordt meestal veroorzaakt door het abrupte afsluiten van bloedvaten op het hart zelf. Daardoor wordt de toevoer van zuurstof en voedingsstoffen naar een deel van de hartspier belemmerd. Als gevolg van het tekort aan zuurstof en voedingsstoffen sterft, afhankelijk van de duur van de afsluiting, een deel van de hartspier en verminderd de pompcapaciteit van het hart. Vaak worden patiënten die getroffen zijn door een hartinfarct op termijn kortademig en hebben ze een verminderde conditie; dit kan variëren van nauwelijks merkbare problemen tot een sterke belemmering om zelfs gewone dagelijkse dingen zoals boodschappen te kunnen doen. De gevolgen van een hartinfarct voor de patiënt zijn afhankelijk van de grootte van het infarct. Hoe kleiner het infarct, hoe beter de vooruitzichten. Het is dan ook letterlijk van levensbelang om de acute grootte van het infarct zo veel mogelijk te beperken. Op dit moment is de beste methode om het acute hartinfarct te behandelen het zo snel mogelijk herstellen van de bloedstroom naar het aangedane stuk hartspier. Dit gebeurt door middel van een dotter- en/of stentbehandeling. Het herstellen van de bloedstroom (reperfusie) heeft ook een keerzijde, het geeft vaak extra schade aan de hartspier; de zogenaamde reperfusieschade. Daarnaast is er binnen het infarctgebied vaak een gedeelte waar de bloedstroom niet onmiddellijk hersteld wordt. Dit gedeelte noemen we “no-reflow”; ook de grootte van dit gebied wordt geassocieerd met de vooruitzichten van de patiënt.

De verminderde pompfunctie als gevolg van het infarct wordt door het hart zelf in eerste instantie gecompenseerd. Dit proces bestaat uit structurele aanpassingen van zowel het infarctgebied als het overlevende weefsel. Het infarctgebied wordt enigszins opgerekt terwijl overlevende hartspiercellen in grootte toenemen en leidt uiteindelijk tot een toename in hartspiermassa en inwendig volume. Dit proces is, afhankelijk van de grootte van het infarct, beperkt en wanneer deze natuurlijke compensatie niet langer toereikend is spreekt men van hartfalen. De vooruitzichten bij diagnose hartfalen zijn meestal slecht, ongeveer de helft van patiënten overlijdt binnen 5 jaar.

In de laatste 20 jaar is enorme vooruitgang geboekt in de diagnose en behandeling van het acute hartinfarct en de vermindering van reperfusieschade, waardoor er veel minder mensen overlijden aan de vroege gevolgen van een acuut hartinfarct. De keerzijde van dit succes is dat het aantal patiënten wat vroeg of laat hartfalen ontwikkelt enorm is toegenomen. Dit benadrukt dat er veel behoefte is aan betere methoden voor diagnose en behandeling van het acute hartinfarct in aanvulling op de huidige richtlijnen. Verbetering van de behandeling dient er zowel op gericht te zijn om kort na het ontstaan van het infarct de infarctgrootte te beperken alsook om op de langere termijn structurele veranderingen van de hartspier te beperken en tegen te gaan.

Dit proefschrift, dat is opgedeeld in 3 delen, presenteert nieuwe methoden om de aanwezigheid en ernst van sterk verminderde doorbloeding van de hartspier of een acuut hartinfarct sneller en nauwkeuriger in kaart te brengen (**Deel 1**). Het grootste deel is echter gewijd aan nieuwe, aanvullende methoden om het acute infarct en de no-reflow te behandelen (**Deel 2**), en de wondheling te verbeteren om het verlies van functie van de hartspier op langere termijn te beperken (**Deel 3**).

Deel I

Na een korte introductie over aderverkalking en doorbloedingsproblemen van de hartspier met de nadruk op het acute hartinfarct in **Hoofdstuk 1,** presenteren we in **Hoofdstuk 2** een varkensproefdiermodel waarin de doorbloeding van de hartspier met opzet en gecontroleerd werd verminderd; als model voor het klinische syndroom van stabiele pijn op de borst. Door verschillende maten van vernauwing van een kransslagader na te bootsen kon de ernst van de verminderde doorbloeding van de hartspier worden gestuurd. Met behulp van nieuwe CT-technieken werd de verminderde doorbloeding erg nauwkeurig en voor het eerst op deze manier in beeld gebracht. Deze methode is niet-invasief, in tegenstelling tot de traditionele meer invasieve angiografie, die als gouden standaard wordt beschouwd. Ook is deze methode in staat om aan te tonen of de allerkleinste bloedvaatjes van het hart doorbloedingsproblemen geven, terwijl er geen grote vernauwingen in de grote kransslagaderen zijn. De verkregen resultaten helpen om sneller en met minder risico inzicht te krijgen wanneer een gedeeltelijke afsluiting van een dichtgeslibde kransslagader daadwerkelijk een beperkend effect heeft op de doorbloeding van het hart zelf en verdere behandeling noodzakelijk maakt. Daarnaast helpt het om het aantal fout-negatieve beoordelingen te verminderen.

Er bestaat de onverminderde behoefte om sneller en preciezer te kunnen voorspellen of er sprake is van een acuut hartinfarct en hoe groot dat is. Daarvoor worden vaak stofjes in het bloed van een patiënt gemeten. Deze stofjes zijn echter niet altijd snel genoeg in het bloed meetbaar of zijn minder specifiek. Zeker in de onderzoekswereld, waar vaak met behulp van proefdieren onderzoek naar nieuwe therapieën voor het acute hartinfarct wordt gedaan, is het van groot belang om de acute grootte van het infarct en de no-reflow snel en precies in kaart te brengen. Op deze manier kan een nauwkeurige startwaarde worden vastgesteld waaraan het succes van de therapie gespiegeld kan worden op het beïnvloeden van infarctgrootte en no-reflow in de loop van de tijd. Hiertoe werd in **Hoofdstuk 3** een herontdekt stofje genaamd hartspecifiek-vetzuurbindend eiwit (hFABP) gemeten in bloed van varkens met een hartinfarct en vergeleken met A) de klinische standaard troponine en B) een kleuring op de uitgenomen harten die heel precies dood van levend hartweefsel kan onderscheiden. De resultaten laten zien dat hFABP sneller dan de klinische standaard zowel de grootte van het hartinfarct als de grootte van no-reflow kan bepalen. Deze resultaten helpen voornamelijk in de proefdierwereld, waar modellen voor het acute hartinfarct nauwkeurig geregisseerd worden, om een betrouwbare inschatting van de acute infarctgrootte en de hoeveel no-reflow te maken. Daarnaast kan hFABP misschien in de klinische realiteit helpen om te bepalen of er al dan niet sprake is van acute hartschade.

Hoofdstuk 4 beschrijft een studie waarin we keken naar stoffen die vaatnieuwvorming kunnen stimuleren. Het stimuleren van vaatnieuwvorming in het infarct wordt gezien als een methode om de wondheling gunstig te beïnvloeden. In deze studie stelden we verschillende typen cellen bloot aan deze zogenaamde groeifactoren onder verschillende experimentele condities om vaatnieuwvorming te bestuderen. Normaal gesproken worden dit soort stoffen getest met cellen uit de navelstreng. Echter is dit niet het celtype dat zich in het hart bevindt en aan de groeifactor blootgesteld zou worden wanneer de groeifactor rechtstreeks in het hart toegediend zou worden. Daarnaast zijn de condities waarin een dergelijke stof ingespoten zou worden in het geïnfarceerde hart behoorlijk anders dan de condities in een traditioneel netwerkvormingsexperiment. Als groeifactor werd het goed bestudeerde vasculair endotheel groeifactor 165A ($VEGF_{165A}$) gekozen en dit werd getest met het traditionele celtype uit de navelstreng, maar ook met het werkelijke doelwit celtype. $VEGF_{165A}$ werd bestudeerd in cardiale microvasculaire endotheelcellen onder condities die weefsel in het geïnfarceerde hart ten dele nabootsen. De resultaten laten duidelijk zien dat de verschillende gekozen experimentele condities van grote invloed zijn op de uiteindelijke vaatnieuwvorming. Dit experiment toont aan dat groeifactoren die ingezet gaan worden om uiteindelijk

in het humane hart vaatnieuwvorming te stimuleren, éérst uitgebreid moeten worden getest onder realistische experimentele condities.

Deel 1 van dit proefschrift wordt afgesloten met een experimentele studie gewijd aan het optimaliseren van stamceltherapie voor de behandeling van het hartinfarct. Hoewel stamceltherapie voor de behandeling van het acute hartinfarct veilig en gematigd succesvol is gebleken, is er nog veel ruimte voor verbetering. Een opvallend probleem in stamceltherapie voor het acute hartinfarct is het feit dat maar een klein gedeelte van de toegediende cellen daadwerkelijk in het hart achterblijft. Er wordt gedacht dat met het verhogen van deze zogenaamde retentie, stamceltherapie betere resultaten zal geven. Uit eerder onderzoek is gebleken dat de stamcellen actief door de bloedvatbekleding van bloedvaten uit het infarct gebied worden gevangen. De moleculen op deze, door het infarct geactiveerde, endotheelcellen zijn verantwoordelijk voor het vastgrijpen van de ingespoten stamcellen. Welke moleculen dat precies zijn is niet volledig bekend, maar vasculair-cellulair adhesiemolecuul 1 (VCAM-1) lijkt een grote rol te spelen. Inderdaad, wanneer we in **Hoofdstuk 5** kijken naar infarctweefsel uit varkens op 1, 3, 7, 14 of 35 dagen na het infarct laten de resultaten zien dat op 3 en 7 dagen na het infarct de aanwezigheid van VCAM-1 enorm verhoogd is (en pas normaliseert na 14 dagen). Onze hypothese dat toedienen van stamcellen uit het beenmerg op deze tijdstippen zou leiden tot een sterk verhoogde celretentie bleek echter onjuist. In deze experimenten bleef de stamcelretentie zeer laag, waaruit geconcludeerd kan worden dat VCAM-1 hooguit ten dele verantwoordelijk is voor stamcelretentie na een infarct en dat toekomstige onderzoeken in dit veld hierover duidelijkheid zullen moeten scheppen.

Deel II van dit proefschrift richt zich op nieuwe behandelingen om acute schade aan het hart te beperken. Wanneer bij een hartinfarct het verstopte bloedvat wordt geopend met een dotter- of stentprocedure en de perfusie wordt hersteld, de zogenaamde reperfusie, ontstaat er vaak extra schade bovenop die van het infarct alleen. Hoewel de exacte oorzaken voor deze zogenaamde reperfusieschade onvolledig bekend zijn, zijn in ieder geval kleinere stolsels en witte bloedcellen die stroomafwaarts van het risicogebied de haarvaatjes afsluiten of schadelijke ontstekingsreacties veroorzaken een onderdeel van dit probleem. Daarnaast kan zwelling van de verse wond kleine bloedvaatjes dichtduwen. De verwachte resultaten van het snel behandelen van deze reperfusieschade zijn beperking van de infarctgrootte en daarbinnen minder no-reflow. We verwachten dat dit soort behandelingen uiteindelijk leiden tot het uitstellen of zelfs voorkomen van hartfalen.

In **Hoofdstuk 6** werd daartoe adenosine in de kransslagaderen van varkens met een hartinfarct gespoten. Adenosine therapie is niet helemaal nieuw, maar eerdere studies laten niet eenduidig een positief effect zien. Adenosine verwijdt de bloedvaatjes in het infarctgebied met als gevolg een betere doorbloeding en we verwachtten dan ook dat er in de allerkleinste bloedvaten minder ongewenste cellen of stolseltjes zullen blijven hangen met als positief resultaat een beperking van de infarctgrootte en de no-reflow. Omdat de werking van adenosine van korte duur is, richtte deze studie zich vooral op het kort- en langdurend toedienen van het medicijn. De resultaten laten zien dat adenosine inderdaad in staat is om de infarctgrootte sterk te beperken ten opzichte van onbehandelde varkens met een infarct. Dit uitte zich ook in een sterk verminderde grootte van de no-reflow in het infarct. Deze resultaten waren weerspiegeld in een verminderde ontstekingsreactie in het infarct. Deze positieve resultaten waren echter alleen waarneembaar in die groepen waarin adenosine hoog gedoseerd en voor een langere periode werd toegediend. Deze belangrijke resultaten plaatsen de negatieve vindingen uit eerdere klinische onderzoeken in perspectief en verklaren deze ten dele. Tenslotte rechtvaardigen deze veelbelovende resultaten verder onderzoek naar adenosine als medicijn voor de additionele behandeling van het hartinfarct in de acute fase.

Deel II van dit proefschrift wordt afgesloten met een onderzoek in varkens met een acuut hartinfarct waarin een zenuwbaan in de hals, de nervus vagus, elektrisch werd gestimuleerd. Het is bekend dat elektrische stimulatie van deze zenuwbaan resulteert in het beperken van de infarctgrootte in kleine proefdieren wanneer dit wordt uitgevoerd tijdens, of voorafgaand aan de periode van het afsluiten van de kransslagader. Omdat dit niet de klinische werkelijkheid nabootst, waar patiënten pas in het ziekenhuis belanden wanneer ze al een hartinfarct hebben, hebben we deze zenuwbaanstimulatie getest in varkens met een acuut hartinfarct. De therapie werd gestart vlak voor de reperfusie, precies zoals het in de kliniek toegepast zou kunnen worden. De resultaten laten zien dat ook in ons grote proefdiermodel elektrische stimulatie van de nervus vagus de infarctgrootte beperkt. Daarnaast bleek de therapie in staat de no-reflow te beperken. De resultaten waren weerspiegeld in de verminderde instroom van witte bloedcellen in het infarctgebied en aanvullende experimenten lieten zien dat stikstofoxide essentieel was voor het therapeutische effect. Al met al is deze vorm van therapie veelbelovend en verdient aanvullend onderzoek.

Hoewel bekend is dat verkleining van het hartinfarct in de acute fase belangrijk is om op de lange termijn hartfalen te voorkomen, is het daarnaast van belang om ook het zogenaamde remodelleringsproces van het hart te beïnvloeden.

Dit proces vindt plaats in de weken en maanden na het acute hartinfarct. De experimenten beschreven in **Deel III** zijn gericht op het beïnvloeden van het proces van wondheling en het in kaart brengen van de langetermijneffecten van nieuwe behandelingen op hartfunctie na een hartinfarct.

In **Hoofdstuk 8** wordt daartoe een nieuwe manier om naar de ontwikkeling van het infarct in de tijd te kijken gepresenteerd. Deze manier is gebaseerd op een MRI opname en verdeelt de linker harthelft digitaal in gelijke plakken. Deze plakken worden vervolgens digitaal opgedeeld in 36 identieke segmenten. Hierna wordt met deze plakken en segmenten de geometrie van het infarct bepaald. Deze gevoelige manier van meten is direct toegepast in **Hoofdstuk 9** waar varkens met een hartinfarct werden behandeld met pacemakers. Deze pacemakers hebben 2 keer per dag 3 keer 5 minuten het infarctgebied elektrisch gestimuleerd. Hartfunctie en infarctgeometrie van deze dieren werd gemeten met MRI een paar dagen na het infarct en 5 weken daarna opnieuw. Hoewel eerder werk in kleine proefdieren en geïsoleerde harten met dit soort pacemakertherapie veelbelovende resultaten liet zien, verbeterde de hartfunctie in onze dieren helaas niet. De vorm van het infarct veranderde echter wel. Pacemakertherapie bleek in staat de verdunning van het infarct, een proces dat normaal gesproken onvermijdelijk verbonden is met de verlittekening van het aangedane hartspierweefsel, sterk te beperken. Ook de samenstelling van het infarct veranderde. Onze pacemakertherapie bleek het aantal van een speciaal gunstig celtype, de myofibroblast, te kunnen verhogen met een verbeterde wondheling als gevolg. Vervolgens is in **Hoofdstuk 10**, opnieuw in een varkensmodel voor het acute hartinfarct, geprobeerd de hoeveelheden myofibroblasten in het infarctgebied met een nieuw medicijn (UM206) te sturen om zo met een verbeterde wondheling het remodelleringsproces, gemeten met echo, gunstig te beïnvloeden. Hoewel de aantallen myofibroblasten in de infarcten van behandelde dieren tegengesteld waren aan die gerapporteerd in hoofdstuk 9 bleek de UM206 therapie de infarctmassa sterk te verkleinen en de negatieve remodellering af te remmen. Deze resultaten laten zien dat we nog niet alles weten over het sturen van myofibroblast-aantallen en op welk moment deze het gunstigst zijn. Wel suggereert dit werk dat het beïnvloeden van myofibroblasten in het infarct met pacemakertherapie, met medicijnen of een combinatie daarvan mogelijk en veelbelovend is.

Van het met groeifactoren stimuleren van vaatnieuwvorming in het infarctgebied wordt aangenomen dat het op korte termijn de wondheling gunstig beïnvloedt en daarmee op langere termijn de schade beperkt. Deze groeifactoren hebben vaak een korte halfwaardetijd, zijn zeer kostbaar en kunnen elders in het lichaam

gevaarlijk zijn door ongewenste vaatgroei te stimuleren. Het is dan ook een doel van velen om lokaal, met behulp van een drager, deze groeifactoren gereguleerd en in het infarct, vaatnieuwvorming te laten stimuleren. Hiertoe hebben we de in hoofdstuk 4 beschreven groeifactor $VEGF_{165A}$ in kleine polymeerbolletjes weten te integreren. De samenstelling van deze pareltjes, het aantal en de inspuitdichtheid zijn zo gekozen dat ze in de kleine vaatjes van het hart blijven hangen zonder zelf schade, in de vorm van celdood of een ontstekingsreactie, te veroorzaken. Deze met het medicijn gevulde, bioafbreekbare “paarlen voor de zwijnen” zijn vervolgens via een katheter direct ingespoten in het risicogebied van varkens met een acuut hartinfarct op het moment van reperfusie. Dit is gedaan in 3 behandelgroepen: placebo, lage dosis VEGF, en hoge dosis VEGF. Het bloed werd vervolgens onderzocht op afgifte van ontstekingsgerelateerde stoffen en hartfunctie van deze dieren werd op 1 en 5 weken na het infarct gemeten met MRI. Ook is met behulp van histologische technieken de vaatdichtheid van het infarct bestudeerd. De met medicijn gevulde bolletjes handhaafden of vergrootten de lokale vaatnieuwvorming op een dosis-afhankelijke manier, terwijl deze in dieren die placebobollen hadden gekregen afnam. Daarnaast bleken beide medicijn-gevulde bollen een remmend effect te hebben op de acute immuunrespons. Helaas verbeterde de hartfunctie van de behandelde dieren niet. Het belangrijkste resultaat van deze studie is dat het mogelijk is gebleken om met dit hypermoderne farmacotherapeutische platform lokaal een effect te bewerkstelligen. Hoewel de resultaten misschien nog niet aardverschuivend zijn, is deze studie een stevig fundament voor de verdere ontwikkeling van lokale, gecontroleerde farmacotherapie.

Samengevat laten de studies uit dit proefschrift zien dat er meerdere succesvolle therapieën in ontwikkeling zijn voor de vroege diagnose en de verbeterde behandeling van het acute hartinfarct. We hebben laten zien dat we de infarctgrootte, de hoeveelheid no-reflow, de acute immuunrespons, de vorm en samenstelling van het infarct en de lokale wondheling gunstig hebben kunnen beïnvloeden en deze gunstige ontwikkelingen verbeterd hebben kunnen vastleggen met CT, MRI of met behulp van stofjes uit het bloed. Tegelijkertijd is er nog veel werk aan de winkel en roepen de studies misschien wel meer vragen op dan ze beantwoorden. Desalniettemin biedt het huidige werk een goede basis voor verder onderzoek en zijn we een stapje dichter bij verbeterde behandeling van het acute hartinfarct.

CHAPTER 14

Fryske gearfetting

In goed funksjonearjend hert en bloedfetstelsel is essinsjeel foar likegoed de oanfier fan soerstof en fiedingsstoffen, as de ôffier fan ôffalstoffen fan en nei alle organen. Sykten oan hert en ieren binne oeral dan ek ferantwurdlik foar in hiel grut tal pasjinten. Dit giet faak mank mei in fermindere kwaliteit fan libjen en in fermindere libbensferwachting. Dizze hert en iersykten bringe dêrneist hiele hege kosten yn de sûnenssoarch mei har mei.

It akute hertynfarkt is ferantwurdlik foar in grut part fan dizze problemen en wurdt meastal feroarsake troch it abrupt ôfsluten fan bloedieren op it hert sels.

Dêrtroch wurdt de tafier fan soerstof en fiedingsstoffen nei in part fan de hertspier behindere. As gefolch fan it tekoart oan soerstof en fiedingsstoffen stjert, ôfhinklik fan de duer fan de ôfsluting, in part fan de hertspier en fermindert de pompkapasiteit fan it hert. Faak wurde pasjinten dy't troffen binne troch in hertynfarkt op termyn koartamich en ha se in fermindere kondysje; dit kin fariearje fan amper merkbere problemen oant in sterke behindering om sels gewoane deistige dingen lykas boadskippen dwaan te kinnen. De gefolgen fan in hertynfarkt foar de pasjint binne ôfhinklik fan de grutte fan it ynfarkt. Hoe lytser it ynfarkt, hoe better de foarútsichten. It is dan ek letterlik fan libbensbelang om de akute grutte fan it ynfarkt safolle mooglik te beheinen. Op dit momint is de bêste metoade om it akute hertynfarkt te behanneljen it sa fluch mooglik herstellen fan de bloedstream nei it oandiene stik hertspier. Dit bart troch in dotter en/of stent behanneling. It herstellen fan de bloedstream (reperfúzje) hat ek in kearside, it jout faak ekstra skea oan de hertspier; de saneamde reperfúzje skea. Dêrneist is der binnen it ynfarktgebiet faak in part wêr't de bloedstream net daliks hersteld wurdt. Dit part neame wy "no-reflow"; ek de grutte fan dit gebiet wurdt assosjearre mei de foarútsichten fan de pasjint.

De fermindere pompfunksje as gefolch fan it ynfarkt wurdt troch it hert sels yn earste ynstânsje kompensearre. Dit proses bestiet út strukturele oanpassingen fan likegoed it ynfarktgebiet as it oerlibjende weefsel. It ynfarktgebiet wurdt in bytsje fergrutte, wylst oerlibjende hertspiersellen yn grutte tanimme en dit laat úteinlik ta in tanimming yn hertspiermassa en ynwindich folume.

Dit proses is, ôfhinklik fan de grutte fan it ynfarkt, beheind en wannear dizze natuerlike kompensaasje net langer foldwaande is sprekt men fan hertfalen. De foarútsichten by diagnoaze hertfalen binne meastal min, ûngefear de helte fan de pasjinten stjert binnen 5 jier.

Yn de lêste 20 jier is enoarme foarútgong boekt yn de diagnoaze en behanneling fan it akute hertynfarkt en de fermindering fan reperfúzje skea, wêrtroch der folle minder minsken stjerre oan de betide gefolgen fan in akút hertynfarkt. De kearside fan dit sukses is dat it tal pasjinten wat ier as let hertfalen ûntwikkelt, enoarm tanommen is. Dit ûnderstreket dat der in protte ferlet is oan bettere metoaden foar diagnoaze en behanneling fan it akute hertynfarkt yn oanfolling op de hjoeddeistige rjochtlinen. Ferbettering fan de behanneling moat der likegoed op rjochte wêze om koart nei it ûntstean fan it ynfarkt de grutte fan it ynfarkt te beheinen, as ek op de langere termyn strukturele feroaringen fan de hertspier te beheinen en tsjin te gean.

Dit proefskrift, dat opdield is yn 3 dielen, presintearret nije metoaden om de oanwêzichheid en earnst fan sterk fermindere trochblieding fan de hertspier of in akút hertynfarkt flugger en krekter yn kaart te bringen (**Diel 1**). It grutste part is lykwols bestege oan nije, oanfoljende metoaden om it akute ynfarkt en de no-reflow te behanneljen (**Diel 2**), en it hieljen fan de wûne te ferbetterjen om it ferlies fan funksje fan de hertspier op langere termyn te beheinen (**Diel 3**)

Diel 1

Nei in koarte yntroduksje oer ierferkalking en trochbliedingssystemen fan de hertspier mei de klam op it akute hertynfarkt yn **Haadstik 1**, presintearje wy yn **Haadstik 2** in proefdiermodel fan in baarch wêryn't de trochblieding fan de hertspier mei opsetsin en kontrolearre fermindere waard; as model foar it klinyske syndroom fan stabile pine op it boarst. Troch ferskillende maten fan fernauwing fan in krânsslachier te simulearjen koe de earnst fan de fermindere trochblieding fan de hertspier stjoerd wurde. Mei help fan nije CT techniken waard de fermindere trochblieding hiel krekt en foar it earst op dizze wize yn byld brocht. Dizze metoade is net ynvasyf, yn tsjinstelling ta de tradisjonele mear ynvasive angiografy, dy't as gouden standert beskôge wurdt. Ek is dizze metoade by steat om oan te jaan as de allerlytste bloedierkes fan it hert trochbliedingsproblemen jouwe, wylst der gjin grutte fernauwingen yn de grutte krânsslachieren binne. De opdiene resultaten helpe om flugger en mei minder risiko ynsicht te krijen wannear foar in diel in ôfsluting fan in tichtslime krânsslachier echt in beheinend effekt hat op de trochblieding fan it hert sels en fierdere behanneling needsaaklik makket. Dêrneist helpt it om it tal fout negative beoardielingen te ferminderjen.

Der bestiet ûnfermindere ferlet om flugger en krekter foarsizze te kinnen as der sprake is fan in akút hertynfarkt en hoe grut dat is. Dêrfoar wurde faak stofkes yn it bloed fan in pasjint metten. Dizze stofkes binne lykwols net altyd fluch genôch

yn it bloed te mjitten of binne minder spesifyk. Benammen yn de ûndersykwrâld, wêr't faak mei help fan proefdieren ûndersyk nei nije terapyen foar it akute hertynfarkt dien wurdt, is it fan grut belang om de akute grutte fan it hertynfarkt en de no-reflow fluch en krekt yn kaart te bringen. Op dizze wize kin in sekuere startwearde fêststeld wurde wêr't it sukses fan de terapy oan spegele wurde kin op it beynfloedzjen fan ynfarktgrutte en no-reflow yn de rin fan de tiid. Hjirta waard yn **Haadstik 3** in wer ûntdutsen stofke neamd hertspesifyk fetsoerbinend aaiwyt (hFABP) metten yn bloed fan bargen mei in hertynfarkt en fergelike mei A) de klinyske standert troponine en B) in kleurjen op de útnommen herten dy't hiel persys dea fan libbend hertweefsel ûnderskiede kinne. De resultaten litte sjen dat hFABP flugger as de klinyske standert likegoed de grutte fan it hertynfarkt as de grutte fan no-reflow bepale kin. Dizze resultaten helpe benammen yn de proefdierewrâld, wêr't modellen foar it akute hertynfarkt krekt regissearre wurde, om in betroubere ynskatting fan de akute ynfarktgrutte en de no-reflow te meitsjen. Dêrneist kin hFABP miskien yn de klinyske realiteit helpe om te bepalen as der al as net sprake is fan akute hertskea.

Haadstik 4 beskriuwt in stúdzje wêryn't wy seagen nei stoffen dy't nijfoarming fan ieren stimulearje kinne. It stimulearjen fan dizze nijfoarming yn it ynfarkt wurdt sjoen as in metoade om it hieljen fan de wûne geunstich te beynfloedzjen. Yn dizze stúdzje stelden wy ferskillende typen sellen bleat oan dizze saneamde groeifaktoaren ûnder ferskillende eksperimintele kondysjes om nijfoarming fan ieren te bestudearjen. Normaal sprutsen wurde dizze stoffen test mei sellen út de nâlestring. Lykwols is dit net it type sel dat yn it hert sit en oan de groeifaktor bleatsteld wurde soe wannear de groeifaktor rjochtstreeks yn it hert tatsjinne wurde soe. Dêrneist binne de kondysjes wêryn't soksoarte stof ynspuite wurde soe yn it ynfarsearre hert behoarlik oars as de kondysjes yn in tradisjoneel netwurkfoarmingseksperimint. As groeifaktor waard it goed bestudearre vaskulêr endoteel groeifaktor 165A ($VEGF_{165A}$) keazen en dit waard test mei it tradisjonele seltype út de nâlestring, mar ek mei it werklike doelwyt type sel. $VEGF_{165A}$ waard bestudearre yn kardiale mikrovaskulêre endoteelsellen ûnder kondysjes dy't weefsel yn it ynfarsearre hert foar in part neimeitsje.

De resultaten litte dúdlik sjen dat de ferskillende keazen eksperimintele kondysjes fan grutte ynfloed binne op de úteinlike nijfoarming fan ieren. Dit eksperimint lit sjen dat groeifaktoaren dy't ynsetten wurde om úteinlik yn it humane hert nijfoarming fan ieren te stimulearjen, earst wiidweidich test wurde moatte ûnder realistyske eksperimintele kondysjes.

Diel 1 fan dit proefskrift wurdt ôfsletten mei in eksperimintele stúdzje wijt oan it optimalisearjen fan stamselterapy foar de behanneling fan it hertynfarkt. Alhoewol stamselterapy foar de behanneling fan it akute hertynfarkt feilich en beskieden suksesfol útwiisd hat, is der noch in protte romte foar ferbettering. In opfallend probleem yn stamsel terapy foar it akute hertynfarkt is it feit dat mar in lyts part fan de tatsjinne sellen echt yn it hert efterbliuwt. Der wurdt tocht dat mei it ferheegjen fan dizze saneamde retinsje, stamsel terapy bettere resultaten jaan sil. Ut earder ûndersyk die bliken dat de stamsellen aktyf troch de beklaaiïng fan ieren út it ynfarkt gebiet fongen wurde. De molekulen op dizze, troch it ynfarkt aktivearre, endoteelsellen binne ferantwurdlik foar it fêstgripen fan de ynspuite stamsellen. Wat foar molekulen dat persys binne is net folslein bekend, mar vaskulêr sellulêr adhesy molekúle 1 (VCAM-1) liket in grutte rol te spyljen. Yndie, wannear wy yn **Haadstik 5** sjogge nei ynfarktweefsel út bargen op 1,3,7,14 of 35 dagen nei it ynfarkt litte de resultaten sjen dat op 3 en 7 dagen nei it ynfarkt de oanwêzichheid fan VCAM-1 enoarm ferhege is (en pas normalisearret nei 14 dagen). Us hypotese dat tatsjinjen fan stamsellen út it bienmoarch op dizze tiidstippen liede soe ta in sterk ferhege selretinsje die bliken dat dit lykwols ûnwier wie. Yn dizze eksperiminten bleau de stamsel retinsje hiel leech, wêrút konkludearre wurde kin dat VCAM-1 heechút foar in part ferantwurdlik is foar stamsel retinsje nei in ynfarkt en dat takomstige ûndersiken yn dit fjild hjir oer dúdlikheid jaan moatte.

Diel II fan dit proefskrift rjochtet him op nije behannelingen om akute skea oan it hert te beheinen. Wannear by in hertynfarkt it ferstoppe bloedfet iepene wurdt mei in dotter behanneling of stent proseduere en de perfúzje hersteld wurdt, de saneamde reperfúzje, ûntstiet der faak ekstra skea boppe op dy fan it ynfarkt allinne. Hoewol de eksakte oarsaken foar dizze saneamde reperfúzje skea net folslein bekend binne, binne der yn elk gefal lytsere bloedproppen en wite bloedsellen dy't fan de stream fan it risikogebiet ôf de hierbuiskes ôfslute of skeadlike ûntstekkingsreaksjes feroarsaakje in ûnderdiel fan dit probleem. Dêrneist kin swollen fan de farske wûne lytse hierbuiskes ticht triuwe. De ferwachte resultaten fan it fluch behanneljen fan dizze reperfúzje skea binne beheining fan de ynfarktgrutte en dêr binnen minder no-reflow. Wy ferwachtsje dat dizze behannelingen úteinlik liede ta it útstellen as sels foarkommen fan hertfalen.

Yn **Haadstik 6** waard dêrta adenosine yn de krânsslachieren fan bargen mei in hertynfarkt spuite. Adenosine terapy is net hielendal nij, mar eardere stúdzjes litte net konkreet in posityf effekt sjen. Adenosine makket de bloedierkes yn it ynfarktgebiet wider mei as gefolch in bettere trochblieding en wy ferwachtsje dan ek dat der yn de allerlytste ierkes minder net winske sellen as bloedpropkes hingjen bliuwe sille

mei as posityf resultaat in beheining fan de ynfarktgrutte en de no-reflow. Omdat de wurking fan adenosine fan koarte duer is, rjochtet dizze stúdzje him foaral op it koarte en langer duorjende tatsjinjen fan it medisyn. De resultaten litte sjen dat adenosine yndie by steat is om de ynfarktgrutte sterk te beheinen oangeande net behannele bargen mei in ynfarkt. Dit uteret him ek yn in sterk fermindere grutte fan de no-reflow yn it ynfarkt. Dizze resultaten waarden wjerspegele yn in fermindere ûntstekkingsreaksje yn it ynfarkt. Dizze positive resultaten wienen lykwols allinne waar te nimmen yn dy groepen wêryn't adenosine heech dosearre en foar in langere perioade tatsjinne waard. Dizze belangrike resultaten pleatsten de negative finingen út eardere klinyske ûndersiken yn perspektyf en ferklearren dizze foar in part. Uteinlik rjochtfeardigen dizze goede resultaten fierder ûndersyk nei adenosine as medisyn foar de addisjonele behanneling fan it hertynfarkt yn de akute faze.

Diel II fan dit proefskrift wurdt ôfsletten mei in ûndersyk yn bargen mei in akút hertynfarkt wêryn't in senuwbaan yn de hals, de nervus vagus, elektrysk stimulearre waard. It is bekend dat elektryske stimulaasje fan dizze senuwbaan resultearret yn it beheinen fan de ynfarktgrutte yn lytse proefdieren wannear dit útfierd wurdt ûnder, of foarôfgeand oan de perioade fan it ôfsluten fan de krânsslachier. Omdat dit net de klinyske wurklikheid simulearret, wêr't pasjinten pas yn it sikehûs belânje wannear se al in hertynfarkt ha, ha wy dizze senuwbaan stimulaasje test by bargen mei in akút hertynfarkt. De terapy waard úteinset flak foar de reperfúzje, persys lykas it yn de klinyk tapast wurde soe.

De resultaten litte sjen dat ek yn ús grutte proefdiermodel elektryske stimulaasje fan de nervus vagus de ynfarktgrutte beheint. Dêrneist blykt de terapy yn steat de no-reflow te beheinen. De resultaten waarden wjerspegele yn de fermindere ynstream fan wite bloedsellen yn it ynfarktgebiet en oanfoljende eksperiminten litte sjen dat stikstofoksyde essinsjeel wie foar it terapeutyske effekt.

Al mei al is dizze foarm fan terapy geunstich en fertsjinnet oanfoljend ûndersyk. Hoewol bekend is dat ferlytsing fan it hertynfarkt yn de akute faze belangryk is om op de lange termyn hertfalen foar te kommen, is it dêrneist fan belang om ek it saneamde remodellearingsproses fan it hert te beynfloedzjen. Dit proses fynt plak yn de wiken en moannen nei it akute hertynfarkt.

De eksperiminten beskreaun yn **Diel III** binne rjochte op it beynfloedzjen fan it proses fan hieljen fan de wûne en it yn kaart bringen fan de lange termyn effekten fan nije behannelingen op hertfunksje nei in hertynfarkt.

Yn **Haadstik 8** wurdt dêrta in nije wize om nei de ûntwikkeling fan it ynfarkt yn de tiid te sjen, presintearre. Dizze manier is basearre op in MRI opname en ferdielt de linker helte fan it hert digitaal yn deselde plakken. Dizze plakken wurde dêrnei digitaal opdield yn 36 identike segminten. Hjirnei wurdt mei dizze plakken en segminten de geometry fan it ynfarkt bepaald. Dizze gefoelige manier fan mjitten is daliks tapast yn **Haadstik 9** wêr't bargen mei in hertynfarkt behannele wurde mei pacemakers. Dizze pacemakers ha 2 x deis 3 kear 5 minuten it ynfarktgebiet elektrysk stimulearre.

Hertfunksje en ynfarkt geometry fan dizze bisten waard in pear dagen nei it ynfarkt metten mei MRI en 5 wike dêrnei opnij. Hoewol earder wurk yn lytse proefdieren en isolearre herten mei dizze pacemaker terapy goede resultaten sjen liet, ferbettere de hertfunksje yn ús bisten spitigernôch net. De foarm fan it ynfarkt feroare lykwols al. Pacemaker terapy blykte yn steat de fertinning fan it ynfarkt, in proses dat normaal sprutsen ûnûntkomber ferbûn is mei it ferlittekenjen fan it oandiene hertspierweefsel, sterk te beheinen. Ek de gearstalling fan it ynfarkt feroare. Us pacemaker terapy blykte it oantal fan in spesjaal geunstich seltype, de myofibroblast, ferheegje te kinnen mei it ferbetterjen fan it hieljen fan de wûne as gefolch. Dêrnei is yn **Haadstik 10**, opnij yn in bargemodel foar it akute hertynfarkt, besocht it tal myofibroblasten yn it ynfarktgebiet mei in nij medisyn (UM206) te stjoeren om sa mei in ferbetterjen fan it hieljen fan de wûne, metten mei echo, geunstich te beynfloedzjen. Hoewol it tal myofibroblasten yn de ynfarkten fan net behannele bisten tsjinsteld wienen oan dy rapportearre yn haadstik 9, blykte de UM206 terapy de ynfarktmassa sterk lytser te meitsjen en de negative remodellearing ôf te remjen. Dizze resultaten litte sjen dat wy noch net alles witte oer it stjoeren fan it tal myofibroblasten en op wat foar momint dizze it geunstichst binne. Wol suggerearret dit wurk dat it beynfloedzjen fan myofibroblasten yn it ynfarkt mei pacemaker terapy, mei medisinen of in kombinaasje der fan mooglik en hoopfol is.

Fan it mei groeifaktoaren stimulearjen fan nijfoarming van ieren yn it ynfarktgebiet wurdt oannommen dat it op koarte termyn it hieljen fan de wûne geunstich beynfloedet en dêrmei op langere termyn de skea beheint. Dizze groeifaktoaren ha faak in koarte healweardetiid, binne hiel kostber en kinne ergens oars yn it lichem gefaarlik wêze troch net winske iergroei te stimulearjen.

It is dan ek in doel fan in protte om lokaal, mei help fan in drager, dizze groeifaktoaren regulearre en yn it ynfarkt, nijfoarming fan ieren stimulearje te litten. Hjirta ha wy yn haadstik 4 beskreaune groeifaktor $VEGF_{165A}$ yn lytse polymeer boltsjes witte

te yntegrearjen. De gearstalling fan dizze peareltsjes, it tal en de ynspuit tichtens binne sa keazen dat se yn de lytse ierkes fan it hert hingjen bliuwe sûnder sels skea, yn de foarm fan seldea of in ûntstekkingsreaksje, te feroarsaakjen. Dizze mei it medisyn folde, bio-ôfbrekbere “paarlen voor de zwijnen” binne dêrnei fia in kateter direkt ynspuite yn it risikogebiet fan bargen mei in akút hertynfarkt op it momint fan reperfúzje.

Dit is dien yn 3 behannelgroepen: plasebo, lege dosis VEGF en in hege dosis VEGF. It bloed waard dêrnei ûndersocht op it ôfjaan fan ûntstekkingsrelatearre stoffen en de hertfunksje fan dizze bisten waard op 1 en 5 wiken nei it ynfarkt metten mei MRI. Ek is mei help fan histologyske techniken de tichtens fan de ieren fan it ynfarkt bestudearre. De mei medisyn folde boltsjes hanthavenen of fergrutten de lokale nijfoarming fan ieren op in dosis ôfhinklike manier, wylst dizze yn bisten dy’t plasebo bollen krigen hienen, ôfnamen. Dêrneist blykten beide medisyn folde bollen in remjend effekt te ha op de akute ymmún respons. Spitigernôch ferbettere de hertfunksje fan de behannele bisten net. It belangrykste resultaat fan dizze stúdzje is, dat it bliken die, dat it mooglik is om mei dit hypermoderne farmakoterapeutyske platfoarm lokaal in effekt te bewurkstelligjen. Hoewol de resultaten miskien noch net spektakulêr binne, is dizze stúdzje in stevich fûnemint foar de fierdere ûntwikkeling fan lokale, kontrolearre farmakoterapy.

Gearfetsjend litte de stúdzjes út dit proefskrift sjen dat der meardere suksesfolle terapyen yn ûntwikkeling binne foar de betide diagnoaze en de ferbettere behanneling fan it akute hertynfarkt. Wy ha sjen litten dat wy de ynfarktgrutte, it tal no-reflow, de akute ymmún respons, de foarm en gearstalling fan it ynfarkt en it lokale hieljen fan de wûne geunstich beynfloedzje kinnen ha en dizze geunstige ûntwikkelingen ferbettere fêstlizze kinne ha mei CT, MRI as mei help fan stofkes út it bloed. Tagelyk is der noch in protte wurk te fersetten en roppe de stúdzjes miskien wol mear fragen op as dat se beäntwurdzje. Lykwols biedt it hjoeddeiske wurk in goede basis foar fierder ûndersyk en binne wy in stapke tichter by ferbettere behanneling fan it akute hertynfarkt

List of Publications

VEGF165A microsphere therapy for myocardial infarction suppresses acute cytokine release and increases microvascular density, but does not improve cardiac function

***A Uitterdijk**, *T Springeling, M van Kranenburg, RWB van Duin, I Krabbendam-Peters, C Gorsse-Bakker, S Sneep, R van Haeren, R Verrijk, RJ van Geuns, WJ van der Giessen, T Markkula, DJ Duncker, HMM van Beusekom

Am J Physiol Heart Circ Physiol; 2015 309(3):H396-H406

Non-rigid Groupwise Image Registration for Motion Compensation in Quantitative MRI

W Huizinga, D Poot, JM Guyader, H Smit, M van Kranenburg, RJ van Geuns, **A Uitterdijk**, HMM van Beusekom, B Coolen, A Leemans, W Niessen, S Klein

International Workshop on Biomedical Image Registration 2014; 8545:184-93

Evolution of reperfusion post-infarction ventricular remodeling: New MRI insights

*T Springeling, ***A Uitterdijk**, A Rossi, C Gorsse-Bakker, P Wielopolski, WJ van der Giessen, GP Krestin, P de Feyter, DJ Duncker, RJ van Geuns

Int J Cardiol 2013; 196(5):354-8

Serial measurement of hFABP and high-sensitivity troponin I post-PCI in STEMI: how fast and accurate can myocardial infarct size and no-reflow be predicted?

A Uitterdijk, S Sneep, RWB van Duin, I Krabbendam-Peters, C Gorsse-Bakker, DJ Duncker, WJ van der Giessen, HMM van Beusekom

Am J Physiol Heart Circ Physiol 2013; 305(7):H1104-10

Quantification of myocardial blood flow by CT perfusion imaging in pigs during various degrees of flow-limiting coronary artery stenosis

*A Rossi, ***A Uitterdijk**, M Dijkshoorn, E Klotz, A Dharampal, M van Straten, WJ van der Giessen, N Mollet, RJ van Geuns, GP Krestin, DJ Duncker, P de Feyter, D Merkus

Eur Heart J CV Imaging 2012; 14(4):331-338

Use of MSCs in a porcine model of acute myocardial infarction; feasibility in-vitro results

D Schop, **A Uitterdijk**, M Bracke, BCW Groenendijk, WJ van der Giessen, JD de Bruijn

Appendix PhD thesis Deborah Schop 2010

Stem Cell Therapy for Chronic Heart Failure

A Uitterdijk, BCW Groenendijk, WJ van der Giessen

Hell J Cardiol 2009; 50(2):127-132

Fat is not all bad: how to make good use of adipose tissue

DJ Duncker, **A Uitterdijk**, WJ van der Giessen

Eur Heart J 2007; 28(21):2565-2567

Individual differences in male rat ejaculatory behaviour: searching for models to study ejaculation disorders.

T Pattij , TR de Jong, **A Uitterdijk**, MD Waldinger, JG Veening, AR Cools, PH van der Graaf , B Olivier

Eur J Neurosci 2005; 22(3):724-34

PhD portfolio

Name PhD student:	André Uitterdijk
ErasmusMC department:	Experimental Cardiology
PhD period:	2007-2015
Promotor:	Prof.dr. D.J. Duncker
Supervisors:	Dr. D. Merkus and Dr. H.M.M. van Beusekom

PhD-training, Courses and Seminars	**Year**	**ECTS**
NHS course “Cardiac function and adaptation”	2008	2
Animal Experimentation Course	2008	4.5
Radiation Protection 5A+5B	2008	0.6
Animal Imaging Workshop	2008	1.2
COEUR courses	2007-2009	6
COEUR seminars	2007-2011	2
Other seminars	2007-2014	8
FACS operator training	2010	0.6
Congresses		
Oral Presentations		
American Heart Association	2011	1.5
BCF Career Event; Academia vs. Industry (invited)	2012	0.3
European Society of Cardiology	2013	1.5
Benelux Congress on Physiology and Pharmacology	2014	0.6
Poster Presentations		
NHS course “Cardiac function and adaptation”	2008	
Shear Stress Symposium (2x)	2009	0.3
Dutch Atherosclerosis Society	2009, 2010	1.2
COEUR PhD-day (award)	2010	0.4
Transcatheter Cardiovascular Therapeutics	2011	
Cardiovascular Conference (2x)	2011	0.6
Dutch-German Joint Meeting	2011	0.9
European Society of Cardiology (3x)	2011, 2012	3
Teaching and Supervising		
Kevin Jonkers, Arjen Poortvliet, Ayla Hoogendoorn Frank-Jan Drost, Felix Kienjet and Bas Wijenberg	2008-2013	12
Total		**47.2**

About the Author

Drevis Berend Uitterdijk was born on the 26th of December 1978. From his birth onwards he was named André. He attended higher education at CSG Oostergo/ Dockinga College in Dokkum. Next, he studied Biotechnology at the University of Professional Education: Noordelijke Hogeschool Leeuwarden/van Hall Instituut Leeuwarden. He completed his final year with an internship at the University of Utrecht at the department of Psychopharmacology in collaboration with the department of Anatomy and Physiology in Nijmegen where he studied sexual psychopharmacology and ejaculation disorders and successfully obtained his bachelor's degree. Following this, André studied Biotechnology at the Wageningen University and Research Centre and specialized in Medical Research. At the department of Process Engineering, division of Marine Biotechnology, he obtained his master of science degree studying metabolism in sponges. Successful completion of his master's study was followed by a voluntary internship in Florida, United States, at the Harbor Branch Oceanographic Institution where he successfully immortalized stem cells from sponges for aquaculture and optimized culture conditions. In 2007, André started his PhD-traineeship at the department of Cardiology; section Experimental Cardiology, Thorax Centre Rotterdam where he worked on novel therapies and diagnostics for ischemic heart disease and acute myocardial infarction. From 2015 onward, he will continue his work in Experimental Cardiology as a post-doctoral researcher.

Dankwoord

Piet Verdouw verwoordde het volmaakt: *“Het niveau van ieder proefschrift is groter dan dat van de promovendus zelf”.* Daar is in dit geval geen woord van gelogen, dit boek bestaat alleen omdat vele handige en slimme mensen er lang en hard aan hebben gewerkt.

Het begon allemaal op 5-6-2007
Beste André,

Met genoegen kan ik je meedelen dat je aangenomen bent op de promotieplaats. Zou je dinsdag 12 juni om 14:30 uur langs kunnen komen om papieren te tekenen en verdere afspraken te maken?
Met vriendelijke groet,

Wim van der Giessen

Beste Wim, je bent er niet meer en dat is een gemis. Ik wil je bedanken voor vertrouwen, wijze lessen en translationele vorming. Je was een unieke brug tussen de onderzoekswereld en de kliniek en stiekem keek ik uit naar een met droge humor gelardeerd en karakteristiek-gedragen laudatio. We zijn je niet vergeten.

Beste Dirk, ik ben dankbaar dat je me opving na het wegvallen van Wim. Het was een voorrecht om jaren de kunst van je af te mogen kijken en met je aan het front van de wetenschap te mogen strijden. Tijdens m’n sollicitatie ontspoorde het gesprek al snel in een lesje no-reflow, ik had er nog nooit van gehoord en werd geïntimideerd door veel te veel citaten, referenties en anekdotes. Eigenlijk werken we nog steeds zo maar kijk ik er net wat minder verbaasd bij. Ik leerde ontzettend veel van je, voornamelijk op het gebied van slimme wetenschap en het intelligent belichten en presenteren van moeilijke data, maar ook management, de PUFA’s, resveratrol en de enneagrammen (type 7) passeerden de revue met een glimlach en een gepaste anekdote tijdens bier en bal. Nog altijd betreed ik je kantoor schoorvoetend en de intellectuele afstand intimideert me onverminderd. Tegelijkertijd doet het me deugd dat ik niet de enige ben met duizend-en-één hobby’s, dat moet bijna wel professorabel zijn.

Daphne, beste Daphne, niemand is zo vrij van ego als jij. Samenwerken gaat altijd gesmeerd en ondanks dat je al associate professor bent, blijf je toegankelijk en neem je de tijd voor elk probleem. Los van je status sta je nog vaak met de poten in de modder, dat inspireert me en bewonder ik. Daarnaast ben je nog akelig slim ook en kan je me zonder uitzondering met moeilijke vragen ontwapenen. U bent een voorbeeld. Geweldig en een voorrecht dat we nog even samen verder mogen.

Beste Beus, orakel van Schiedam. Ik moest even aan je manier van werken wennen maar het heeft me uitstekend geleerd hoe belangrijk protocolvastheid en voorbereiding wel niet zijn. Ik heb enorm geprofiteerd van je grote histopathologische kennis en je maakte me veel beter in het verkopen van resultaten waarvan ik het belang niet inzag, niemand debatteert en presenteert zo goed als jij, ik heb er veel van geleerd. Ik koester de vele fietstochtjes die zonder uitzondering ontspoorden/ evolueerden in levensbeschouwing met alle onderwerpen van de hele wereld, via gastronomie en vrijmetselarij naar sport, logica en complexe wijsbegeerte. Ik bewonder je vermogen de kleine geneugten in het leven te herkennen en hoewel niet alle ideeën tot manuscripten hebben geleid ben ik blij met het hFABP- en Octobolmanuscript.

Ik dank de leden van de leescommissie, de hoogleraren van Geuns, Koudstaal en van Royen voor het razendsnel beoordelen van de promotiewaardigheid en academische merites van dit boek. Daarnaast een hartelijk dank voor prof. Prinzen en Dr. Essers voor het deelnemen aan de grote commissie. Ik kijk uit naar de gedachtenwisseling.

Twee mensen zijn belast met de wat mij betreft discutabele eer van paranimf zijn. Wat van oudsher een actieve erebaan zou zijn, is vandaag de dag verwaterd tot een uur stilstaan. Dat heb ik nooit goed begrepen en misschien is de tijd dan ook wel rijp om deze twee heren actief te betrekken in wat peri-dissertatiële ruggespraak en ze wat meer aan het woord te laten bij de verdediging.

Allereerst Richard Willem Benjamin, onze chronisch-goedgeluimde womenmagnet en vleesgeworden trapleuning. Hoewel de “grap” met de stekker onvergefelijk ver beneden niveau was heb je m’n avontuur op de ExpCard jarenlang verrijkt met humor en koffie. Vele experimenten op akelig-onsympathieke tijdstippen werden stukken dragelijker met een lekker stuk muziek (whoa-oa-ooh, yeah yeah), creatief geknutsel, oneindige toneelstukjes en ontelbaar veel grappen. Ik ben je dankbaar en kijk uit naar de van-Dune-reinforced-suspension-bridge, HARDER RANCID 4evâh.

Het is dat een ondankwoord niet is toegestaan, daarom op deze plek speciaal voor mijn 2e ~~paraninja~~ paranimf, kleine broertje, middelmatigman en drammerig-stampvoetkereltje ~~Incontinenticent~~ Vincent “zeg ken jij de twister” de Beer (met die gekke moedervlek op je bil) een hartelijk “Ik heb je nooit gemogen.” Ik heb genoten van onze vergevorderde onwelvoeglijkheden, spitsvondige beledigingen en hartverwarmend levensbeschouwen rondom de Krav Maga, congressen,

borrels en bacchanalen. Je bent de enige in de hele wereld die 2 uiterste emoties in me losmaakt, soms de antireligieuze, verongelijkte betweter des ultrairritaties die tegelijkertijd en volledig tegenstrijdig alles van wanmerk des kuddedieres Apple aanbidt en soms een hartelijke vent en begripvolle vriend met luisterend (maar lelijk en onfris) oor. Je bent een unieke man met ultrahumor en er zijn maar weinigen die dat gepast naar waarde kunnen schatten, het is een gave alsook talent, één plus één is honderd. Ik ben het beste wat je ooit is overkomen.

~~Steelpan~~, ~~Sesam~~, Stefan "The Eye of the Tiger" Sneep. Slimme vent die alles kan (r^2=1), ik heb ontzettend veel aan je gehad in vele studies en minstens zoveel doodlopende proefballonnen. Zonder jou was ons rockconcert niks geworden, heel bijzonder dat je in korte tijd diverse instrumenten leerde bespelen. Ik mis het koffiedrinken en de broodje/bootje tochtjes, succes met werk en studie, laten we snel ergens onbeperkt saté gaan eten.

Lieve Lot, unieke rechtsblonde hart-op-de-tong-vrouw, ondanks dat je alcohol in m'n gezicht gooide, in m'n vinger knipte en in m'n duim hechtte kijk ik met een grote glimlach terug op je onbetaalbare bijdrage aan een berg studies en je kraakheldere levensvisie, ik wens je het beste.

Bianca, intelligente vrouw, ik ben dankbaar dat de PID/3B het boek heeft gehaald, het is een mooi meerlagig geheel geworden waar we trots op mogen zijn. Ik wens je veel zonneschijn toe, dat je maar mag vinden wat je zoekt.

Rorry van Haeren, hartelijk dank voor je hulp bij het vullen van het archief, ik ben altijd onder de indruk geweest van je kennis van de histologie en heb prettig met je gewerkt, het ga je goed.

Ik heb altijd de arbeidsethos bewonderd van Oana (alleen Roy wist dat je het eigenlijk als 0ana spelt), lieve Oana, harde werkster, dank voor je wijsheid, bemoedigende woorden en humor, ik bewonder je, pas goed op jezelf laten we snel weer de forellen verbaasd laten kijken.

Jarenlang was Mieke mijn buurvrouw, Mieke, hartelijk dank voor veel goede gesprekken en het organiseren van de beste borrels, de SinterKerst cocktail party, 't avondje New Kids, en de ultraMeloen BBQ zijn legendarisch.
Na Mieke werd Nienke "die Nase" van Ditzhuijzen mijn buurvrouw, Nina, we zijn het exact nul keer met elkaar eens geweest maar daar zal je het wel weer niet mee eens zijn, trek alsjeblieft dit keer wat fatsoenlijks aan.

Ilona! Laat ik het voorzichtig verwoorden, we moesten wat aan elkaar wennen in het prille begin. Vandaag de dag waardeer ik je echter als slimme en hardwerkende collega, ik heb veel van je geleerd en kijk uit naar verdere samenwerking, dankjewel. M'n eerste van vele katheters mocht ik met veel humor leren plaatsen met die lelijke vent van je, Stefan "Wakschaatser" Krabbendam, ik zeg www.steefit.nl, hartelijk dank.

Marc "stug met een zachte G" van Houwelingen, hoe zat het ook alweer met die Bratwurst en dat Sauerkraut? Ook daarom ben je een held, maar weet je misschien waar mijn winterpeen is?

Elza, zuster van Deel, onvoorstelbaar dat je op Alestorm in slaap viel en te gek dat we op jouw feestje onze ego's konden voeden. Ik hoop dat je het Rembo&Rembo licht nog mag zien.

Voor mijn Ottomaanse broeder en blufturk Tuncay Yetgin, Gekke Turk, kameraad, succes met het afronden van je boek en veel geluk met je opleiding, ik kijk uit naar je verdediging, kom gauw weer eens meetrainen of heb je toch liever een lawashje kalfsvlees?

Hartelijk dank aan de McGyvers van de afdeling, Liesbeth (m'n noodles zijn op, gaan we binnenkort naar de boot?) en Rob (ons filmpje is al 332192 keer bekeken!), dank voor alle ondersteuning als de boel het weer eens begaf. Bedankt voor koffie en de vele relativerende gesprekken.

Vele experimenten mocht ik profiteren van de kennis en ervaring van de biotechnische ruggengraat van de afdeling, Maaike. Lieve M, zonder jou werd het niks, ik heb veel van je geleerd en zonder uitzondering met een glimlach met je gewerkt, heel erg bedankt.

Voor M-Honey, als ik het kan, dan jij zeker, houdt moed, afronden die shit en op naar een Slippies/Onepiece party? Yanti en Marion, altijd goed voor een glimlach, dank.

Monique, onze poortwachter, dank voor je hulp, ik beloof je dat ik ook dit jaar weer keurig vergeet hoe ik m'n vakantiekaart moet invullen. Elles, ik ben je niet vergeten, een hartelijke groet.

Anouchska, samen zwalkend door de homobuurten van Parijs heb ik je als een waardevolle en intelligente collega leren kennen. Succes met begeleiden.

Beste Roy, krasse ouwe gek, het is een gemis dat je te vroeg bent weggevallen. Ik heb je arbeidsethos altijd bewonderd en keek uit naar de ferme handdruk die misschien wel bij het afronden van dit boek zou hebben gepast, we zijn je niet vergeten.

Daphne Meijler, Kelly (1000 burpees!), Ruben, Annemarie “hij moet er toch echt in”, Chris, ga nou als Tetris, Ihsan en Maarten, dank voor collegialiteit.

Een hartelijke groet aan oud collega’s Marcel de jong, Liz, Maaike H, Inge, Olivier, Yannick, Monique de W, Diederik en Sylvana, het ga jullie goed.

Ik dank broeder-Remko voor de unieke omslag, je hebt volmaakt Gorefest’s Freedom met Sabaton’s Coat of Arms verenigd samen met He-Man, het subliminale en wat hart, goed werk man.

Distaal van de klapdeuren woonden eertijds de collega’s van de moleculaire cardiologie, een hartelijke groet aan Weiland den Dekker, Remco “Herman” Haasdijk. Petra B, essentieel betrokken bij elk stuk promotiecabaret! Renate+Jaco, ik schaam me ervoor dat samenwerken niet aan de orde was. Esther en Lau, gelukkig zijn jullie blijven hangen, heel waardevol! In het bijzonder dank ik Dennipedia, met je koffiedrinken, mopperen over onze “begeleiders” en het wetenschappelijke beschouwen (niet te verwarren met afzeiken) van met name andermans “werk” zorgde zonder uitzondering voor een welkome glimlach.

Het was een groot voorrecht om te mogen werken met moderne klinische beeldvormingstechnieken als CT en MRI. Het blijft uniek om het hart, hartfunctie en regionale doorbloedingsproblematiek van onze varkens in beeld te mogen brengen met dezelfde machines waarin een uurtje later “gewoon” weer een patiënt ligt. Dit zou niet mogelijk zijn geweest zonder de steun van prof. Krestin en het fundament wat mijn voorgangers legden. Vele uren bracht ik op erbarmelijke tijdstippen door met mijn eigen scandiva Tirza Springeling. Lieve T, we moesten wat aan elkaar wennen maar hebben er toch maar mooi 3 artikelen uit geperst, dank voor je vele inspanningen en de verhelderende gesprekken over de klinische werkelijkheid, ik heb veel van je geleerd en kijk uit naar jouw verdediging. Na Tirza mocht Matthijs de laatste handvol Octo’s scannen, Matthijs bedankt en succes met de laatste loodjes.

The perfect example of the smoothest interdepartmental collaboration in history was the CT-perfusion work together with my dearest Alexia (Ciao Bella!), it was a pleasure working with you.

I have had the pleasure of collaborating with several partners, thank you Eric Mokelke, Ruud Verrijk, Trent Fischer and Richard Cornelussen for smooth and constructive work. Een hartelijke groet aan de collega's in Maastricht, Evangelos, Kevin en W Matthijs.

Op de achtergrond van proefdierkundig onderzoek speelt zich een hoop af. Van dierverzorging, sterilisatie van instrumenten tot het opruimen en afvoeren van bebloed en onfris afval. Een hartelijk dankjewel voor de onmisbare collega's van het EDC, 2x Dennis, Kim "Hammer Smashed Face" Moerkerke, Marcel "de Zwarte Poema" Boersma, Calinda, Ed en Dominique. Michael, Ruud, Ludwig, Ridoe en Brito, hartelijk dank voor jullie inspanningen, we kunnen niet zonder. Georgia en Urbanic, uw werk is belangrijk en wordt gewaardeerd, van u beiden kerstkaarten te mogen ontvangen heeft me ontroerd en herinnert me er aan wat écht belangrijk is.

Door de jaren heen mocht ik met een aantal bijzondere studenten werken. Hartelijk dank Kevin "Febo" Jonkers, Arjen "nou-maar-Charlotte-zei" Poortvliet, Ayla "the Tavern Wench" Hoogendoorn, Frank-Jan "Milow" Drost (vraag Richard maar, ik zie het niet), Felix "Appetite for Destruction" Kienjet en Bas "A" Wijenberg. Ik heb zonder uitzondering een hoop van jullie geleerd en wens jullie het beste.

Een hartelijke groet voor vrienden en trainers van de Krav Maga, de Trojan "workout" en m'n huidige broeders en zusters bij Staal&Kracht. Hartelijk dank voor het chronisch aanpakken van m'n vele fysieke en mentale beperkingen, ik heb het nodig.

Wiger en Hendrik, freonen fan eartiids en freonen fan hjoed by wa't ik altiid gewoan Drevis wêze kin, wat tolerearje we elkoar al lang. Fan sûpe yn it dowehok en fiskje by "Bartele Merkus" oant krinkjespuie en wiisprate op de bettere musyk. Mar gauw wer ris ôfprate.

Een hartelijke groet voor mijn lieve schoonouders, broers en zus, ik voel me thuis bij jullie en kijk al weer uit naar het kerstdiner met slagroomspuit.

Ik haw twa nuvere susters, elts mei hun eigen bysûndere libbens. Ik bin grutsk op jimme, mar ferjit net, ik bin de moaiste fan ús trijen, lit dat dúdlik wêze.

Hikke en tein yn it skitterjende Driezum bin ik lokkich mei myn alderleafste Heit&Memke. Tige tank dat der troch de jierren hinne altiid romte wie om fierder te learen en my ûntwikkeljen te bliuwen. Der is gjin thús sa thús is as thús-thús, de tritichste fan Desimber bakke we wer oaljekoeken. Goed op jimsels passe.

De beste plek van dit boek is voor mijn allerliefste Sanne, mijn prachtige vrouw die niet eens bijna zo onschuldig is als ze er uit ziet en glimlacht als ze slaapt. Moppie, ik ben ontzettend trots op je. Je wilde op me wachten om samen op 1 dag het promotieavontuur af te sluiten en dat is een geweldig cadeau, ook daarom hou ik van je. Je bent slim en grappig, soms geknotst en soms de koàrraep, soms de rockchick, soms de bikerbabe, soms in je chillpakje op de bank en soms de dure mevrouw. Maar altijd mijn allerliefste die de meest mooie woorden verzint die niet bestaan maar ik onmiddellijk begrijp. Samen de shit lief, samen sterk, samen onder de apelbeam, samen.
Een kus van je allergrootste fan.

Now I see it all through different eyes,
where I'm going, where I've gone.
All I know, I'm still surprised,
that the road goes on.

Toto – The Road Goes On